4 c
3763

VAPOUR TRANSPORT IN ALTERNATING - BLOCK AND GRAFT COPOLYMERS OF POLYDIMETHYLSILOXANE

by

MICHAEL JOHN LLEWELLYN WILLIAMS,
B.Sc., A.R.C.S.

A thesis presented for the degree of

DOCTOR OF PHILOSOPHY

in the University of London

Physical Chemistry Department,
Imperial College,
London.

September, 1978.

ABSTRACT

MICHAEL JOHN LLEWELLYN WILLIAMS, B.Sc., A.R.C.S.

VAPOUR TRANSPORT IN ALTERNATING-BLOCK AND GRAFT COPOLYMERS OF POLYDIMETHYLSILOXANE

Studies have been made of the transport and sorption of propane in alternating-block copolymers of polydimethylsiloxane (PDMS) and poly(bisphenol-A carbonate) (BPAC) and in the pure components PDMS and BPAC at several temperatures in the range 20 to 60°C. Two distinct series of membranes, each with a fixed PDMS block length but variable BPAC block length were investigated in the composition range 25 to 83% PDMS. Sorption equilibria and kinetics were obtained with an electronic vacuum microbalance and permeability and diffusion coefficients from flow across a thin membrane.

Sorption in PDMS obeys Henry's Law. For BPAC, non-linear isotherms were obtained and an analysis made in terms of the dual mode sorption theory for gases in glassy polymers; the results indicate a strong component of Langmuir-type immobilisation to the sorption although an analysis of the concentration dependence of the diffusion coefficient indicates that there is a definite degree of mobility to this component of sorption.

With the copolymers, non-linear isotherms were obtained for materials with high BPAC contents. The permeability data strongly support a partial microphase separation of the two components and depart markedly from theoretical expressions for transport in media consisting of a dispersion of one component in a continuum of the other. By allowing for some degree of mixing of BPAC with the PDMS continuum, most of the features of the transport measurements can be accounted for.

Finally in relation to the dual-mode sorption theory as applied to glassy polymers, the sorption of propane in a poly(vinyl acetate) phase dispersed in a crosslinked silicone rubber network has been measured above and below the glass transition temperature. The results establish that the curvature in the isotherm for the glassy polymer attributed to localised sorption in microcavities is not present above the transition temperature.

ACKNOWLEDGEMENTS

I am greatly indebted to Dr. J. A. Barrie for his interest and guidance throughout this research.

I am grateful to the Science Research Council for a bursary for this work, the General Electric Co. Research and Development Centre (U.S.A.) for gifts of material samples and Dr. G. S. Parry of the Department of Chemical Engineering for the electron micrographs.

Finally, I should like to thank Mr. Keith Munday for the many fruitful discussions of the past three years.



DEDICATION



To my parents, without whose help and encouragement this would not have been possible.

Also to the memory of my father, the late Jack Llewellyn Williams.

CONTENTS

	Page
LIST OF TABLES	9
LIST OF ILLUSTRATIONS	11
CHAPTER 1 : INTRODUCTION	13
1.1 Basic principles	13
1.2 Definitions of $\overline{P}$, D and S.	14
1.3 Kinds of penetrant	15
1.4 Factors that affect $\overline{P}$, D and S.	16
1.4.1 Temperature dependence	16
1.4.2 Effect of glass transition	17
1.4.3 Crosslinking	18
1.4.4 Plasticisation	18
1.4.5 Nature of penetrant	18
1.4.6 Physical nature of the polymer	19
1.4.7 Heterogeneous polymer systems	19
1.5 Copolymers	20
1.5.1 Block copolymers	20
1.5.2 Graft copolymers	21
1.6 This investigation	22
CHAPTER 2 : THEORY	24
2.1 Basic equations of diffusion	24
2.2 Solution of Fick's equations	25
2.2.1 Steady-state	25
2.2.2 Transient-state	27
2.2.3 Sorption- and desorption-kinetics	29
2.3 Molecular diffusion theories	33

	Page
2.4 Dual-mode sorption theory	34
2.4.1 Heats of solution	35
2.4.2 Diffusion model for the theory	36
2.4.3 Novel solutions	37
CHAPTER 3 : LITERATURE REVIEW	40
3.1 Introduction	40
3.2 Transport in heterogeneous media	40
3.2.1 Review of theoretical models	40
3.2.2 Review of experimental testing of the models	44
3.3 Review of the dual-mode sorption theory	49
3.4 Review of PDMS/BPAC copolymers literature	56
CHAPTER 4 : EXPERIMENT	59
4.1 Materials	59
4.1.1 Alternating-block copolymers of poly(dimethyl siloxane (PDMS) and poly(bisphenol-A carbonate)(BPAC)	59
4.1.2 Poly(bisphenol-A carbonate).	59
4.1.3 Poly ((c.ℓ.)-dimethylsiloxane).	60
4.1.4 Poly ((c.ℓ.)-dimethylsiloxane-g-vinyl acetate),PDMS-g-PVAc	60
4.1.5 Physical properties of the membranes	60
4.1.6 Penetrant vapour	61
4.2 Apparatus	61
4.2.1 The permeability system	61
4.2.2 The sorption system	64
4.3 Experimental procedure	68
4.3.1 Permeation measurements	68
4.3.2 Sorption measurements	
CHAPTER 5 : RESULTS AND DISCUSSION, PART 1 : BPAC, PDMS and PDMS-g-PVAc	71
5.1 BPAC	71
5.1.1 Equilibrium sorption	71

	Page
5.1.2 Sorption kinetics	82
5.2 PDMS	90
5.2.1 Equilibrium sorption	90
5.3 PDMS-g-PVAc	93
5.3.1 Equilibrium sorption	93
CHAPTER 6 : RESULTS AND DISCUSSION PART 2 : PDMS-b-BPAC membranes	101
6.1 Preliminary remarks	101
6.2 Densities and Tg's	101
6.3 Transient permeation results	105
6.3.1 Permeabilities	105
6.3.2 The delta-phi analysis (DPA)	107
6.3.3 Physical interpretation of DPA.	110
6.3.4 Permeability temperature coefficients	113
6.3.5 Time-Lag diffusion and solubility coefficients	120
6.4 Equilibrium sorption	122
6.5 Steady-state diffusion coefficients	144
6.6 Effect of annealing on sorption	148
CHAPTER 7 : CONCLUSIONS	153
7.1 Summary and appraisal of results	153
7.1.1 Transport and sorption of propane in pure BPAC.	153
7.1.2 Sorption of propane in PVAc.	154
7.1.3 Alternating PDMS-b-BPAC copolymers	154
7.2 Concluding remarks	155
7.2.1 Churchill thermocirculator	155
7.2.2 Suggestions for further study.	155

	Page
CHAPTER 8 : APPENDIX	157
8.1 Other expressions for permeation in heterogeneous media	157
8.2 Transient permeation : sample calculations and estimation of errors	160
8.3 Equilibrium and transient sorption : sample calculations and estimation of errors	162
8.3.1 Equilibrium sorption	162
8.3.2 Transient sorption	163
8.4 Sorption data : BPAC	166
8.5 Sorption data : PDMS	170
8.6 Sorption data : PDMS-g-PVAc and PVAc (extracted).	172
8.7 Transient permeation data for PDMS-b-BPAC/propane	177
8.7.1 20-block membranes	177
8.7.2 40-block membranes	179
8.7.3 Misc. membranes	181
8.8 Equilibrium sorption data for PDMS-b-BPAC/propane	182
8.8.1 20-block membranes	182
8.8.2 40-block membranes	188
8.8.3 Misc. membranes	193
8.9 Electron microscopy	196
REFERENCES	198

ADDENDUM: J.A. Barrie, K. Munday and M.J.L. Williams. "Sorption and Diffusion of Hydrocarbon Vapours in Glassy Polymers." Polymer Engineering and Science (in press).

LIST OF TABLES

Page

CHAPTER 3 : LITERATURE REVIEW

3.1 Some methods for interpreting heterogeneous permeability data. 42

CHAPTER 4 : EXPERIMENT

4.1 Some physical properties (of the membranes) 63

CHAPTER 5 : RESULTS AND DISCUSSION,
PART 1 : BPAC, PDMS and PDMS-g-PVAc

5.1 Sorption parameters for BPAC/propane 71

5.2 Enthalpies of sorption for BPAC/propane 77

5.3 Enthalpy comparisons 78

5.4 Diffusion coefficients for BPAC/propane 85

5.5 Activation energies of diffusion for BPAC/propane 87

5.6 Solubility coefficients for PDMS/propane 93

5.7 Sorption parameters for propane in PDMS-g-PVAc and "extracted" PVAc. 96

5.8 Enthalpies of sorption for propane in PDMS-g-PVAc and PVAc. 100

CHAPTER 6 : RESULTS AND DISCUSSION,
PART 2 : PDMS-b-BPAC MEMBRANES

6.1 Permeabilities at 50°C. 105

6.2 Delta-phi analyses 109

6.3 Permeability temperature coefficients. 114

6.4 Delta-phi analysis using E_P's 119

6.5 Transient values of D, S (at 50°C), E_D and $\Delta\overline{H}_S$. 121

6.6 Sorption parameters for PDMS-b-BPAC/propane (20-blocks). 122

6.7 Sorption parameters for PDMS-b-BPAC/propane (40-blocks). 123

6.8 Sorption parameters for PDMS-b-BPAC/propane (Misc.). 124

6.9 Values of k_D, S_L and B at 50°C. 139

6.10 Enthalpies of solution for PDMS-b-BPAC/propane. 144

6.11 Steady-state D's at 50°C and activation energies. 146

6.12 Effect of annealing on sorption parameters. 150

Page

CHAPTER 8 : APPENDIX

8.1.A Equilibrium sorption data for BPAC/propane at 30 and 40°C. 167

8.1.B Equilibrium sorption data for BPAC/propane at 50 and 60°C. 168

8.2 Sorption kinetics data for BPAC/propane 169

8.3 Equilibrium sorption data for PDMS/propane. 171

8.4.A. Equilibrium sorption data for PDMS-g-PVAc/propane, below T_g. 173

8.4.b. Equilibrium sorption data for PDMS-g-PVAc/propane, above T_g. 174

8.5.A. Equilibrium sorption data for PVAc(extracted)/propane below T_g. 175

8.5.B Equilibrium sorption data for PVAc(extracted)/propane above T_g. 176

8.6 - 8.10 PDMS-b-BPAC/propane transient permeation data : 20-block membranes. 177-179

8.11 - 8.15 PDMS-b-BPAC/propane transient permeation data : 40-block membranes. 179-180

8.16 - 8.18 PDMS-b-BPAC/propane transient permeation data : miscellaneous block membranes. 181

8.19 - 8.23 PDMS-b-BPAC/propane sorption data: 20-blocks. 183-187

8.24 - 8.28 PDMS-b-BPAC/propane sorption data : 40-blocks. 188-192

8.29 - 8.31 PDMS-b-BPAC/propane sorption data : misc.blocks. 193-195

LIST OF ILLUSTRATIONS

Page

CHAPTER 3 : LITERATURE REVIEW

3.1 Proposed morphology of alternating PDMS-b-BPAC copolymers 57

CHAPTER 4 : EXPERIMENT

4.1 Chemical structure of alternating PDMS-b-BPAC copolymers 59

4.2 Permeability system 62

4.3 Permeation cell 65

4.4 Microbalance beam 65

4.5 Sorption system 66

CHAPTER 5 : RESULTS AND DISCUSSION,
PART 1 : BPAC, PDMS and PDMS-g-PVAc.

5.1 BPAC/propane isotherms 72

5.2 Van't Hoff plots : k_D, $\overline{k}_D$, B, $\overline{B}$, S_L, $\overline{S}_L$ for BPAC/propane 75

5.3 $\Delta\overline{H}_S$ vs. concentration for BPAC/propane. 81

5.4 $\overline{D}_S$ vd. concentration for BPAC/propane at 30.1°C and 40.05°C. 83

5.5 $\overline{D}_S$ vs. concentration for BPAC/propane at 50.1°C and 60.0°C 84

5.6 $\overline{D}_S.Y^{-1}$ vs. X. Y^{-1} for BPAC/propane 86

5.7 Arrhenius plots : D_m, D_i, $D_{C=O}$ for BPAC/propane. 88

5.8 PDMS/propane isotherms. 91

5.9 Van't Hoff plot for PDMS/propane 92

5.10 Sorption isotherms for PDMS-g-PVAc/propane. 94

5.11 Sorption isotherms for PVAc (extracted)/propane. 95

5.12 Van't Hoff plots : k_D, S_L for PDMS-g-PVAc/propane 98

5.13 Van't Hoff plots : k_D, S_L for PVAc (extracted)/propane 99

CHAPTER 6 : RESULTS AND DISCUSSION,
PART 2 : PDMS-b-BPAC MEMBRANES

6.1 Density vs. volume fraction of PDMS. 102

	Page
6.2 T_g vs. $(\overline{DP})^{-1}$ for BPAC.	104
6.3 $\overline{P}(50^{o})$ vs. volume fraction of PDMS.	104
6.4 $\overline{P}(50^{o})$ vs. Φ_A : models - DPA comparison	111
6.5 E_p vs. volume fraction of PDMS.	115
6.6 Temperature dependence of $\overline{P}$	116
6.6 (continued).	117
6.7 - 6.11 Sorption isotherms (20-blocks).	125-129
6.12 - 6.16 Sorption isotherms (40-blocks).	130-134
6.17 - 6.19 Sorption isotherms (misc.).	135-137
6.20 k_D vs. volume fraction of PDMS.	140
6.21 S_L vs. volume fraction of PDMS.	141
6.22 Heats of solution vs. Φ_A.	143
6.23 Diffusivity vs. Φ_A.	147
6.24 Activation energy of diffusion vs. Φ_A.	149
6.25 Effect of annealing on sorption : PDMS-60(80:14.6)/propane at 50°C.	151
6.26 Effect of annealing on sorption : PDMS-60(40:7.2)/propane at 50°C.	152

CHAPTER 8 : APPENDIX

8.1 PDMS-25 (20:17.8) x 120,000 (including silicon analysis).	197
8.2 PDMS-25 (20:17.8) x 50,000 (including silicon analysis).	197

CHAPTER 1

INTRODUCTION

1.1 Basic Principles

When small molecules pass through a polymer membrane, the rate of transmission can generally be expressed in terms of the physical characteristics of the membrane. It was Graham, in 1866, who first described the main features of the phenomenon of gaseous transport or "permeation", through polymer membranes on a quantitative level (1). Essentially, the process consists of three steps:

(a) Sorption. The penetrant molecules sorb into the ingoing surface of the membrane from the gaseous phase.

(b) Diffusion. The sorbed molecules pass through the membrane by random displacements within the polymer matrix leading to a net transport across the membrane.

(c) Desorption. At the outgoing surface of the membrane the penetrant molecules evaporate into the gaseous phase.

Generally, steps (a) and (c) occur almost instantaneously and the diffusion step (b) is considered to be rate-determining for the overall process. It should be noted that the process of solution of a gas or vapour in a polymer is often exothermic and that diffusion is an activated process with a positive energy of activation. Permeation is the resultant effect of these two processes and can have associated with it either a positive or negative temperature coefficient depending on the relative magnitudes of the enthalpy of solution and the activation energy of diffusion for the system in question.

The interpretation of both permeation and solubility data is extremely valuable in studying the mechanism of transport phenomena and elucidating the microstructure of the polymer itself. Several reviews have appeared which relate the chemical properties and physical structure of both the individual penetrants and the polymers to the transport characteristics associated with such systems (2-6).

The interpretation and analysis of permeation and solubility data is generally in terms of Fick's equations and these will be discussed later.

1.2 Definitions of $\bar{P}$, D and S

Three important quantities must be defined:

(a) The permeability coefficient, $\bar{P}$ is defined as the amount of penetrant at S.T.P. passing through a membrane of unit cross-sectional area and of unit thickness under unit pressure difference in unit time whilst the system is in the steady state.

From this definition,

$$\bar{P} = \frac{V \cdot \ell}{A_c \cdot t \cdot (P_1 - P_2)} \qquad \ldots (1.1)$$

where V = volume of penetrant (cm^3STP) passing through the membrane in t seconds when the system has reached the steady state,

ℓ = membrane thickness (cm),

A_c = membrane cross-sectional area (cm^2),

P_1, P_2 = ingoing and outgoing pressures of penetrant (cm Hg), respectively.

Typical units of permeability are $\left(\frac{cm^3 STP.cm}{cm^2.s.cm\ Hg}\right)$, which are used throughout this work.

(b) The diffusion coefficient (or diffusivity), D is the amount of penetrant at S.T.P. passing through a membrane of unit area under unit concentration gradient in unit time.

$$D = \frac{V}{A_c.t} \Big/ \frac{\partial C}{\partial x} \qquad \ldots (1.2)$$

where C = concentration of penetrant in the membrane ($cm^3 STP.cm^{-3}$),

x = distance parameter measured normal to the faces of the membrane.

The units of diffusivity are ($cm^2.s^{-1}$).

(c) The solubility coefficient, S is the amount of penetrant at S.T.P. in unit volume of dry polymer when in equilibrium with the surrounding penetrant at unit pressure. The units used in this work are $\frac{cm^3 STP}{cm^3.cmHg}$.

In the Henry's Law region,

$$S = \frac{C}{P} \qquad \ldots (1.3)$$

Rewriting (1.2) for a uniform concentration gradient,

$$D = \frac{V.\ell}{A_c.t.(C_1-C_2)} \qquad \ldots (1.4)$$

and substituting (1.3), yields

$$D = \frac{V.\ell}{A_c.t(S.P_1-S.P_2)} = \frac{1}{S} \cdot \frac{V.\ell}{A_c.t(P_1-P_2)} \qquad \ldots (1.5)$$

Substituting (1.1) now gives

$$D = \frac{\overline{P}}{S} \qquad \ldots (1.6)$$

When $\overline{P}$, D and S are independent of concentration, or in the limit $C \to 0$, then

$$\overline{P} = D.S. \qquad \ldots (1.7)$$

1.3 Kinds of penetrant

Experimental work has shown that the usefulness of equation (1.7) is limited by the restriction that both D and S (and, by inference $\overline{P}$) should be independent of concentration. To a large extent it is the penetrant that determines the degree to which D will be dependent on concentration and three main groups of penetrants, viz. permanent gases, organic vapours and water, may be discerned and are briefly considered.

(a) Permanent gases

As a general rule, (1.7) holds good when the penetrant interacts only weakly with the polymer and with itself whilst sorbed in the polymer (7,8). This is the case with permanent gases such as nitrogen, oxygen, hydrogen, helium and carbon dioxide in many polymers. This weak interaction is reflected in low solubilities. No example has been found of concentration dependence of D for permanent gases (8).

(b) Organic vapours

For these systems, polymer-penetrant interactions are relatively strong leading to high solubilities, plasticisation of the polymer matrix and hence increased segmental mobility. D generally increases with increased concentration as does S in many instances (9).

(c) Water

For water as penetrant, the situation is relatively more complex and seems to depend principally on whether the polymer itself is hydrophilic or hydrophobic (10). In the former case, the penetrant-polymer interactions appear to be the most important. The water swells the membrane and behaves very much like an organic vapour with D increasing as the concentration increases.

In the latter case, however, clustering of the water molecules due to hydrogen bonding occurs leading to D decreasing as concentration increases because of the relative immobility of water molecules in the clusters. The dominant interactions in this kind of system tend to be of the penetrant-penetrant type.

A brief mention should be made at this stage concerning the solubility of organic vapours in glassy polymers. Solubility isotherms obtained experimentally at relatively low penetrant pressures are generally curved concavely to the pressure axis. It is widely accepted that two distinct sorption mechanisms, acting simultaneously, are responsible for this phenomenon. Firstly, there is the usual Henry's Law-type dissolution of the penetrant in the glassy matrix; secondly, there is sorption of the penetrant into well-defined "microvoids" existing in the matrix and this can best be represented mathematically by a Langmuir-type relationship.

These two processes constitute part of the dual-mode sorption theory which is discussed more fully in chapter 2.

1.4 Factors that affect $\overline{P}$, D and S

These have been reviewed in detail before (3-6, 8, 11) and are mentioned but briefly here.

1.4.1 Temperature dependence

The effect of temperature on the diffusion coefficient in gas/polymer systems was first identified as an activated process by Barrer (12). It is a typical Arrhenius-type relationship:-

$$D = D_o \cdot \exp(-E_D/RT) \qquad \ldots (1.8)$$

where D_o = pre-exponential constant,
E_D = activation energy of diffusion

It has been shown that in the case of elastomers, E_D tends to decrease with increasing temperature (6,13). However, for comparatively small temperature ranges, E_D may be regarded as constant. It is always positive and hence D always increases with increasing temperature.

A van't Hoff relationship, mathematically similar to (1.8), exists for solubility coefficients:-

$$S = S_o \exp(-\Delta\overline{H}_S/RT) \qquad \ldots (1.9)$$

where S_o = pre-exponential constant,
$\Delta\overline{H}_S$ = heat of solution

The heat of solution may be regarded as comprising two terms, namely, (a) the latent heat of condensation, and (b) the heat of dilution. In the case of permanent gases, the heat of condensation is negligible, hence $\Delta\overline{H}_S$ is essentially the heat of dilution and is often small and positive (5). For organic vapours, however, the heat of condensation is dominant and $\Delta\overline{H}_S$ values in these cases are usually negative and often quite large. For a positive $\Delta\overline{H}_S$, then, S will increase with increasing temperature and vice versa.

Combination of equations (1.7), 1.8) and 1.9) gives

$$\overline{P} = \overline{P}_o \cdot \exp(-E_P/RT), \quad \ldots (1.10)$$

where $E_P = E_D + \Delta\overline{H}_S$ ... (1.11)

and $\overline{P}_o = D_o \cdot S_o$ ... (1.12)

As described earlier, permeation is the end result of diffusion and solution, and E_P may be positive or negative depending on the relative magnitudes of E_D and $\Delta\overline{H}_S$. Often E_P is positive, which means that $\overline{P}$ will increase with temperature. However, in highly permeable polymers (e.g. silicone rubbers) exactly the opposite trend may be observed: E_P is negative and $\overline{P}$ decreases with increasing temperature.

1.4.2 Effect of Glass Transition

When the temperature of a polymer is lowered towards its glass transition temperature (T_g), segmental motions and rotations slow down considerably. Below T_g, the polymer becomes a hard brittle glass with large-scale segmental motions all but frozen out. The effect of the glass transition on $\overline{P}$, D and S hinges upon the size of penetrant molecule relative to the average cavity size characteristic of the polymer.

The free volume theory (14) postulates that the largest energy barrier to diffusion is that of hole formation and it is argued, in terms that are compatible with the theory, that the number of pre-existing holes that exist in the polymer below T_g does not significantly alter above T_g (15). Rather, it is the physical size of the holes which changes, which is to say that the amplitude of the segmental oscillations or rotations increases.

Thus when a penetrant molecule is small compared to the average hole size, the penetrant will diffuse easily into the polymer. E_D should therefore remain constant above and below T_g, and this is indeed the case for the diffusion of many gases through polyethyl methacrylate (16) and through a vinyl chloride-vinylacetate copolymer(15,17).

However, when the size of the gas molecule is comparable to the average cavity size, it is observed for a large number of polymer-gas systems that E_D is lower below T_g than above (17).

The solubility too can also be affected directly by the glass transition. For several gases in polyvinyl acetate, sharp increases in $\Delta\overline{H}_S$ were recorded by raising the temperature of the polymer through its T_g (18, 19).

It follows that these changes in E_D and $\Delta\overline{H}_S$ will be reflected in similar changes in E_P on passing through the glass transition.

When an organic vapour causes significant swelling of the polymer, the diffusion process is more complex and may be accompanied by slow relaxation-controlled processes. In the systems studied for this project, the degree of swelling was negligible and this aspect of transport in polymers is not dealt with further.

1.4.3 Crosslinking

It has been shown that as the degree of crosslinking (or "vulcanisation") increases, so the diffusion coefficient decreases due to the decreased mobility of some of the polymer segments (20,21). Since it causes little or no change in solubility, it follows that the permeability will decrease as the degree of crosslinking increases. This is especially true for large size penetrants. Under normal circumstances however only very light crosslinking is encountered and this tends to have little effect on $\overline{P}$ and D.

1.4.4 Plasticisation

The addition to a polymer membrane of plasticisers (typically high boiling-point liquids) effectively lowers the glass transition temperature and increases the diffusivity and, to a lesser extent if any, the solubility. The overall effect can be regarded as lubrication.

1.4.5 Nature of penetrant

The size of the penetrant is naturally extremely important. In general, the larger the molecule, the larger is E_D and hence the smaller is the diffusion coefficient. It has been shown that D decreases exponentially with increasing molar volume of penetrant (4). There appears to be a critical size of penetrant for a given polymer: above the critical value, penetrant size seems to have little

effect on E_D (4); but below it there appears in some cases to be an almost linear correlation between E_D and penetrant molecular diameter (8).

Branching in the molecular structure of the penetrant is another extremely important parameter(21), and indeed penetrant shape is usually more crucial in determining the magnitude of the diffusion coefficient than the actual molecular size.

As regards solubility, a general principle of "like dissolves like" applies. Organic vapours will dissolve more readily than water in hydrophobic polymers and for hydrophilic polymers the reverse is true. It is also generally found that the higher the boiling point of the penetrant, the greater is its solubility in a given polymer.

1.4.6 Physical nature of the polymer

Since density can be regarded as a measure of the "looseness" of the polymer, then generally the lower the density, the higher the diffusion coefficient and permeability.

Changes in the molecular weight of the polymer have little or no effect on permeability and diffusivity except in the region of low molecular weights.

The mode of preparation of a polymer membrane can affect its transport characteristics. For example, films of glassy polymers cast from solution may have variable properties depending on the type of solvent employed. Often the poorer the solvent, the higher is the permeability.

Although the thickness of a membrane should not in principle affect $\overline{P}$, D and S, differences in morphology can sometimes occur near the surface of the polymer leading to an apparent dependence of D on sample thickness (11).

1.4.7 Heterogeneous Polymer Systems (22)

Until now, mention has been made of only homogeneous polymeric materials, that is to say single-phase systems. In heterogeneous polymer systems, more than one phase is present.

Crystalline regions in a semi-crystalline polymer constitute a second phase and act in a similar way to crosslinks by holding the amorphous matrix together. Such regions are generally impermeable and as the degree of crystallinity increases so the permeability, diffusivity and solubility all decrease.

The introduction of fillers into a polymer often leads to the same effect; these may be porous or non-porous. Non-porous fillers act in a similar fashion to crystallites and tend to reduce $\overline{P}$, D and S. However, aggregation of filler particles can lead to the formation of additional flow paths which may reduce the blocking action of the filler. With porous fillers the possibility of additional flow paths within the filler particles arises.

Laminated membranes are also regarded as heterogeneous polymer systems. Two polymer sheets A and B can be laminated in the form AB, ABA, ABAB, ... etc. Triple laminates such as ABC can also be obtained. Rigorous mathematical treatments of the permeability and time-lag (and hence the diffusion coefficient) have been developed for such systems where D is constant and subsequently verified to a large extent (23).

Polymer blends are typically regarded as simple physical mixtures of non-covalently bonded, chemically distinguishable polymers.

Possibly the most complex of two-polymer heterogeneous systems are dispersions of A in a continuum of polymer B. The transport properties of such systems are affected by the volume fraction of each component, the spatial distribution, size and shape of the dispersed domains as well as the individual permeation characteristics of pure A and pure B. Exact solutions of the diffusion equations have not been found, but there are various approximate steady-state models available which have been reviewed (22, 24-27). Typical domain/continuum systems are found in block and graft copolymers, where the two polymers are, as is often the case, incompatible.

1.5 Copolymers (28-32)

There are essentially two types of copolymer systems: block copolymers and graft copolymers. The former is generally characterised by both the polymer chains constituting the "backbone" of the material with few or no side-chain attachments; the latter, in contrast, is basically one polymer forming the backbone of the material with the other polymer being grafted on to this as side-chain attachments.

1.5.1 Block copolymers. These can be prepared in various ways. Perhaps the most important method is anionic polymerisation which has the special advantage of being able to avoid spontaneous termination by the judicious choice of experimental conditions (33, 34) and it affords a large degree of control over the molecular weight and the molecular weight distribution of the polymer.

The method produces stable polymer carbanions (called "living polymers"), which can be reacted, at the experimenter's leisure, with additional monomer, a different monomer or perhaps a reagent which will finally terminate the polymerisation. Alternate additions of two monomers to a living polymer under carefully controlled conditions can produce alternating-block copolymers.

The process can be initiated either by electron transfer from alkali-metal complexes (such as sodium naphthalene in ether) to monomer, or by organoalkali compounds, e.g. the isomers of butyl lithium. In the former case a dianiomic species is formed and two initiator molecules are consumed for each chain that is formed. The latter type of iniation is more versatile however and is characterised by direct anionic attack with the chains growing at one end only.

These are also mechanical methods for preparing block copolymers. When polymer chains are broken under mechanical stress such as vibromilling, mastication etc., free-radical sites are produced at the severed ends. In the presence of a monomer, free-radical polymerisation can be initiated and in the presence of another polymer in the same condition mutual termination of the macroradicals can occur either reforming the respective homopolymers or producing a di-block copolymer. The block copolymers which are produced in each of the above cases tend to have rather random configurations in sharp contrast to those produced by anionic polymerisation.

1.5.2 Graft copolymers These can be prepared in several ways, the principal ones being radiation, chemical and mechanical methods.

(i) Radiation methods (35-38). The predominant feature here is attack by radicals produced by radiation (typically from a gamma ray source or an electron beam). More than one technique can be employed. In the pre-irradiation technique, the polymer is first irradiated on its own and is then, being highly activated, allowed to react with the monomer. This procedure reduces the chances of the monomer simply reacting with itself and producing unwanted homopolymer as opposed to the required graft copolymer. However, if the free-radical sites thereby produced are very short-lived, then this method is unsuitable. Better, in that case, is the simultaneous irradiation technique where the monomer is added to the polymer to which it is to be grafted first

of all, and then the irradiation takes place. Whilst being highly suitable for short-lived radicals, it does run the risk of initiating homopolymerisation of the polymer.

(ii) Chemical methods. This category tends to encompass many different mechanisms. Various methods for radical polymerisation have been employed including peroxide initiation, hydroperoxide initiation, initiator attack on the α hydrogen atom of a double bond, redox initiation and using the removal of a labile atom to terminate a chain growth by chain transfer.

(iii) Mechanical methods. Although block copolymers are the usual result of mechanical degradation, a graft copolymer can be obtained if the two polymers involved undergo disproportionation. This has been achieved in both solution and the solid state.

1.6 This Investigation

The major objective of the project presented here was to investigate the effect of block-length distribution on the transport properties of an alternating-block copolymer and to compare the results obtained with some of the current steady-state permeation models for heterogeneous media. The penetrant used was propane and the copolymer under examination was poly(dimethyl siloxane - b - bisphenol - A carbonate), which is abbreviated to PDMS - b - BPAC.

Samples of this material fall into three distinct groups, the first two being distinct series and the third being miscellany. In the first series, the block-length of the PDMS is kept constant at 20 mer units and the block-length of BPAC is varied. The second series is similar except that the block-length of the PDMS is now kept constant at 40 mer units. This then provides the basis for examining changes in microstructure with block-length size and composition.

The second part of the investigation consists of two critical tests for the dual mode sorption theory which, in simple terms, states that vapour sorption into a glassy-phase polymer consists of a Henry's law-type dissolution together with a Langmuir-type condensation in microcavities in the glassy matrix:

(i) One assumption in the theory assumes that in the transient state, the vapour in the microcavities in completely immobile. This is to be tested by investigating the sorption kinetics of propane sorbing into pure BPAC.

(ii) A major premise of the dual mode sorption theory is that below T_g the Langmuir-type mechanism exists, whilst above T_g it vanishes completely. Whilst this is generally held to be true, the premise is to be tested directly by sorbing propane into PDMS-g-poly(vinyl acetate) (containing 44.2% PVAC by volume) both above and below the T_g of PVAC.

The use of a PVAC graft copolymer was considered to be preferable to using a pure glassy film or microspheres for several reasons. The experimental system in use required that a glassy film should be ultra-thin (so as to obtain reasonable equilibration times) and yet there must be sufficient weight of it in order to obtain adequate sorption of penetrant. Below T_g this was difficult but certainly not impossible. Indeed 200 cm^2 of thin film could be cast on glass and wound into a coil with copper wire spacers as was done with BPAC. The difficulty would arise above T_g when the film sagged and started to flow. Crosslinking the film might have helped, but the vulcanisation of an ultra-thin glassy film with a T_g near room temperature presents serious difficulties.

Microspheres would have advantages below T_g in terms of reasonable equilibriation times, but above T_g the problem of tackiness would again present difficulties. PVAC grafted on to PDMS, its probable morphology being glassy microsphere-sized domains embedded in a highly permeable continuum, circumvented the problem.

CHAPTER 2

THEORY

2.1 Basic equations of diffusion

It was Fick (39) who first set the process of diffusion on a quantitative basis by adapting the mathematical formulation of Fourier (40) who, some years previously, had developed a theory of heat transfer by conduction. Fick recognised its analogy to matter transfer by diffusion.

For an isotropic medium, diffusion is governed by Fick's first equation,

$$F = -D \cdot \frac{\partial C}{\partial x} \qquad \ldots (2.1)$$

and by Fick's second equation,

$$\frac{\partial C}{\partial t} = D \cdot \frac{\partial^2 C}{\partial x^2} \qquad \ldots (2.2)$$

where F = rate of transfer of diffusing matter through a section of unit area,

C = concentration of diffusing matter at a point x along the direction of flow measured normal to the section at time t,

D = diffusion coefficient.

When F and C are expressed in terms of the same units of amount, then D is independent of such units and has the dimensions $(\text{length})^2.(\text{time})^{-1}$, e.g. $cm^2.s^{-1}$.

The negative sign in (2.1) arises because the flow of diffusing matter is in the opposite direction to that of the concentration gradient, i.e. the matter flows from high to low concentration.

Equation (2.2) can be derived from (2.1) by applying the principle of conservation of matter. However, (2.2) is only applicable for a diffusion coefficient that is constant. When D is a function of concentration, Fick's second equation must be expressed as

$$\frac{\partial C}{\partial t} = \frac{\partial}{\partial x}\left(D(C). \frac{\partial C}{\partial x} \right) \qquad \ldots (2.3)$$

For the definition implicit in (2.1) to be complete, the section through which diffusion takes place must be carefully specified (41). Several frames of reference fixed with respect to the volumes or masses

of components have been defined and the various diffusion coefficients discussed by Crank (25). For a two-component system with zero volume change of mixing, diffusion can be described by a single coefficient referred to as the mutual diffusion coefficient. When the change on mixing is not zero, a single diffusion coefficient can still be used to describe the diffusion process using fixed-mass frames of reference. For zero volume change on mixing, the diffusion coefficients measured relative to fixed-mass sections can be related to the mutual diffusion coefficient. In the limit of zero volume fraction of one component, the mutual and fixed-mass coefficients become identical. No significant swelling of the polymer by the penetrant was observed in this work and the diffusion coefficient is largely independent of the frame of reference.

2.2 Solution of Fick's equations

Whilst no analytical solution has yet been found for (2.3), exact solutions have been obtained for a wide variety of boundary conditions and sample geometries when D is constant (25, 42-44).

Only those solutions concerned with diffusion through a plane sheet are presented here.

The solutions fall into two distinct groupings, viz., steady-state and transient-state systems.

2.2.1 Steady-state

(a) For constant D

Consider a membrane of thickness ℓ, subject to the following boundary conditions:

$C = 0 \qquad 0 < x < \ell \qquad t = 0$

$C = C_o \qquad x = 0 \qquad t \geqslant 0$

$C = C_\ell \qquad x = \ell \qquad t \geqslant 0,$

i.e. the two faces of the membrane (x=0, x=ℓ) are maintained at C_o and C_ℓ respectively having been initially at zero.

Since the "steady state" implies that the concentration at any point x is independent of time, it follows that

$$\frac{\partial C}{\partial t} = 0 \qquad \ldots (2.4)$$

Thus (2.2) reduces to

$$\frac{\partial^2 C}{\partial x^2} = 0 \qquad \ldots (2.5)$$

Integration of this, subject to the boundary conditions gives

$$\frac{x}{\ell} = \frac{C_o - C}{C_o - C_\ell} \qquad \ldots (2.6)$$

which shows that the concentration gradient across the membrane from x=0 to x=ℓ is constant.

Combination of (2.1) and (2.6) yields

$$F = D \frac{(C_o - C_\ell)}{\ell} \qquad \ldots (2.7)$$

and it follows from (1.7) that

$$F = \overline{P} \frac{(P_o - P_\ell)}{\ell} \qquad \ldots (2.8)$$

where P_o, P_ℓ are the pressures corresponding to C_o, C_ℓ respectively.

(b) for D varying with C.

Equation (2.1) is still valid and (2.4) still applies, hence (2.3) reduces to

$$\frac{\partial}{\partial x}\left(D(C) \cdot \frac{\partial C}{\partial x} \right) = 0 \qquad \ldots (2.9)$$

which remains analytically unsolved.

However, with $C_o >> C_\ell$, equation (2.7) becomes

$$F = \frac{1}{\ell} \int_o^{C_o} D(C).\, dC \qquad \ldots (2.10)$$

By measuring the steady-state flux for a series of ingoing pressures, the dependence of F on P_o can be plotted. If next the solubility of the penetrant in the membrane is directly measured by equilibrium sorption studies, then an F v. C_o relationship can be derived and plotted graphically. Now differentiation of eq. (2.10) leads to

$$\left(\frac{dF}{dC} \right)_{C=C_o} = \frac{1}{\ell} D(C_o) \qquad \ldots (2.11)$$

Thus from the tangents (equivalent to dF/dC) to the F v. C_o graph, an empirical D(C) v. C relationship may be obtained.

Alternatively one can use the form of eq. (2.7) and re-define D as an average $\overline{D}$,

$$F = \overline{D} \frac{(C_o - C_\ell)}{\ell} = \frac{1}{\ell} \int_{C_\ell}^{C_o} D(C).dC \qquad \ldots (2.12)$$

hence

$$\overline{D} = \frac{1}{C_o - C_\ell} \int_{C_\ell}^{C_o} D(C).dC \qquad \ldots (2.13)$$

It is possible to extract a D(C) v. C relationship empirically when there is fairly strong concentration dependence.

2.2.2. Transient-state

(a) Constant D

(i) Time Lag

The "transient state" can generally be described as that state in which the penetrant-polymer system exists prior to the establishment of the steady state. Thus it is in this state that both the concentration at any point in the sheet and the rate of flow of penetrant through the sheet will vary with time.

If the membrane is initially free of penetrant and the ingoing and outgoing concentrations are kept constant with the latter negligible relative to the former (i.e. $C_o >> C_\ell$), then the following boundary conditions apply

$$C = 0 \qquad 0 < x < \ell \qquad t = 0$$

$$C = C_o \qquad x = 0 \qquad t \geqslant 0$$

$$C = 0 \qquad x = \ell \qquad t \geqslant 0$$

and the solution of (2.2) becomes

$$\frac{Q_t}{\ell.C_o} = \frac{D.t}{\ell^2} - \frac{1}{6} - \frac{2}{\pi^2} \sum_{n=1}^{\infty} \frac{(-1)^n}{n^2} \exp\left(\frac{-Dn^2\pi t}{\ell^2}\right) \qquad \ldots (2.14)$$

where Q_t = amount of penetrant which passes completely through the membrane in time t.

The steady state is approached as t becomes very large ($t \to \infty$) and (2,14) reduces to

$$Q_t = \frac{D.C_o}{\ell}\left(t - \frac{\ell^2}{6D}\right) \qquad \ldots (2.15)$$

Hence a graph of Q_t v. t will, at sufficiently large values of t, yield a straight line which, on extrapolation, yields an intercept on the t-axis which is referred to as the time lag, L (42, 45)

$$L = \frac{\ell^2}{6D} \qquad \ldots (2.16)$$

This is an extremely useful expression for determining D, provided of course that no concentration dependence is involved.

(ii) Small-times analysis

It is not always experimentally practicable to wait for t to become sufficiently large such that the steady state is reached. In such cases, the small-times approach is most valuable (45). The alternative solution to equation (2.2) is

$$\frac{dQ_t}{dt} = C_o \left(\frac{4D}{\pi t} \right)^{\frac{1}{2}} \sum_{n=o}^{\infty} \exp \left(\frac{-\ell^2 (2n+1)^2}{4Dt} \right) \qquad \ldots (2.17)$$

For small times only the first term of the infinite series is important and (2.17) reduces to

$$\ln \left(t^{\frac{1}{2}} \cdot \frac{dQ_t}{dt} \right) = \frac{1}{2} \ln \left(\frac{4 C_o^2 D}{\pi} \right) - \frac{\ell^2}{4Dt} \qquad \ldots (2.18)$$

Thus a graph of $\ln(t^{\frac{1}{2}} \cdot dQ_t/dt)$ vs. $(1/t)$ may be expected to be a straight line of slope $(-\ell^2/4D)$ for small times and for constant D.

(b) D a function of C

(i) Time lag

Whilst it has not been possible to solve (2.2) for D = D(C), expressions for the time lag have nevertheless been obtained (47). For the same boundary conditions as before,

$$L = \frac{\int_o^{\ell} x \cdot C_s(x) \cdot dx}{\int_o^{C_o} D\,(C) \cdot dC} \qquad \ldots (2.19)$$

where $C_s(x)$ = concentration distribution of penetrant in the membrane in the steady state.

Provided that the D(C) v. C relationship is of a known form or can be assumed to satisfy an arbitrary analytical expression containing unknown parameters, then such parameters can be numerically evaluated from a series of measurements of the time lag. The only difficulty lies in determining $C_s(x)$ which is found, in principle, from the equation

$$\int_{C_s}^{C_o} D(C)\, dC = \frac{x}{\ell} \int_0^{C_o} D(C) \cdot dC \qquad \ldots (2.20)$$

Graphical methods and series expansions have been used; further considerations of this are to be found elsewhere (48).

(ii) Small-times analysis

Strictly speaking the small-times analysis can only be used for constant D systems. However, the method has been successfully applied to variable D systems to evaluate D(C) at C=0 (i.e. D(0))(49). This is possible because the extrapolation involved is towards t=0 and it is at this time that C→0. Evaluation of D(0) can be of use in determining the unknown parameters mentioned in the last section.

2.2.3 Sorption- and desorption-kinetics

When a polymer has a very low permeability, the measurement of that property using the steady-state permeation method is not always practicable. It is a necessary practical requirement that the magnitude of the rate of increase of pressure due to desorbing penetrant on the outgoing side of the membrane should be very large compared to any rate of increase of pressure due to unavoidable leaks, slow desorption of vapours from the glass apparatus, etc. For a glassy polymer, say, this would mean casting an ultra-thin membrane. This in turn would run the very great risk of being flawed by dust particles etc., which could then contribute to a leak.

The method using sorption- and desorption-kinetics derives S and D (and hence $\overline{P}$) and avoids such complications and will be discussed in the next chapter.

Sorption in a membrane of thickness ℓ, initially free of vapour, exposed on both sides by vapour at concentration C_o can be represented by the following boundary conditions

$$C = 0 \qquad 0 < x < \ell \qquad t = 0$$
$$C = C_o \qquad x = 0,\ell \qquad t \geqslant 0$$

Desorption of the same membrane having reached equilibrium is described by

$$C = C_o \qquad 0 < x < \ell \qquad t = 0$$
$$C = 0 \qquad x = 0,\ell \qquad t \geqslant 0$$

(a) Constant D

For both sets of boundary conditions, two equivalent solutions exist

for equation (2.2)

$$\frac{M_t}{M_\infty} = 4\left(\frac{Dt}{\ell^2}\right)^{1/2}\left(\frac{1}{\pi^{\frac{1}{2}}} + 2\sum_{n=o}^{\infty}(-1)^n \text{ ierfc } \frac{n\ell}{2(Dt)^{\frac{1}{2}}}\right) \qquad \ldots (2.21)$$

and

$$\frac{M_t}{M_\infty} = 1 - \frac{8}{\pi^2}\sum_{m=o}^{\infty}\frac{1}{(2m+1)^2}\exp\left(\frac{D(2m+1)^2\pi^2 t}{\ell^2}\right) \qquad \ldots (2.22)$$

where M_t = amount of penetrant sorbed by the membrane at time t (for sorption) or desorbed by the membrane at time t (for desorption).

M_∞ = amount of penetrant absorbed by the membrane as $t \to \infty$ (for sorption) or at t=0 (for desorption) i.e. the equilibrium uptake of penetrant.

Equation (2.21) is useful for comparatively small values of t when the summation terms become negligible and the equation reduces to

$$\frac{M_t}{M_\infty} = \frac{4}{\ell}\left(\frac{Dt}{\pi}\right)^{1/2} \qquad (2.23)$$

Thus a plot of M_t vs. $t^{1/2}$ should yield a straight line through the origin of slope $4M_\infty D^{1/2}/\ell\pi^{1/2}$ from which D is obtained. Eq. (2.23) is usually valid up to $M_t = M_\infty/2$.

Equation (2.22) can be used in two ways. Firstly for moderate and large values of t only the first summation term (m=0) in the expression is important, thus the equation reduces and rearranges to give

$$\ln\left(1 - \frac{M_t}{M_\infty}\right) = \ln\left(\frac{8}{\pi^2}\right) - \frac{D\pi^2 t}{\ell^2} \qquad \ldots (2.24)$$

Hence D can be derived from the slope of the graph $\ln(1 - M_t/M_\infty)$ vs. t provided that $M_t/M_\infty > 0.5$.

Secondly, and perhaps more accurately, by taking just the first two summation terms (m=0 and m=1) and setting $M_t/M_\infty = 0.5$, equation (2.22) reduces and re-arranges to give

$$\frac{(t)_{0.5}}{\ell^2} = \frac{-1}{\pi^2 D}\ln\left(\frac{\pi^2}{16} - \frac{1}{9}\left(\frac{\pi^2}{16}\right)^9\right) \qquad \ldots (2.25)$$

where $(t)_{0.5}$ = "half-time" of the equilibration, i.e. the value of t at $M_t/M_\infty = 0.5$.

The error introduced by such a series truncation is approximately 0.001% and (2.25) now re-arranges as

$$D = \frac{0.04919.\ell^2}{(t)_{0.5}} \qquad \ldots (2.26)$$

This equation has been found, during the course of this work, to be very convenient to use and extremely reliable.

(b) For D varying with C.

For a variable D, equations (2.23), (2.24) and (2.25) can still be used, but the D thereby determined will be some average, $\overline{D}$, which is not necessarily the same one as that derived from permeation methods. Thus the equations become

$$\frac{M_t}{M_\infty} = \frac{4}{\ell}\left(\frac{\overline{D}t}{\pi}\right)^{1/2}, \qquad \ldots (2.27)$$

$$\ln\left(1 - \frac{M_t}{M_\infty}\right) = \ln\left(\frac{8}{\pi}\right)^2 - \frac{\overline{D}\,\pi^2 t}{\ell^2} \qquad \ldots (2.28)$$

and $$\overline{D} = \frac{0.04919.\ell^2}{(t)_{0.5}} \qquad \ldots (2.29)$$

One can measure $\overline{D}$ as a function of C. The next step is to extract the D vs. C. dependence from these data and there are several procedures available for the derivation of D(C).

(i) Successive approximations

It has been shown that for any one sorption/desorption experiment (50)

$$\overline{D} \approx \frac{1}{C_o}\int_o^{C_o} D(C)\,.\,dC \qquad \ldots (2.30)$$

Differentiation at $C = C_o$ yields

$$C_o\left(\frac{d\overline{D}}{dC}\right)_{C=C_o} + \overline{D}_{C=C_o} = D(C_o) \qquad \ldots (2.31)$$

Thus a graph of $\overline{D}$ vs. concentration can be plotted, tangents drawn or computed for each value of C_o to evaluate $(d\overline{D}/dC)_{C=C_o}$ and a crude approximation to D(C) vs. C relationship obtained.

By the use of numerical methods, fresh sorption/desorption curves can be constructed from the D(C) vs. C relationship, new values of $\overline{D}$ evaluated using equations (2.27) and (2.29), and finally a second approximation to the D(C) vs. C relationship obtained from (2.31). The whole process can be repeated (with relative ease using a computer)

until there is good agreement between the observed and calculated values of $\overline{D}$ (51). However the overall accuracy of this method tends to be limited by the accuracy of the derivation of $(d\overline{D}/dC)_{C=C_o}$ in equation (2.31).

(ii) Sorption + desorption mean $\overline{D}$

A modification of the previous method is simply to determine the values of $\overline{D}$ for sorption and $\overline{D}$ for desorption, written as $\overline{D}_s$ and $\overline{D}_d$ respectively and to use the mean value of the two rather than either one in the procedures described in the last section. Some workers have even used this mean value without further correction (52, 53) since

$$\frac{\overline{D}_s + \overline{D}_d}{2} = \frac{1}{C_o} \int_0^{C_o} D(C) \, . \, dC \qquad \ldots (2.32)$$

proves to be a much better approximation than (2.30). Others however feel that determinations of this sort are best carried out at small concentrations rather than high ones (54).

(iii) Successively small intervals.

Another procedure involves performing a series of sorption experiments with the equilibrium concentration, C_o, kept constant throughout, but the initial uniform concentration in the membrane, C_i, being varied for each run (55). Rewriting equation (2.27) for unit volume of polymer as

$$C_t = K.t^{1/2} \qquad \ldots (2.33)$$

where C_t = concentration of penetrant in the polymer at time t, and K is a function of C_i.

When $C_o - C_i \to 0$ then D will be approximately constant so that

$$K = \frac{4}{\ell} (C_o - C_i) \, (D(C_o)/\pi)^{1/2} \qquad \ldots (2.34)$$

where $D(C_o) = D_{C=C_o}$.

As the value of C_i approaches C_o for successive runs, so the curve of K vs. C_i will approach a tangent of slope $-4D(C_o)^{1/2}/\pi^{1/2}\ell$, hence $D(C_o)$.

By repeating the same series of experiments for different values of C_o the $D(C_o)$ vs. C_o relationship (which is equivalent to the D(C) vs. C relationship) can be obtained. Once again there is a limitation due to the difficulty in accurately positioning the tangent to which the K vs. C_i curve makes its asymptotic approach.

(iv) Weighted-mean Diffusion Coefficients (50)

Numerical solutions have established that the initial rates of sorption and desorption are accurately represented by weighted-mean diffusion coefficients

$$\text{where} \quad \overline{D}_s = p\, C_o^{-p} \int_0^{C_o} C^{p-1} \,.\, D(C).dC \qquad \ldots (2.35)$$

$$\text{and} \quad \overline{D}_d = q\, C_o^{-2} \int_0^{C_o} (C_o - C)^{q-1} \,.\, D(C).dC \qquad \ldots (2.36)$$

where p = 1.67 or 1.85 for systems where D(C) increases or decreases with concentration, respectively,

q = 1.85 or 1.67 for similar systems (56, 57).

More will be said of these equations in connection with the dual mode sorption theory which is discussed later in this chapter.

(v) Other methods

Various alternatives to the methods described above are known (58 - 62), and are described together elsewhere (25).

2.3 Molecular Diffusion Theories

Since most of the widely-used theories are reviewed elsewhere (14), only a brief resume is presented here.

The free-volume theory postulates that the probability of permeant molecule undergoing a single diffusion step is directly related to the probability of an element of free volume, specifically larger than some critical volume, being available for the molecule to jump into. It compares molecules diffusing through a polymer matrix to hard spheres travelling through a liquid and suggests that diffusion is not an activated process, but rather it occurs as a result of the redistribution of the free volume in the liquid (63).

In contrast, Barrer's Zone theory is based almost entirely on energy considerations derived from the assumption of diffusion being an activated process. The premise is that the activation energy required in order for the molecule to move to successive equilibrium positions is shared by both the penetrant and surrounding polymer segments so that a "hot" zone is created through the normal fluctuations of the thermal energy of the system. This energy is derived from the system's many degrees of freedom (64, 65).

Brandt developed this theory further using molecular considerations (66).

Other workers have developed a volume fluctuation theory for transport in the glassy state and a molecular theory for diffusion in elastomeric systems (67 - 69).

2.4 Dual-Mode Sorption Theory (70)

The theory generally applies to sorption in glassy media and it postulates that two concurrent modes of sorption exist which together produce non-linear isotherms concave to the pressure axis. The first mode is normal Henry's Law-type dissolution and the second mode, which is responsible for the isotherm curvature, is a non-linear Langmuir-type part which represents the immobilisation of penetrant molecules in "microvoids" or "microcavities" which are distributed throughout the glassy matrix.

At equilibrium and at constant temperature,

$$C = C_D + C_H = k_D.P + \frac{C_H' \cdot B \cdot P}{1 + B \cdot P} \qquad \ldots (2.37)$$

where C = overall concentration in cm^3STP/cm^3 polymer

C_D = concentration of the dissolved species in cm^3STP/cm^3 polymer

C_H = similarly, for the immobilised species

k_D = Henry's Law solubility coefficient in cm^3STP/cm^3 polymer/cmHg

P = pressure in cm Hg

C_H' = hole saturation constant in $cm^3STP.cm^{-3}$ polymer where $0 \leqslant C_H \leqslant C_H'$

B = hole affinity constant in $cmHg^{-1}$ and represents the ratio of the rate constants for sorption and desorption of penetrant in the holes.

At very high pressure,

$$C = k_D \cdot P + C_H' \qquad \ldots (2.38)$$

which represents the assymptote towards which the isotherm tends as the pressure increases. Achievement of high pressure experimentally then facilitates the estimation of both k_D and C_H'. When this is not possible, however, the sorption parameters k_D, C_H' and B can be evaluated using mathematical iterative procedures on a computer, and a programme was developed in this laboratory for this purpose (71).

At very low pressures, (2.37) becomes

$$C = k_D.P + C_H'.B.P \qquad \ldots (2.39)$$

and

$$S_L = \frac{C}{P} = k_D + C_H'.B \qquad \ldots (2.40)$$

where S_L is the limiting Henry's Law solubility coefficient as $C \to 0$ and represents the initial slope of the dual mode sorption isotherm.

2.4.1 Heats of solution

Three heats of solution are involved with dual mode sorption: the enthalpy of dissolution, the enthalpy of hole-filling and the overall heat of solution which are designated $\overline{\Delta H}_D$, $\overline{\Delta H}_H$ and $\overline{\Delta H}_S$ respectively.

$\overline{\Delta H}_D$ is evaluated using the van't Hoff expression

$$k_D = k_{DO} \exp - \frac{\overline{\Delta H}_D}{RT} \qquad \ldots (2.41)$$

A plot of $\ln k_D$ vs. T^{-1} is expected to yield a line of slope $- \overline{\Delta H}_D/R$

$\overline{\Delta H}_H$ is similarly evaluated using

$$B = B_o \exp - \frac{\overline{\Delta H}_H}{RT} \qquad \ldots (2.42)$$

$\overline{\Delta H}_S$, since it is dependent on concentration, is best evaluated using the Clapeyron-Clausius equation,

$$\left(\frac{\partial \ln P}{\partial (1/T)} \right)_{C=C_o} = - \frac{\overline{\Delta H}_S}{R} \qquad \ldots (2.43)$$

Thus for a given value of C_o, a graph of ln P vs. T^{-1} can be plotted and the corresponding value of $\overline{\Delta H}_S$ can be determined.

Although no simple relationship exists between $\overline{\Delta H}_D$, $\overline{\Delta H}_H$ and $\overline{\Delta H}_S$, at very high pressures the Langmuir contribution to the isotherm becomes negligible and hence

$$\lim_{P \to \infty} (\overline{\Delta H}_S) = \overline{\Delta H}_D \qquad \ldots (2.44)$$

The limiting value of $\overline{\Delta H}_S$ as $C \to 0$ can be evaluated from the van't Hoff expression for S_L,

$$S_L = S_{LO} \exp - \frac{\overline{\Delta H}_{S(C=0)}}{RT} \qquad \ldots (2.45)$$

2.4.2 Diffusion model for the theory (72)

One of the assumptions of the theory is that there is local equilibrium between the dissolved species of penetrant and those species immobilised in the microvoids at all times throughout the medium, i.e. the kinetics of the immobilisation are very rapid compared to the diffusion of the dissolved species and hence the diffusion process is the rate-determining step. A further assumption is that the penetrant sorbed according to the Langmuir mode is totally immobilised, thus only diffusion of the dissolved species occurs, being driven by its concentration gradient. The diffusion coefficient of the dissolved species has been referred to as the "true" diffusion coefficient and for Henry's Law dissolution will be independent of concentration and position in the membrane.

There are several methods for determining the "true" diffusivity few of which involve analytic expressions.

The method of Vieth and Sladek is described more fully elsewhere (70, 72) and is mentioned but briefly here.

Equation (2.1) must be rewritten as

$$F = -D(C).\frac{\partial C}{\partial x} = D_{eff}.\frac{\partial C}{\partial x} \qquad \ldots (2.45)$$

where D_{eff} is the experimentally observed "effective" diffusion coefficient which is concentration dependent. According to the dual mode sorption theory, the flux can also be expressed solely in terms of the mobile species,

$$F = -D_m.\frac{\partial C_m}{\partial x} \qquad \ldots (2.47)$$

for a one-dimensional flow where the subscript m refers to the mobile species and D_m is the "true" diffusivity, which is treated as a constant. Eliminating F from (2.46) and (2.47) yields

$$D_{eff} = D_m.\frac{\partial C_m}{\partial C} \qquad \ldots (2.48)$$

Since C_m equals C_D, the concentration of dissolved species, then from equation (2.37),

$$\frac{\partial C_m}{\partial C} = \frac{\partial C_D}{\partial P} \Big/ \frac{\partial C}{\partial P} = k_D \Big/ \left(k_D + \frac{C'_H.B}{(1+B.P)^2}\right) \qquad \ldots (2.49)$$

Substituting (2.49) into (2.48) gives

$$D_{eff} = D_m \left(1 + \frac{C'_H B/k_D}{(1+B.P)^2}\right)^{-1} \quad \ldots (2.50)$$

As $P \to 0$, (2.50) can be written as

$$D_{eff} = D_m \left(1 + \frac{C'_H B}{k_D}\right)^{-1} \quad \ldots (2.51)$$

D_m can therefore be determined by measuring diffusivities at very low pressures.

Alternatively, as $P \to \infty$, D_{eff} tends to the value of D_m, i.e., at sufficiently high pressures, the experimentally measured diffusion coefficient is the "true" value.

For this project however, sufficiently high pressures were not available and sufficiently low pressures could not be employed with satisfactory accuracy.

Equation (2.50) can be used for normal pressure regions, but its usefulness is limited by the accuracy of the evaluation of D_{eff} from experimental observations.

For diffusivity data derived from normal pressure regions, Vieth and Sladek (72) describe a lengthy procedure for a numerical solution using finite difference tecnhiques.

2.4.3 Novel solutions

Other methods of solution for D_m have been developed during the course of this project and are presented here.

(i) Tangential method

This is simply an extension of the method that employs equation (2.50). An expression can be derived for D_{eff} that utilises sorption (or desorption) kinetics data.

Taking the weighted-mean equation (2.35) and differentiating w.r.t. C_o gives

$$\frac{d\bar{D}_s}{dC_o} = \frac{p.D(C_o)}{C_o} - \frac{p}{C_o}\left(p\, C_o^{-p} \int_o^{C_o} C^{p-1}.\, D(C).dC\right) \quad \ldots (2.52)$$

$$= p.\frac{D(C_o)}{C_o} - p.\frac{\bar{D}_s}{C_o} \quad \ldots (2.53)$$

Since $D(C_o)$ represents D_{eff} at $C = C_o$, then

$$D_{eff} = D(C_o) = \frac{C_o}{p}\left(\frac{d\overline{D}_s}{dC_o}\right) + \overline{D}_s \qquad \ldots (2.54)$$

(C.f. equation (2.31))

Substituting into (2.50) at $P = P_o$ gives

$$D_m = \left(\overline{D}_s + \frac{C_o}{p}\left(\frac{d\overline{D}_s}{dC_o}\right)\right)\left(1 + \frac{C_H' \cdot B}{k_D(1+B.P_o)^2}\right) \qquad \ldots (2.55)$$

D_m can be determined from a graph of $\overline{D}_s$ vs. C_o and drawing tangents at various points. It is however the limited accuracy of $(d\overline{D}_s/dC_o)$ that is the major failing with this method.

(ii) Integral method

A more satisfactory approach is the integral method. Substituting equation (2.48) into (2.35) produces:

$$\overline{D}_s = p\, C_o^{-p} \int_o^{C_o} C^{p-1} \cdot D_m \cdot \frac{\partial C_m}{\partial C} \cdot dC \qquad \ldots (2.56)$$

Integration by parts yields:-

$$\overline{D}_s = p\, C_o^{-p} \left(D_m \left(C^{p-1} \cdot C_m \right)_o^{C_o} - D_m \int_o^{C_o} C_m(p-1) \cdot C^{p-2} \cdot dC \right) \ldots (2.57)$$

Substituting $(C_m)_{C=C_o} = k_D \cdot P_o$ gives

$$\overline{D}_s = D_m.p.C_o^{-p} \left(C_o^{p-1} \cdot k_D.P_o - k_D(p-1) \int_o^{C_o} C^{p-2}.P.dC \right) \qquad \ldots (2.58)$$

The integral $\int_o^{C_o} C^{p-2}.P.dC$ can be determined by rewriting equation (2.37) for P, viz.,

$$P = \frac{\left((C_H'B + k_D - B.C)^2 + 4\, k_D.B.C\right)^{1/2} - (C_H'B + k_D - B.C)}{2k_DB} \qquad \ldots (2.59)$$

substituting, and then using numerical integration on a computer. Thus D_m can be determined using just $\overline{D}_s$, C_H', B and k_D.

(iii) Modification for partial immobilisation

The above methods are easily adapted to make provision for the possibility of partially mobile Langmuir species. Since D_m is designated the diffusivity of the mobile species, then D_i is proposed as the diffusion coefficient for the "immobile" species. Correspondingly C_i

shall be equal to C_H, the concentration of the immobilised species.

Equation (2.42) becomes

$$F = -D_m \cdot \frac{\partial C_m}{\partial x} - D_i \cdot \frac{\partial C_i}{\partial x} \quad \ldots (2.60)$$

and equation (2.43) becomes

$$D(C) = D_m \cdot \frac{\partial C_m}{\partial C} + D_i \cdot \frac{\partial C_i}{\partial C} \quad \ldots (2.61)$$

The corresponding final equation for the tangential method is

$$A' = D_m \cdot B' + D_i \cdot C' \quad \ldots (2.62)$$

where $$A' = \frac{C_o}{p}\left(\frac{d\overline{D}_s}{dC_o}\right) + \overline{D}_s \quad \ldots (2.63)$$

$$B' = \left(1 + \frac{C_H' \cdot B}{k_D(1+B.P_o)^2}\right)^{-1} \quad \ldots (2.64)$$

$$C' = \frac{C_H' \cdot B}{C_H' \cdot B + k_D(1+B.P_o)^2} \quad \ldots (2.65)$$

A', B' and C' can be determined from $\overline{D}_s$, $d\overline{D}_s/dC_o$, C_H', B and k_D at various values of P_o or C_o. D_m and D_i are both regarded as constants and can be determined by a least squares method.

Better, however, is the final equation for the integral method:

$$\overline{D}_s = X \cdot D_m + Y \cdot D_i \quad \ldots (2.66)$$

where

$$X = p\, C_o^{-p}\left(C_o^{p-1} \cdot k_D \cdot P_o - k_D(p-1)\int_o^{C_o} C^{p-2} \cdot P \cdot dC\right) \quad \ldots (2.67)$$

and

$$Y = p\, C_o^{-p}\left(C_o^{p-1} \cdot \frac{C_H' B \cdot P_o}{1 + B.P_o} - (p-1)\int_o^{C_o} C^{p-2} \cdot \frac{C_H' \cdot B.P}{1 + B.P} \cdot dC\right) \quad \ldots (2.68)$$

Both X and Y depend solely on k_D, C_H', B and C_o. Values are computed using numerical integration and D_m and D_i are subsequently determined by a least-squares method.

CHAPTER 3

LITERATURE REVIEW

3.1 Introduction

In this chapter a general survey of the literature connected with the two principal areas of this project (diffusion through heterogeneous media and sorption/diffusion in glassy polymers) is presented, concentrating on those aspects which are the more important and relevant.

Gas/vapour transport in disperse heterogeneous polymer media seems to have attracted relatively little attention in the past five years. There exist many theoretical models for the various kinds of systems mentioned in chapter 1, but relatively few serious attempts to test the theoretical expressions experimentally have been recorded. A fully comprehensive model has still to be developed.

Gas/vapour transport in the glassy state has, in contrast, attracted considerable attention recently. Interest has focussed largely on the dual mode sorption theory, which was first suggested over twenty years ago. Whilst commanding wide acceptance as an experimentally useful analysis, there still exist various aspects (which will be discussed later) that require further examination before the theory and its physical interpretation can stand as fully validated.

Finally, a brief review of some of the work carried out on PDMS/BPAC alternating block copolymers is presented in the final section.

3.2 Transport in Heterogeneous Media

3.2.1 Review of theoretical models

A detailed survey is not attempted here since several excellent reviews exist already (22, 24-27). The most useful analyses are related to the steady-state behaviour, since analysis of the transient state poses formidable theoretical difficulties.

A representative selection of the many methods which can be used to interpret the permeability data of heterogeneous polymer systems is given in Table 3.1. Others are simply referenced here (87-90).

An exhaustive study of every method was not considered feasible during the course of this project. Four approaches, those of Maxwell,

Bruggeman, Higuchi and Lichtenecker, were selected and employed in the final analysis of the permeation data because they effectively covered a wide range of heterogeneous systems, and are discussed further here. The Böttcher model, although possessing the unique feature of being independent of whether a component forms the continuous or the disperse phase, was found to be unsuitable when the permeability of one phase is negligible compared to the other.

Expressions for most of the methods presented in Table 3.1 (except those which are discussed below) are given in Chapter 8 (Appendix 8.1).

The following system of notation is used throughout:

$\overline{P}_m$ = permeability of the heterogeneous medium

$\overline{P}_C$ = permeability of the continuous phase

$\overline{P}_D$ = permeability of the disperse phase

Φ_C = volume fraction of the continuous phase

Φ_D = volume fraction of the disperse phase

Clearly,

$$\Phi_C + \Phi_D = 1 \qquad \ldots (3.1)$$

(a) Maxwell model

The simplest classical model was proposed by Maxwell (73) in 1873. An expression was derived for a single sphere in a continuous medium

$$\overline{P}_M = \overline{P}_C \left(\frac{\overline{P}_D + 2\overline{P}_C - 2\Phi_D (\overline{P}_C - \overline{P}_D)}{\overline{P}_D + 2\overline{P}_C + \Phi_D (\overline{P}_C - \overline{P}_D)} \right) \qquad \ldots (3.2)$$

Due to assumptions implicit in the model, equation (3.2) is only applicable for dilute suspensions of identical spheres such that the perturbation of the lines of flux around any one sphere is not affected by the perturbations associated with neighbouring spheres.

For $\overline{P}_C >> \overline{P}_D$, equation (3.2) reduces to

$$\overline{P}_M = \overline{P}_C \left(\frac{1 - \Phi_D}{1 + \Phi_D/2} \right) = \overline{P}_C \left(\frac{2\Phi_C}{3 - \Phi_C} \right) \qquad \ldots 3.3)$$

when $\overline{P}_C << \overline{P}_D$, (3.2) becomes

$$\overline{P}_M = \overline{P}_C \left(\frac{1 + 2\Phi_D}{1 - \Phi_D} \right) = \overline{P}_C \left(\frac{3 - 2\Phi_C}{\Phi_C} \right) \qquad \ldots (3.4)$$

TABLE 3.1 Some methods for interpreting heterogeneous permeability data.

Method	Type of solution	Type of system	Comments
(i) Maxwell (73)	Exact	Identical spherical domains	Applies to dilute suspensions only. Neglects domain interactions.
(ii) Bruggeman (74)	Approximate	Large range of spherical domain sizes	Considers domain interaction.
(iii) Bruggeman/ Meredith & Tobias (75)	Approximate	Identical spherical domains.	A modified form of (ii).
(iv) Böttcher (76)	Approximate	Random spherical domains	Makes no distinction between the continuous and disperse phase.
(v) Rayleigh & Runge (77,78)	Exact series (truncated)	Ordered, identical spherical domains	Considers domain interactions. Meaningless beyond the limit for close packing of spheres.
(vi) Rayleigh/Meredith & Tobias (79)	Exact series (truncated)	Ordered, identical spherical domains	Meredith & Tobias employ a different activity gradient function to (v) and extend the truncation.
(vii) Series/parallel (80)	Empirical	Laminated sheets	Simplest views of permeation.
(viii) Higuchi (81,82)	Empirical	Random dispersion of spherical domains	Considers domain interaction and introduces an empirical weighting, K.
(ix) Lichtenecker (83)	Empirical	Homogeneous blend	Useful when there is no phase separation
(x) Fidelle & Kirk (84)	Numerical	Ordered, identical spherical domains	(As for (v)).
(xi) Bell & Crank (85)	Numerical	Ordered, identical rectangular block domains	Applicable to other systems.
(xii) Baxley, Nicholas and Couper (86)	Numerical-statistical	Random, irregular shaped domains	A computer based model, thought to require further development (25).

The Bruggeman model adapted by Meredith and Tobias (75), the Rayleigh model adapted by Runge (78) and Meredith and Tobias' modification of the Rayleigh model (79) all reduce to the Maxwell expression as $\Phi_C \rightarrow 1$.

(b) The Bruggeman model (74)

Derived for electrical conductivities in disperse heterogeneous systems, the Bruggeman model suggests that as the volume fraction of the disperse phase becomes large, the lines of diffusive flux will be a function of the permeability of the composite medium, $\overline{P}_M$, rather than that of the continuous phase, $\overline{P}_C$.

$$\Phi_C \left(\frac{\overline{P}_D - \overline{P}_C}{\overline{P}_D - \overline{P}_M}\right) = \sqrt[3]{\frac{\overline{P}_C}{\overline{P}_M}} \qquad \ldots (3.5)$$

It is an approximate treatment.

For $\overline{P}_C >> \overline{P}_D$, (3.5) becomes

$$\overline{P}_M = \overline{P}_C \cdot \Phi_C^{3/2} = \overline{P}_C \cdot (1 - \Phi_D)^{3/2} \qquad \ldots (3.6)$$

For $\overline{P}_C << \overline{P}_D$, (3.5) becomes a crude approximation,

$$\overline{P}_M \approx \frac{\overline{P}_C}{\Phi_C^3} = \overline{P}_C (1 - \Phi_D)^{-3} \qquad \ldots (3.7)$$

The model is applicable for spherical particles as the disperse phase with large ranges of domain sizes, but does not correspond with any specific, well-defined structure.

(c) Higuchi model (81, 82)

This model is represented by

$$\overline{P}_M = \overline{P}_C \left(\frac{(\overline{P}_D + 2\overline{P}_C - X) - \Phi_D(2\overline{P}_C - 2\overline{P}_D - X)}{(\overline{P}_D + 2\overline{P}_C - X) + \Phi_D(\overline{P}_C - \overline{P}_D + X)} \right) \qquad \ldots (3.8)$$

where $$X = \frac{K(\overline{P}_D - \overline{P}_C)^2}{(2\overline{P}_C + \overline{P}_D)} \qquad \ldots (3.9)$$

Equation (3.8) closely resembles the Maxwell expression (3.2). K is an empirical constant, chosen as 0.78 to give the best fit for a collection of data. K represents a "neglected" function of Φ_D and was originally expected to be dependent on Φ_D, but was found to be a constant.

For $\bar{P}_C >> \bar{P}_D$, (3.8) becomes

$$\bar{P}_M = \bar{P}_C \cdot \frac{3.22 \cdot \Phi_C}{6 - 2.78 \cdot \Phi_C} \qquad \ldots (3.10)$$

When $\bar{P}_C << \bar{P}_D$, the expression reduces to

$$\bar{P}_M = \bar{P}_C \cdot \frac{c - 2.78\ \Phi_C}{0.22\ \Phi_C} \qquad \ldots (3.11)$$

The Higuchi expression (3.8) clearly reduces to the Maxwell expression for K = 0.

(d) The Lichtenecker rule (83)

For two completely miscible polymer components A and B, the following expression is often found to apply,

$$\ln \bar{P}_{AB} = \Phi_A \cdot \ln \bar{P}_A + \Phi_B \cdot \ln \bar{P}_B \qquad \ldots (3.12)$$

or

$$\bar{P}_{AB} = \left(\bar{P}_A\right)^{\Phi_A} \cdot \left(\bar{P}_B\right)^{\Phi_B} \qquad \ldots (3.13)$$

where subscripts A and B refer to pure components and AB refers to the composite.

Random copolymers unable to phase-separate generally appear to obey the Lichtenecker relationship also. Equations (3.12) and (3.13) do not, however, have any a priori theoretical basis.

3.2.2. Review of experimental testing of the models

This section concerns the kind of scrutiny which some of the models mentioned in the last section have undergone. Of the many models that exist, it has been found that relatively few have received serious attention insofar as gas/vapour transport in polymers is concerned : the expressions of Maxwell and Higuchi have been used most in this respect. The validity of the Lichtenecker rule (although rarely termed in the literature as such) has been clearly indicated by work on permeation through two-component blends and this aspect will be discussed later in more detail.

Mitoff (91) believes that for the vast majority of heterogeneous systems, only three models need to be considered with each having special advantages under specific conditions. For a system where the permeabilities are of comparable magnitude (or at least within an order

of magnitude of each other), the Lichtenecker rule (83) is favoured. For spherical and for randomly oriented particles suspended in a continnum, the Maxwell (73) and Fricke (87) expressions respectively are advocated.

Mitoff also makes the important point that the difference between many of the existing models in mathematical terms is so slight in some cases that testing them in a meaningful way requires painstaking care and precision.

The Higuchi theory (81, 82) has been examined by at least three workers (27, 92, 93).

Peterson (92) determined the oxygen permeabilities for several disperse heterogeneous films. In each case the continuous phase was poly (vinyl acetate) (Φ_C for which was maintained constant at 0.72) and the disperse phase in turn was polystyrene, poly (vinylidene chloride) and poly (methyl methacrylate). Two of the systems were studied at two different temperatures.

The results correlated very well with Higuchi model predictions, but since Φ_C was not varied at all, no firm general conclusions can be drawn from this study.

Peterson recognised that for the systems involving polystyrene and poly (methyl methacrylate) the permeability coefficients were pressure dependent. This is consistent with the model developed later by Paul and Koros (94), which is discussed in section 4.3.

A similar investigation was carried out by Ziegel (93) for a series of penetrant gases in compression moulded block copolymers having both glassy and elastomeric blocks. Ziegel produced evidence in support of some of Higuchi's assumptions but did not make a direct comparison of the results with the Higuchi model predictions. Instead an alternative model is proposed.

Sheer (27) recently tested several models with data for water vapour transport through poly (dimethyl siloxane) - g - poly (vinyl acetate) films. Solubility and transport measurements were made for several PVAc volume fractions over a range of temperature and concentration. Although the experimental data could be "reasonably" represented by the Bruggeman and Böttcher models, the Higuchi model gave the best fit. The systematic approach of measuring $\overline{P}$'s at different temperatures meant that correlations between experimental and predicted values could be examined not only for the permeability

data itself but for the energies of permeation for the various grafted compositions also.

The majority of the models discussed produce two sets of results for a given two-component system depending on which of the two polymers constitutes the continuous matrix and which forms the disperse (domain) phase, especially when the two respective permeabilities are widely different (c.f. equations (3.3) and (3.4) for the Maxwell model for example). Robeson et al (95) have postulated that for an immiscible binary polymer system (say A and B), polymer A will be the continuous phase at high Φ_A and the disperse phase at low Φ_A, and similarly for polymer B. In other words for high Φ_A the expression for polymer A - continuous will be valid, and for low Φ_A the expression for polymer B - continuous will hold. It is further postulated that at intermediate values of Φ_A and Φ_B, both polymers will contribute continuous phase characteristics to the matrix and the modified Maxwell expression is given as

$$\overline{P}_C = X_A \cdot \overline{P}_A \left(\frac{\overline{P}_B + 2\overline{P}_A - 2\Phi_B (\overline{P}_A - \overline{P}_B)}{\overline{P}_B + 2\overline{P}_A + \Phi_B (\overline{P}_A - \overline{P}_B)} \right)$$

$$+ X_B \cdot \overline{P}_B \left(\frac{\overline{P}_A + 2\overline{P}_B - 2\Phi_A (\overline{P}_B - \overline{P}_A)}{\overline{P}_A + 2\overline{P}_B + \Phi_A (\overline{P}_B - \overline{P}_A)} \right) \quad \ldots (3.31)$$

where X_A and X_B are arbitrary weighting factors subject to $X_A + X_B = 1$.

Phase inversion is assumed to occur at $X_A = X_B = 0.5$ and the corresponding value of Φ_A can be determined graphically by observing where equation (3.31) (with $X_A = X_B = 0.5$) intersects the experimental data curve.

Using their own oxygen and nitrogen permeability data for $(AB)_n$ type block copolymers of polysiloxanes (PSX) and polysulphones (PSF), Φ_{PSX} for phase inversion was observed at 0.53, though in practice the transition appears to take place over a broad range of volume fractions.

The results which Robeson et al achieve appear to be consistent with an independent analysis of the elastic modulus behaviour of the system but the physical significance of X_A and X_B remain unclear. Furthermore it is not evident how the authors envisage the morphology of the continuous phase at intermediate volume fractions, whether it

whether it is seen as two interpenetrating continuous phases, a miscible or semi-miscible blend or perhaps something else. The assumption that $X_A = X_B = 0.5$ at the point of phase inversion would appear to have no a priori theoretical basis.

Although based on arbitrary mathematical weightings, the approach developed by Robeson et al is nevertheless novel and forms a useful method of tackling the problem of phase inversion at intermediate volume fractions. Its application need not be restricted to the Maxwell model.

Barnabeo et al (96) utilised the above approach to interpret oxygen and carbon dioxide permeability data for block copolymers and random copolymers of poly(methacrylonitrite) (PMAN) and polystyrene at 25°C. They concluded that the block copolymer series is a two-phase system which is continuous in PMAN at high Φ_{PMAN} and continuous in polystyrene at low Φ_{PMAN} because the data, when plotted as $\ln \overline{P}$ vs. Φ_{PMAN}, is well represented by an S-shaped curve which Robeson et al (95) predict.

By contrast, a similar plot for the random copolymers produced a much gentler curve which had no discernible inflection. The plot had been expected to be linear (i.e. to obey the Lichtenecker rule); perhaps the small amount of curvature was indicative of a small degree of phase separation.

Huang and Kanitz (97) have investigated the permeation of nitrogen, oxygen and carbon dioxide through polyethylene-g-polystyrene using the time-lag technique. A plot of gas permeability vs. % styrene grafting decreased initially, passed through a minimum at 20-30% and then began to increase again. To explain this they postulated that the permeability at first decreased with increasing % graft due to the system's free volume being "filled in" by the polystyrene and that above 30% graft the crystallites might be disrupted resulting in increased permeability. It is not clear why they did not attempt to explain the initial permeability decrease in terms of the addition of a component having a relatively much lower permeability. Increased diffusive tortuosity and reduced cross-sectional area are not discussed, nor are any theoretical models.

In a later study by the same authors (98) it is reported that modification of polyethylene by graft copolymerisation slightly improves

the system's gas separation efficiency. The observed $\overline{P}$'s and D's for gas mixtures agreed well with those of the pure components and could be predicted by single transport coefficients.

Toi, Igarashi and Tokuda (99) studied the same system as Huang and Kanitz but in contrast regarded the graft copolymer as a distinct two-phase system. They demonstrated simple linear additivity between solubility coefficients as a function of volume fraction but found that more complex relationships exist for diffusivities. Toi et al also supported Huang and Kanitz's idea of crystallite disruption at high % graft (97). Their study underlines the importance of the detailed nature of the individual phase morphology and its effects on the transport characteristics of heterogeneous media.

Odani, Taira, Nemoto and Kurata (100) present permeability and diffusion data for helium, argon, krypton, xenon and nitrogen in styrene-butadiene-styrene block copolymers. By judicious choice of solvent casting and thermal treatments, two domain structures (confirmed by electron microscopic observation) were prepared: (i) polystyrene rods dispersed in a polybutadiene matrix, and (ii) alternating lamellae of styrene and butadiene. The permeation data were interpreted in terms of the simple limiting series and parallel models, the latter being generally favoured. The diffusion data were interpreted by employing a tortuosity factor and a chain immobilisation factor.

The nitrogen permeability of a series of blends of natural rubber and other elastomers has been reported by Barbier (101). The results are not analysed according to any particular model, but Hopfenberg and Paul (102) have recently suggested that one of the series of blends (between natural rubber and a butadiene - acrylonitrite copolymer), if analysed according to the Maxwell model, could be interpreted as natural rubber forming a disperse phase over virtually all the composition range studied. A cursory examination of Barbier's data, however, reveals that other models might be equally applicable, including the Lichtenecker rule.

The most extensive experimental study of polymer blends has been the work of Rånby (103) and Shur and Rånby (104 - 107). The early studies concerned mechanical blends of poly(vinyl chloride) (PVC) with ethylene - vinyl acetate copolymers (EVA) and with acrylonitrite -

butadiene copolymers (NBR).

With the EVA copolymer initially containing 45% PVAc, the PVC/EVA-45 blend was milled at 160°C and produced a (ln $\overline{P}$) vs. (wt % of EVA) plot curved concave to the composition axis. With the PVAc content in EVA raised to 65%, the blend was milled at 185°C and the same plot was effectively linear indicating increased compatibility according to the Lichtenecker rule. This was confirmed by other physical measurements. Similar effects were observed for the PVC/NBR system. The less compatible blends gave indications of phase inversions at low % EVA and NBR.

Ito (108), Pieski (109) and Stallings, Hopfenberg, and Stannett (110) have all studied gas/vapour transport through polymer blends.

Recently, Frisch (111) produced a highly mathematical paper on permeation and sorption in inhomogeneous polymer membranes.

3.3 Review of the dual mode sorption theory (70)

On the basis of solubility and diffusivity measurements for several gases in poly(vinyl acetate) above and below T_g, Meares (18, 19, 112) was the first to suggest that a single (Henry's Law) mode of sorption existed above T_g and that two modes, Henry's Law dissolution and "microcavity filling", existed below T_g. In particular, he observed that the enthalpy of sorption for each gas became more negative below T_g compared with its value above the transition.

This idea was first put into a mathematical form in 1958 by Barrer, Barrie and Slater (113) who studied the sorption of C_4 and C_5 hydrocarbons in ethyl cellulose at several temperatures and up to 18 cm Hg pressure. Non-linear isotherms, concave to the pressure axis were recorded in each case. They proposed that sorption might occur by penetrant molecules entering pre-existing gaps in the glassy polymer matrix in addition to the more typical dissolution that was known to occur in elastomers and presented the idea mathematically by quoting the currently accepted expression for the "dual mode sorption" model (see chapter 2, equation (2.37)).

Although these investigators did not pursue this analysis quantitatively at that time, the same data were recently re-examined by Chan et al (114) who concluded the results were indeed quantitatively consistent with the DMS model.

Poly(ethylene terephthalate) (P.E.T.) has been examined by at least four groups of investigators (115-118). The earliest work appears to be that of Michaels, Vieth and Barrie (115) who in 1963 studied the solution of helium, nitrogen, oxygen, argon, methane, carbon dioxide and ethane in both glassy and partially crystalline P.E.T. using time-lag and static sorption methods. Only the latter two penetrants exhibited any isotherm curvature (i.e. deviation from Henry's Law behaviour).

Crystallinity was found to reduce gas solubility in the glassy polymer, but not in direct proportion to the decrease in the amorphous volume (except in the case of helium). It was suggested that this was because the crystallisation process tended to leave in the residual amorphous phase a greater number of microvoids than present in the completely amorphous polymer. It should be noted that the concept of "microvoids" (or "microcavities") was well established at this time.

Vieth, Alcalay and Frabetti (116) extended this work by studying the solubilities of several gases in oriented P.E.T. A graphical method of extracting the sorption parameters C'_H , B and k_D was briefly described and subsequently adopted as a standard procedure. More recently, Koros et al (119) have shown that the method is not sufficiently rigorous and have suggested modifications; more will be said about this at a later stage.

The carbon dioxide/P.E.T. system was examined further by Toi (117) who measured diffusivities and showed their apparent dependence on pressure for both the amorphous and the partially crystalline glassy polymer. Koros et al (118) later confirmed this view of the CO_2/P.E.T. system and proved that permeability also can be pressure dependent. (This work will be discussed more thoroughly later).

The earliest model for diffusion in a glassy polymer in terms of the dual mode sorption theory appears to be that proposed by Michaels, Vieth and Barrie (120) following on their sorption studies (115). They made the assumption that the driving force for diffusion was not the overall concentration gradient, but rather the concentration gradient of the dissolved species. They showed that gas diffusion in both the glassy and rubbery states of P.E.T. is Fickian and also verified experimentally the theoretical prediction that the diffusivities for the Henry's Law penetrant population in glassy P.E.T. are larger than those observed experimentally and that diffusivities are independent

of pressure in the Henry's Law region.

Vieth and Sladek (72) extended the analysis to cover the region of non-linear Langmuir-type sorption and postulated that the Langmuir penetrant population was totally immobilised and made no contribution at all to the diffusive flux.

It was further postulated firstly that the kinetics of the immobilisation process are very rapid compared with the rate of diffusion of the dissolved (mobile) species, and secondly that the diffusion coefficient for the mobile species is a constant, independent of concentration. From this basis numerical solutions for the modified form of Fick's second equation were obtained using finite difference techniques which are applicable to fixed-volume sorption experiments where pressure decay is observed.

Vieth, Frangoulis and Rionda (121) successfully used the Vieth-Sladek technique to interpret the kinetics of sorption of methane in glassy polystyrene at several temperatures and pressures of up to 30 atmospheres. The concept of microvoids plays a prominent role in the discussion presented, and it is suggested that weak dispersion forces bind the penetrant molecules to the polymer matrix, the intensity of the binding being greater in the microvoids "... perhaps owing to the focusing of force fields of polymer chain segments which compose the hole periphery." (Sic).

Vieth, Tam and Michaels (122) investigated the solubility of carbon dioxide, methane, argon and nitrogen in oriented and unoriented polystyrene films at 25°C up to pressures of 20 atmospheres. Each penetrant showed deviation from Henry's Law (although in the case of argon and nitrogen this is very slight) and each of the isotherms analysed lent solid support to the DMS theory. As expected, the oriented films exhibited less solubility than the unoriented ones. Also, the Henry's Law solubility coefficients (k_D) and the hole affinity constants (B) were correlated with Lennard-Jones force constants (ε/k), and the hole saturation constants (C'_H) were correlated with the predicted areas occupied by individual penetrants, again for both the oriented and unoriented polystyrene films.

In 1969, Paul (123) conducted a critical examination of the basic assumptions of the dual mode sorption theory. He pointed out that if immobilisation of penetrant species were occurring, then the standard expression derived for the time-lag technique could not be quantitatively

applied without some modification. Suggesting that sorption kinetics were not a sensitive enough test for the theory, Paul argues that since analytical solutions of Fick's second equation (derived in terms of the DMS theory) are not available or indeed even feasible, one could resort to Vieth-Sladek type numerical procedures, but this would make a critical survey unwieldy. Observation of the time-lag for permeation would be a far more critical and sensitive test, and Paul presents an analytical solution for the time-lag (which Petropoulos (124) notes, was given in an earlier study of a formally identical system (125)).

Petropoulos (124) pursues the same theme and stresses the need to validate the DMS theory's more important assumptions, viz., that (i) rapid equilibrium between the two penetrant populations is effectively maintained, (ii) the penetrant molecules described by the Langmuir expression are completely immobilised, (iii) the diffusivity of the dissolved species is a constant, independent of concentration and position. He describes the driving force for diffusion not in terms of a concentration gradient but in terms of a gradient of chemical potential which leads to thermodynamic diffusion coefficients. The major innovation here is in postulating a diffusion coefficient for the so-called "immobile" penetrant molecules, which is the basis of the "partial immobilisation" DMS theory for which there is currently growing evidence.

Patel, Patel, Patel and Patel (126) used Paul's time-lag technique (123) to interpret the transport of helium, oxygen, nitrogen and carbon dioxide in poly(methyl methacrylate) while Davis and Rooney (127) examined the transport properties of sulphur dioxide in polyethylene, polycarbonate and polyamide at subatmospheric pressures.

These latter investigators discovered some apparently curious effects whilst determining the effect of pressure on the permeability of each system. A plot of $\overline{P}$ vs. pressure for polyethylene produced a straight line indicating $\overline{P}$ increasing gently with increasing pressure and a similar effect was observed for polyamide. The graph for polycarbonate however, despite a certain amount of scatter, indicated for increasing pressure a decrease in $\overline{P}$ followed by a broad minimum and then a steady increase.

Sorption of sulphur dioxide in polycarbonate and polyamide was strong and exhibited characteristic DMS curvature whilst the weak

polyethylene sorption isotherm was adequately described by Henry's Law. Sorption-desorption kinetics indicated that SO_2 diffusion in polyethylene and polyamide was Fickian for the pressure range studied; for polycarbonate however the diffusion process appears to be Fickian at pressures up to approximately 25 cm Hg, becoming distinctly "non-Fickian" at higher pressures. This they believed to be consistent with the anomalous permeability pressure dependence.

Polycarbonate was further studied by Vieth and Eilenberg (128) who investigated the sorption kinetics of carbon dioxide over a range of temperatures and at pressures between 3 and 22 atmospheres. The Vieth-Sladek technique (72) is used to interpret the characteristic DMS data and no anomalous diffusion behaviour was observed perhaps because, in contrast to the previous case, carbon dioxide sorbs much less relative to sulphur dioxide.

The value for the energy of diffusion led the authors to suggest that a combined mechanism of activated diffusion plus slip flow might be present and that polymer micromotions might be contributing significantly to the diffusion process, but on a lesser scale than in elastomeric systems.

Kubo and Dole (129) in 1973 investigated the solubility of permanent gases in polyethylene but, as in the case of Michaels and Bixler's earlier study of the same polymer (130), no isotherm curvature was observed essentially because measurements were not made at high enough pressures. By now then the picture is emerging that perhaps <u>any</u> gas or vapour should exhibit a Langmuir-type sorption isotherm in glassy polymers over a certain range of pressure.

Tshudy and von Frankenberg (131) have developed the dual mode sorption theory further by relaxing the earlier postulate that a rapid equilibrium exists between the two penetrant populations. They assumed that the immobilisation process could be described in terms of reversible bimolecular kinetics which, in effect, makes the theory applicable to those systems where the rate of diffusion is comparable to the rate of "hole-filling".

The authors did not, however, include the concept of microvoids in their theoretical model. Instead they went back to the basics of the Langmuir isotherm and considered a fixed number of immobilisation sites uniformly distributed throughout the medium and fixed in position. On this basis they developed expressions for transient sorption,

equilibrium sorption, time-lag (equivalent to Paul's earlier expression (123) and steady-state permeability.

Paul and Kemp (132) performed both transient sorption and permeation experiments using helium, nitrogen, methane and carbon dioxide as penetrants in silicone rubber membranes containing a dispersion of highly adsorptive molecular sieves. The DMS model is clearly applicable to this non-glassy system although the mathematical form of the isotherm has to be modified slightly by considering the volume fractions of the two respective phases. Tne agreement between the experimental time-lags and those computed from Paul's earlier analysis (123) was excellent.

In a later paper (133) on the same system, the same authors found that after appropriate analysis which takes account of the effects of immobilisation, sorption kinetics, steady-state permeation and time-lag results could be interpreted by a single "true" diffusion coefficient, D_m, which is effectively concentration independent. This was perhaps only to be expected however since D_m is characteristic of the mobile penetrant population which was diffusing through a typical elastomeric matrix.

Vieth, Douglas and Bloch (134) and Vieth and Amini (135) have extended the generality of the DMS model by examining water structural interactions in reverse osmosis which lead to positive deviations from Henry's Law behaviour (curvature concave to the concentration axis). It is postulated that the polymer matrix swells as the penetrant is sorbed, thus exposing more immobilisation sites and thereby increasing the level of sorption synergistically.

NMR relaxation techniques have been employed by Assink (136) to validate the assumption of rapid equilibrium between the two penetrant populations of ammonia in polystyrene. However, the attempt to validate the assumption of zero mobility for the adsorbed species was less conclusive. Indeed, the possibility that the "immobile" species might have a small degree of mobility (Assink quotes $\sim$ 5% that of the mobile species) could not be eliminated.

The crucial question as to whether the adsorbed species could possess any mobility was effectively answered by Paul and Koros (94) and Koros, Paul and Rocha (119).

Paul and Koros (94) introduced the notion of mobility for the adsorbed species by employing a simple diffusive flux relation which is equivalent to the sum of two separate but parallel processes, one for the Henry's Law population, the other for the Langmuir population. Two different theoretical approaches were formulated, one based on concentration gradients, the other on chemical potential gradients (first suggested by Petropoulos (124)). Both formulations produced three equivalent predictions.

Firstly, total immobilisation of the adsorbed species will result in a constant permeability coefficient and a time-lag which strongly decreases with pressure.

Secondly, no immobilisation will produce a constant time-lag with a permeability which strongly decreases as pressure increases.

Thirdly, partial immobilisation will result in the permeability and the time-lag both decreasing with increasing pressure, but neither as strongly as in the two previous limiting cases.

Koros, Paul and Rocha (119) put these predictions to the test by reporting the transport characteristics of carbon dioxide in polycarbonate between 1 and 30 atmospheres pressure at 35^{o}C. Both the permeability and the time lag decreased with increasing pressure thus supporting the partial immobilisation model. The mobility of the Langmuir species was estimated at about 10% that of the Henry's Law species.

Another important development recorded in this paper was the mathematical extraction of the sorption parameters from the isotherm data. A non-linear least-squares regression analysis (possibly similar to the one developed independently at this laboratory (71) was perfromed on a computer to produce the best possible fit to the data. The results indicated that the graphical method hitherto employed was not the best method and that contrary to previous assumptions few, if any, isotherm sorption plots had been carried out at sufficiently high pressures to justify estimating an asymptote visually.

Koros, Paul, Fujii, Hopfenberg and Stannett (118) made a similar study on the effect of carbon dioxide transport in poly(ethylene terephthalate) and their results give similar quantitative support to the partial immobilisation model. The authors also stress the importance of reporting pressure levels used in transport experiments

when the processes involved are pressure dependent.

More recently, Barrie, Munday and Williams (137) (see attached copy in appendix) have studied vapour sorption in polystyrene, polycarbonate and polyvinylacetate. As predicted, the Langmuir component to sorption is shown to become small as the glass transition is approached from below and vanishes above it. The sorption kinetics results for the propane/polycarbonate system have been analysed in a novel way and show evidence of mobility in the adsorbed population.

Stern and de Meringo (138) have studied the solubility of carbon dioxide in symmetric (dense) cellulose 2.4-acetate at temperatures ranging from 0^{o} - 70^{o}C and up to 45 atmospheres pressure. The dual mode sorption theory appears to represent accurately the data up to 60^{o}C but not between 60^{o} and 70^{o}C, possibly because of a second-order transition in that temperature region

3.4 Review of PDMS/BPAC copolymers literature

Alternating block copolymers of poly(dimethyl siloxane) and poly (bisphenol-A carbonate) of the type investigated in this project were first synthesised by Vaughn (139, 140) although silicon-containing polycarbonate polymers were previously reported by Goldberg (141). Vaughn studied tensile strength and elongation at break for several different copolymer compositions with PDMS block lengths of 20 and 40. It was found that the tensile strength appeared to increase monotonically with increasing BPAC content, irrespective of the block lengths examined. The elongation at break was shown to decrease dramatically with increasing BPAC content and then approaches a constant value. However, the graph for the PDMS 40-blocks was consistently lower than that for the 20 blocks indicating that this property for the former set of films decreased more sharply than the latter for increasing BPAC content.

Kambour (142) has carried out torsion pendulum studies on some of these films and found that the upper glass transition temperature decreased steadily as a function of the reciprocal degree of polymerisation of the BPAC block thus indicating that the temperature dependence on block length is effectively analogous to the dependence of T_g on molecular weight in homopolymers.

Kambour also showed that each material investigated exhibited strong low-angle x-ray scattering with an interference peak suggesting the presence of a domain/continuum microstructure. The tentative

conclusions drawn from Kambour's study, which included electron microscopy, were that a microdomain structure did exist. At low BPAC content, discrete but irregularly shaped particles composed principally of BPAC blocks exist; at high BPAC content, discrete silicon aggregates exist in a BPAC continuum; and at intermediate concentrations, both BPAC and PDMS continua are assumed to exist.

LeGrand (143) has studied the mechanical and optical properties of these materials and surmised that some of the BPAC blocks are associated to form domains which act as crosslinks, but the matrix is probably composed of both PDMS and BPAC blocks (see Fig. 3.1). A later study by Magila and LeGrand (144) supported this view and suggested that the stress-strain behaviour of such materials is governed not only by the presence of domains, which act as filler and cross-links, but more importantly by the nature of the chain between such regions.

LeGrand later found that single crystals of these materials could be prepared (145) and contributed further to the earlier model by obtaining high-resolution proton magnetic resonance spectra for the swollen polymers (146). The results indicated that the mobility of the aromatic protons depends on block length, while this is not the case for the gem dimethyl and siloxane methyl protons.

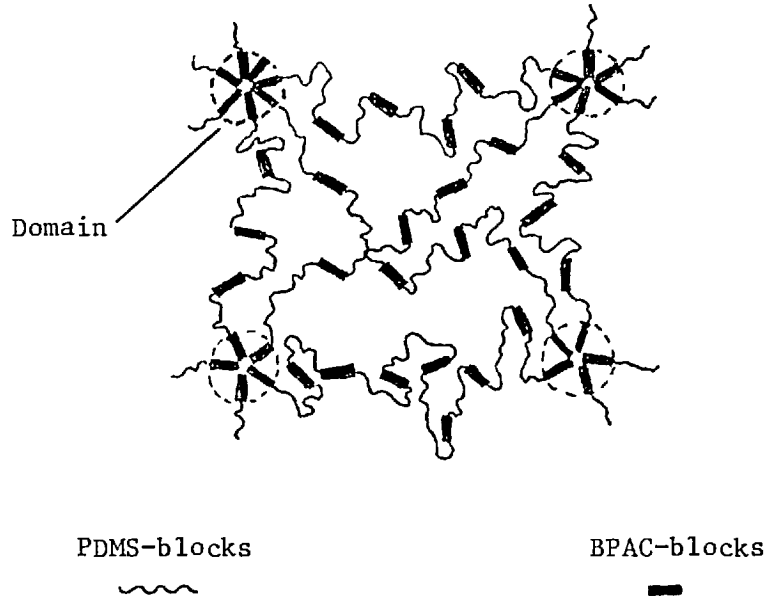


Fig. 3.1 Proposed morphology of alternating PDMS-b-BPAC copolymers (143).

The same author (147) investigated the optical anisotropy of the statistical segment in these block copolymers and the effect of several different swelling fluids. The results were generally in support of the earlier model (142, 143).

The picture has emerged then that the morphology of these copolymers can be adequately described in terms of partial microphase separation. LeGrand's model (Fig. 3.1) is consistent with Krause's prediction, based on thermodynamic considerations, that microphase separation becomes more difficult as the number of blocks increases for a given composition of copolymer (148), i.e., as the block lengths get shorter.

The exact nature of the continuous phase remains unresolved however. Kambour (142) suggested the two interpenetrating continua exist while Dawkins (149), in a discussion concerning LeGrand's model, has suggested that $(AB)_n$ block copolymers will often resemble random copolymers.

CHAPTER 4

EXPERIMENT

4.1 Materials

4.1.1 Alternating-block copolymers of poly(dimethyl siloxane (PDMS) and poly (bisphenol-A carbonate) (BPAC).

Powder samples of these copolymers were synthesised and supplied by the General Electric Research and Development Centre (140). The chemical structure is given in Fig. 4.1.

An α, ω - dichloropoly (dimethyl siloxane) oligomer undergoes condensation with excess bisphenol-A in a pyridine-methylene chloride

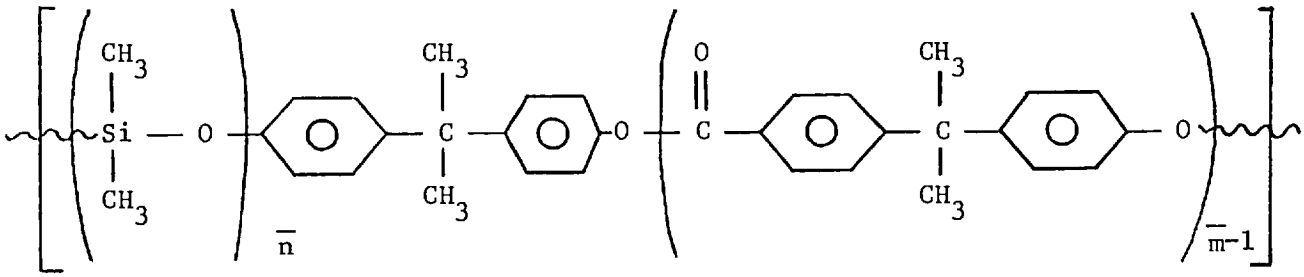


Fig. 4.1 Chemical structure of alternating PDMS-b-BPAC copolymers

solution. Phosgene and additional bisphenol-A are then added to the produce to form the polycarbonate blocks in situ. The copolymer is isolated either by evaporation of the solvent or precipitation with methanol.

In Fig. 4.1, $\bar{n}$ is the number average degree of polymerisation of the PDMS blocks and is determined by end group analysis of the initial oligomer. The number average degree of polymerisation of the BPAC blocks, $\bar{m}$, is calculated from sample's overall composition.

Whilst $\bar{n}$ could be controlled within sharply defined limits, $\bar{m}$ was less easily controlled and figures quoted for this quantity are mean values.

The samples were cast as films on clean mercury from a 10% methylene chloride solution and then outgassed in a vacuum oven between 135 and 145°C for 48 hours.

4.1.2 Poly (bisphenol-A carbonate).

Glassy beads of BPAC were supplied by BDH Chemicals Ltd. and cast as a thin film on clean glass from a 10% methylene chloride

solution. The sheet was then outgassed in a vacuum oven between 50 and 60°C for 48 hours.

4.1.3 Poly ([c.ℓ.] - dimethyl siloxane)

Sheets of this material were supplied by Dow Corning Ltd. PDMS gum had been press cured with 1% by weight 2,4-dichlorobenzoyl peroxide at 115°C for five hours and then post cured at 200°C for four hours.

The membrane sample was refluxed in a sohxlet containing ethyl acetate for 24 hours to remove any low molecular weight material and then outgassed in a vacuum oven at 50-50°C.

4.1.4 Poly ([c.ℓ.] - dimethyl siloxane-g-vinyl acetate), (PDMS-g-PVAc)

The single sample used in this project was supplied by Dr. A. Sheer (27) of this laboratory. The membrane was prepared by exposing [c.ℓ.] - PDMS swollen with vinyl acetate monomer to ^{60}Co γ-radiation at room temperature in the absence of air. The sample was then refluxed in a sohxlet containing ethyl acetate for 6-7 days until constant weight was attained and finally outgassed under high vacuum at room temperature.

The [c.ℓ.]-PDMS was the same as that described in section 4.1.3 and the vinyl acetate monomer was supplied by Hopkin and Williams Ltd.

4.1.5 Physical properties of the membranes

The PDMS-b-BPAC copolymer films varied from being tough and transparent at high BPAC content to being clear and rubbery at high PDMS content. The PDMS-g-PVAc was tough and opaque. Some of the physical properties of the membranes are presented in Table 4.1.

The lower (PDMS) glass transition temperatures for the membranes, pure PDMS and pure BPAC were measured by differential scanning calorimetry (D.S.C.) using a Du Pont 990 Thermal Analyser in an independent project in this laboratory (150); the higher Tg's for the BPAC component in the membranes were determined from mechanical loss measurements using a Rheovibron (150).

Densities were measured by the water displacement method, and volume fractions of PDMS (Φ_{PDMS}) were derived from the weight fractions and densities of the two pure components. The data for PDMS-g-PVAc are those of Sheer (27). The results presented in Table 4.1 are discussed in chapter 6.

In listing the PDMS-b-BPAC membranes, the weight % of PDMS will be shown followed in parenthesis by the PDMS : BPAC block lengths. E.g. PDMS-64(20:3.5) indicates a sample containing 64% PDMS by weight; the length of the PDMS blocks is 20 mer units and the average length of the BPAC blocks is 3.5 mer units.

The PDMS-83(61:36) is anomalous in that it contains a binodal distribution of BPAC block lengths. The figure of 3.6 for the average block of BPAC in this membrane is an arbitrary mean having no true physical significance.

Membrane PDMS-54 (40:10) was originally quoted by the sample suppliers as having a BPAC block length of 14, which would make the block length distribution incompatible with the weight % of PDMS. This error was rectified and the use of 10 as the value for the BPAC block length has produced no anomalies during this project.

4.1.6 Penetrant vapour

Glass bulbs of propane were supplied by the National Physical Laboratory with a certified purity of 99.9 moles %. To "top up" the bulbs for some of the later experiments, propane was withdrawn from a cylinder supplied by Matheson Gas Products Ltd.

4.2 Apparatus

4.2.1 The permeability System (Fig. 4.2)

About 10^{-5} mm Hg. could be achieved by the Edwards two-state rotary oil pump (P) working in conjunction with the three-stage mercury diffusion pump (D) and the liquid nitrogen cold trap (CT). The power supply for the diffusion pump was connected through a device which automatically switched off if the water supply used for condensing the mercury vapour fell below a certain pressure.

To prevent mercury vapour entering the sensitive Baratron head (B), two pieces of gold foil (F) were inserted into the apparatus.

An Edwards Pirani guage (G) was fitted to the high vacuum line and was used to detect leaks and the extent of outgassing.

(i) High pressure (ingoing) side

Vapour from the reservoir (R) was supplied to the ingoing side of the cell (C) which included a 1000 cm^3 buffer volume (V_1) to maintain an effectively constant ingoing pressure. The pressure itself was measured on the strain-guage transducer (TR) (Type 4-327-0003; Bell and Howell Ltd) supplied with a steady 10V d.c. A sensitive potentiometer measured the transducer's voltage signal (mV) which had been previously calibrated against the mercury manometer (M).

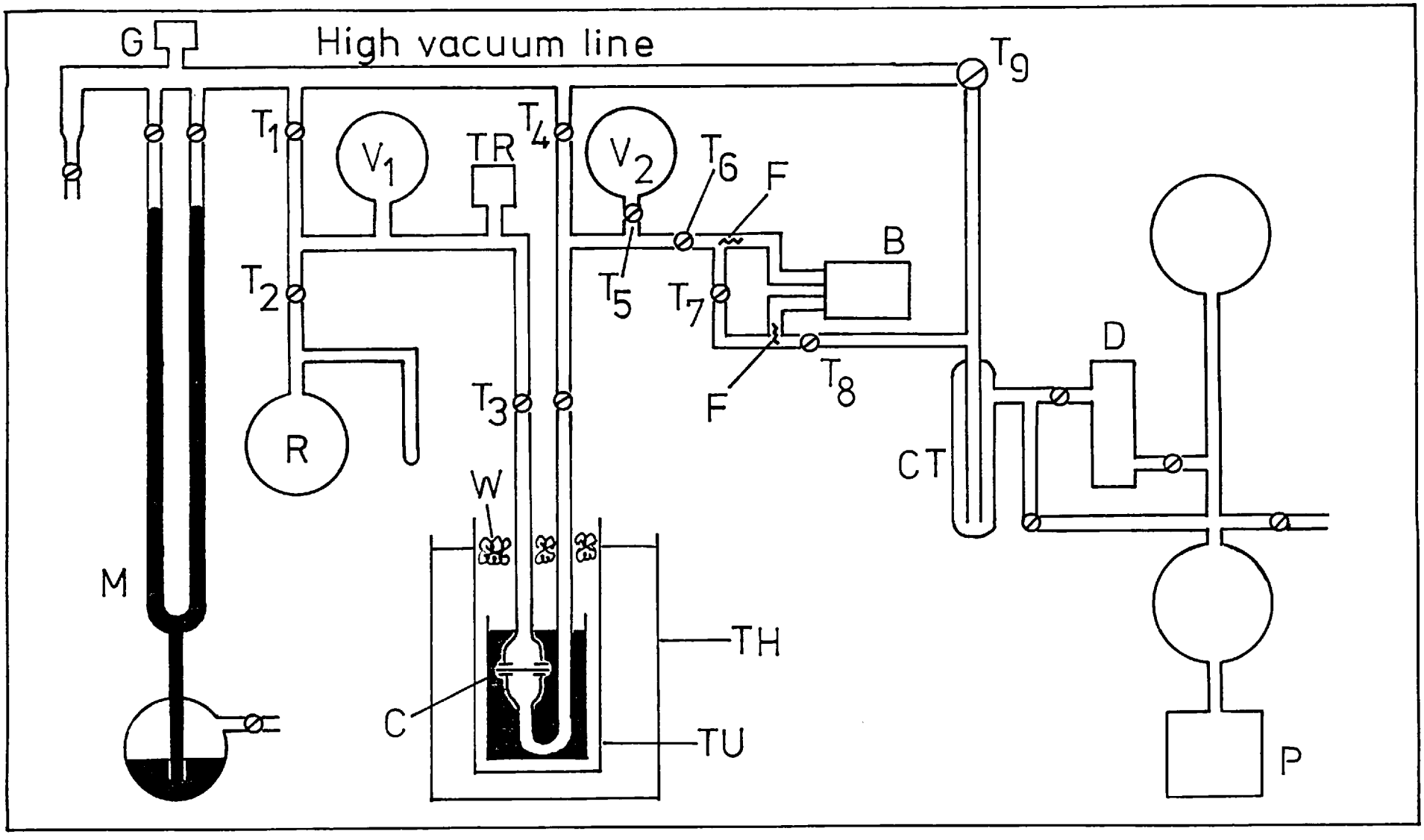


FIG. 4.2 PERMEABILITY SYSTEM

Table 4.1 Some physical properties

Density, ρ; volume fraction of PDMS, Φ_{PDMS}; glass transition temperature, T_g.

Polymer	ρ/g.cm^{-3}	Φ_{PDMS}	T_g(PDMS)/^oC	T_g(BPAC)/^oC
BPAC	1.178	0.000	-	+ 147 (by D.S.C.)
PDMS-25(20:17.8)	1.147	0.287	-	+ 141
PDMS-34(20:11)	1.104	0.384	-	+ 127
PDMS-50(20:6)	1.097	0.547	-	+ 93
PDMS-60(20:3.9)	1.052	0.644	-	+ 68
PDMS-64(20:3.5)	1.040	0.682	- 117	+ 67
PDMS-49(41:12.4)	1.070	0.537	-	+ 135
PDMS-54(40:10)	1.081	0.586	- 123	+ 121
PDMS-60(40:7.2)	1.076	0.644	- 122	+ 116
PDMS-64(40:7)	1.049	0.682	- 120	+ 98
PDMS-82(40:3)	1.012	0.846	- 117	-
PDMS-60(80:14.6)	1.047	0.644	- 123	+ 126
PDMS-64(100:16.5)	1.046	0.682	- 123	+ 157.5
PDMS-83(61:3.6)	1.013	0.855	- 120	-
PDMS	0.975	1.000	- 122	-
PDMS-g-PVAc (44.2% by volume PVAc)	1.081	0.558	- 122	T_g(PVAc) + 32 (by D.S.C.)

(ii) Low pressure (outgoing) side

The pressure of the vapour on the outgoing side (including the 500 cm^3 buffer volume (V_2)) was measured by a sensitive Baratron capacitance manometer (B) (type 90H-3E; M.K.S. Instruments Inc.) operating in the pressure range 10^{-4} - 3 mmHg.

The Baratron measures differences in pressure between the two inlets of the head system, one of which was directly connected to the mercury diffusion pump so that the instrument effectively measured the absolute pressure. In the head an ultra-thin metal diaphragm is clamped between two electrodes so as to form a capacitor circuit. A

pressure difference across the diaphragm displaces it relative to the electrode assembly and registers as a change in capacitance in the circuit which is measured on a capacitance bridge. The out-of-balance signal is then transformed to a pressure reading obtained directly on a digital volt meter.

(iii) The permeation cell.

This is illustrated in Fig. 4.3. The membrane (M) was held between two glass 'cups' (C) and was glued to the same at the periphery by a silicone-based sealant (S) (Silastic, supplied by Dow Corning Ltd.). The sample was supported from below by a fixed copper guaze (G) on top of which was placed a piece of hardened filter paper (F). This arrangement did not impede the effusant vapour and prevented distortion of the membrane when under a pressure gradient by the criss-cross pattern of the guaze. The cell was sealed around the edges with more sealant and then left for 24 hours to cure.

Additional sealant bonding (A) (Araldite Rapid, supplied by Ciba Geigy Ltd.) completed the cell system. After the final seal had reached full strength (about eight hours), it was set in a beaker of mercury (see Fig. 4.2) to seal it effectively. This rested on lead shot at the bottom of a copper tube (TU) which was topped with cotton wool (W) to reduce convection currents. The copper tube stood in the thermostat tank (TH) which was controlled by a mercury contact thermometer to within $\pm$ 0.05^{o}C.

4.2.2 The sorption system

This is shown in Fig. 4.5.

(i) The pumping system

This is essentially the same as that for the permeability system and only the cold trap (CT), Pirani guage (G), vapour reservoir (R) and transducer (TR) need be illustrated.

(ii) The microbalance

A vacuum electronic microbalance (Model 4102, Sartorius U.K.), accurate to within 1 μg, was used for the transient and equilibrium sorption studies.

The polymer sample (S) and the copper counterweight (C) were suspended from the quartz tubular beam (B) by two identical platinum wires hanging on aluminium stirrups. The surrounding glass tubes (TU) (which were sprayed internally with metal salts and earthed to minimise

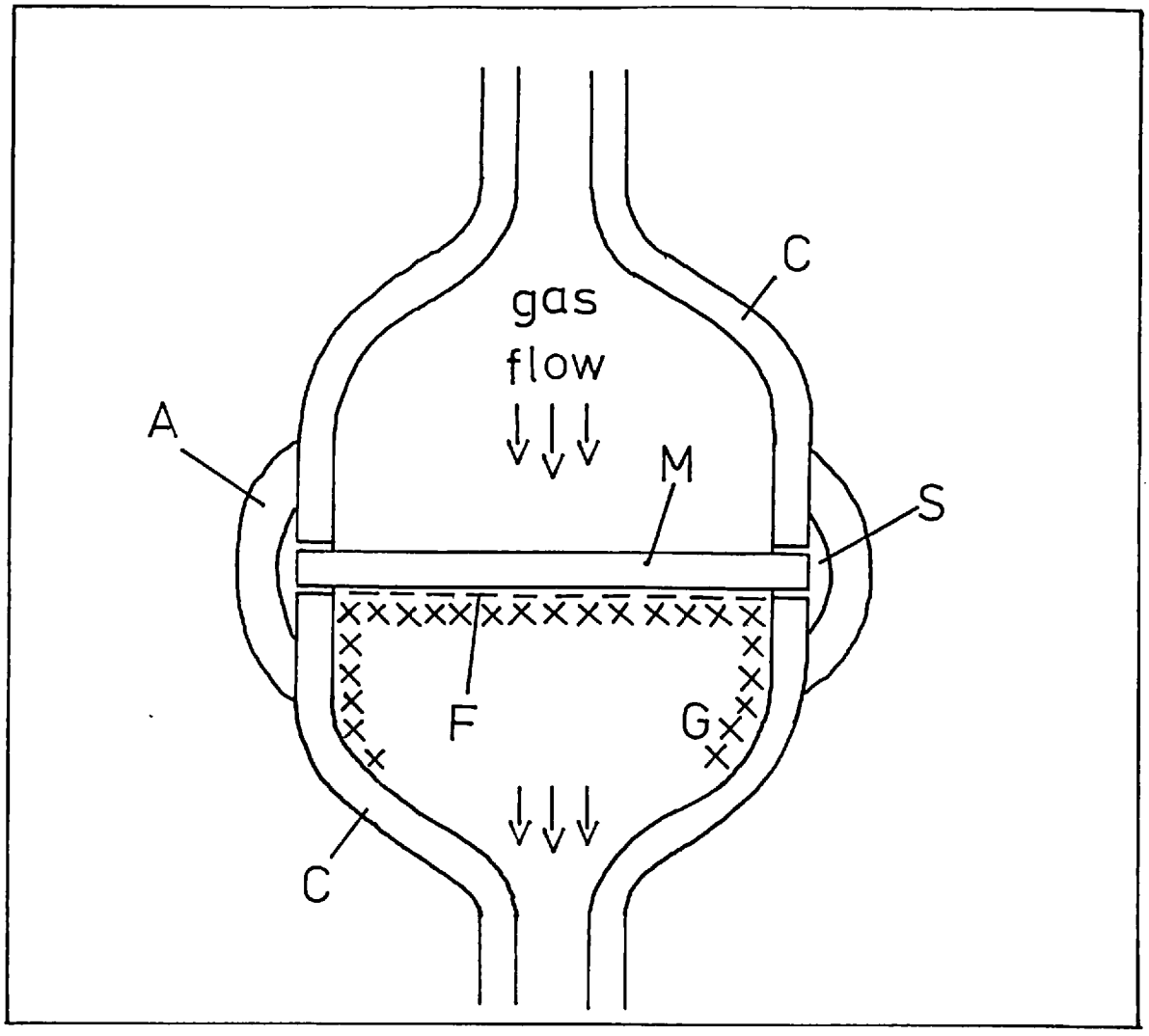


FIG. 4.3 PERMEATION CELL

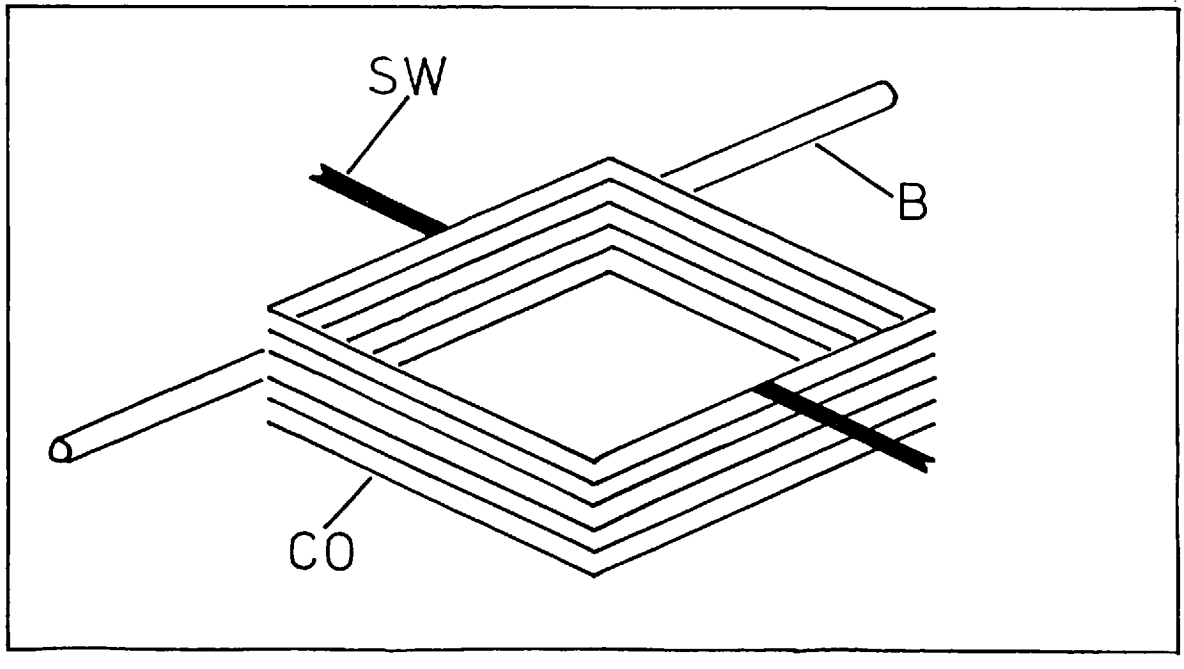


FIG. 4.4 MICROBALANCE BEAM

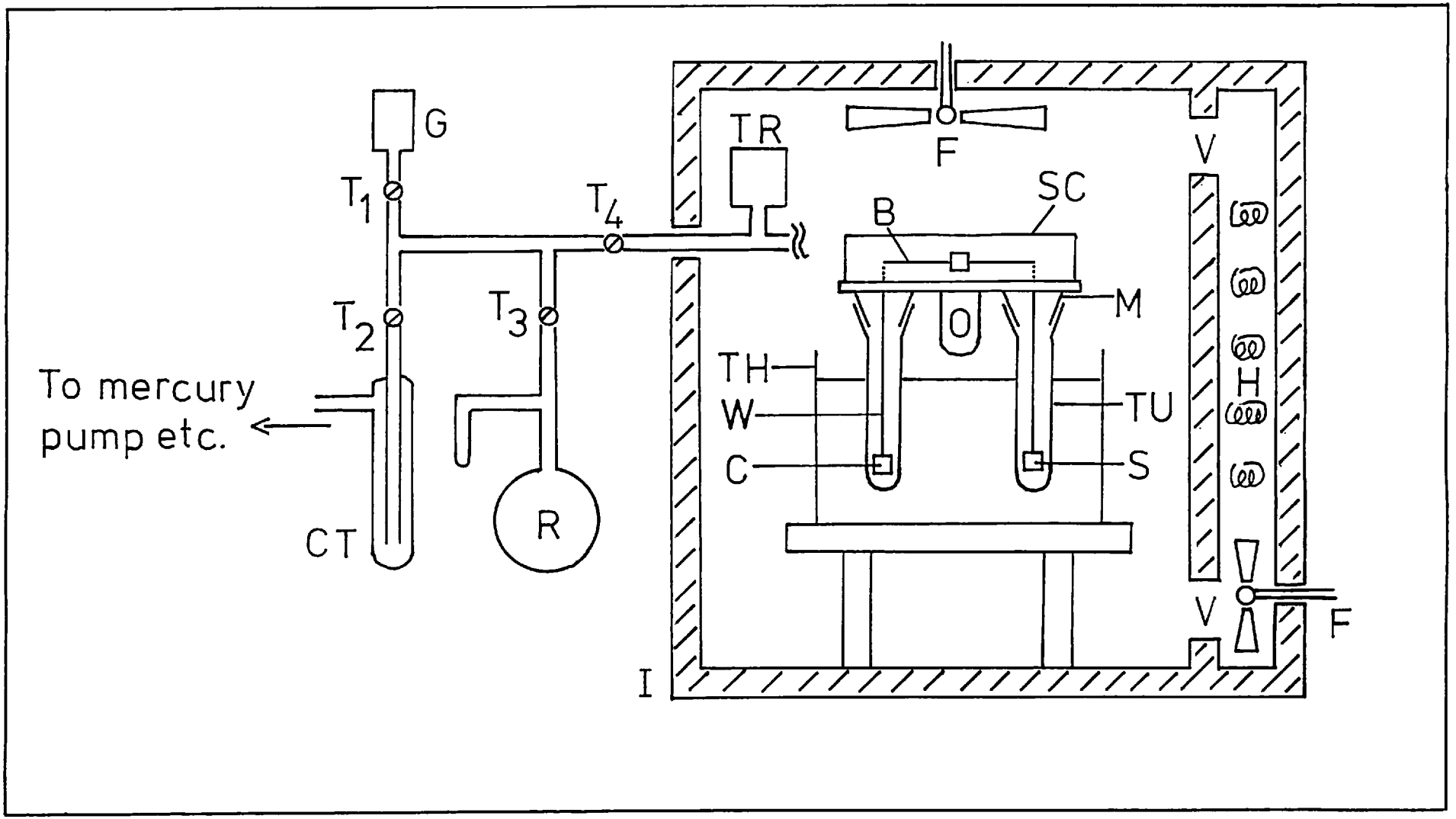


FIG. 4.5 SORPTION SYSTEM

static) were attached by silicone greased joints to metal cones (M) tightly screwed to the base of the stainless steel casing (SC). The outlet (O) of the balance head was connected to the vacuum system through a metal flange and a flexible bellows-type coupling (not shown).

The balance is a continuous null-point instrument which depends upon an automatic compensatory torque being applied to counterbalance any load-induced moment. The beam assembly is illustrated in Fig. 4.4 and consists of a moving copper field coil (CO) supported by two silver torsion wires (SW) and to which is attached the quartz tubular beam (B). The field coil is placed around a permanent magnet (not shown) and attached to this on one side parallel to the field coil are two fixed oscillator coils (not shown).

A displacement of the beam from the horizontal causes the moving coil to receive a high frequency signal from the oscillator coils' H.F. field. This detecting signal is then passed to the amplifier for rectification phase adjustment and amplification and is finally returned as a compensating direct current to restore the beam to equilibrium. This compensating current is measured and converted for reading in terms of weight change.

Returning to Fig. 4.5, the microbalance was mounted on wall brackets and contained within an insulated air thermostat (I) which had a window in the door and which could be illuminated internally.

The lower ends of the glass tubes (TU) extended into the glass thermostat bath (TH) which was regulated to within $\pm$ 0.1^{o}C by a thermocirculator (Churchill Instruments Ltd. - the standard model was used for the temperature range 20-60^{o}C; below 20^{o}C, the refrigerating model was employed).

Air thermostatting was achieved with a column of 500W heaters (H) controlled by a mercury contact thermometer fixed inside the air thermostat. Hot air emanated through two vents (V) and convection was effected by two fans (F).

The read-out system was a Honeywell two-pen chart recorder (Electronik 194) which simultaneously registered signals from the microbalance and the pressure transducer (TR) which was calibrated against a mercury manometer.

4.3 Experimental procedure

4.3.1 Permeation measurements (Fig. 4.2)

(i) The Baratron

With both inlets of the Baratron head connected to the pumping system and the head thermostat set at 150°C, the instrument was baked out for 24 hours under a pressure of $\sim 10^{-5}$ mm Hg. for 24 hours. The head was then allowed to cool to its working temperature of 50°C which was subsequently maintained. With the two inlets connected via tap (T_7) and taps (T_6) and (T_8) closed, the Baratron system was zeroed and adjusted for minimum quadrature. During the permeation runs, taps (T_6) and (T_8) remained open and tap (T_7) was kept closed.

(ii) Outgoing volume

The volume into which the vapour expands after diffusing through the membrane was determined by successive expansions of air at known pressure from buffer volume (V_2). The volume of (V_2) including the volume of the barrel of tap (T_5), was measured before attachment to the apparatus by weighing the vessel first empty and then full of water. Air was admitted into the system and the pressure measured on the Baratron; the pressure was less than 3 mm Hg - the maximum pressure which could be measured accurately with the head. Tap (T_5) was then closed and the remaining outgoing volume evacuated. On expansion of the gas into the outgoing volume again, the new pressure was noted and the procedure repeated several times. A simple gas law calculation yielded the outgoing volume.

(iii) The cell (Fig. 4.3)

Prior to assembly the internal diameter of the cell was measured with calipers in order to estimate the cross-sectional area of the membrane to be exposed to the penetrant.

The membrane was cut to fit the external cross-section of the cell thereby allowing the 'cups' a firm grip on the sample. The thickness of the membrane was measured using a micrometer.

After the cell was assembled and glass-blown on to the apparatus, the membrane was outgassed and the outgoing volume leak rate determined. A leak rate of less than 0.5% of the steady-state flux rate was considered tolerable.

(iv) The run

With taps (T_1) and (T_3) closed, vapour was admitted to the high-pressure side of the system via (T_2), the pressure being monitored by the transducer (TR). The low-pressure side was evacuated with tap (T_7) closed and taps (T_4), (T_5), (T_6) and (T_8) open. Tap (T_4) was closed seconds before (T_3) was opened to start the run. The stopwatch was started at this point and the increase in pressure followed as a function of time. Pressure readings were taken when the steady-state (a linear plot of pressure vs. time) was reached. The ingoing pressure was measured at the beginning of the run and periodically thereafter to check for constancy as was the case for room temperature.

The pressure of vapour in the outgoing side was never allowed to increase beyond 1% of the ingoing pressure as the boundary conditions would be no longer satisfied and errors would be introduced into the time-lag and permeability measurements. When it appeared that this would happen, the 500 cm^3 outgoing buffer volume (V_2) was replaced with a larger volume.

At the end of each run the vapour, first on the ingoing side and then on the outgoing side of the cell, was frozen back into the reservoir (R) using the side-arm attachment with liquid nitrogen. To remove any traces of air, the frozen vapour was pumped via taps (T_1) and (T_9) before tap (T_2) was closed.

Some runs were repeated at the same temperature and ingoing pressure to check for reproducibility of results and also at different ingoing pressures to check for pressure-dependence of the permeability and time-lag.

Between runs the cell was outgassed for periods of time not less than ten time-lags; for changes of membrane temperature, 24 hours were allowed for thermal equilibration.

Sample calculations and an estimation of errors are given in Chapter 8 (Appendix 8.2).

4.3.2 Sorption measurements (Fig. 4.5)

The membrane sample (S) was weighed and then suspended from the right-hand support wire (W) of the microbalance by means of a small piece of platinum wire, and a suitable counterweight of copper wire (C) suspended from the left-hand support wire (W) sufficient to bring the balance read-out on scale. For the pure BPAC sample only, shorter suspension wires were used because of the larger sample dimensions;

a sheet 20 cm x 10 cm was rolled up to form a cylinder 10 cm long and with copper wire spacers between layers to prevent contact between adjacent layers.

The system was outgassed and allowed to come to thermal equilibrium. It was found that in order to produce a steady zero baseline for the microbalance signal, the air thermostat had to be set a few degrees lower than the water thermostat. Occasionally, the steady baseline drift would be minimised but not completely eliminated; where such a drift might seriously affect the results, a suitable correction was applied. The leak rate into the system was checked for each new temperature using the Pirani guage (G).

At 10^{-5} mm Hg pressure, taps (T_1) and T_2) were closed and vapour admitted to the system from the reservoir (R) through taps (T_3) and (T_4). For equilibrium studies, the rate of admission of vapour was unimportant; for the kinetic studies, the vapour was admitted as quickly as possible. The pressure and the weight increase were followed as a function of time on the two-pen charter recorder. The run was considered to be finished when no further weight increase was being recorded.

For the equilibrium measurements, the vapour was then either frozen back into the reservoir using the side-arm attachment with liquid nitrogen to check that the outgassed weight of sample returned to its original value; alternatively, more vapour was admitted and the new equilibrium weight up-take subsequently measured. The former method was more time-consuming and except, perhaps, when a large zero baseline drift was encountered, showed no advantage over the latter method which was used extensively. For some membranes, especially those with a high volume fraction of glassy component, measurements were carried out "up" and "down" the isotherm to check whether hysteresis effects existed; none were observed.

At the end of kinetic runs, the vapour was frozen back and pumped out each time and a fresh start made for each ingoing pressure.

Sample calculations and treatment of errors are given in Chapter 8 (Appendix 8.3).

CHAPTER 5

RESULTS AND DISCUSSION, PART I: BPAC, PDMS and PDMS-g-PVAc

5.1 BPAC

5.1.1 Equilibrium sorption

The BPAC/propane isotherms are shown in Fig. 5.1 and the sorption parameters derived for each isotherm in Table 5.1. The two dashed lines in Fig. 5.1 are asymptotes to the computed curves for 50.1°C and 60.0°C, intersecting the C-axis at the appropriate value of C_H' for that temperature. The isotherm data are given in Chapter 8 (Appendix 8.4).

Two sets of sorption parameters are given in Table 5.1. The first set k_D, C_H' and B were computed for each individual isotherm taken separately using a non-linear regression computer programme developed in this laboratory (71). The objective achieved by this programme was to produce values of k_D, C_H' and B such that the mean deviation between the predicted concentrations and the experimental concentrations was minimised.

Table 5.1 Sorption parameters for BPAC/propane

Henry's Law solubility, k_D; hole saturation constant, C_H'; hole affinity constant, B; limiting Henry's Law solubility (as concentration → 0), S_L.

T/°C	$10^2 k_D$ / $(\frac{cm^3 STP}{cm^3 cmHg})$	C_H' / $(\frac{cm^3 STP}{cm^3})$	B/cm Hg^{-1}	$10.S_L$ / $(\frac{cm^3 STP}{cm^3 cmHg})$
30.1	6.03 (± 7%) 6.45	1.67 (± 11%) 1.55	0.311 (± 30%) 0.340	5.79 (± 18%) 5.91
40.05	5.01 (± 2%) 4.91	1.25 (± 4%) 1.28	0.254 (± 9%) 0.248	3.68 (± 5%) 3.67
50.1	4.01 (± 8%) 3.79	1.02 (± 21%) 1.04	0.167 (± 43%) 0.183	2.10 (± 19%) 2.29
60.0	2.55 (± 17%) 2.98	1.22 (± 31%) 0.93	0.094 (± 50%) 0.139	1.40 (± 19%) 1.58

The programme then proceeded to estimate by what amount the sorption parameters could be altered within the limits of the mean deviation and still give a reasonable fit to the experimental data. These results are quoted as an average percentage in parenthesis after the values of the sorption parameters.

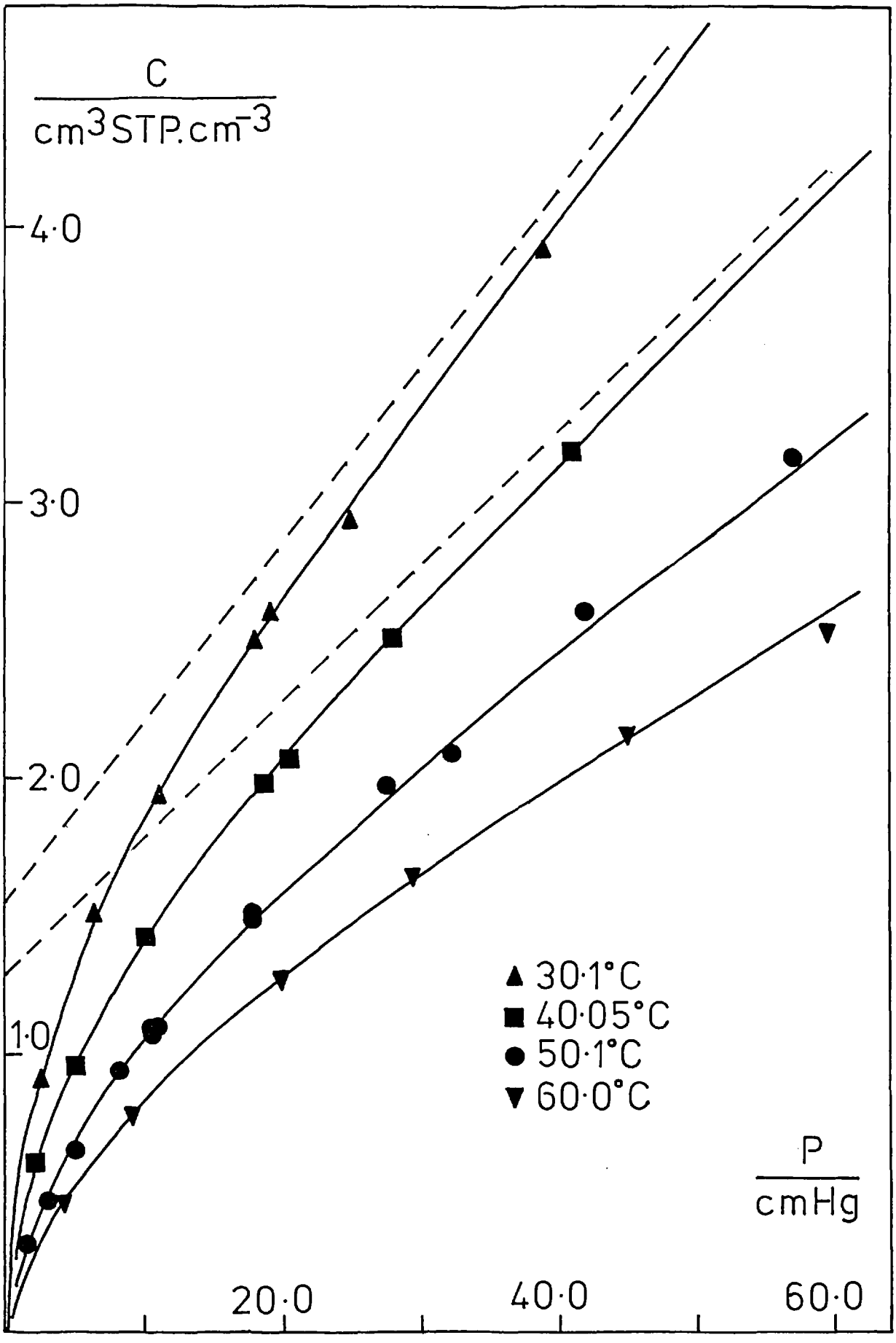


FIG. 5.1 BPAC/PROPANE ISOTHERMS

Inspection of the dual mode isotherm equation (2.37) (see also equation (5.2)) reveals that a maximum value of k_D corresponds to a minimum value of C'_H and a maximum value of B, and vice versa.

Values of S_L (= $k_D + C'_H.B$) and the adherent uncertainties were obtained using the values of the sorption parameters in Table 5.1 as it was not possible to measure the slopes of the isotherms as concentration → 0.

The relatively large uncertainties in k_D, C'_H and B prompted a further examination of the analytical procedure which led to a second set of the sorption parameters, $\overline{k}_D$, $\overline{C'_H}$, $\overline{B}$ and $\overline{S}_L$ which appear below the first set of values in each case in Table 5.1. The bar superscript is used solely to distinguish that these parameters were determined using a different analytical procedure.

Any analysis of sorption isotherms exhibiting characteristic "dual mode" sorption curvature requires first the estimation of k_D (70). With this established, the Langmuir component, C_H, of the isotherm can be analysed. Re-arranging equation (2.37),

$$C_H = C - k_D.P = \frac{C'_H.B.P}{1 + B.P} \qquad \ldots (5.1)$$

which can be re-written as

$$\frac{1}{C_H} = \left(\frac{1}{C'_H.B}\right)\frac{1}{P} + \frac{1}{C'_H} \qquad \ldots (5.2)$$

A plot of C_H^{-1} vs. P^{-1} then yields a straight line of slope $(C'_H.B)^{-1}$ and a vertical intercept of $(C'_H)^{-1}$ and hence both B and C'_H are determined. However, any uncertainty in the initial estimation of k_D will be subsequently compounded in the derivation of C'_H and B.

It was decided therefore to attempt to estimate values of the sorption parameters with the following constraints:

(i) the values lay within the quoted uncertainty limits,

(ii) the values for k_D and B satisfied a van't Hoff-type of dependence on temperature,

(iii) isotherms predicted using these values were in good agreement with the experimental data.

Essentially this procedure differs from the more conventional method with the introduction of constraint (ii). For gas sorption in polymers in the region of Henry's Law, sorption experiments have shown that over shorter ranges of temperature a plot of $\ln k_D$ vs. T^{-1} is linear. It seems reasonable

therefore to anticipate this behaviour and select values of $\overline{k}_D$ which produce the best straight line for the plot of ln k_D vs. T^{-1} whilst subject to constraints (i) and (iii).

With these values of $\overline{k}_D$, equation (5.2) was used to derive values of $(C'_H)^{-1}$ and $(C'_H.B)^{-1}$, and hence values of B. These "intermediate" values of B were designated B*.

According to the theoretical development of the Langmuir isotherm, the parameter B is given by equation (2.42) (151)

$$B = B_o \exp - \frac{\overline{\Delta H}_H}{RT} \qquad \ldots (2.42)$$

where $\overline{\Delta H}_H$ is the enthalpy of "hole-filling" which according to the model is constant and independent of coverage. For this reason values of $\overline{B}$ were selected which gave the best straight line for a plot of ln B* vs. T^{-1}. The semilog plots for B (with error bars) and $\overline{B}$ are shown in Fig. 5.2.

Having now estimated $\overline{k}_D$ and $\overline{B}$ for each isotherm, $\overline{C'_H}$ was calculated by taking the mean value of $\overline{C'_H}$* where this quantity is defined by re-arranging equation (2.37) and substituting $\overline{k}_D$ and $\overline{B}$.

$$C'_H* = \frac{(C - \overline{k}_D.P)(1 + \overline{B}.P)}{\overline{B}.P} \qquad \ldots (5.3)$$

For N sorption points on an isotherm,

$$\overline{C'_H} = \frac{1}{N} \sum C'_H* \qquad \ldots (5.4)$$

The first test for the values of $\overline{k}_D$, $\overline{B}$ and $\overline{C'_H}$ was to determine values of $\overline{S}_L$ and check for a linear van't Hoff plot of ln $\overline{S}_L$ vs. T^{-1}. To within 2-3%, the test was successful as Fig. 5.2 shows.

In each case the selected values of $\overline{k}_D$, $\overline{B}$ and $\overline{C'_H}$ lie within the uncertainty limits of the original estimations of k_D, B and C'_H. Moreover, the semilog plots for $\overline{k}_D$, $\overline{B}$ and $\overline{S}_L$ are effectively without the scatter which plots for the original parameters (see Fig. 5.2) clearly suffer from.

The second, perhaps most important, test was to compare the values predicted by the constrained parameters with the experimental data. The results are illustrated in Fig. 5.1 and a numerical comparison is listed in Appendix 8.4. The solid lines and asymptotes were not computed from the originally determined sorption parameters, but from the set of mutually compatible parameters. The fit is excellent.

The question now arises as to whether the constrained parameters are more significant than the original parameters. For the individual isotherms

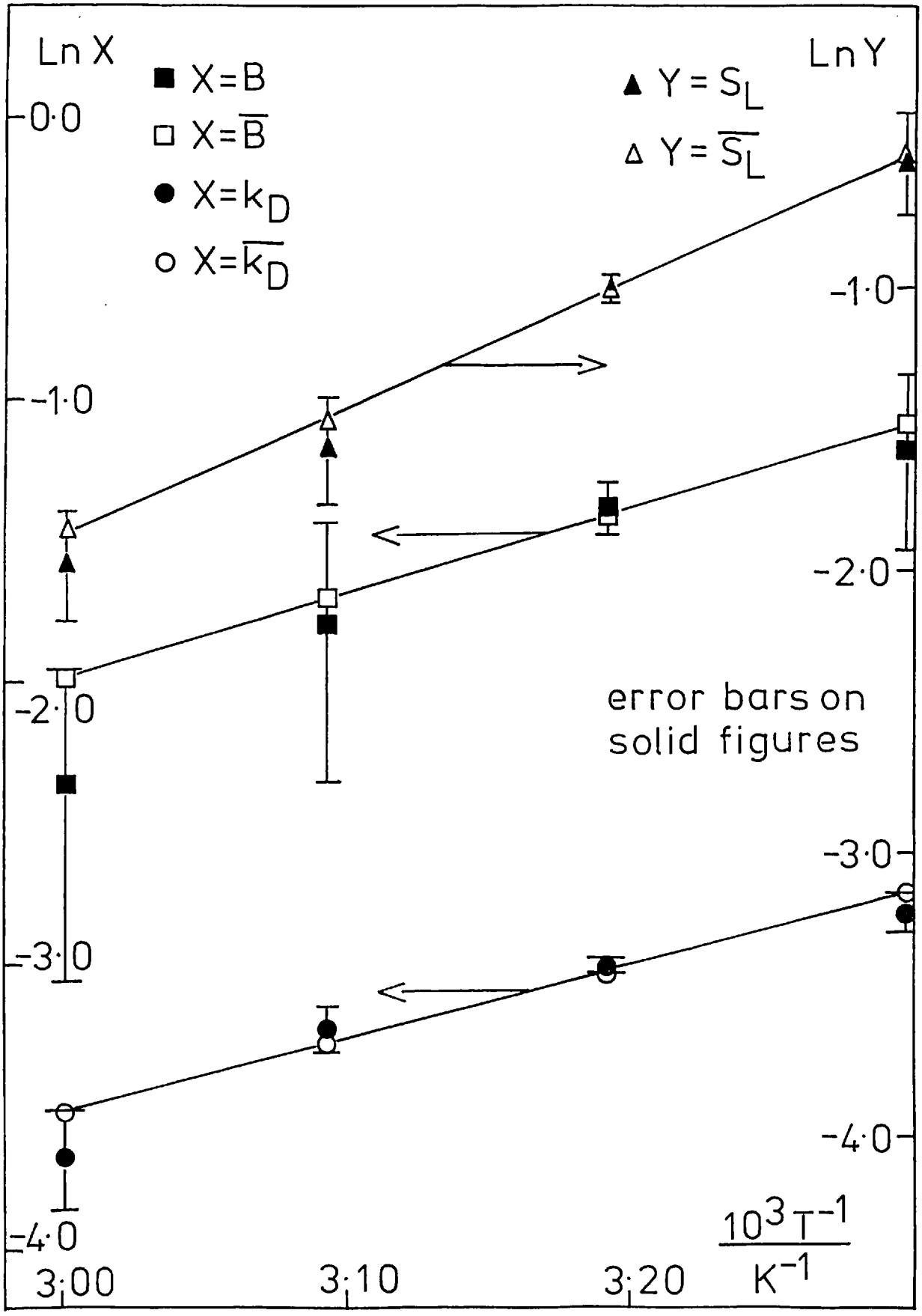


FIG. 5.2 BPAC/PROPANE
VAN'T HOFF PLOTS: k_D, $\overline{k_D}$, B, $\overline{B}$, S_L, $\overline{S_L}$

taken separately the former produce a very good fit to the experimental data but not the "best" fit which is characterised by a minimum mean deviation and is produced by the latter parameters.

Perhaps a small indication that the contrained parameters are more significant is the temperature dependence of C_H' (Table 5.1). The hole saturation constant is expected to decrease with increasing temperature and eventually to disappear when the glass transition is reached. In this respect the C_H' data for 50.1°C and 60.0°C might appear anomalous but for the attendant uncertainty. However, the data for $\overline{C}_H'$ clearly reveal the expected trend.

What this analytical approach has shown is that sorption parameters exist which obey van't Hoff relationships for $\overline{k}_D$, $\overline{B}$ and $\overline{S}_L$ and which can adequately predict the experimental data. For this reason the constrained parameters will be emphasised for the remaining analysis of the BPAC/propane system.

The figures themselves exhibit expected trends with all the parameters decreasing with increasing temperature (with the exception of the values of C_H' for 50.1°C and 60.0°C).

C_H' has decreased by 30-40% (depending on which data are inspected) by raising the temperature by 30°C; this behaviour has been attributed to increased segmental mobility and the consequent disappearance of some microcavities (121). This is not an entirely satisfactory explanation since it would imply that by lowering the temperature of the polymer the microcavity volume, and hence the free volume of the polymer is increased. Furthermore, it might also be expected that C_H' should somehow be related to the coefficient of thermal expansion for the glass and therefore show an <u>increase</u> with increasing temperature, i.e., the volume of the microcavities should increase as the glass expands thereby providing more sites for adsorption. Any such microcavity volume expansion, however, would be extremely small.

C_H' in terms of the original Langmuir isotherm for gas adsorption on a surface represents the maximum possible coverage and should therefore be almost independent of temperature. It is clear then that the Langmuir relationship for gas/vapour sorption in the glassy state is not completely analogous to the relationship for surface adsorption.

The possibility that for higher temperatures the same level of saturation (C_H') in the microcavities is not achieved at high pressures because of steric effects between the more highly excited penetrant molecules is unlikely.

Since C'_H must be a function of the space (or number of sites) available to the penetrant for immobilisation, it is proposed that C'_H is a function of the free volume frozen into the polymer below T_g. It is further proposed that since the total free volume of the polymer is regarded as effectively constant below the glass transition temperature a proportion of the free volume is relatively mobile and somewhat analogous in its behaviour to the free volume above T_g. The residual proportion of free volume is completely immobilised.

The mobile free volume will contribute to the transport of the Henry's Law penetrant population; the immobile free volume is responsible for the Langmuir penetrant population. The proportion of mobile free volume increases with the temperature until T_g is reached when the free volume becomes totally mobile in the rubbery state. As the temperature is lowered, the proportion of immobile free volume increases, more Langmuir immobilisation becomes possible and so C'_H increases. The total free volume remains essentially unaltered.

This model suggests that, at low enough temperatures (not necessarily absolute zero), sorption would be described simply by a Langmuir relationship, the Henry's Law component being absent.

The enthalpies of sorption for the BPAC/ propane system are presented in Table 5.2

Table 5.2 Enthalpies of sorption for BPAC/propane

Enthalpy of dissolution, $\Delta\overline{H}_D$; enthalpy of "hole-filling", $\Delta\overline{H}_H$; heat of solution (C = 0), $\Delta\overline{H}_{S(C=0)}$

	$\Delta\overline{H}_D$/kJ.mole^{-1}	$\Delta\overline{H}_H$/kJ.mole^{-1}	$\Delta\overline{H}_{S(C=0)}$/kJ.mole^{-1}
From k_D, C'_H, B	- 20.8 (± 5%)	- 33.5 (± 34%)	- 40.6 (± 22%)
From $\overline{k}_D$, $\overline{C}'_H$, $\overline{B}$	- 21.7	- 25.2	- 37.3

The three enthalpies were calculated from equation (2.41), (2.42) and (2.45) using a least-squares plot. The errors for the values based on the original sorption parameters were determined graphically from the error bars (Fig. 5.2).

The observation that $\Delta\bar{H}_D < \Delta\bar{H}_H < \Delta\bar{H}_{S(C=O)}$ in terms of absolute magnitude appears to be generally consistent with the results of other investigations (114, 121, 128) and a comparison is made in Table 5.3.

The enthalpies were derived from sorption parameters presented in each of the references quoted using the method of least squares for the appropriate equations. For the first three systems in the table, the sorption parameters were apparently determined using the "graphical method" favoured by Vieth and Sladek (72) which was discussed in Chapter 3. Stern and DeMeringo (138) studied the CO_2/ cellulose acetate system at several temperatures and analysed the data using not only the graphical method but also a non-linear regression computer programme of the type used in this project. This produced two sets of sorption parameters and hence two corresponding sets of enthalpies are presented for that system with the upper set being derived from data obtained by the graphical method. The figures for the ethyl cellulose system (which was studied at six or seven temperatures for each penetrant) were calculated from data presented by Chan, Koros and Paul (114) who carefully analysed the earlier experimental results of Barrer, Barrie and Slater (113).

Table 5.3 Enthalpy comparisons

(Same symbols as for Table 5.2)

System	$\Delta\bar{H}_D$/kJ.mole^{-1}	$\Delta\bar{H}_H$/kJ.mole^{-1}	$\Delta\bar{H}_{S(C=O)}$/kJ.mole^{-1}
CH_4/glassy polystyrene (121)	- 6.3	-15	-26
CH_4/oriented polystyrene (128)	- 2.2	-14	-23
CO_2/polycarbonate (128)	-24	-13	-21
CO_2/cellulose acetate (138)	-24 -25	-24 -28	-27 -29
n-C_4H_{10}/ethyl cellulose (114)	-18	-14	-36
i-C_4H_{10}/ethyl cellulose (114)	- 814?	- 9.4	-35
n-C_5H_{12}/ethyl cellulose (114)	-30	-46	-44
i-C_5H_{12}/ethyl cellulose (114)	-21	-32	-47
neo-C_5H_{12}/ethyl cellulose (114)	-38	-39	-40

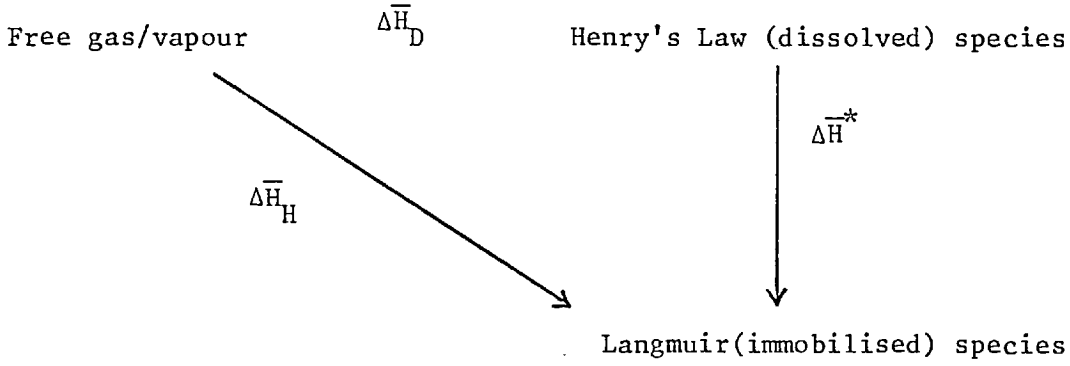
In general, $|\ \Delta\overline{H}_D\ | < |\ \Delta\overline{H}_H\ | < \Delta H_{S(C=O)}|$ is true for most of the systems presented within the scatter of the semilog plots. Perhaps the most serious discrepancy occurs for the CO_2/polycarbonate system. However, it must be pointed out that this system (and the two systems mentioned above it in Table 5.3) was studied for only three temperatures and this seriously affected the accuracy of the enthalpies. In this particular case the range of values for $\Delta\overline{H}_D$ was estimated as being between -6 and -32 $kJ.mole^{-1}$. Fortunately the scatter in most of the other systems suffered from far less scatter in the semilog plots.

No simple relationship exists between $\Delta\overline{H}_D$, $\Delta\overline{H}_H$ and $\Delta\overline{H}_{S(C=O)}$ because of the fact that C'_H is a strong function of temperature. If, as in the simple Langmuir model, C'_H is treated as temperature independent, then it is easily shown that

$$\Delta\overline{H}_{S(C=O)} = \frac{k_D.\ \Delta\overline{H}_D + C'_H.B.\ \Delta\overline{H}_H}{k_D + C'_H.B} \qquad \ldots (5.5)$$

and therefore $\Delta\overline{H}_{S(C=O)}$ must lie between the limits of $\Delta\overline{H}_H$ and $\Delta\overline{H}_D$. The fact that $\Delta\overline{H}_{S(C=O)}$ is generally greater than both $\Delta\overline{H}_H$ and $\Delta\overline{H}_D$ is a reflection of the strong temperature dependence of C'_H.

The enthalpy of hole-filling can be regarded as the sum of the enthalpy of dissolution, $\Delta\overline{H}_D$ and the enthalpy change in going from the dissolved state to the immobilised state, designated $\Delta\overline{H}^*$



$$\Delta\overline{H}_H = \Delta\overline{H}_D + \Delta\overline{H}^* \qquad \cdots (5.6)$$

The classic Langmuir expression for a gas adsorbing as a monolayer onto a surface can be derived by introducing rate constants for sorption (k_1) and desorption (k_{-1}), and postulating that adsorption depends on the gas pressure, P, and the number of non-adsorbed sites whilst desorption depends solely on coverage, θ.

The rate of attainment of equilibrium, R, is then given by

$$R = k_1 P(1 - \theta) - k_{-1}\theta \qquad \ldots (5.7)$$

At equilibrium, R = 0 and (5.7) re-arranges to give the familiar Langmuir isotherm,

$$\theta = \frac{BP}{1 + BP} \qquad \ldots (5.8)$$

where

$$B = \frac{k_1}{k_{-1}} \qquad \ldots (5.9)$$

Tshudy and von Frankenberg (131) have discussed the dual mode sorption mechanism in kinetic terms and suggested that in the context of microcavities dispersed in a glassy matrix, the pressure term in (5.7) should be replaced by a concentration term for the dissolved species, i.e. $k_D P$. Equation (5.9) is then replaced by

$$B = \frac{k_1 \cdot k_D}{k_{-1}} \qquad \ldots (5.10)$$

where k_1 and k_{-1} must be redefined in terms of sorption and desorption between the immobile and dissolved states.

Taking logs and differentiating (5.10) w.r.t. T^{-1} yields

$$\Delta\bar{H}_H = \frac{\partial \ln (k_1/k_{-1})}{\partial (1/T)} - \Delta\bar{H}_D \qquad \ldots (5.11)$$

Comparison with (5.6) produces

$$\Delta\bar{H}^* = \frac{\partial \ln (k_1/k_{-1})}{\partial (1/T)} \qquad \ldots (5.12)$$

From equation (5.6) it is clear that if $|\Delta\bar{H}_H| > |\Delta\bar{H}_D|$ is generally true, then $\Delta\bar{H}^*$ is negative.

Total enthalpy of solution

The graph of $\Delta\bar{H}_S$ vs. total penetrant concentration is shown in Fig. 5.3 and was determined using the Clapeyron-Clausius equation (2.43). Isotherms were theoretically generated using the constrained sorption parameters and values of P for each isotherm were calculated for a series of constant values of C. The value of $\Delta\bar{H}_S$ for each value of C was then determined using a least-squares method for equation (2.43).

The graph passes through a minimum at approximately C = 0.9 $cm^3 STP.cm^{-3}$; the reason for this feature is not known but may be associated with the

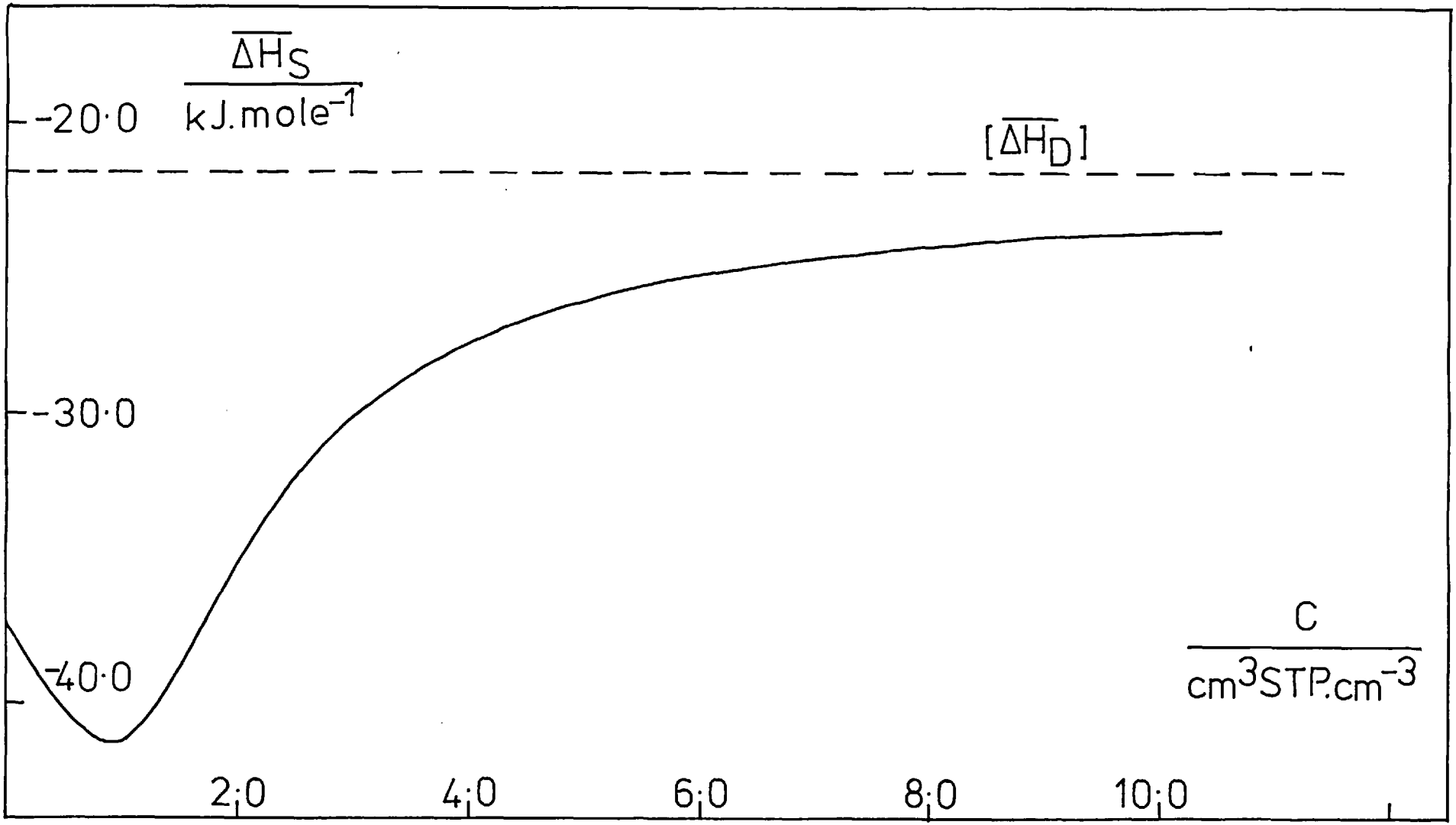


FIG. 5.3
$\overline{\Delta H_S}$ vs. CONCENTRATION

temperature dependence of C_H'. At higher concentrations the Henry's Law mode predominates and the graph tends towards the asymptote representing the value of $\Delta\overline{H}_D$ (the dashed line in Fig. 5.3).

5.1.2 Sorption kinetics

The results for $\overline{D}_s$ (diffusion coefficient derived from sorption kinetics) are listed in Chapter 8 (Appendix 8.4) and are illustrated as a function of total concentration in Figs. 5.4 and 5.5. The data were calculated from "half-times" using equation (2.29).

It was initially attempted to analyse the data in terms of the dual mode sorption theory incorporating the constraint of total immobilisation of the Langmuir penetrant population. Using the weighted mean equation for sorption kinetics (2.35) two equations, which have been discussed in Chapter 2, were developed.

The first, equation (2.55) was eventually found to be impractical since it required the drawing of tangents to curves based on scattered experimental data.

The second, equation (2.58) was found to be far more satisfactory. D_m, the diffusivity for the mobile species, could be determined from $\overline{D}_s$ and the sorption parameters k_D, C_H' and B.

However, the values of D_m obtained from equation (2.58) decreased smoothly with concentration. Furthermore, for each temperature it was not possible to provide any sort of fit to the experimental data using a single mean value of D_m.

It was thought that perhaps by varying the sorption parameters to the extremes of their respective uncertainties it might be possible to force some sort of fit to the experimental data. It was found, however, that the theoretical line generated by a single mean value of D_m was relatively insensitive to variations in k_D, C_H' and B.

In order to force some sort of fit to the experimental data at each of the four temperatures, the sorption parameters used for the evaluation of D_m had to be distorted well beyond their known uncertainties.

For this reason, the notion of mobility for the Langmuir population was developed, independently of Paul (123) and Petropoulos (124). Equation (2.58) was modified to include the term D_i (the diffusivity of the "immobile" species), and the final analytical form is described by equations (2.66), (2.67) and (2.68).

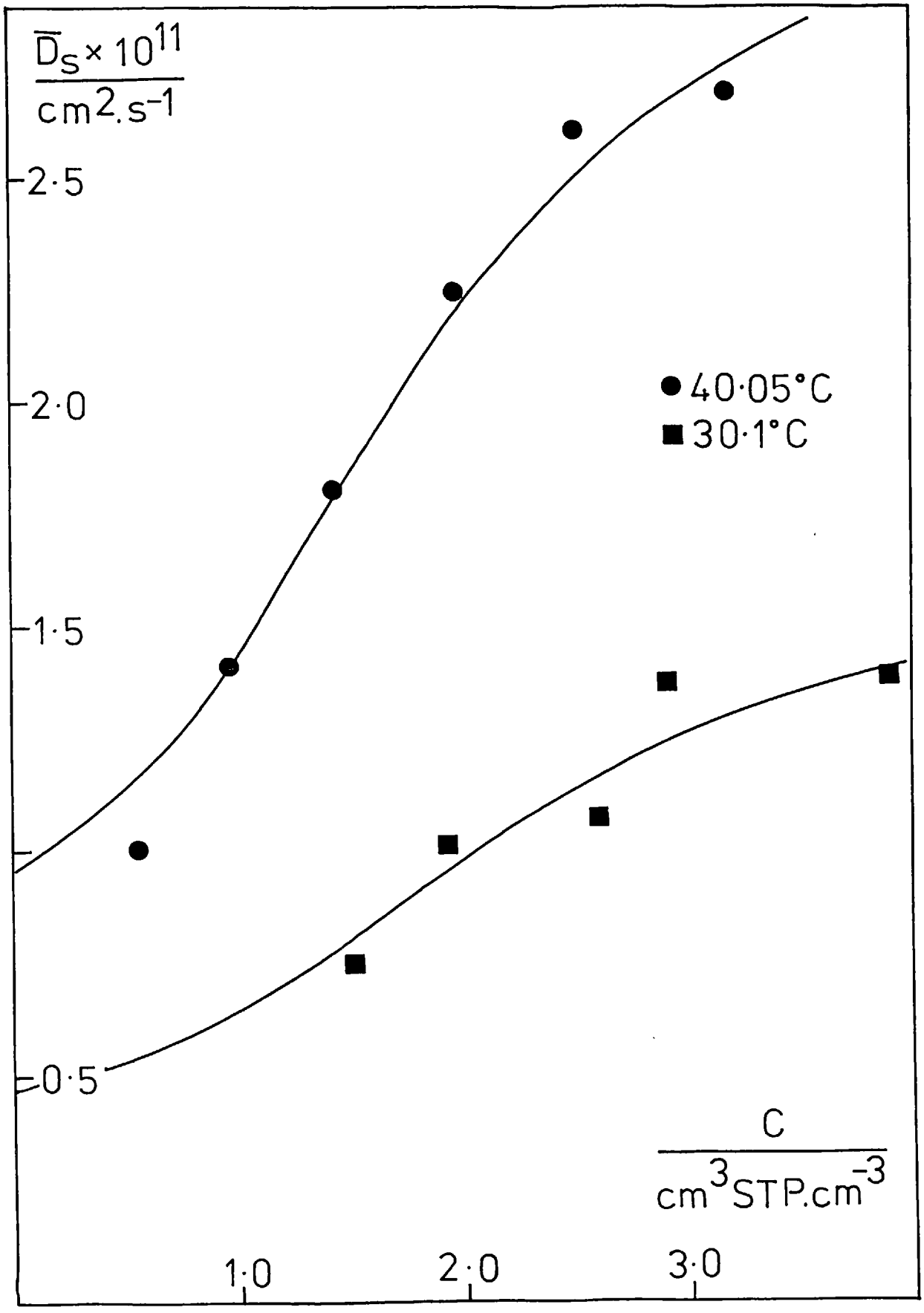


FIG. 5.4 BPAC / PROPANE

$\overline{D}_s$ v. C (30·1°C AND 40·05°C)

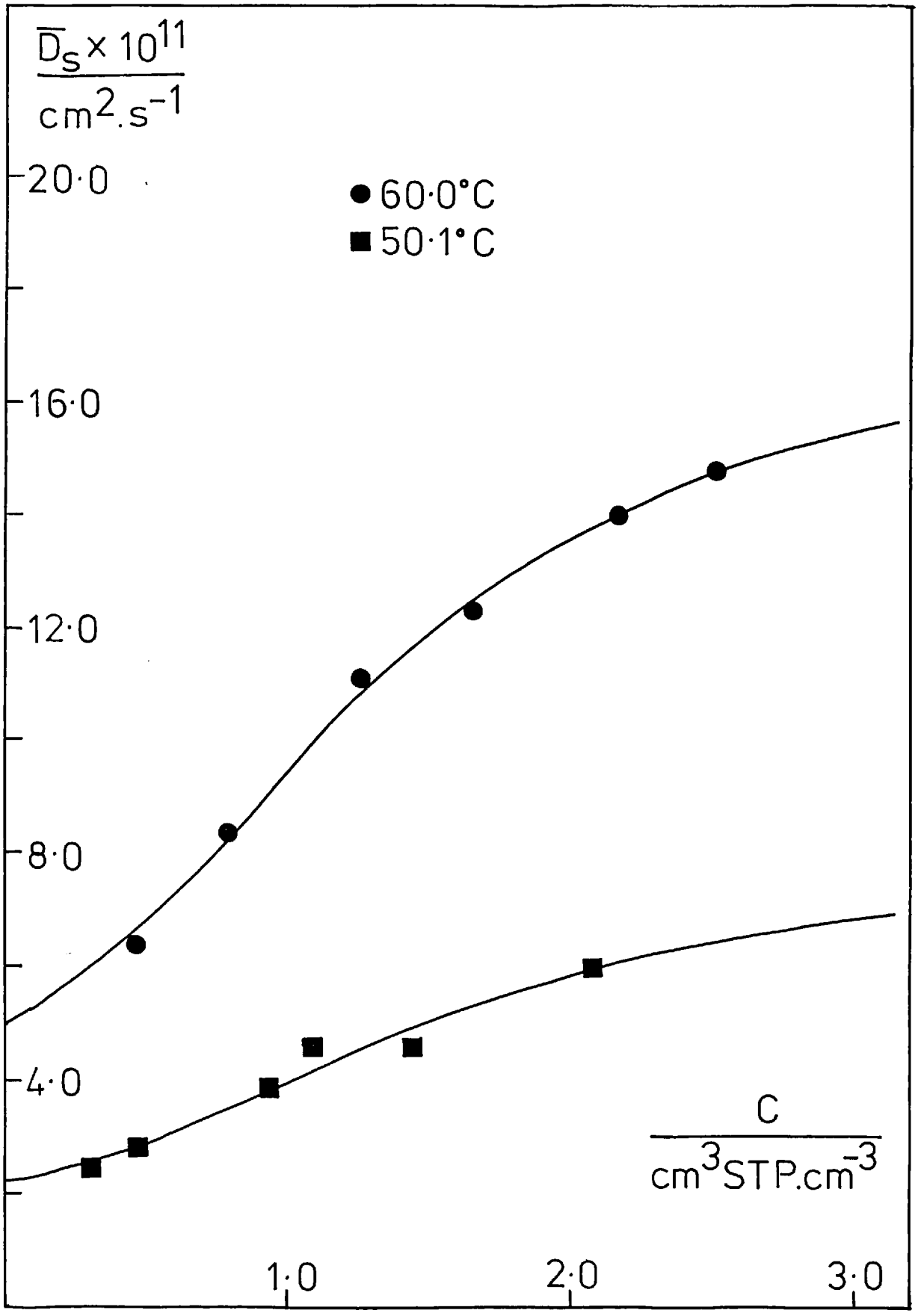


FIG. 5.5 BPAC / PROPANE

$\overline{D}_s$ v. C (50·1°C AND 60·0°C)

The results are presented in Table 5. They were derived using the constrained sorption parameters and were used to compute the sigmoidal solid lines in Figs. 5.4 and 5.5. The uncertainties were derived statistically from the scatter in the plots illustrated in Fig. 5.6. Any variation of the sorption parameters made only marginal differences to the theoretical lines. The constrained parameters produced the best visual fit however.

Table 5.4 Diffusion coefficients for BPAC/propane

For the Henry's Law (mobile) population, D_m; for the Langmuir ("immobile") population, D_i; and the overall diffusivity as $C \to 0$, $D_{C=0}$.

$T/^oC$	$10^{11}.D_m/cm^2.s^{-1}$	$10^{12}.D_i/cm^2.s^{-1}$	$10^{11}D_{C=0}/cm^2.s^{-1}$	D_i/D_m
30.1	1.74(± 0.12)	3.16(± 2.20)	0.471(± 0.183)	18.2%
40.05	3.46(± 0.10)	5.74(± 1.64)	0.960(± 0.128)	16.5%
50.1	8.29(± 0.35)	10.2 (± 3.76)	2.23 (± 0.255)	12.3%
60.0	18.38(± 0.20)	18.7 (± 4.13)	4.98 (± 0.300)	10.2%

Values of $D_{C=0}$ were determined using a simple weighted equation derived from equation (2.61),

$$D(C) = D_m \cdot \frac{\partial C_m}{\partial C} + D_i \cdot \frac{\partial C_i}{\partial C} \qquad \ldots (2.61)$$

This can be re-written as

$$D(C) = \left(D_m \cdot \frac{\partial C_m}{\partial P} + D_i \cdot \frac{\partial C_i}{\partial P}\right) / \frac{\partial C}{\partial P} \qquad \ldots (5.13)$$

As $C \to 0$, equation (5.13) becomes

$$D_{C=0} = \frac{D_m.k_D + D_i.C'_H.B}{k_D + C'_H.B} \qquad \ldots (5.14)$$

which was used to evaluate $D_{C=0}$.

Fig. 5.6 illustrates the method by which values of D_m and D_i were obtained. Equation (2.66) is re-arranged to give

$$\frac{\overline{D}_s}{Y} = \frac{X}{Y} \cdot D_m + D_i \qquad \ldots (5.15)$$

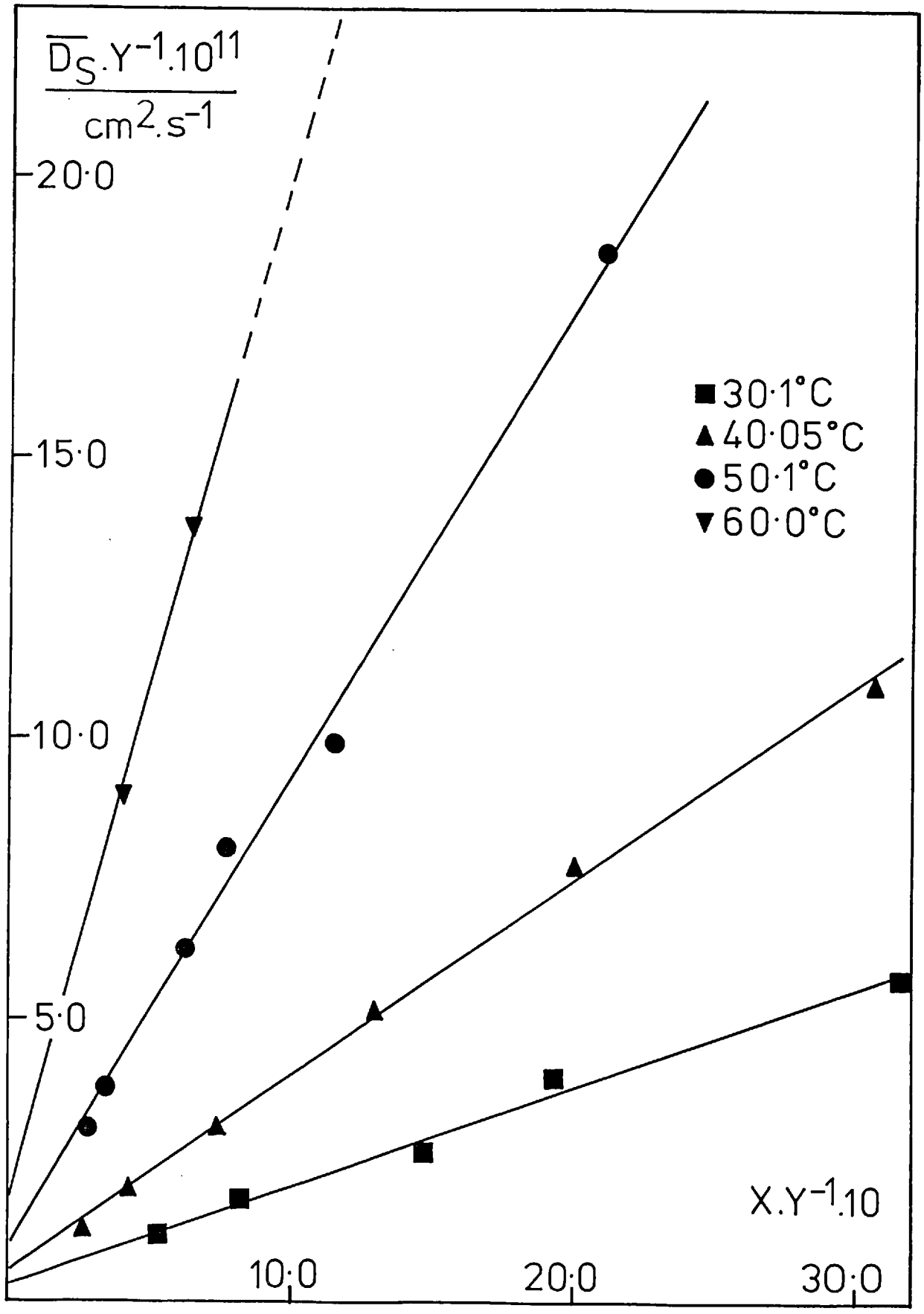


FIG. 5.6
$\overline{D_S}.Y^{-1}$ vs. $X.Y^{-1}$

A graph of $\bar{D}_s.Y^{-1}$ vs. $X.Y^{-1}$ for each temperature produces a linear plot of slope D_m and intercept D_i. X and Y are dimensionless functions described by equations (2.67) and (2.68). The linearity of these plots plus the excellent fit of the theoretical lines to the experimental data in Figs. 5.4 and 5.5 effectively justify the important assumption of partial mobility for the Langmuir species.

The ratio of D_i/D_m has been included to illustrate its dependence on temperature. Both D_m and D_i behave normally and increase with temperature, but clearly D_m increases more rapidly than D_i. One might expect D_i/D_m to tend towards zero as the glass transition is approached, although a crude extrapolation indicates a value of 2-3% at BPAC's T_g.

Other workers have determined values of D_m and D_i for other systems using approaches markedly different from the one used in this project. Koros, Paul and Rocha (119) found D_i/D_m to be approximately 10% for CO_2/polycarbonate at 35°C although Koros, Chan and Paul (152) later revised this figure to 7.8%. The same authors also investigated methane, argon, nitrogen and helium transport in polycarbonate at 35°C and calculated D_i/D_m to be 11.5, 18.0, 28.9 and 133% respectively. (The last figure, however, they considered to be anomalous and put it statistically closer to, though necessarily greater than 100%).

Assink's work on the ammonia/polystyrene system (136) produced an estimate of $\sim$ 5% for D_i/D_m at 23°C.

The temperature dependences of D_m, D_i and $D_{C=0}$ are presented in Table 5.5 and illustrated in Figure 5.7.

Table 5.5 Activation energies for diffusion for BPAC/propane

Energy of diffusion for Henry's Law species, E_{D_m}; for the Langmuir species, E_{D_i}; overall activation energy for diffusion at C = 0, E_{DO}.

E_{D_m} /kJ.mole^{-1}	E_{D_i} /kJ mole^{-1}	E_{DO} /kJ.mole^{-1}
66.8 (± 5%)	49.8 (± 48%)	66.6 (± 11%)

The Arrhenius plots are remarkably linear and uncertainties in the E_D's determined from the statistical scatter in the points are consequently misleadingly low. The uncertainties which are quoted in Table 5.5 were

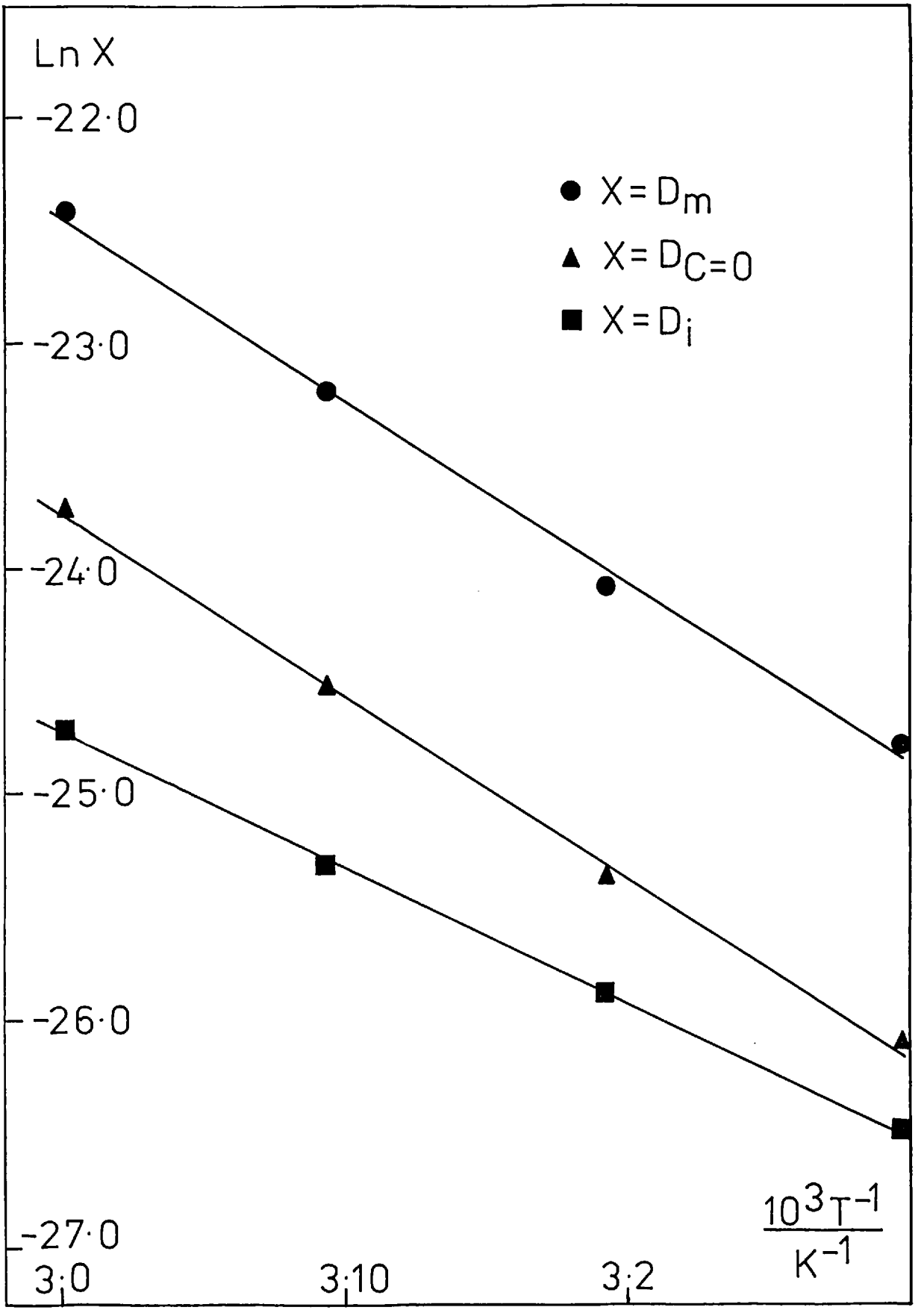


FIG. 5.7 BPAC/PROPANE
ARRHENIUS PLOTS: D_m, D_i, $D_{C=0}$

assessed graphically using the estimated errors given in Table 5.4.

E_{D_m} is so close to E_{DO} that one wonders if this is more than coincidence. A requirement for such a condition to be true is that

$$\frac{D_{(C=O)}}{D_m} = \text{constant, } K' \qquad \ldots (5.16)$$

which in terms of (5.11) requires

$$\frac{(D_m/D_i)\ C'_H\ B + k_D}{C'_H\ B + k_D} = K' \qquad \ldots (5.17)$$

to be true for all temperatures. Unfortunately, reliable data are not currently at hand from other systems to test such a hypothesis.

Chan, Koros and Paul (114) have estimated values of E_{D_i} and E_{D_m} for several hydrocarbons in ethyl cellulose. The Arrhenius plots produced for D_i suffer from serious scatter however and one is hesitant to attach too much significance to the results. One of the more convincing plots indicates $E_{D_m} = 32$ kJ.mole^{-1} and $E_{D_i} = 60$ kJ.mole^{-1} (for n-pentane). Other plots indicate values for E_{D_i} sometimes smaller, sometimes larger than that for E_{D_m}. It was also interesting to note that for neo-pentane, D_i was estimated as zero, i.e., the Langmuir population was surmised to be totally immobilised.

The physical processes associated with E_{D_m} and E_{D_i} are not self-evident. One might have expected E_{D_m}, the activation energy of diffusion for the Henry's Law species to be less than E_{D_i}, which is associated with the Langmuir species, reflecting the difference in the mobilities of the two species.

It is unlikely that E_{D_i} characterises an activated transition from one microcavity to another. It is more reasonable to suggest that the parameter is associated with a transition between the immobile and mobile states.

Thus for the Henry's Law species,

$$\{\text{Mobile molecule, dissolved in matrix}\} \xrightarrow{E_{D_m}} \{\text{Activated transition}\} \rightarrow \{\text{Mobile molecule, dissolved in matrix}\}$$

and for the Langmuir species,

$$\{\text{Immobile molecule, in microcavity}\} \xrightarrow{E_{D_i}} \{\text{Activated transition}\} \rightarrow \{\text{Mobile molecule dissolved in matrix}\}$$

For E_{D_i} to differ from E_{D_m} would imply that the two activated transition states are not the same. Interpeting the results in terms of this model,

a penetrant molecule requires less energy to enter into a dissolved state adjacent to the wall of a microcavity than it does to diffuse through the matrix.

The lower value of D_i compared to D_m can be attributed to entropy factors which reduce the probability of escape from the microcavity. This interpretation of the results must, however, be treated with some degree of caution; it is conceivable that E_{D_i} and E_{D_m} do not differ significantly within the experimental errors of measurement.

A simple extrapolation shows that D_i would be greater than D_m only at temperatures below $-30^{\circ}C$.

One can reasonably expect a single penetrant molecule to spend part of its lifetime in the dissolved state and part in microcavities. The relative amount of time spent in each depends on the number of microcavities encountered (thermodynamic considerations apart), which itself could be sensitive to the sample's thermal history. In this respect thermal pretreatment might be expected to affect those parameters associated with the Langmuir species more than those which characterise the Henry's Law species.

5.2 PDMS

Before proceeding to examine the sorption properties of the PDMS-g-PVAc graft copolymer (section 5.3), the solution properties of propane in PDMS itself were characterised for the temperature range over which the graft was to be studied.

5.2.1 Equilibrium sorption

The data are shown in Fig. 5.8 and are listed in Appendix 8.5. Good straight lines were obtained for all the temperatures examined, although the possibility of very slight curvature concave to the concentration axis (symptomatic of membrane swelling at high concentrations) could not be completely discounted at $T = 1.5^{\circ}C$.

The solubility coefficients are presented in Table 5.6. For the analysis of the PDMS-g-PVAc data, interpolations of these values will be employed based upon the van't Hoff plot which is shown in Fig. 5.9.

The enthalpy of solution was determined as -17.18 ($\pm$ 0.10) kJ/mole, which is within 1% of the value previously recorded in this laboratory (153).

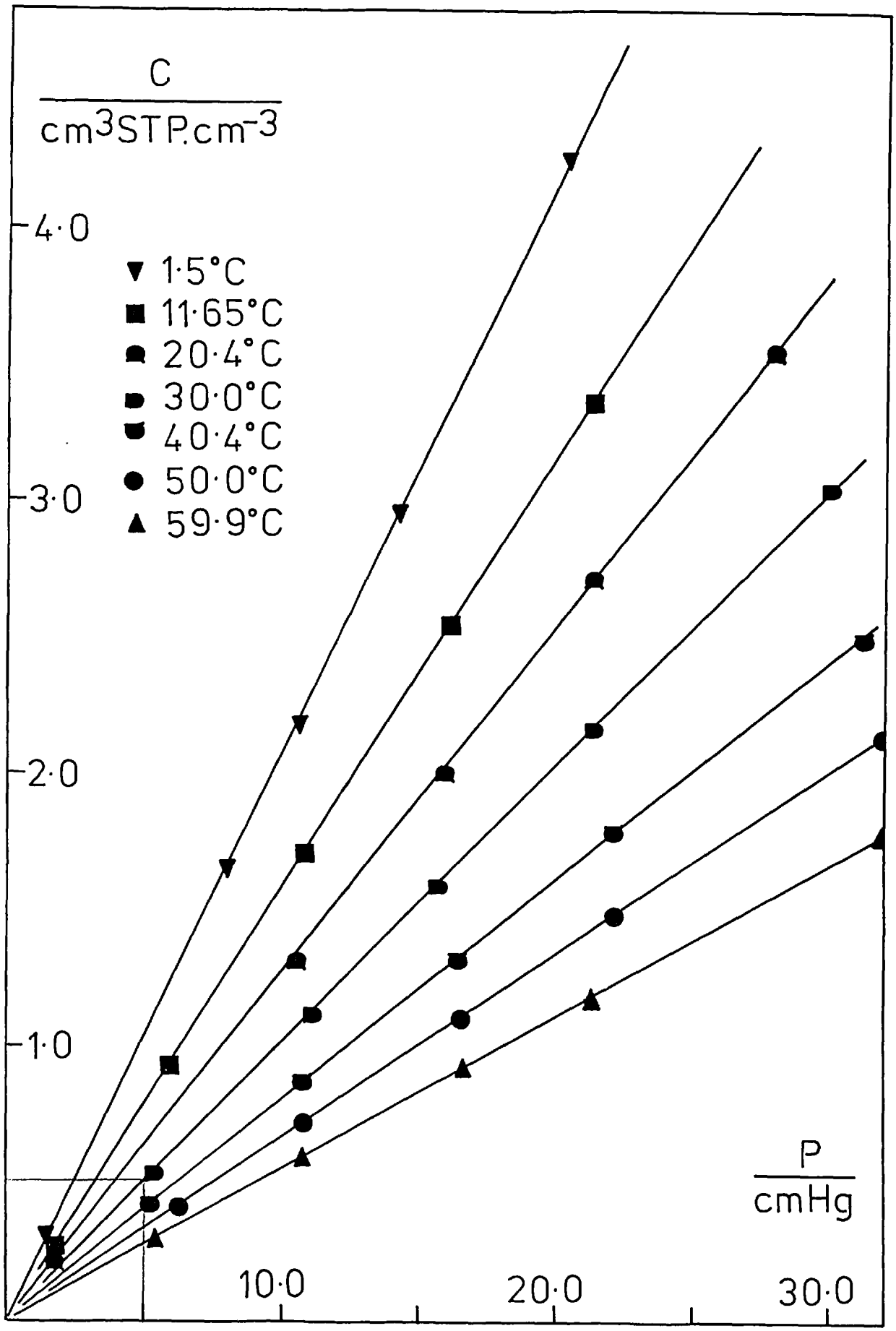


FIG. 5.8 PDMS/PROPANE ISOTHERMS

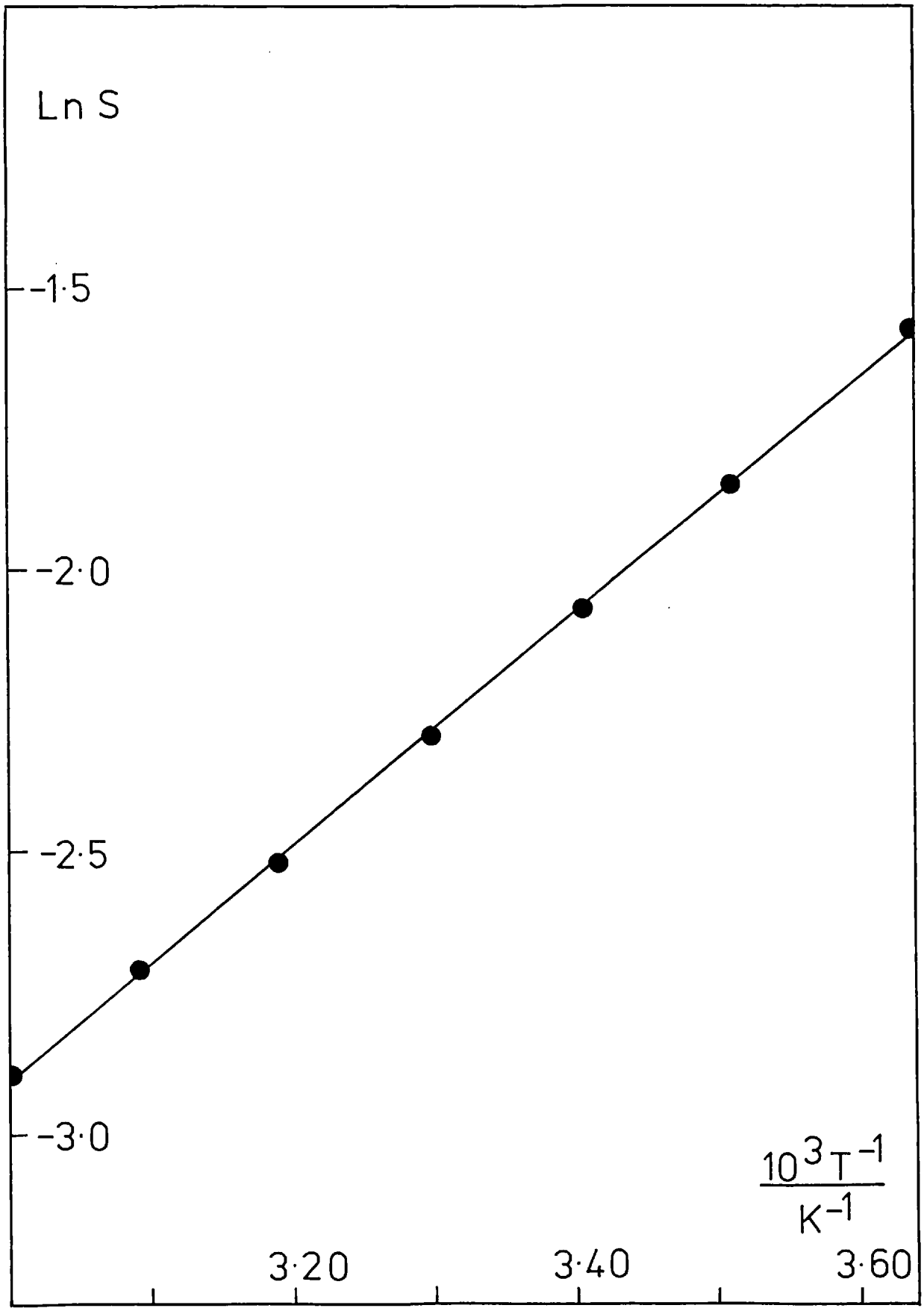


FIG. 5.9 PDMS/PROPANE
VAN'T HOFF PLOT

Table 5.6 Solubility coefficients for PDMS/propane

T/°C	1.5	11.65	20.4	30.0	40.4	50.0	59.9
$10^2.S$ / ($\frac{cm^3 STP}{cm^3.cmHg}$)	20.74	15.73	12.61	10.08	8.07	6.66	5.55

5.3 PDMS-g-PVAc

Sheer (27) has shown that solubility coefficients for water in PDMS-g-PVAc copolymers obey a simple additivity rule. The solubility coefficient of a particular sample is adequately described by the sum of the coefficients of the two pure components weighted according to their respective volume fractions so that

$$S_{AB} = \Phi_A.S_A + \Phi_B.S_B \qquad (5.18)$$

For the purpose of analysis, it is assumed that the solubility addivity rule also holds for propane as penetrant.

Isotherm data for PVAc itself were deduced from the copolymer sorption data multiplying (5.18) by P (pressure) and re-arranging:

$$C_{PVAc} = \frac{C_{Copolymer} - 0.558.\ S_{PDMS}.P}{0.442} \qquad \ldots (5.19)$$

It becomes clear that the mean deviation for values of C_{PVAc} will be effectively double that of values of $C_{Copolymer}$.

5.3.1 Equilibrium sorption

The experimental data for the graft copolymer and the "extracted" PVAc are listed in Appendix 8.6 and are shown in Figs. 5.10 and 5.11. The main feature of these results is that the Langmuir-type curvature present below T_g vanishes above T_g to give normal Henry's Law sorption. A cursory observation of Fig. 5.10 might indicate that there was little significant curvature in the isotherms below T_g. A more careful scrutiny establishes that it is impossible to draw a straight line through the data points and the origin given the experimental accuracy of the system (c.f. for example the isotherms of 5.10 above T_g or those of Fig. 5.8). One can confidently state that significant curvature of the Langmuir type is present in the graft copolymer below T_g.

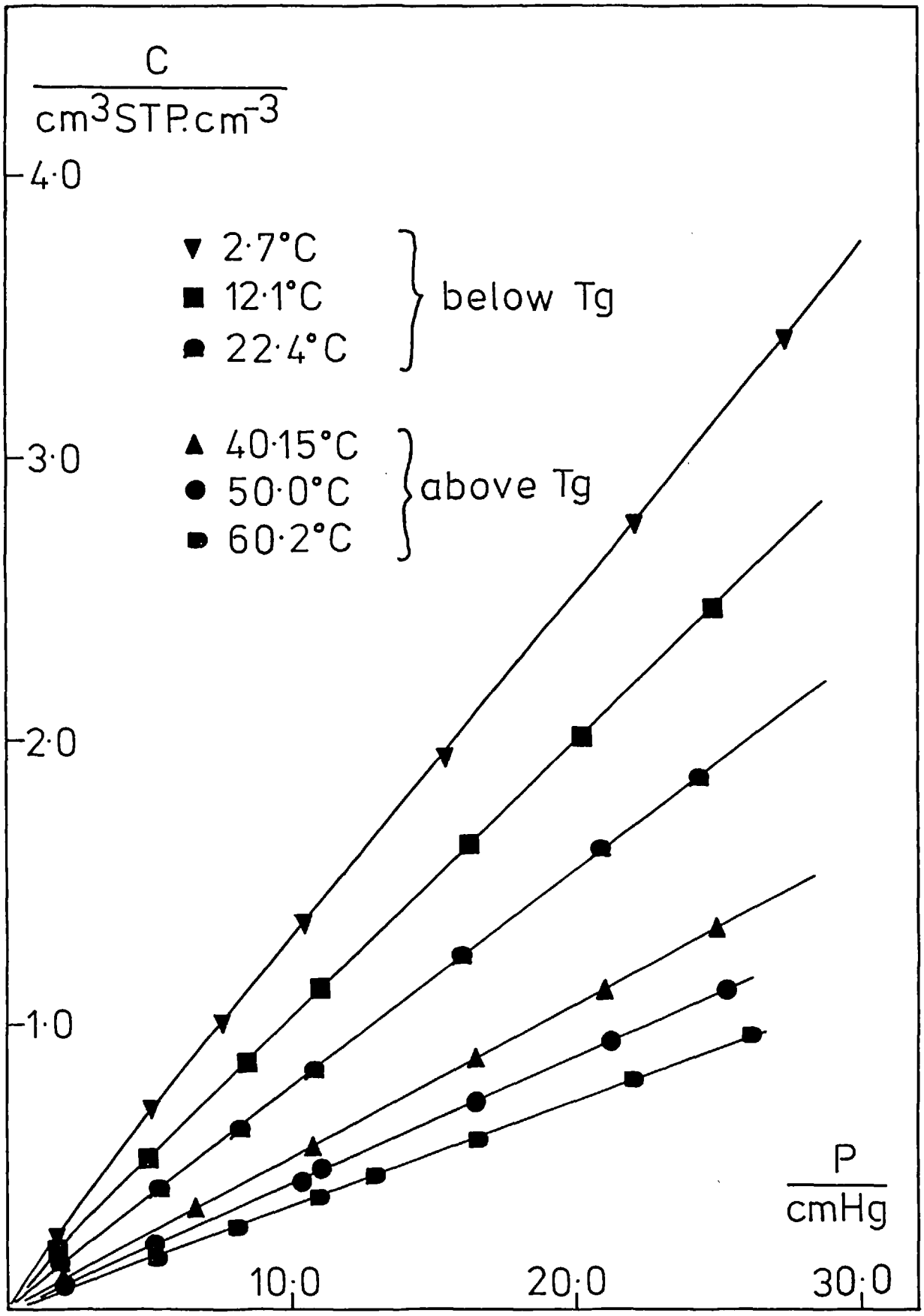


FIG. 5.10 PDMS-g-PVAc/PROPANE SORPTION ISOTHERMS

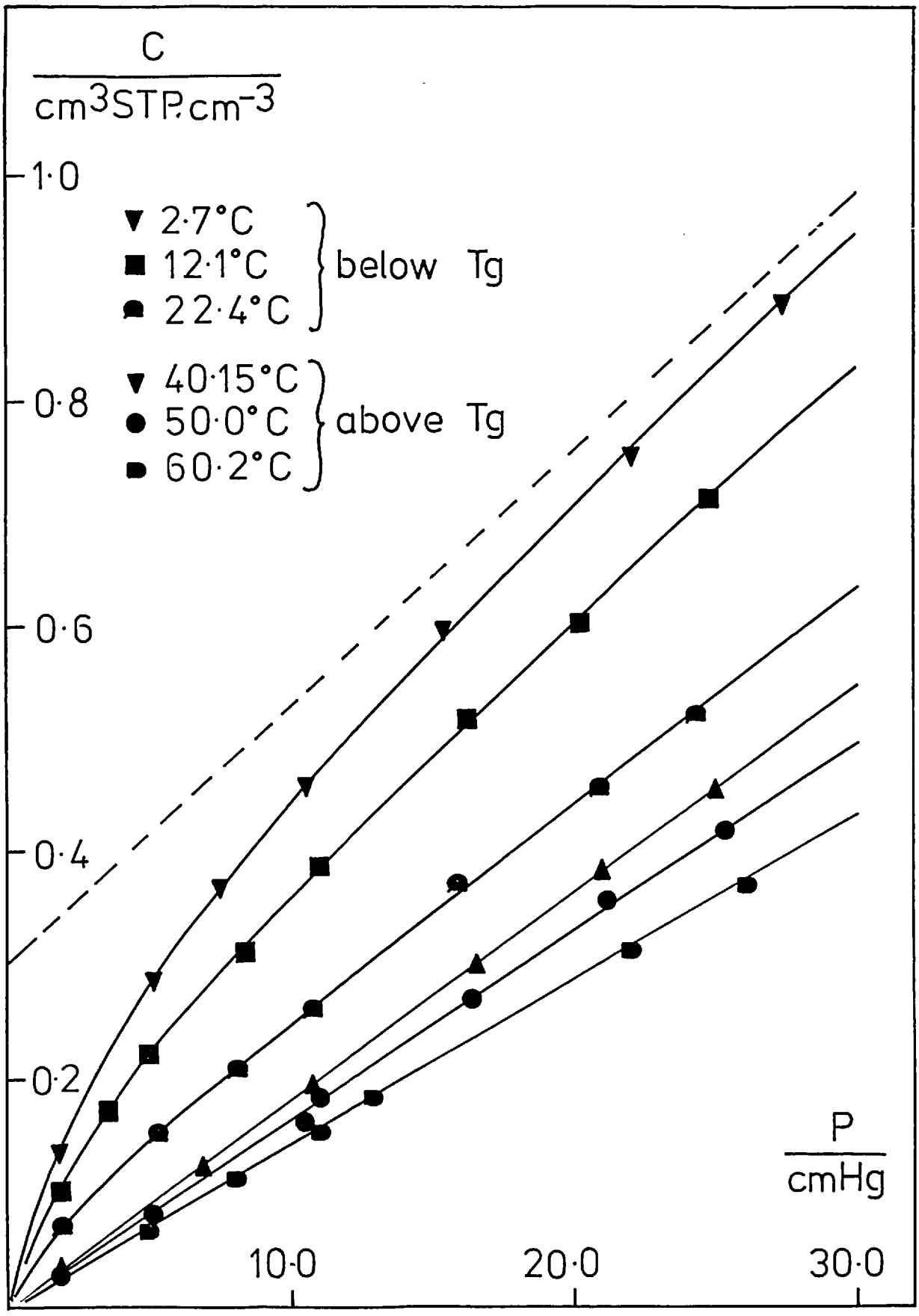


FIG. 5.11 PVAc("EXTRACTED")/PROPANE SORPTION ISOTHERMS

A dual mode sorption analysis has been made of the isotherms in Fig. 5.10 and the "extracted" isotherms of Fig. 5.11. The results are presented in Table 5.7, together with the solubility coefficients for PDMS interpolated from the results presented in Table 5.6.

Table 5.7 Sorption parameters for propane in PDMS-g-PVAc and "extracted" PVAc

Symbols and units as for Table 5.1

		Below T_g			Above T_g		
T/°C		2.7	12.1	22.4	40.15	50.0	60.2
(PDMS: $10^2.S$		19.92	15.56	12.09	8.14	6.66	5.47)
PDMS-g-PVAc:	$10^2.k_D$	12.12 (± 0.5%)	9.68 (± 1%)	7.58 (± 1%)	5.35 (± 1%)	4.45 (± 1%)	3.69)± 1%)
	C'_H	0.133 (± 12%)	0.079 (± 19%)	0.032 (± ∿50%)	-	-	-
	B	0.255 (± 21%)	0.316 (± 35%)	0.464 (± >100%)	-	-	-
	$10^2.S_L$	15.51 (± 2%)	12.17 (± 4%)	9.07 (-)	-	-	-
PVAc("extracted"):	10^2k_D	2.29 (± 5%)	2.24 (± 5%)	1.89 (± 5%)	1.83 (± 1%)	1.66 (± 5%)	1.45 (± 3%)
	C'_H	0.300 (± 13%)	0.179 (± 19%)	0.073 (± ∿50%)	-	-	-
	B	0.257 (± 22%)	0.315 (± 36%)	0.459 (± >100%)	-	-	-
	$10^2.S_L$	9.99 (± 8%)	7.86 (± 14%)	5.22 (-)	-	-	-

Since the Langmuir component in the graft copolymer isotherms is small, there are considerable errors attached to the dual mode sorption parameters. However, it is gratifying that the values of B obtained from both analyses are the same, and further that the values of C'_H are in the ratio of 0.442:1 which is the volume fraction of PVAc in the graft copolymer.

The isotherm for "extracted" PVAc at 22.4°C appears anomalous with an apparently low value of k_D (see Fig. 5.13). This may be due to the experimental uncertainty; on the other hand interpretation of the results

in the region of T_g is complicated by the possible existence of a two-phase glassy/rubbery structure over a certain range of temperature. Thus Meares (18,19) found anomalous sorption behaviour for helium, neon and hydrogen in PVAc just below the glass transition.

From the accuracy of the analysis it is not possible to comment with any degree of certainty on the temperature variation of B.

The system has suffered from two distinct disadvantages:

(i) Propane sorbs more strongly in PDMS than in PVAc hence a given uncertainty in concentration for the copolymer is proportionately larger for the PVAc fraction when it is "extracted" (scaled up to unit volume fraction).

(ii) The determination of sorption parameters to a high degree of accuracy requires the experimental data to be commensurately precise and this has not been possible in this project, principally because of (i). Furthermore, as C'_H and B become progressively smaller, they consequently become more difficult to estimate. The results reflect this.

The results are therefore best regarded in qualitative rather than quantitative terms. Nevertheless they demonstrate the presence of a Langmuir population just below T_g and its disappearance just above the transition.

It would be an advantage to repeat the measurements with a gas which showed a higher preferential sorption for the PVAc component and covering a wider temperature range.

For the sake of completeness, the van't Hoff plots of k_D and S_L for the graft copolymer and for PVAc are presented in Figs. 5.12 and 5.13. It was felt that a plot for B would not yield any significant results.

In Fig. 5.12, the semilog plot of k_D for the graft copolymer at first glance suggests that it could be adequately described by a single straight line regardless of the glass transition. This may be the case, but it is just beyond the bounds of the experimental uncertainty and it is believed that the overwhelming influence of the PDMS is masking the real effect which is revealed in Fig. 5.13.

Meares' (19) semilog plots for helium hydrogen and neon solubility in PVAc were linear above T_g but showed distinct curvature and a minimum just below the transition. This trend suggested by the dashed line in Fig. 5.13 seems consistent with Meares' results at least qualitatively.

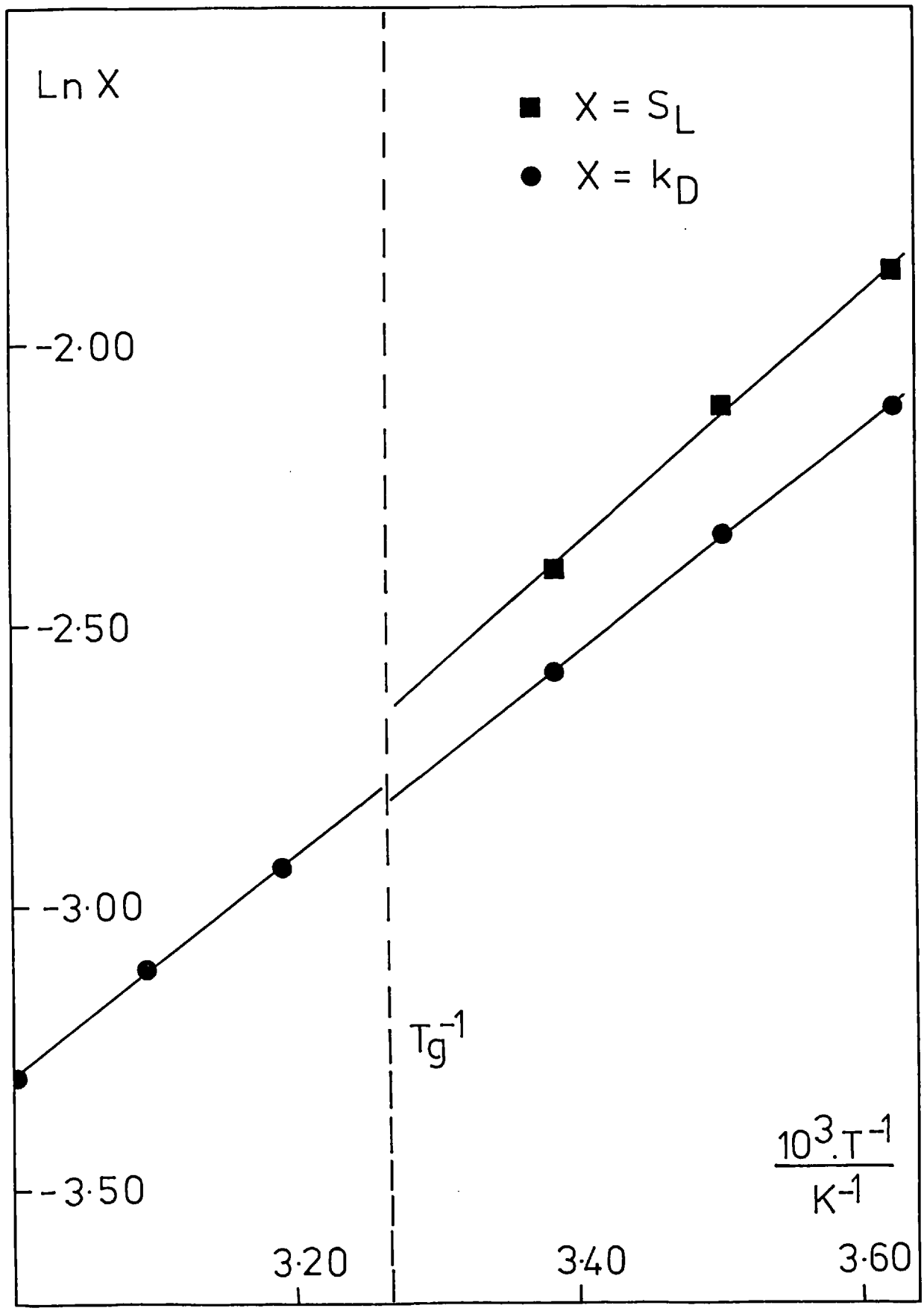


FIG. 5.12 PDMS-g-PVAc/PROPANE

VAN'T HOFF PLOTS: k_D, S_L

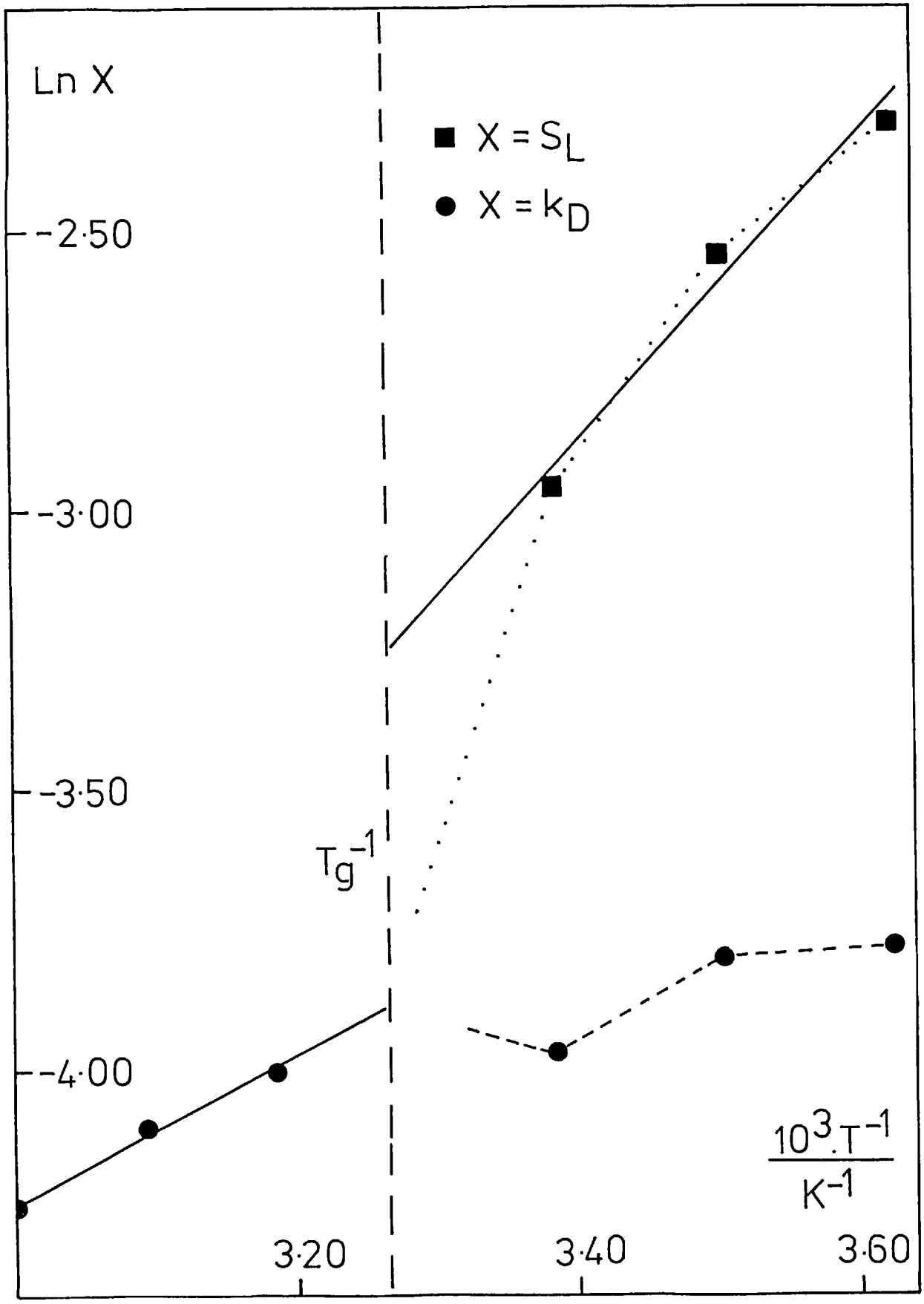


FIG. 5.13 PVAc("EXTRACTED")/PROPANE
VAN'T HOFF PLOTS: k_D, S_L

There is no a priori justification for assuming linearity for any of the semilog plots in Figs. 5.12 and 5.13 since they occur in the glass transition region. One might have expected the plot for S_L to tend towards that of k_D as the transition is approached and $C'_H.B$ becomes very small. Perhaps the plot for this parameter curves downwards as the transition is approached (suggested by the dotted line in Fig. 5.13) and intersects at a "triple point" for S_L, k_D ($> T_g$) and k_D ($< T_g$) at the glass transition temperature.

The enthalpies of solution for PDMS-g-PVAc and PVAc (extracted) (together with that of PDMS for comparison) are presented in Table 5.8.

Table 5.8 Enthalpies of sorption for propane in PDMS-g-PVAc and PVAc

Symbols as for Table 5.2

	Below T_g		Above T_g
	$\Delta\bar{H}_D$/kJ.mole^{-1}	$\Delta\bar{H}_{S(C=O)}$/kJ.mole^{-1}	$\Delta\bar{H}_D$/kJ.mole^{-1}
(PDMS			-17.18)
PDMS-g-PVAc	-16.1	-18.5	-16.0
PVAc	-	-22.3(?)	-10.2

The significance of the values obtained below T_g is doubtful and should be reviewed with some scepticism.

CHAPTER 6

RESULTS AND DISCUSSION, PART 2: PDMS-b-BPAC MEMBRANES

6.1 Preliminary remarks.

The following notation will be used in this chapter: the letter A used as a subscript will indicate PDMS; the letter B will similarly be used to indicate BPAC. E.g., $\Phi_A \equiv$ volume fraction of PDMS, $\overline{P}_B \equiv$ permeability of BPAC. The notation for the copolymers themselves will be the same as that used in chapter 4 (section 4.1.5), e.g., PDMS-25 (20:17.8) represents the copolymer containing 25% PDMS by weight and possessing a block length distribution of 20 PDMS mer units to (an average of)17.8 BPAC mer units. Also, the phrases "20-blocks", "40-blocks" etc. will be commonly used. They refer specifically to the series of copolymers where each sample contains 20 PDMS mer units and 40 PDMS mer units respectively in each AB block.

The transient permeation results are to be interpreted in terms of the corresponding data for the two pure components, PDMS and BPAC. Since it was not possible to obtain these data for BPAC, the results for this polymer presented for purposes of comparison were estimated from the transient sorption results presented in chapter 5 and represent those values at C = 0. The transient permeation data for pure PDMS are taken from Alexopoulos, Barrie, Tye and Fredrickson (154); those for PDMS-25 (20:17.8), PDMS-50(20:6) and PDMS-64 (20: 3.5) are the work of Spencer (155) who employed the same apparatus that was used for this project.

6.2 Densities and T_g's

The density and glass transition data for most of the PDMS-b-BPAC have been presented in chapter 4 (Table 4.1). The densities are illustrated in Fig. 6.1 where the dashed line connects the two values for the pure components and represents the prediction of simple density additivity. Clearly all the data are not adequately represented by the line and this suggests the possibility of interaction between the PDMS and BPAC segments.

Total microphase separation has previously produced linear ρ vs. Φ plots for grafted copolymers (27). The converse of that observation might apply here, i.e., the non-linearity of the plot in Fig. 6.1 suggests

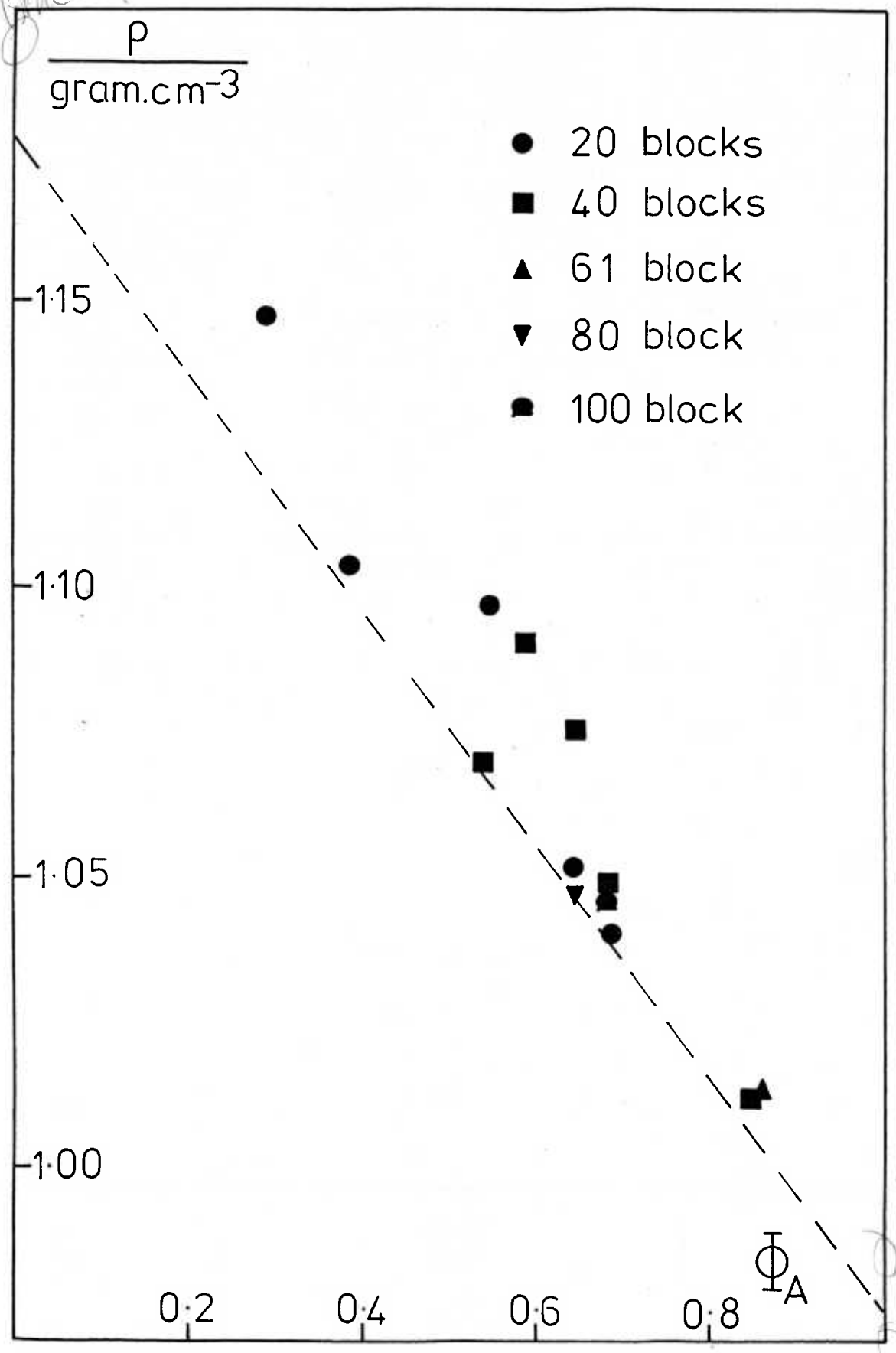


FIG. 6.1 PDMS–b–BPAC

DENSITY vs. VOLUME FRACTION OF PDMS

incomplete microphase separation, and this is consistent with the model for the morphology which has been proposed by LeGrand (143).

However, the density data do not represent a very sensitive test since the measurements were made using the crude water displacement method which is very susceptible to error, and is more useful when the spectrum of densities is relatively wide. Perhaps the use of a density column might have increased the reliability of the measurements.

The T_g data have been treated in a manner similar to that suggested by Kambour (142) are illustrated in Fig. 6.2. Values of $\overline{DP}$ for BPAC were not assumed as those quoted by G.E.C. in the sample documentation, since some could only be regarded as approximations. Instead, values of $\overline{DP}_B$ were estimated from

$$\overline{DP}_B = \frac{(100 - W_A) \cdot \overline{DP}_A \cdot M_A}{W_A \cdot M_B} \qquad \ldots (6.1)$$

where $\overline{DP}_A$ = degree of polymerisation of the PDMS block,
W_A = % PDMS by weight in the sample,
M_A = molecular weight of a single PDMS mer unit,
M_B = molecular weight of a single BPAC mer unit.

Kambour's data are also shown for the purposes of comparison. Instead of the abscissa being the reciprocal of the block molecular weight ($\overline{M_n}$), it was felt that the reciprocal of the degree of polymerisation ($\overline{DP}$) would suffice.

The data appear to be adequately represented by a curve (drawn as a visual guide only) and seem to be independent of the PDMS component. This supports Kambour's thesis that the temperature dependence of the BPAC block length is effectively analogous to the dependence of T_g on molecular weight in homopolymers. The higher values of T_g obtained in Grohmann's study (150) are a consequence, at least in part, of the higher frequence employed namely 11 Hz compared with 0.3 to 3Hz characteristic of the torsion pendulum used by Kambour (156).

Also, Kambour has not quoted the thermal history of the samples he used; nor is it clear whether the membranes were outgassed of solvent at all. Residual solvent could plasticise the polymer and effectively lower its T_g.

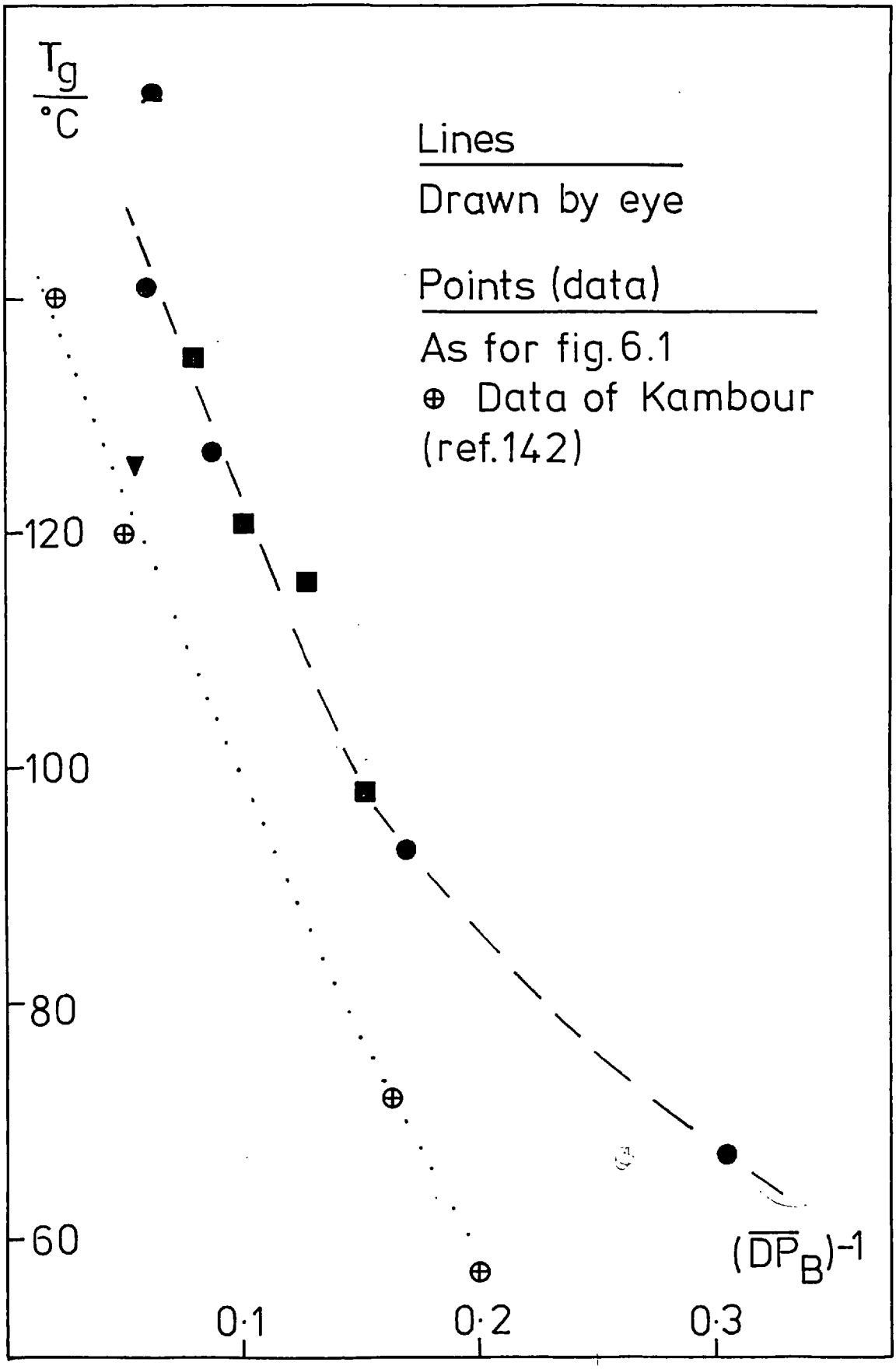


FIG. 6.2
T_g vs. $(\overline{DP})^{-1}$ FOR BPAC

PDMS-b-BPAC

6.3 Transient permeation results

6.3.1 Permeabilities

The permeability data for the membranes at all the temperatures studied were calculated using equation (1.1) and are listed in Appendix 8.7. Values of $\overline{P}$ interpolated to 50°C for purposes of comparison are presented in Table 6.1 and illustrated in Fig. 6.3.

Table 6.1 Permeabilities at 50°C

Permeability, $\overline{P}$; volume fraction of PDMS, Φ_A.

Membrane	Φ_A	$10^7 . \overline{P}$ / ($\frac{cm^3 STP . cm}{cm^2 . s . cm\ Hg}$)
BPAC (estimated)	0.000	5.24×10^{-5}
20-blocks :		
PDMS-25 (20:17.8)	0.287	0.200
PDMS-34 (20:11)	0.384	0.465
PDMS-50 (20:6)	0.547	0.925
PDMS-60 (20:3.9)	0.644	1.26
PDMS-64 (20:3.5)	0.682	1.46
40-blocks :		
PDMS-49 (41:12.4)	0.537	1.49
PDMS-54 (40:10)	0.586	1.78
PDMS-60 (40: 7.2)	0.644	1.90
PDMS-64 (40:7)	0.682	2.27
PDMS-82 (40:3)	0.846	3.36
Misc. :		
PDMS-60 (80:14.6)	0.644	2.24
PDMS-64 (100:16.5)	0.682	3.09
PDMS-83 (61:3.6)	0.855	3.99
PDMS	1.000	5.05 (154)

The only membrane to exhibit a concentration-dependent permeability was PDMS-25 (20: 17.8); the value quoted here is for $C \rightarrow 0$.

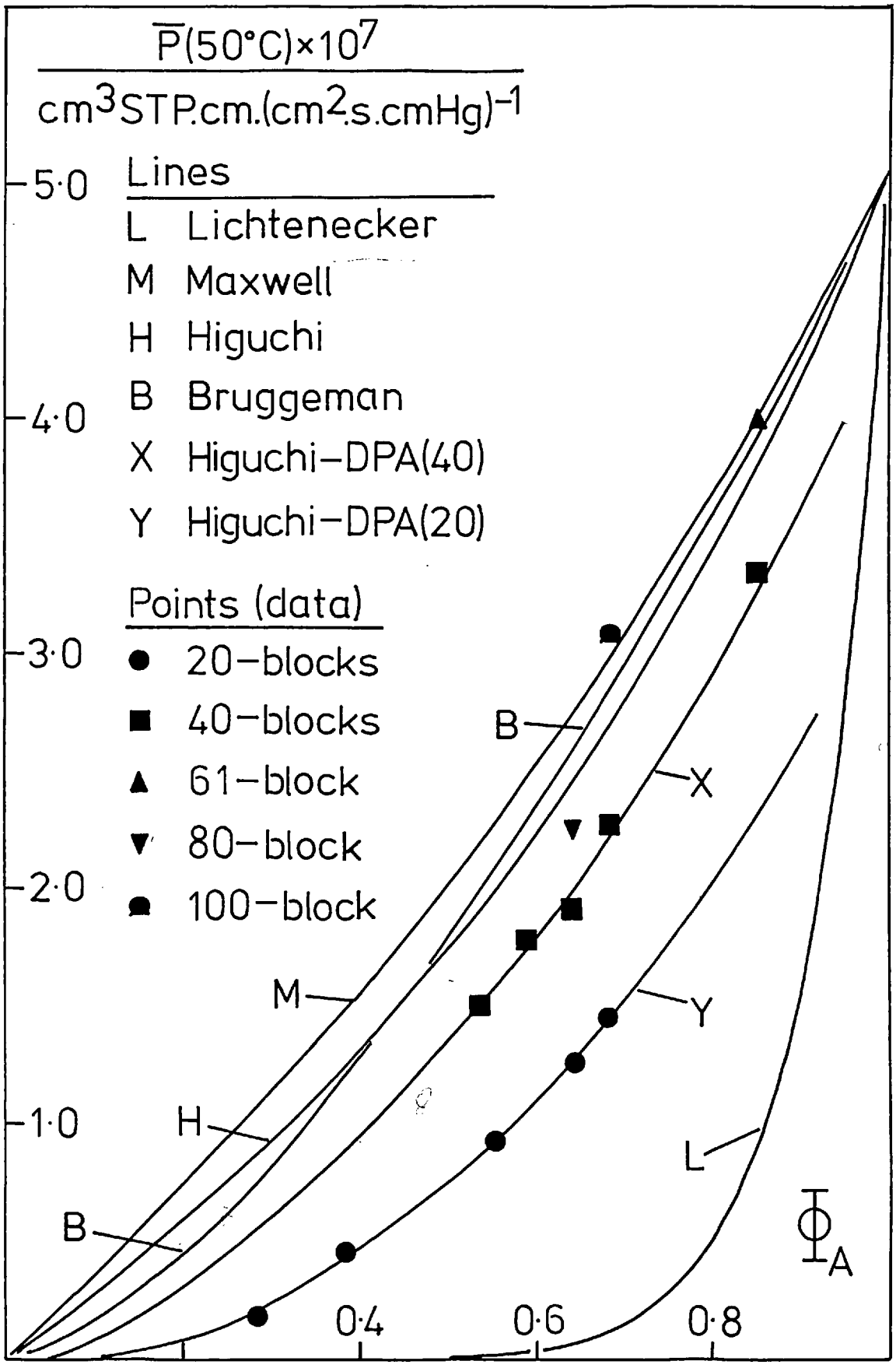


FIG. 6.3 PDMS–b–BPAC/PROPANE
$\overline{P}(50°C)$ vs. VOLUME FRACTION OF PDMS

The graphs representing the expressions of Maxwell, Bruggeman, Higuchi and Lichtenecker were computed from equations (3.3), (3.6), (3.10) and (3.13) respectively. Except in the case of Lichtenecker, which does not apply to disperse systems, the expressions correspond to systems where PDMS is the continuous phase and BPAC is the disperse phase. The graphs for BPAC as the continuous phase take exceedingly small values within the PDMS volume fraction range of 0 - 0.95 and hence those expressions were not considered further.

It is immediately clear from Fig. 6.3 that with few exceptions, the data fall well below the values predicted by the expressions of Maxwell, Bruggeman and Higuchi, and are well above the graph for the Lichtenecker relationship. The 20-blocks and the 40-blocks appear to form two distinct curves. It is also clear that for a given composition, the longer the block lengths the greater the permeability of the sample.

An analysis of the 20-block and 40-block data in terms of the approach developed by Robeson et al (95) using an expression containing arbitrarily weighted Maxwell expressions (see chapter 3, equation (3.31)) was attempted. The results predicted a phase inversion for the 20-blocks at $\Phi_A = 0.705$ and one for the 40-blocks at $\Phi_A = 0.245$.

Although the prediction for the 40-blocks might seem feasible, the interpretation of the result for the 20-blocks is that BPAC is the more abundant component in the continuous phase for each of the samples in the 20-block series. Such a conclusion seems intuitively disputable.

There seemed to be no advantage to be gained by employing Robeson et al's approach with other theoretical expressions.

A novel analysis which attempts to explain the experimental data has been developed during the course of this project and is presented below.

6.3.2 The delta-phi analysis (DPA)

Probably without exception, the models which attempt to describe the permeability of a disperse heterogeneous polymer system implicitly assume that both the disperse phase and the continuous phase are composed of pure components respectively.

It is proposed here to retain the assumption of a disperse phase consisting of pure BPAC, but to discard the notion of a pure continuous phase and assume that it is a dilute miscible blend (or homogeneous random

copolymer) of BPAC and PDMS.

Such assumptions are consistent with the morphology suggested by LeGrand (143), but they define the continuous phase more specifically and in terms that are amenable to mathematical analysis. The suggestion of Kambour (142) (a co-worker with LeGrand), that two distinct continua of PDMS and BPAC exist, is modified; here, a single homogeneous continuum is assumed.

It is further proposed to treat the data in terms of the Maxwell, Bruggeman and Higuchi models whilst simultaneously treating the continuous phase in terms of the Lichtenecker rule.

To do so we must consider a membrane containing PDMS and BPAC, with volume fractions Φ_A and Φ_B respectively, and let us assume that a portion, $\Delta\Phi$, of BPAC exists in the continuous phase to form a homogeneous PDMS/BPAC blend.

It follows that the continuous phase volume fraction, Φ_C, and the disperse phase volume fraction, Φ_D, must be redefined as

$$\Phi_C = \Phi_A + \Delta\Phi, \qquad \ldots (6.2)$$

and

$$\Phi_D = \Phi_B - \Delta\Phi. \qquad \ldots (6.3)$$

The permeability of the continuous phase, $\overline{P}_C$, must also be redefined. Within the continuous phase itself, the volume fraction of PDMS, V_A is given by

$$V_A = \frac{\Phi_A}{\Phi_C} = \frac{\Phi_A}{\Phi_A + \Delta\Phi} \qquad \ldots (6.4)$$

Similarly, the volume fraction of BPAC in the continuous phase alone is given by

$$V_B = \frac{\Delta\Phi}{\Phi_C} = \frac{\Delta\Phi}{\Phi_A + \Delta\Phi} \qquad \ldots (6.5)$$

Treating the continuous phase as a dilute blend, and applying the Lichtenecker relationship (equation 3.13), we obtain

$$\overline{P}_C = (\overline{P}_A)^{V_A} \cdot (\overline{P}_B)^{V_B} = (\overline{P}_A)^{\left(\frac{\Phi_A}{\Phi_A + \Delta\Phi}\right)} \cdot (\overline{P}_B)^{\left(\frac{\Delta\Phi}{\Phi_A + \Delta\Phi}\right)} \qquad \ldots (6.6)$$

Equation (6.6) can be rearranged to yield

$$\overline{P}_C = \overline{P}_A \left(\frac{\overline{P}_B}{\overline{P}_A} \right)^{\left(\frac{\Delta\Phi}{\Phi_A + \Delta\Phi} \right)} \qquad \ldots (6.7)$$

Substituting (6.2) into equations (3.3) (3.6) and (3.10), of Maxwell, Bruggeman and Higuchi respectively, the following corresponding modified expressions are found,

$$\overline{P}_{AB} = \overline{P}_C \cdot \frac{2(\Phi_A + \Delta\Phi)}{3 - (\Phi_A + \Delta\Phi)} \qquad \ldots (6.8)$$

$$\overline{P}_{AB} = \overline{P}_C \cdot (\Phi_A + \Delta\Phi)^{3/2} \qquad \ldots (6.9)$$

$$\overline{P}_{AB} = \overline{P}_C \cdot \frac{3.22\ (\Phi_A + \Delta\Phi)}{6 - 2.78\ (\Phi_A + \Delta\Phi)} \qquad \ldots (6.10)$$

where $\overline{P}_C$ is defined by equation (6.7).

These expressions were tested with the experimental data for the 20-block and 40-block series of membranes. For each membrane a value of $\Delta\Phi$ was computed using a mathematically iterative procedure. The results are presented in Table 6.2.

Table 6.2 : Delta-phi analyses.

Φ_A	$\Delta\bar{\Phi} \times 10^2$		
	Maxwell	Bruggeman	Higuchi
20-blocks			
0.287	5.60	4.57	4.94
0.384	4.90	4.07	4.19
0.547	5.24	4.75	4.49
0.644	5.40	5.10	4.71
0.682	5.15	4.91	4.50
Mean $\Delta\Phi$	5.26	4.68	4.57
40-blocks			
0.537	2.13	1.60	1.43
0.586	1.90	1.45	1.20
0.644	2.45	2.12	1.78
0.682	1.85	1.58	1.21
0.846	1.42	1.35	1.00
Mean $\Delta\Phi$	1.95	1.62	1.32

Perhaps surprisingly, $\Delta\Phi$ seems remarkably constant within a particular series, and furthermore the variation in $\Delta\Phi$ values between the different models is not large. It could be inferred from the results that the continuous phase is a dilute blend of BPAC in PDMS with a composition in the range 7-17% BPAC by volume for the 20-block polymers and 2-3% BPAC by volume for the 40-block series.

For both series and for each of the three theoretical expressions, a mean $\Delta\Phi$ was determined and substituted back into equations (6.8), (6.9) and (6.10) respectively. The equations were subsequently replotted to see how good a fit was obtained with the experimental data.

The results for the Higuchi model treated according to the delta-phi analysis are given for both 40- and 20-blocks in Fig. 6.3 (lines X and Y respectively). The fit in each case is excellent. Indeed the fit for all three models taking a mean $\Delta\Phi$ was extremely good.

As a check on the sensitivity of $\overline{P}_{AB}$ to changes in $\Delta\Phi$, equations (6.8), (6.9) and (6.10) were replotted using firstly the maximum value of $\Delta\Phi$ recorded for the particular model, and then the respective minimum value. The results are shown in Fig. 6.4.

For each series, the upper line for each model was plotted using $\Delta\Phi_{min}$ for the particular model; the lower line corresponds to the particular $\Delta\Phi_{max}$.

The models compare extremely well. The experimental data all fall within the narrow confines of the lines.

6.3.3. Physical interpretation of DPA.

The criterion for the homogeneous mixing of two polymers can be expressed in terms of the Gibbs free energy of mixing, ΔG.

$$\Delta G = \Delta H - T.\Delta S \qquad \ldots (6.11)$$

where ΔH is the enthalpy of mixing and ΔS is the change in entropy on mixing. Mixing occurs when ΔG is negative. In the absence of specific interactions between the two components leading to a negative ΔH, mixing will only occur for positive entropies of mixing such that $T.\Delta S > \Delta H$. Generally, mixtures of two different macromolecules tend to be imcompatible as S, although positive, is small for the mixing of two polymer molecules and a small positive ΔH is sufficient to prevent mixing except for very high values of the temperature. If, however, ΔH is close to zero or negative then partial or complete mixing becomes possible.

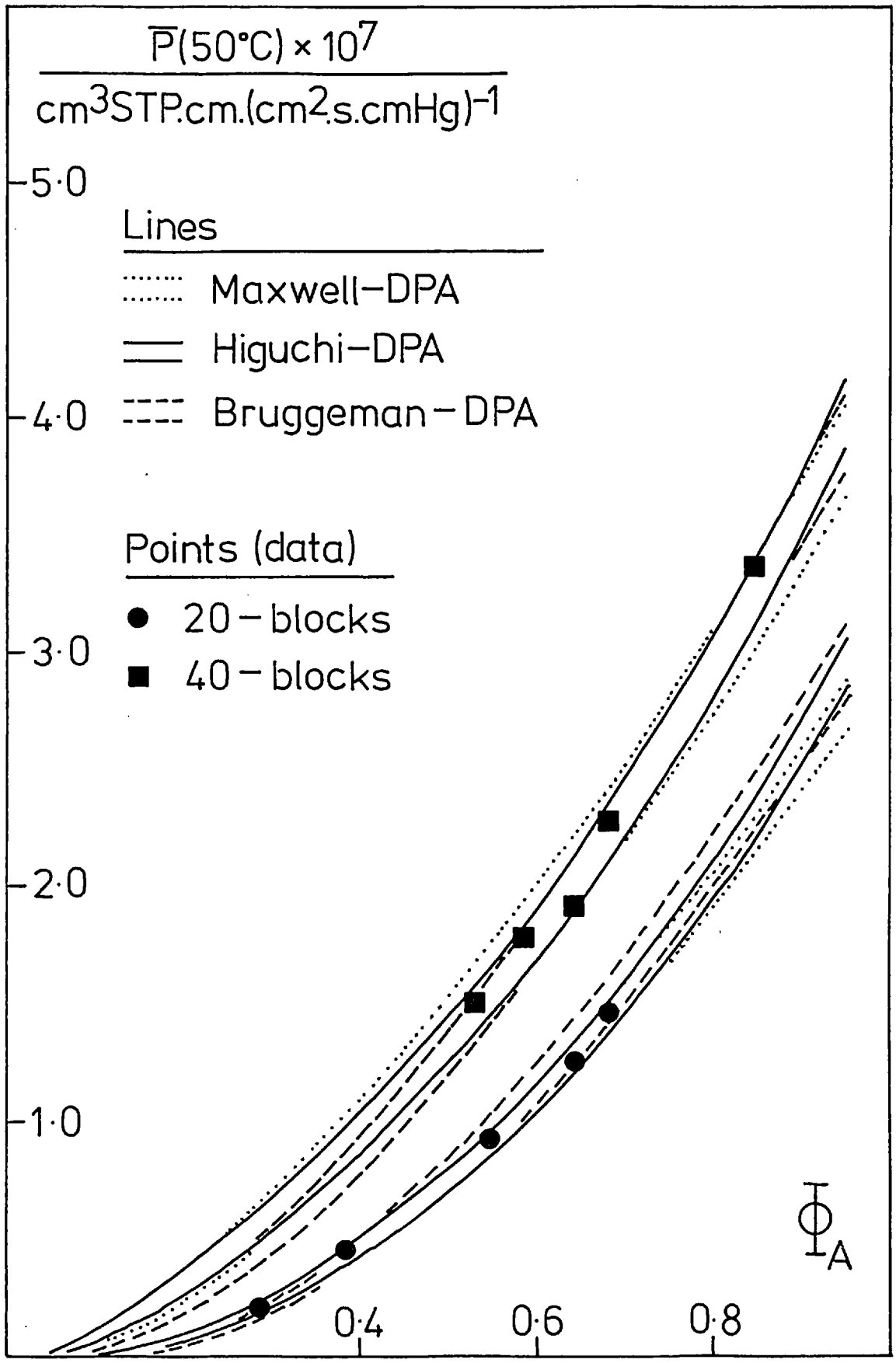


FIG. 6.4 PDMS–b–BPAC/PROPANE
$\overline{P}(50°C)$ vs. Φ_A : MODELS–DPA COMPARISON

The Lichtenecker relationship has been proposed for completely miscible homogeneous blends where ΔG is negative. The Maxwell-type model applies to heterogeneous systems consisting of a dispersion of one phase in a continuum of another and in this instance would relate to systems where ΔG is positive over most of the composition range.

The experimental data for the 20-blocks and 40-blocks fall between these extremes and hence possess characteristics of both, i.e., a domain structure embedded in a homogeneous two-component continuum. The closer the data are to the Maxwell, Bruggeman, Higuchi predictions, the greater is the degree of phase-separation and the more heterogeneous is the system; the converse applies the closer the data are to the Lichtenecker predictions.

The results therefore indicate that the block-length size has a direct effect on the degree of phase-separation and, by inference, the ΔG of mixing. If one assumes that the ΔH of mixing for a given composition is independent of block-length considerations, then it follows that the block-length size has a direct effect on ΔS causing it to increase as the blocks get shorter. This trend might be deduced intuitively by comparing the relative "order" characteristic of completely phase-separated domain/continuum morphologies to the random homogeneity which would be enforced sterically by very short block-lengths.

Referring to Fig. 6.4, the position of the data for the 100-block and the 61-block suggest that their morphology is one close to complete phase-separation. The datum for the 80-block indicates for that particular composition that phase-separation is not quite complete. The reason why the 61-block appears to have a higher degree of phase separation than the 80-block is not certain at this stage, but might be connected with the former's binodal distribution of BPAC blocks.

The value of $\Delta\Phi$, since it relates directly to the degree of phase-separation, must be directly associated with the ΔG of mixing and, by inference, ΔS. This trend might be deduced intuitively by comparing the entropy of a pure component continuous phase (where $\Delta\Phi = 0$) to the increased entropy of an impure, dilute blend of one component in the other as the continuous phase (where $\Delta\Phi$ is small and positive). It should also be noted on a more quantitative level that the Maxwell-DPA expression, i.e.,

$$\overline{P}_{AB} = \overline{P}_A \left(\frac{\overline{P}_B}{\overline{P}_A} \right)^{\left(\frac{\Delta\Phi}{\Phi_A + \Delta\Phi} \right)} \cdot \frac{2(\Phi_A + \Delta\Phi)}{3 - (\Phi_A + \Delta\Phi)} \qquad \ldots (6.12)$$

reduces to the classical Maxwell expression at $\Delta\Phi = 0$, and reduces to the Lichtenecker relationship at $\Delta\Phi = \Phi_B$. The Bruggeman-DPA and Higuchi-DPA expressions also possess analogous characteristics.

However, before $\Delta\Phi$ can be confidently proposed as a "real" quantity as opposed to a convenient "arbitrary" weighting factor, the observation that $\Delta\Phi$ can be regarded as a constant for a particular series of membranes must be examined more closely. It is suggested here that $\Delta\Phi$, apart from being a function of block-length distribution, is indeed a function of Φ_A though not a very strong one. At very high and very low values of Φ_A, the block length of one component becomes very large relative to the other. Under such conditions there would be no impedance (thermodynamic considerations apart) to the system adopting a completely phase-separated morphology. Therefore if one accepts that at very high and very low values of Φ_A complete phase-separation occurs, then one must accept that $\Delta\Phi$ is zero for both cases but small and positive at intermediate values of Φ_A.

Furthermore, extrapolation of the lines described by the Higuchi-DPA expression for the 20-blocks and 40-blocks (lines Y and X in Fig. 6.3) to $\Phi_A = 1$ produces two different values of $\overline{P}$ for PDMS well below the accepted value. The value of $\Delta\Phi$ must get smaller in each case as $\Phi_A \rightarrow 1$ if the lines are to tend towards the value of $\overline{P}$ for PDMS.

It should be remembered that the 20-blocks cover 0.4 and the 40-blocks 0.3 of the Φ_A spectrum. Data covering a much wider range might have indicated a stronger Φ_A - dependence in the values of $\Delta\Phi$ produced. Nevertheless, the observation remains that for the range of volume fractions covered, a constant mean $\Delta\Phi$ is adequate to achieve a good fit to the experimental data.

6.3.4. Permeability temperature coefficients.

Values of E_P determined using van't Hoff plots of equation (1.10), are presented in Table 6.3 and illustrated in Fig. 6.5. The dashed lines in this figure were drawn by eye and are a visual guide only. The van't Hoff plots are shown in Fig. 6.6.

The Maxwell, Bruggeman and Higuchi expressions can generally be expressed as

$$\overline{P} = \overline{P}_C . f(\Phi_C) = \overline{P}_o \exp - \frac{E_P}{RT}$$

$$= \overline{P}_{Co} . f(\Phi_C) . \exp - \frac{E_P}{RT} \qquad \ldots(6.13)$$

where the subscript o refers to a pre-exponential constant, C refers to the

continuous phase and f is the characteristic function of volume fraction for each of the three theoretical expressions.

Table 6.3 : Permeability temperature coefficients

Membrane	Φ_A	E_P/kJ. mole^{-1}
BPAC	0.000	+ 29.3
20-blocks		
PDMS-25 (20:17.8)	0.287	- 2.90 (± 0.35)
PDMS-34 (20:11)	0.384	- 1.92 (± 0.45)
PDMS-50 (20:6)	0.547	+ 2.34 (± 0.16)
PDMS-60 (20:3.9)	0.644	+ 1.76 (± 0.24)
PDMS-64 (20:3.5)	0.682	+ 1.69 (± 0.72)
40-blocks		
PDMS-49 (40:12.2)	0.537	- 2.96 (± 0.21)
PDMS-54 (40: 10)	0.586	- 1.98 (± 0.19)
PDMS-60 (40:7.2)	0.644	- 1.12 (± 0.13)
PDMS-64 (40:7)	0.682	- 0.97 (± 0.23)
PDMS-82 (40:3)	0.846	- 1.51 (± 0.11)
Misc.		
PDMS-60 (80:14.6)	0.644	- 2.55 (± 0.16)
PDMS-64 (100:16.5)	0.682	- 2.60 (± 0.05)
PDMS-83 (61:3.6)	0.855	- 1.91 (± 0.14)
PDMS	1.000	- 2.9

It follows that, provided $f(\Phi_C)$ is not a function of temperature, then

$$\overline{P}_o = \overline{P}_{Co} \cdot f(\Phi_C), \qquad \ldots (6.14)$$

and

$$E_P = E_{PC} \qquad \ldots (6.15)$$

This means that the experimentally observed E_P for a disperse two-phase system for which $\overline{P}_C >> \overline{P}_D$ should be equal to the E_P of the continuous phase and should remain constant for that range of Φ_C for which the continuous phase composition remains constant. For a completely phase-separated disperse heterogeneous system containing only the pure components A and B,

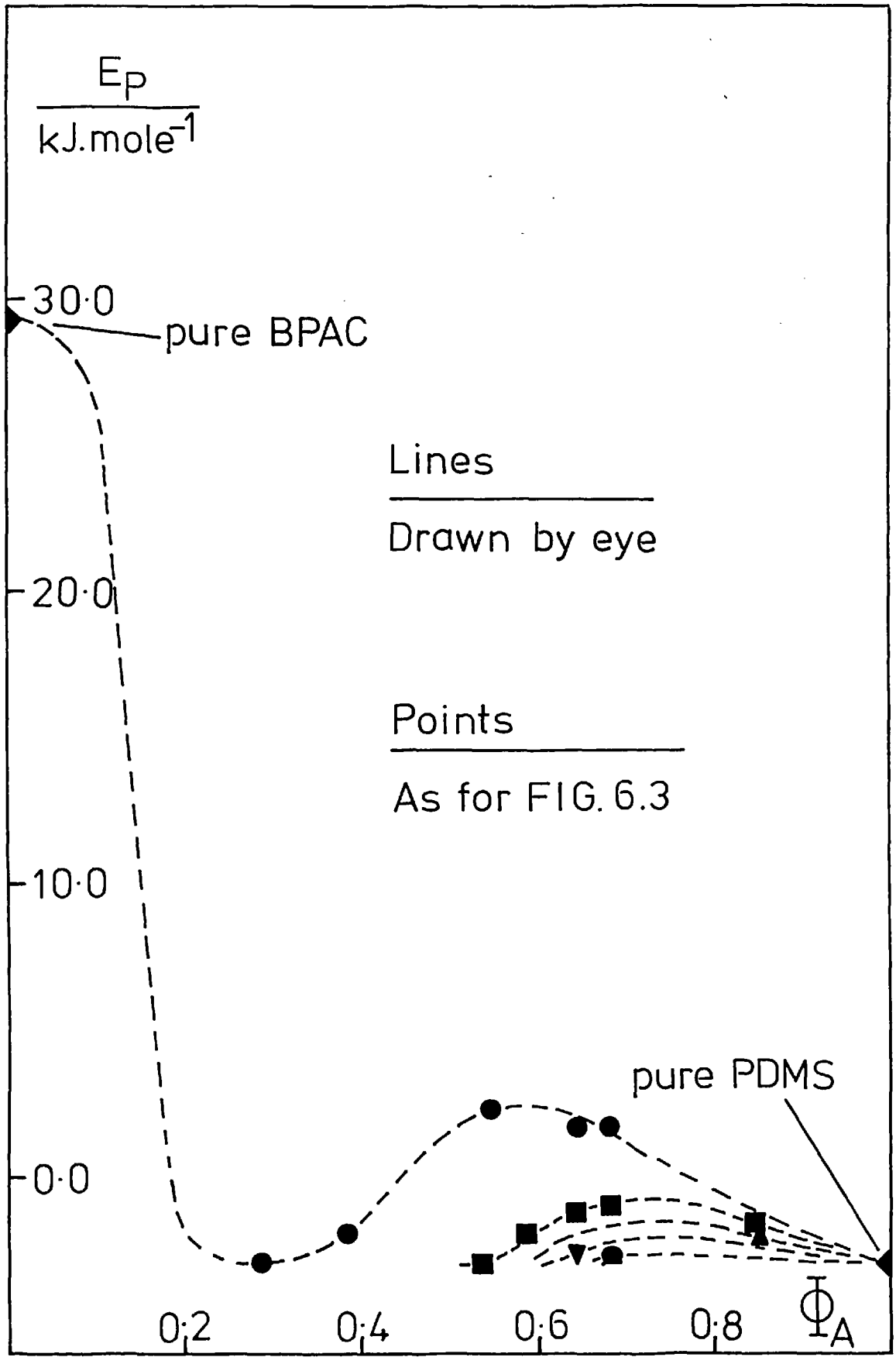


FIG. 6.5 PDMS–b–BPAC/PROPANE
E_P vs. VOLUME FRACTION OF PDMS

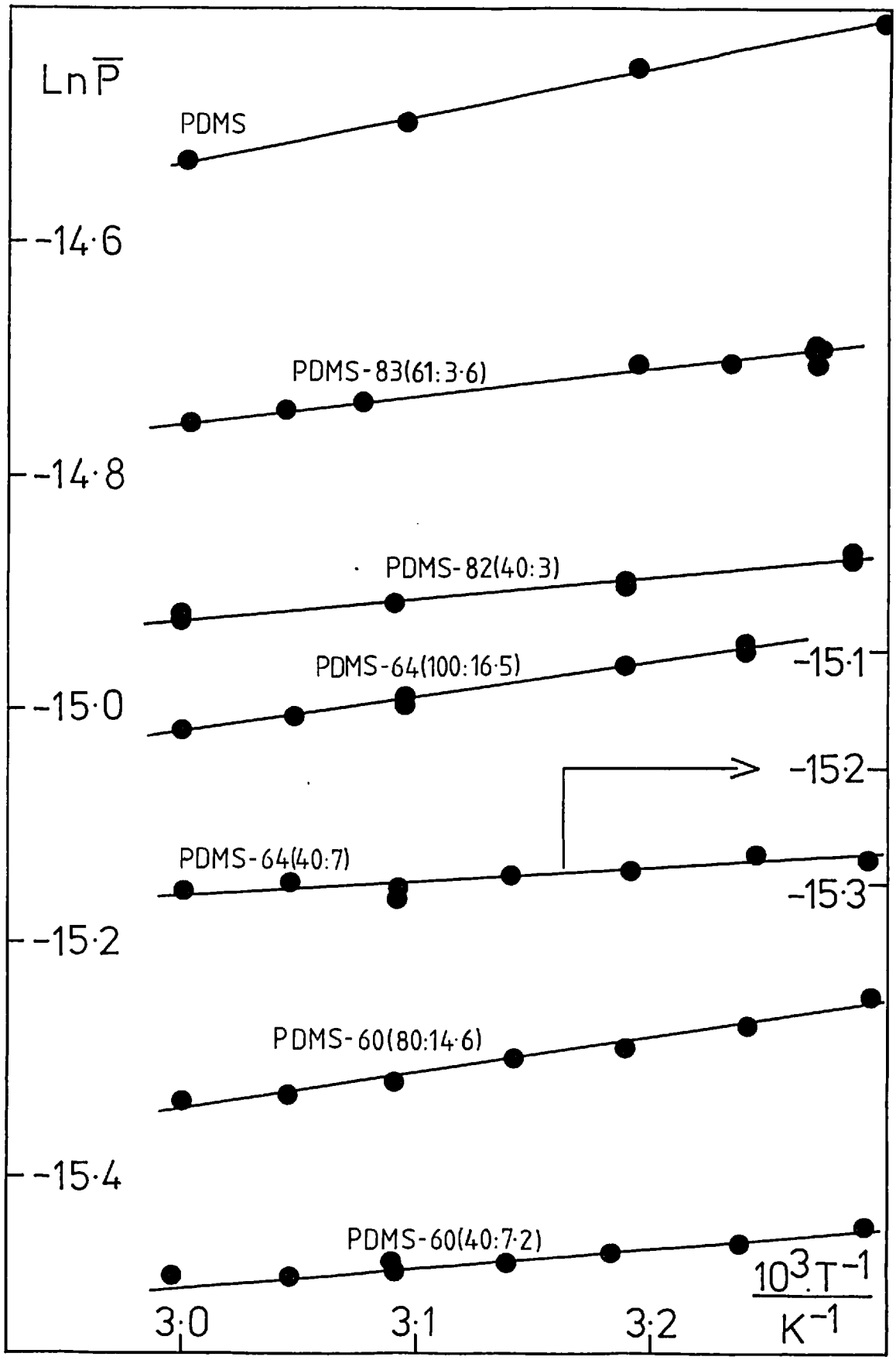


FIG. 6.6 PDMS-b-BPAC/PROPANE
TEMPERATURE DEPENDENCE OF $\overline{P}$

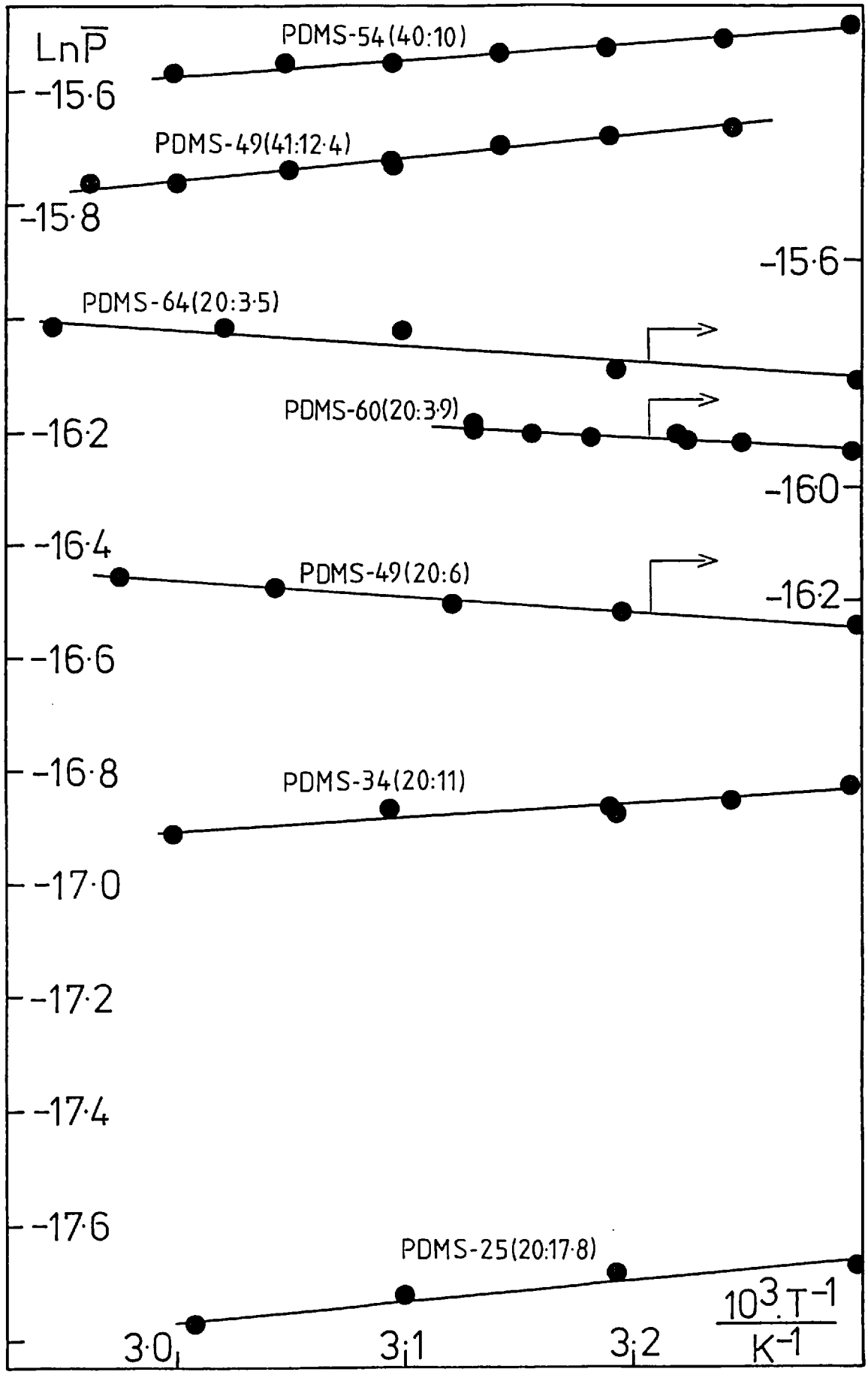


FIG. 6.6 (continued).

E_P for the system would be expected to be equal to E_{PA} for A continuous (high Φ_A) and equal to E_{PB} for B continuous (high Φ_B); a transition between the two E_P's corresponding to phase inversion should occur at intermediate values of Φ_A and Φ_B.

(It can be noted at this stage that all the E_P results lie in a region fairly close to the value for pure PDMS indicating this component's abundance in the continuous phase. The prediction based upon Robeson et al's analysis (see section 6.31) of phase inversion for the 40-blocks at $\Phi_A = 0.245$ still appears feasible; however, the prediction of phase inversion for the 20-blocks at $\Phi_A = 0.705$ is clearly not valid.)

The Lichtenecker rule, when treated in a similar way to equation (6.13) produces the following relationship,

$$E_P = \Phi_A \cdot E_{PA} + \Phi_B \cdot E_{PB} \qquad \ldots (6.16)$$

which represents a straight line (not shown) on Fig. 6.5 connecting the values of E_P for the two pure components. In this case there is a single, continuous phase and E_P is a linear function of Φ_A.

As in the case of the permeabilities, the experimental data tend to fall between the two extremes as represented by equations (6.15) and (6.16). The delta-phi analysis can be used to attempt to interpret the results, but the quantitative correlations suffer from extreme sensitivity of the E_P predictions to parameters such as E_P for BPAC, for PDMS and $\Delta\Phi$ itself.

The DPA expression (6.12) in the general case can be written as

$$\overline{P} = \left(\overline{P}_{AO} \exp - \frac{E_{PA}}{RT} \right) \left(\frac{\overline{P}_{BO}^{\left(\frac{\Delta\Phi}{\Phi_A + \Delta\Phi} \right)}}{\overline{P}_{AO}^{\left(\frac{\Delta\Phi}{\Phi_A + \Delta\Phi} \right)}} \cdot \exp - (E_{PB}.\Delta\Phi/(\Phi_A + \Delta\Phi)RT) \right) \cdot f(\Phi_A + \Delta\Phi)$$

$$= \overline{P}_0 \exp - \frac{E_P}{RT} \qquad \ldots (6.17)$$

from which it follows that

$$\overline{P}_{AO} \left(\frac{\overline{P}_{BO}}{\overline{P}_{AO}} \right)^{\left(\frac{\Delta\Phi}{\Phi_A + \Delta\Phi} \right)} \cdot f(\Phi_A + \Delta\Phi) = \overline{P}_0 \qquad \ldots (6.18)$$

Equation (6.17) now reduces to

$$E_P = E_{PA} + (E_{PB} - E_{PA}) \cdot \frac{\Delta\Phi}{\Phi_A + \Delta\Phi} \quad \ldots (6.19)$$

At $\Delta\Phi = 0$, equation (6.19) reduces to (6.15); at $\Delta\Phi = \Phi_B$, the equation reduces to (6.16).

Equation (6.19) has limited practical use due to the considerable uncertainty attributable to the product $(E_{PB} - E_{PA}).\Delta\Phi$ which is a very large quantity multiplied by a very small quantity. It is also clear from the mathematical form of (6.19) that for a constant $\Delta\Phi$, the equation would describe a curve possessing no inflexions such as appear in the lines drawn as visual guides in Fig. 6.5. Any further mathematical description of the behaviour of E_P as a function of Φ_A would require the development of a theoretical expression of $\Delta\Phi$ as some function of Φ_A. This has not been attempted.

Nevertheless it was decided to determine values of $\Delta\Phi$ based upon the E_P data presented in Table 6.3. Solving equation (6.19) for $\Delta\Phi$,

$$\Delta\Phi = \frac{\Phi_A(E_P - E_{PA})}{E_{PB} - E_P} \quad .. (6.20)$$

The results are presented in Table 6.4 and are compared with those values of $\Delta\Phi$ obtained from the permeability data for 50°C. For the purposes of comparison, the results derived using the Maxwell, Bruggeman and Higuchi expressions have been averaged and presented as a single figure for each value of Φ_A.

Table 6.4 Delta-phi analysis using E_P's

Φ_A	$10^2.\Delta\Phi$ (from $\bar{P}$'s)	$10^2.\Delta\Phi$ (from E_P's)
20-blocks:		
0.287	5.04	0
0.384	4.39	1.2
0.547	4.83	10
0.644	5.07	11
0.682	4.85	11
40-blocks:		
0.537	1.72	- 0.1
0.586	1.52	1.7
0.644	2.12	3.8
0.682	1.55	4.4
0.846	1.26	3.8

Considering the level of uncertainty in the values of E_P and the value of E_{PB} (which was estimated from sorption kinetics), the level of

agreement between the values of $\Delta\Phi$ determined by the two different methods is remarkably good. As expected, $\Delta\Phi$ for the 20-blocks is generally larger than the values for the 40-blocks indicating a higher BPAC content in the continuous phase for the former series.

6.3.5 Time-lag diffusion and solubility coefficients

Although some significant dependence of $\overline{P}$ and D on pressure was observed only for the membrane containing the high amount of BPAC (sample PDMS-25 (20:17.8)), a very weak dependence was presumably present in at least some of the other membranes. A full assessment of this dependence would require a large range of ingoing pressures which would extend beyond the practical limit imposed to prevent distortion of the rubbery sample. For this reason a quantitative assessment was not attempted.

Langmuir-type immobilisation of penetrant in the microcavities which are presumed still to exist in the glassy domains in each sample is held accountable for the pressure dependence. In such cases the relationship between the time-lag and D as expressed in equation (2.16) requires modification (123). Nevertheless since for the most part no significant pressure dependence was observed, equations (2.16) and (1.7) were used to determine transient diffusion and solubility coefficients respectively.

Values for D and S interpolated at $50^{o}C$ for comparison along with the activation energies of diffusion and the heats of solution are presented in Table 6.5. The experimental data are listed in Appendix 8.7. The values for PDMS-25 (20:17.8) are those for $P \rightarrow 0$. The results for BPAC quoted for purposes of comparison were derived from the sorption kinetics discussed in Chapter 5. The data for PDMS were taken from Alexopoulos et al (154).

The uncertainties in the values of E_D and $\Delta\overline{H}_S$ were determined statistically from the scatter in the respective semilog plots (not illustrated).

The scatter in the results presented in Table 6.5 appear to reflect the limited accuracy of the time-lag technique. The diffusion coefficients reveal trends for the 20-blocks and 40-blocks which are comparable to those for the permeability coefficients. The solubility coefficients are seriously scattered: this reflects the fact that S accumulates the errors in $\overline{P}$ and D and also that the difference in the solubility coefficients for the two pure components are not vastly different.

Table 6.5 Transient values of D. S (at 50°C), E_D and $\Delta\overline{H}_S$

Membrane	$10^6 D/cm^2.s^{-1}$	$E_D/kJ.mole^{-1}$	$10^2 S/cm^3 STP.cm^{-3}.cmHg^{-1}$	$\Delta\overline{H}_S/kJ.mole^{-1}$
BPAC				
20-blocks:				
PDMS-25 (20:17.8)	0.335	26.26(±0.68)	5.95	-29.2 (±0.3)
PDMS-34 (20:11)	0.860	19.98(±0.61)	5.41	-21.9 (±0.9)
PDMS-50(20:6)	1.75	21.92(±0.18)	5.30	-19.4 (±0.2)
PDMS-60(20:3.9)	2.23	17.00(±0.42)	5.66	-15.24(±0.48)
PDMS-64(20:3.5)	2.48	18.40(±0.39)	5.78	-16.68(±0.40)
40-blocks:				
PDMS-49(41_12.4)	2.37	15.51(±1.09)	6.29	-18.47(±1.21)
PDMS-54(40:10)	2.87	17.43(±0.32)	6.19	-19.41(±0.43)
PDMS-60 (40:7.2)	3.47	16.30(±0.11)	5.48	-17.42(±0.13)
PDMS-64 (40:7)	3.78	15.58(±0.41)	6.00	-16.56(±0.36)
PDMS-82 (40:3)	5.09	15.36(±0.30)	6.60	-16.86(±0.31)
Misc.:				
PDMS-60(80:14.6)	3.77	16.13(±0.23)	5.93	-18.69(±0.30)
PDMS-64 (100:16.5)	3.76	18.41(±0.80)	8.21	-21.01(±0.80)
PDMS-83(61:3.6)	5.84	14.23(±0.34)	6.84	-16.14(±0.40)
PDMS	8.9	13.4	5.7	-16.3

It has been suggested that the time-lag itself could be sensitive to the design of the permeation cell (157), specifically the amount of membrane periphery overlap which is gripped by the two "cups" (see chapter 4) and the membrane thickness. Too much overlap for a sizable thickness would distort the lines of diffusive flux at the membrane periphery, increasing the effective flow path and hence increasing the time-lag. Transient D's might therefore appear anomalously low. Permeability coefficients might also be affected, though to a far lesser extent. Any such "edge-effects" are difficult to quantify.

The scatter in the values of E_D and $\Delta\overline{H}_S$ suggest uncertainties far beyond the statistical errors determined from the scatter in the semilog plots. This suggests that extraneous effects such as "edge-effects" may be the cause of the discrepancies. A graphical comparison between the transient and steady-state results will be made at a later stage.

6.4 Equilibrium sorption results

Significant curvature was present in the sorption isotherms for many of the membranes that were examined. This was believed to be due to a Langmuir component in the glassy BPAC phase. The data were therefore interpreted in terms of the dual mode sorption theory.

The parameters associated with the sorption of propane in all the alternating PDMS-b-BPAC copolymers are presented in Tables 6.7-6.9. Where the uncertainty of C'_H or B was found to be greater than 100%, no percentage error has been quoted; in such cases however the derived value of S_L will have an uncertainty considerably less than 100%.

Table 6.6 Sorption parameters for PDMS-b-BPAC/propane, (20-blocks)

Membrane	T/°C	$10^2 k_D / (\frac{cm^3 STP}{cm^3 cmHg})$	$10.C'_H / (\frac{cm^3 STP}{cm^3})$	$10.B / cmHg^{-1}$	$10.S_L (\frac{cm^3 STP}{cm^3 cmHg})$
PDMS-25(20:17.8)	19.95	7.15(± 5%)	8.21(± 15%)	2.30(± 24%)	2.60 (± 8%)
	30.35	5.14(± 4%)	7.42(± 14%)	1.39(± 18%)	1.55 (± 4%)
	40.3	4.22(± 7%)	5.02(± 27%)	1.32(± 31%)	1.09 (± 5%)
	50.1	3.41(± 4%)	3.59(± 20%)	1.05(± 23%)	0.718(±3.5%)
PDMS-34(20:11)	20.05	6.31(± 7%)	5.23(± 42%)	1.46(± 56%)	1.39 (± 11%)
	30.1	4.77(± 4%)	3.65(± 23%)	1.31(± 31%)	0.955(± 6%)
	40.1	3.69(± 8%)	3.09(± 59%)	0.89(± 63%)	0.644(± 10%)
	50.0	3.37(± 2%)	1.02(± 28%)	1.65(± 40%)	0.505(± 5%)
PDMS.50(20:6)	20.2	8.54(± 3%)	0.55	5.1	1.14
	30.45	6.63(± 2%)	0.75	1.3	0.759
	40.85	5.42(± 1%)	0.30	1.7	0.591
	49.95	4.48(± 1%)	0.75	0.3	0.473
PDMS-60(20:3.9)	20.1	8.50(±<1%)	-	-	-
	30.05	6.77(±<1%)	-	-	-
	40.05	5.52(±<1%)	-	-	-
	50.1	4.54(±<1%)	-	-	-
PDMS-64(20:3.8)	20.1	8.90(±<1%)	-	-	-
	30.45	7.14(±<1%)	-	-	-
	40.7	5.75(±<1%)	-	-	-
	50.1	4.79(±<1%)	-	-	-

Table 6.7 Sorption parameters for PDMS-b-BPAC/propane, (40-blocks)

Membrane	T/°C	$10^2 k_D$/($\frac{cm^3 STP}{cm^3 cmHg}$)	$10.C'_H$/($\frac{cm^3 STP}{cm^3}$)	$10.B/cmHg^{-1}$	$10.S_L$/($\frac{cm^3 STP}{cm^3 cmHg}$)
PDMS-49(41:12.4)	20.6	7.17(± 3%)	4.53(± 25%)	1.37(± 35%)	1.39 (± 6%)
	30.75	5.78(± 3%)	3.32(± 32%)	1.10(± 44%)	0.942(± 6%)
	40.4	4.67(± 2%)	2.47(± 26%)	0.95(± 34%)	0.702(± 4%)
	50.0	4.12(± 2%)	0.83(± 33%)	1.99(± 50%)	0.576(± 6%)
PDMS-54(40:10)	20.0	8.27(± 1%)	2.08(± 17%)	2.31(± 28%)	1.31 (± 5%)
	30.2	6.62(± 1%)	1.21(± 11%)	2.20(± 18%)	0.928(± 3%)
	40.55	5.23(± 1%)	1.05(± 21%)	1.45(± 29%)	0.677(± 3%)
	49.75	4.36(±<1%)	0.62(± 8%)	1.57(± 12%)	0.533(± 1%)
PDMS-60(40:7.2)	19.75	8.58(± 1%)	1.23(± 19%)	2.21(± 34%)	1.13 (± 4%)
	30.1	6.93(±<1%)	0.38(± 17%)	5.84(± 45%)	0.917(± 7%)
	40.05	5.66(± 1%)	0.18	6.94	0.694
	50.0	4.65(±<1%)	-	-	-
PDMS-64(40:7)	20.15	9.06(± 1%)	0.32	8.7	1.18
	30.05	7.18(±<1%)	0.29(± 18%)	3.2(± 39%)	0.810(± 3%)
	40.4	5.84(± 1%)	-	-	-
	50.0	4.83(±<1%)	-	-	-
PDMS-82(40:3)	19.9	10.93(±<1%)	-	-	-
	30.15	8.61(±<1%)	-	-	-
	40.05	7.01(±<1%)	-	-	-
	50.0	5.73(±<1%)	-	-	-

Table 6.8 Sorption parameters for PDMS-b-BPAC/propane, (misc.).

Membrane	T/°C	$10^2 k_D / (\frac{cm^3 STP}{cm^3 cmHg})$	$10.C_H' / (\frac{cm^3 STP}{cm^3})$	$10.B / cmHg^{-1}$	$10.S_L / (\frac{cm^3 STP}{cm^3 cmHg})$
PDMS-60(80:14.6)	19.8	8.84(±<1%)	1.83(± 1%)	2.97(± 3%)	1.43 (± 1%)
	30.15	6.93(±<1%)	1.41(± 9%)	2.42(± 17%)	1.03 (± 3%)
	40.2	5.57(±<1%)	0.89(± 10%)	2.05(± 19%)	0.739(± 3%)
	50.0	4.53(±<1%)	0.93(± 13%)	1.17(± 18%)	0.562(± 3%)
PDMS-64(100:16.5)	20.25	9.44(± 1%)	3.38(± 9%)	2.62(± 15%)	1.83 (± 3%)
	30.35	7.50(± 1%)	2.40(± 12%)	2.48(± 23%)	1.35 (± 5%)
	40.55	6.00(±<1%)	1.86(± 5%)	1.75(± 8%)	0.926(± 1%)
	49.8	4.87(± 2%)	1.67(± 23%)	1.19(± 29%)	0.686(± 3%)
PDMS-83(61:3.6)	20.05	11.14(±<1%)	-	-	-
	30.1	8.83(±<1%)	-	-	-
	40.4	7.13(±<1%)	-	-	-
	50.0	5.84(±<1%)	-	-	-

At certain temperatures for some membranes, no values of C_H', B and S_L are quoted because those particular isotherms were effectively linear and therefore not amenable to analysis by the dual mode sorption theory.

The sorption isotherms are illustrated in Figs. 6.7 - 6.19; in some cases asymptotes for the two lowest temperatures have been drawn also. Full listings of the data are to be found in chapter 8 (Appendix 8.8).

With few exceptions the parameters reveal the expected trends and decrease with increasing temperature. Despite the sometimes large uncertainties in some of the parameters, some general conclusions can be drawn concerning the effect of block-length distribution.

The dependence of C_H' upon block length for a given weight composition appears to be fairly strong. Comparison of the results for PDMS-50(20:6) and PDMS-49(41:12.4) reveals that by effectively doubling the block lengths C_H' is increased by as much as a factor of eight.

Comparison of the results for PDMS-60(20:3.9), PDMS-60(40:712) and PDMS-60(80:14.6) reveals a similar, if less dramatic pattern. For the 20-block sample, C_H' is effectively zero at all temperatures; for the 40-block, C_H' has values of between 0.123 and 0; the corresponding range for the 80-block is 0.183 - 0.093.

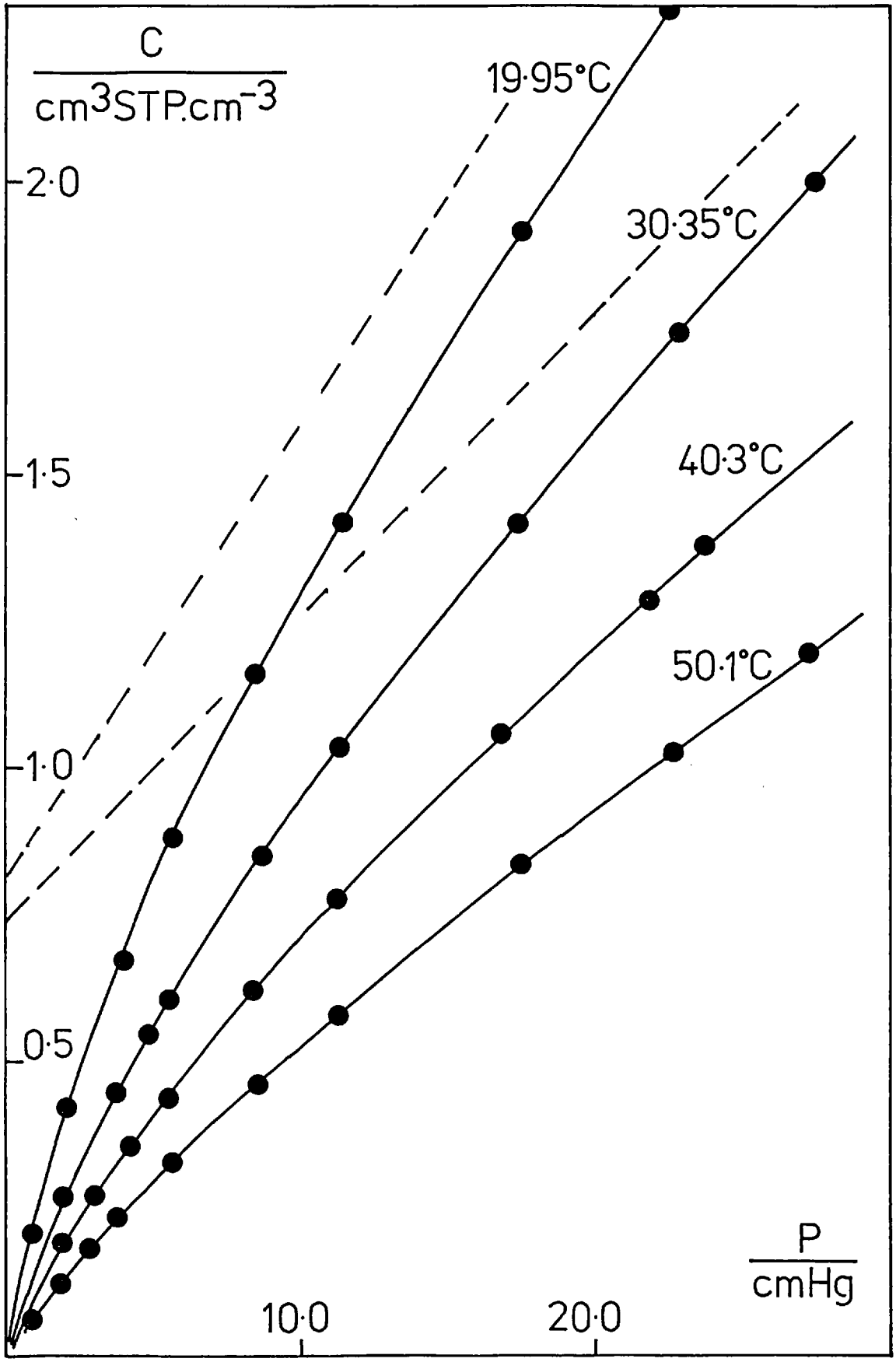


FIG. 6.7 PDMS-25(20:17·8)/PROPANE SORPTION ISOTHERMS

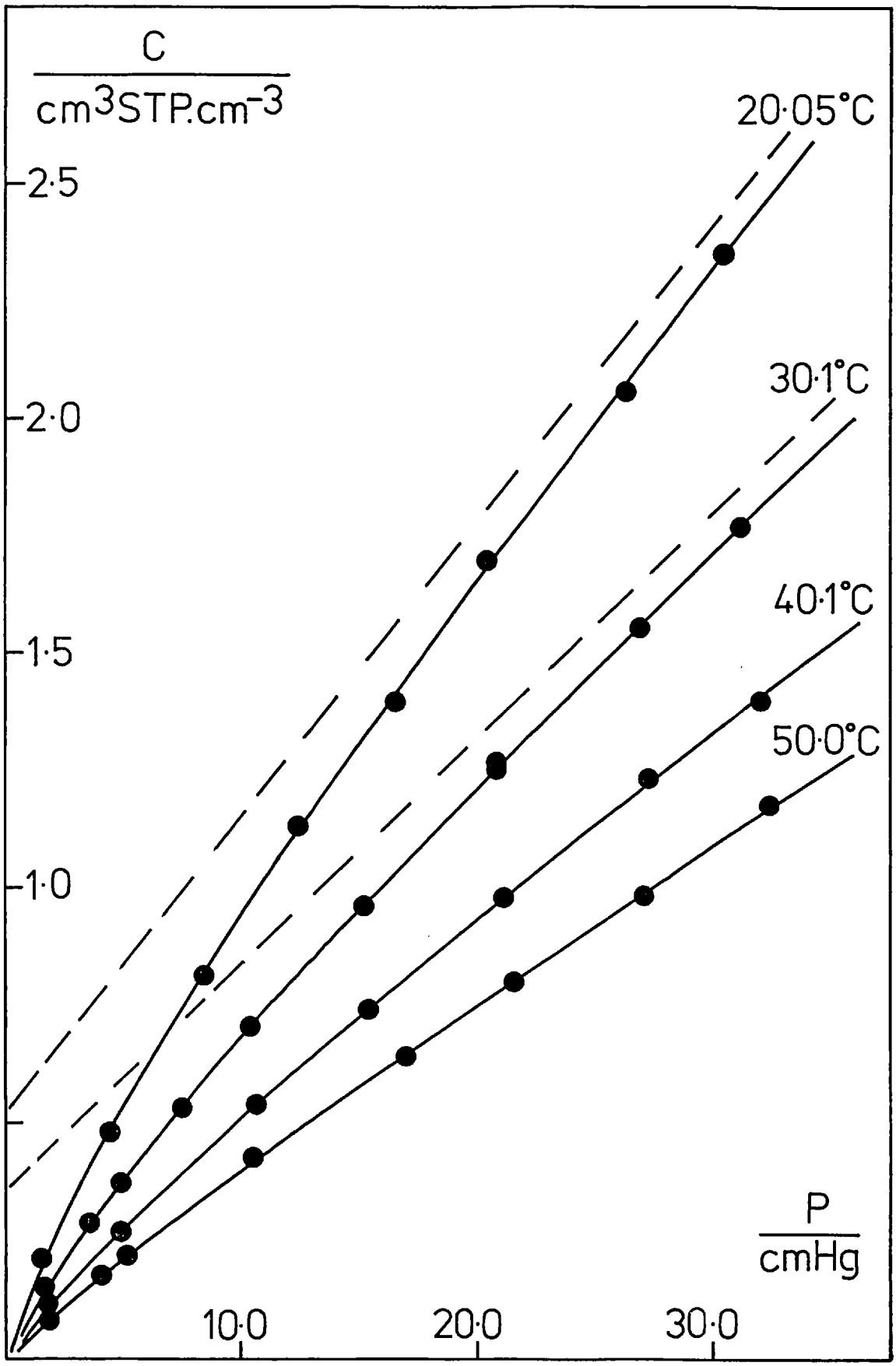


FIG. 6.8 PDMS-34(20:11)/PROPANE SORPTION ISOTHERMS

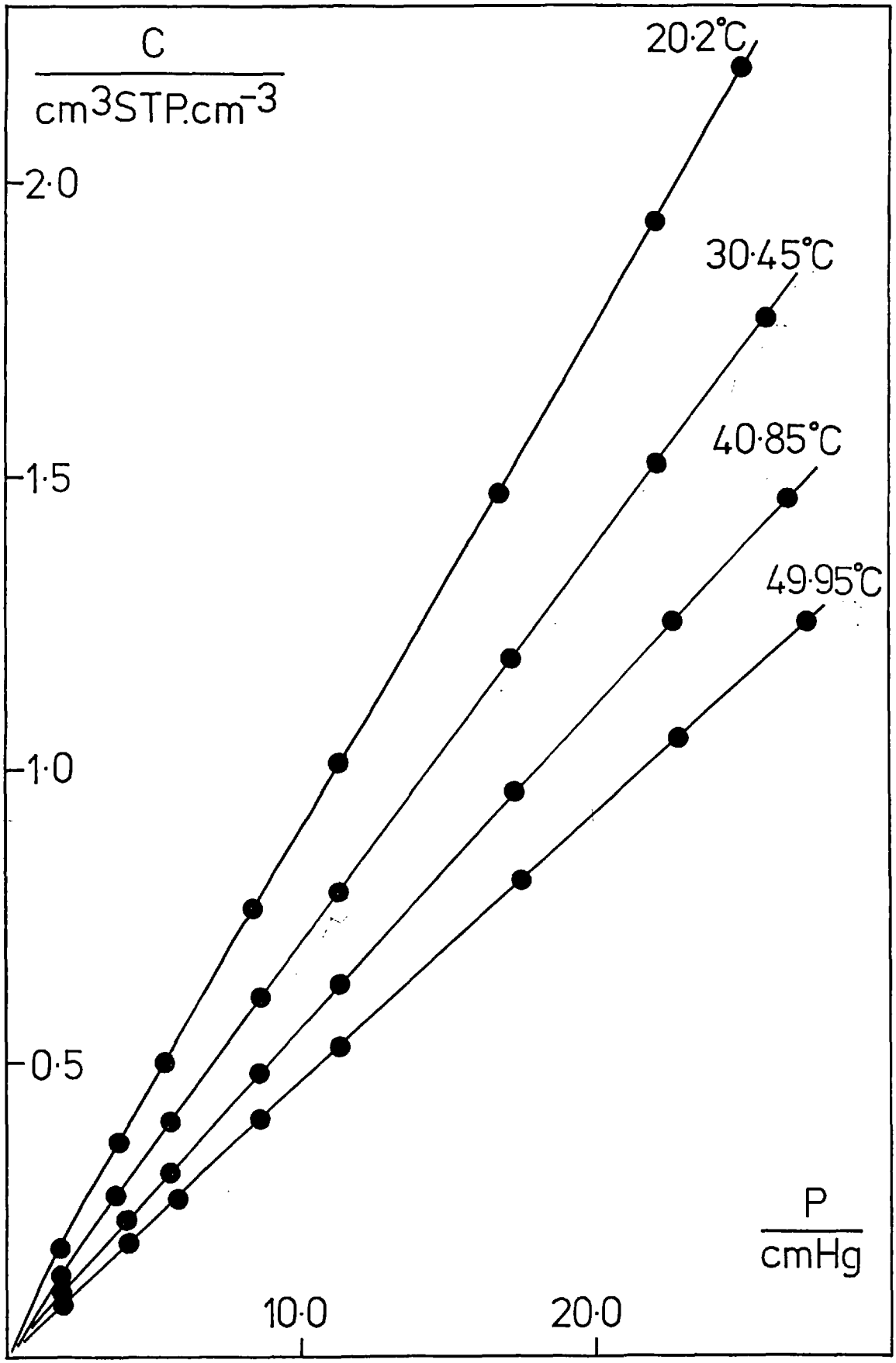


FIG. 6.9 PDMS-50(20:6)/PROPANE SORPTION ISOTHERMS

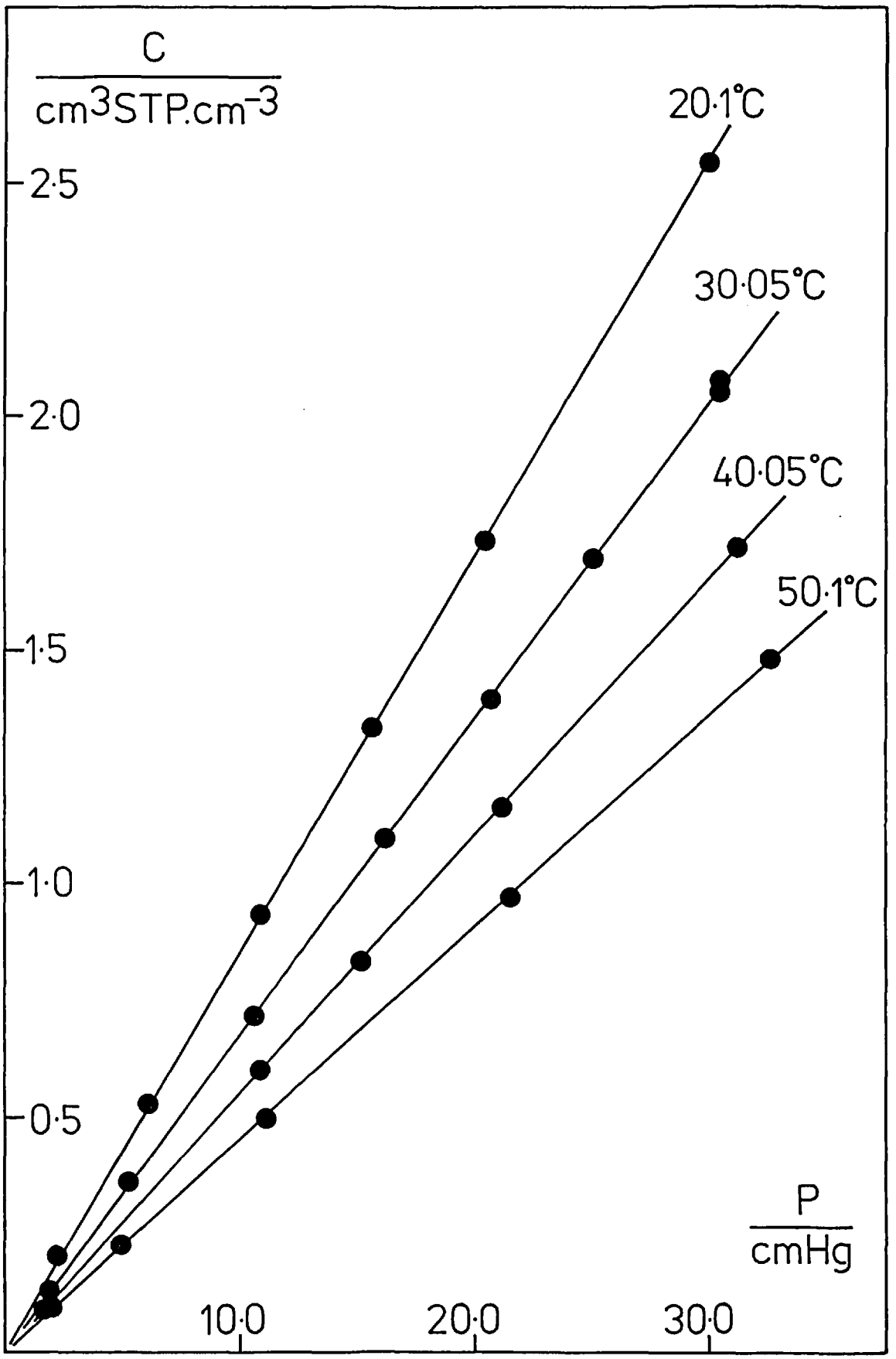


FIG. 6.10 PDMS-60(20:3·9)/PROPANE SORPTION ISOTHERMS

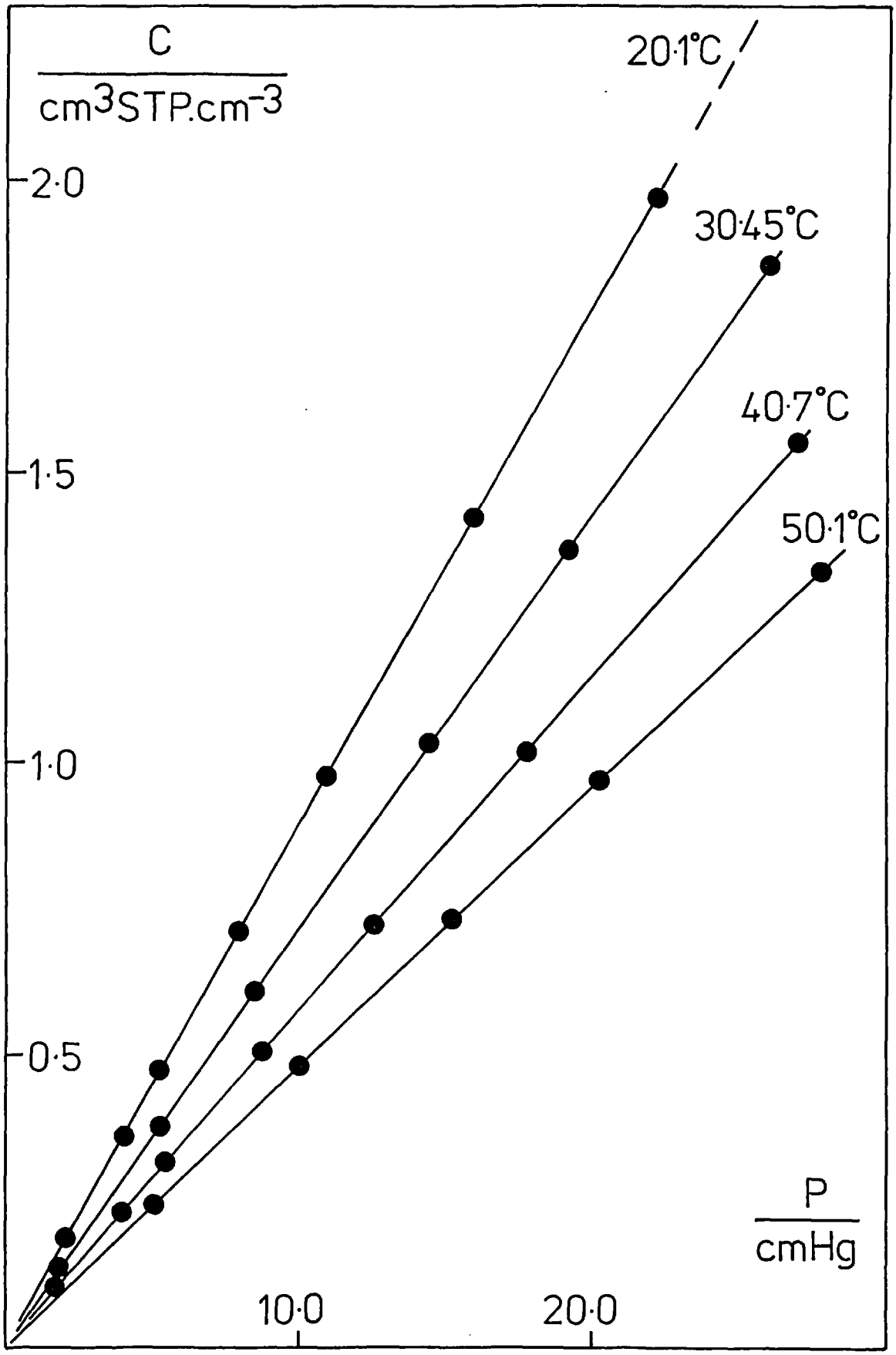


FIG. 6.11 PDMS-64(20:3·5)/PROPANE SORPTION ISOTHERMS

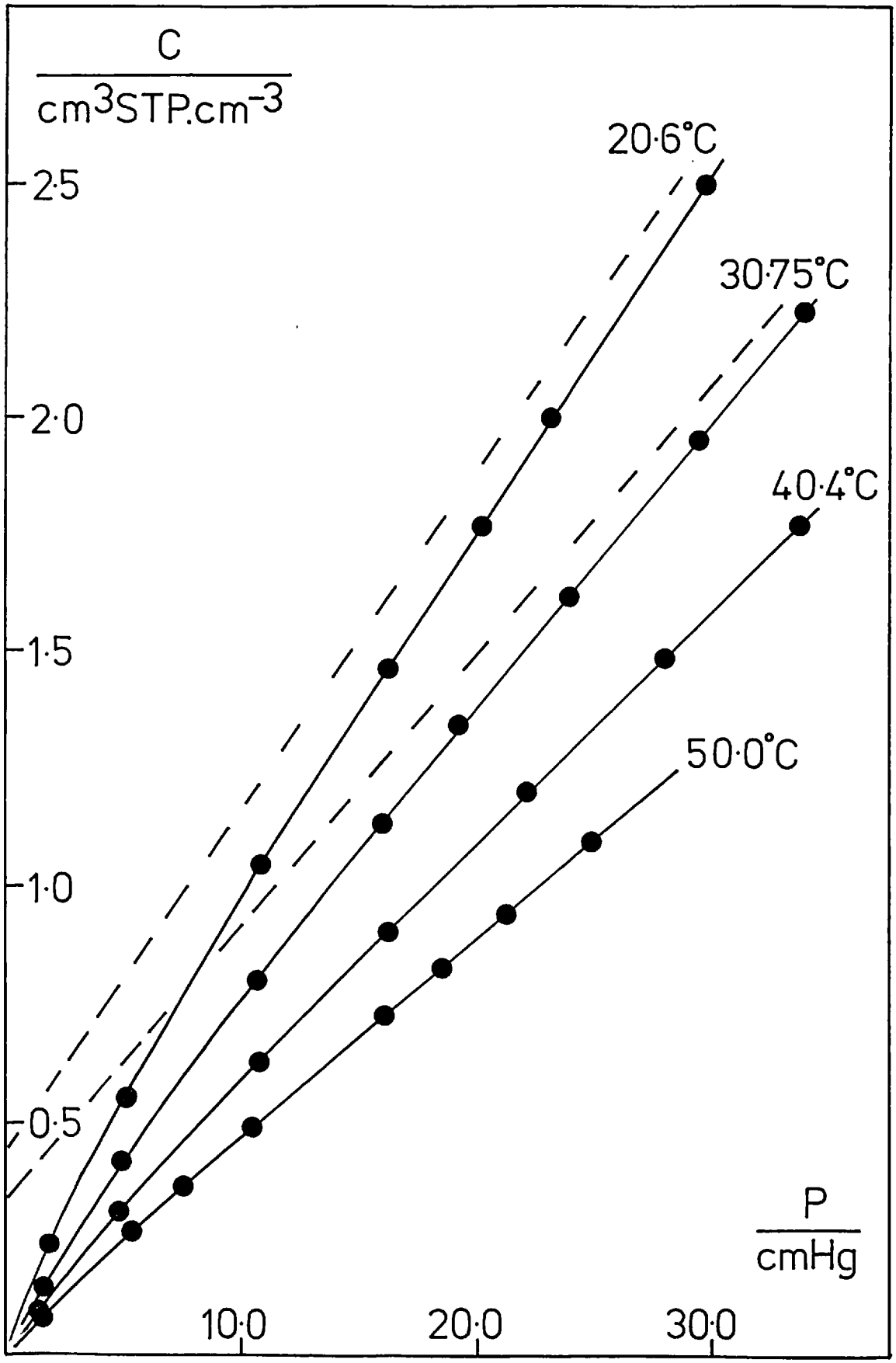


FIG. 6.12 PDMS-49(41:12·4)/PROPANE SORPTION ISOTHERMS

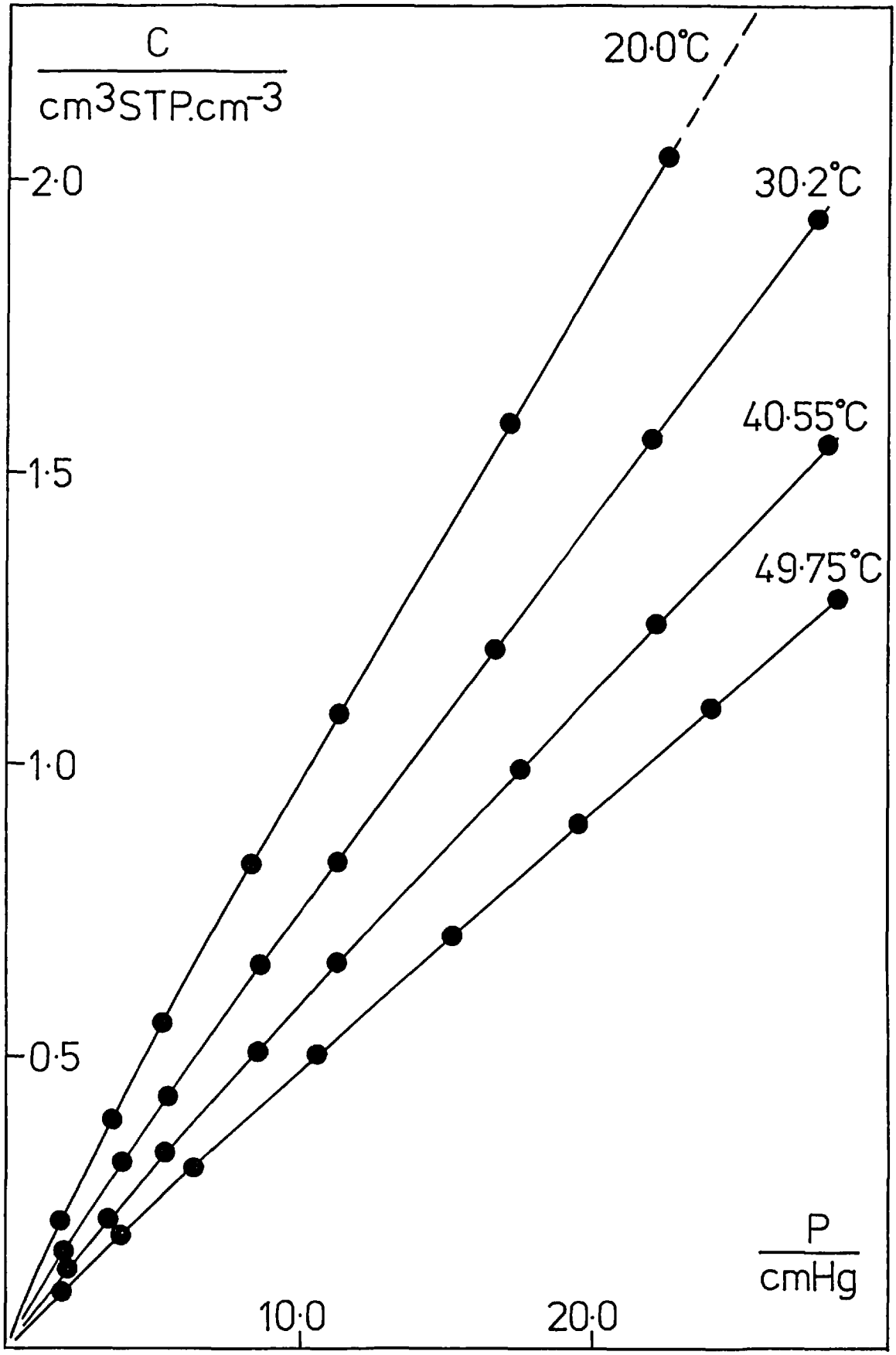


FIG. 6.13 PDMS-54(40:10)/PROPANE SORPTION ISOTHERMS

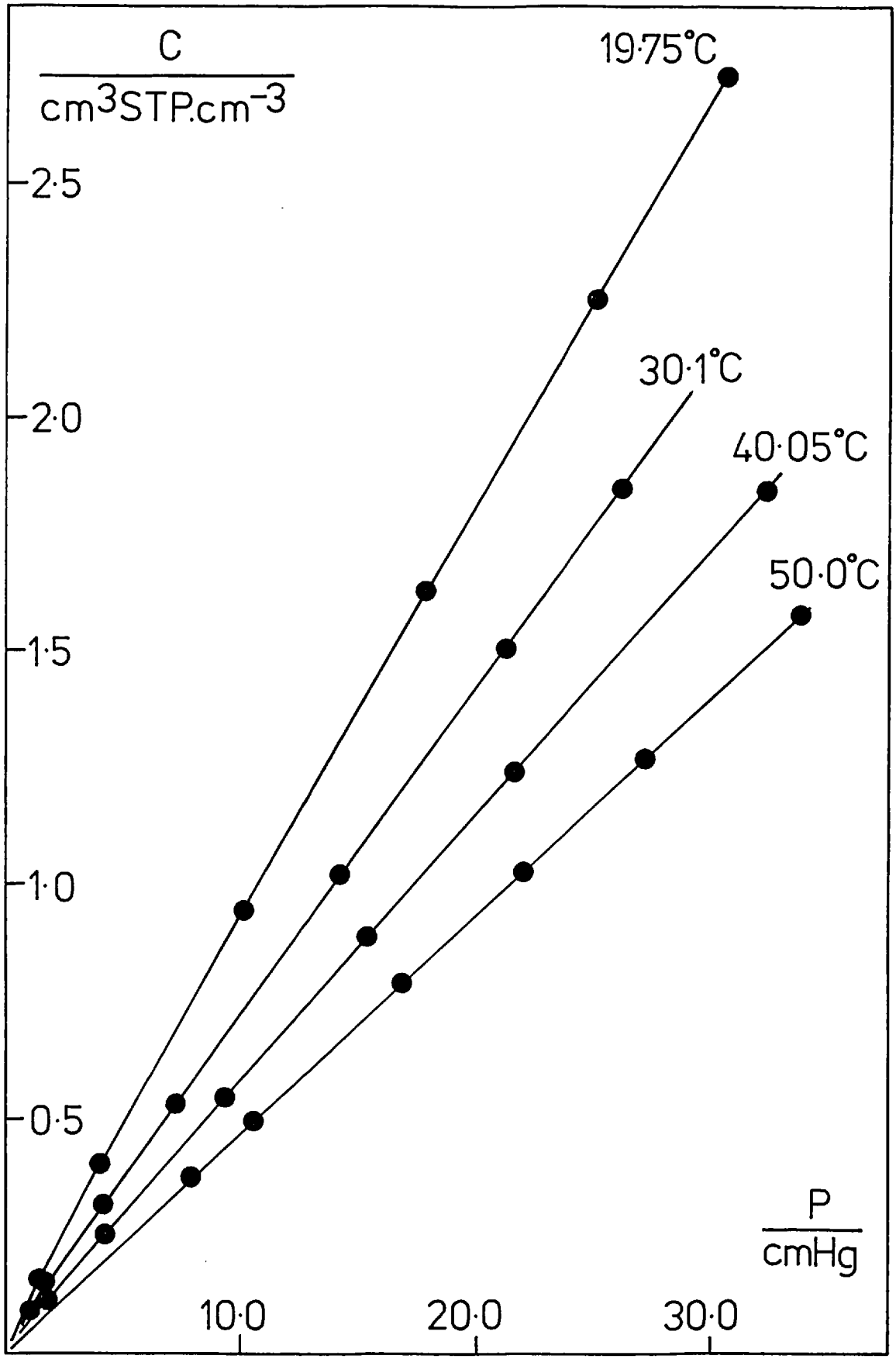


FIG. 6.14 PDMS-60(40:7·2)/PROPANE SORPTION ISOTHERMS

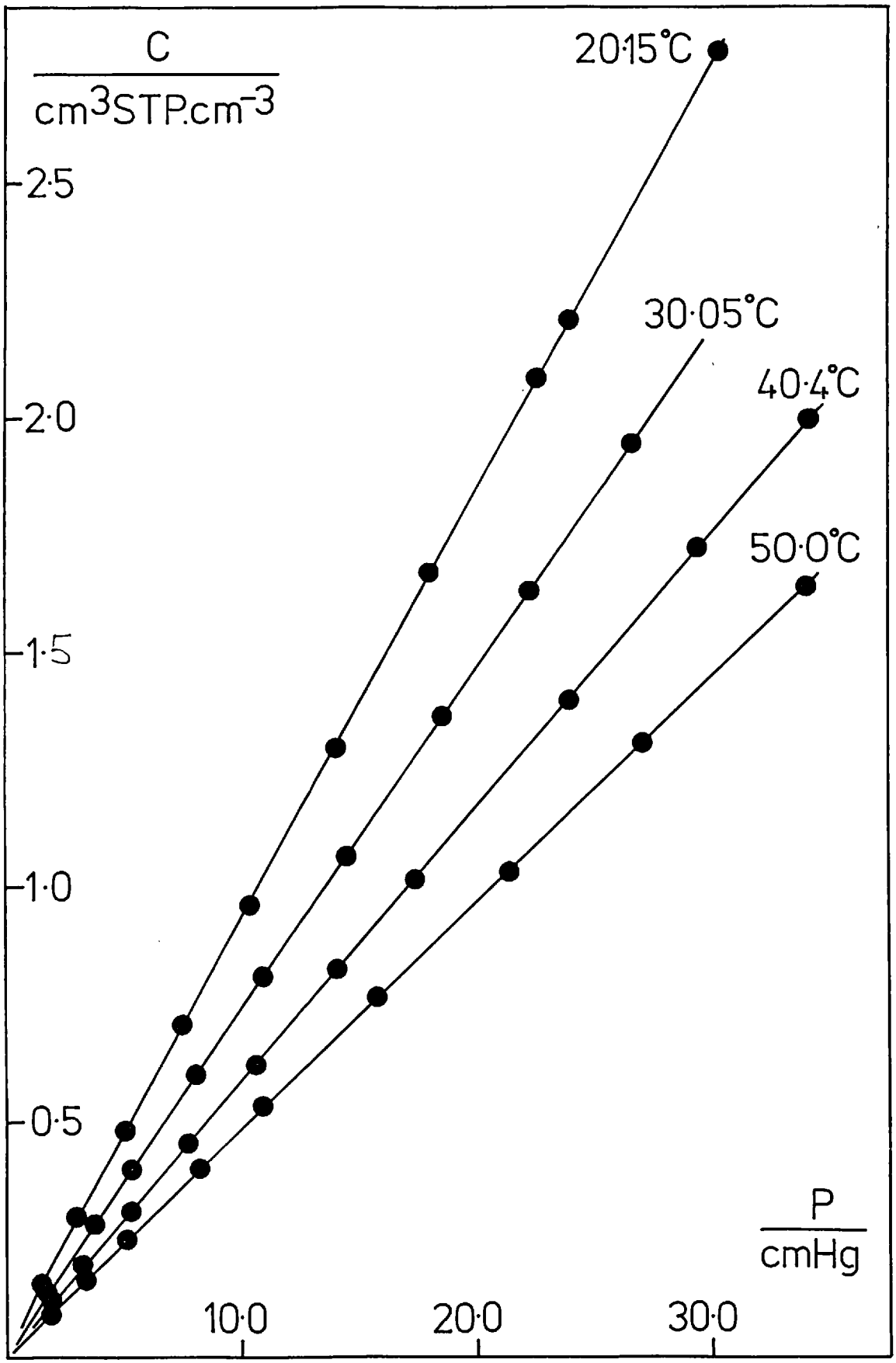


FIG. 6.15 PDMS-64(40:7)/PROPANE
SORPTION ISOTHERMS

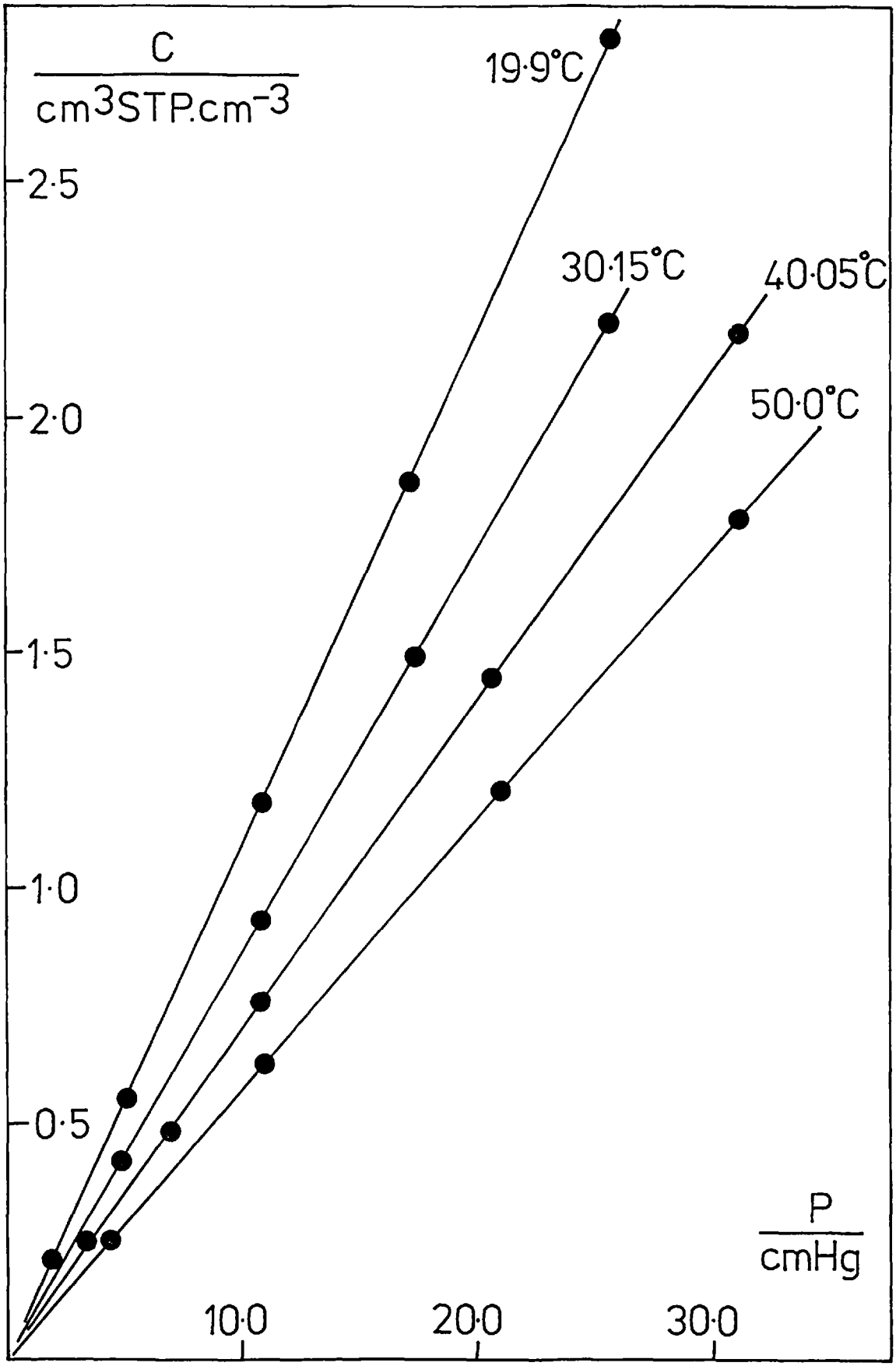


FIG. 6.16 PDMS-82(40:3)/PROPANE SORPTION ISOTHERMS

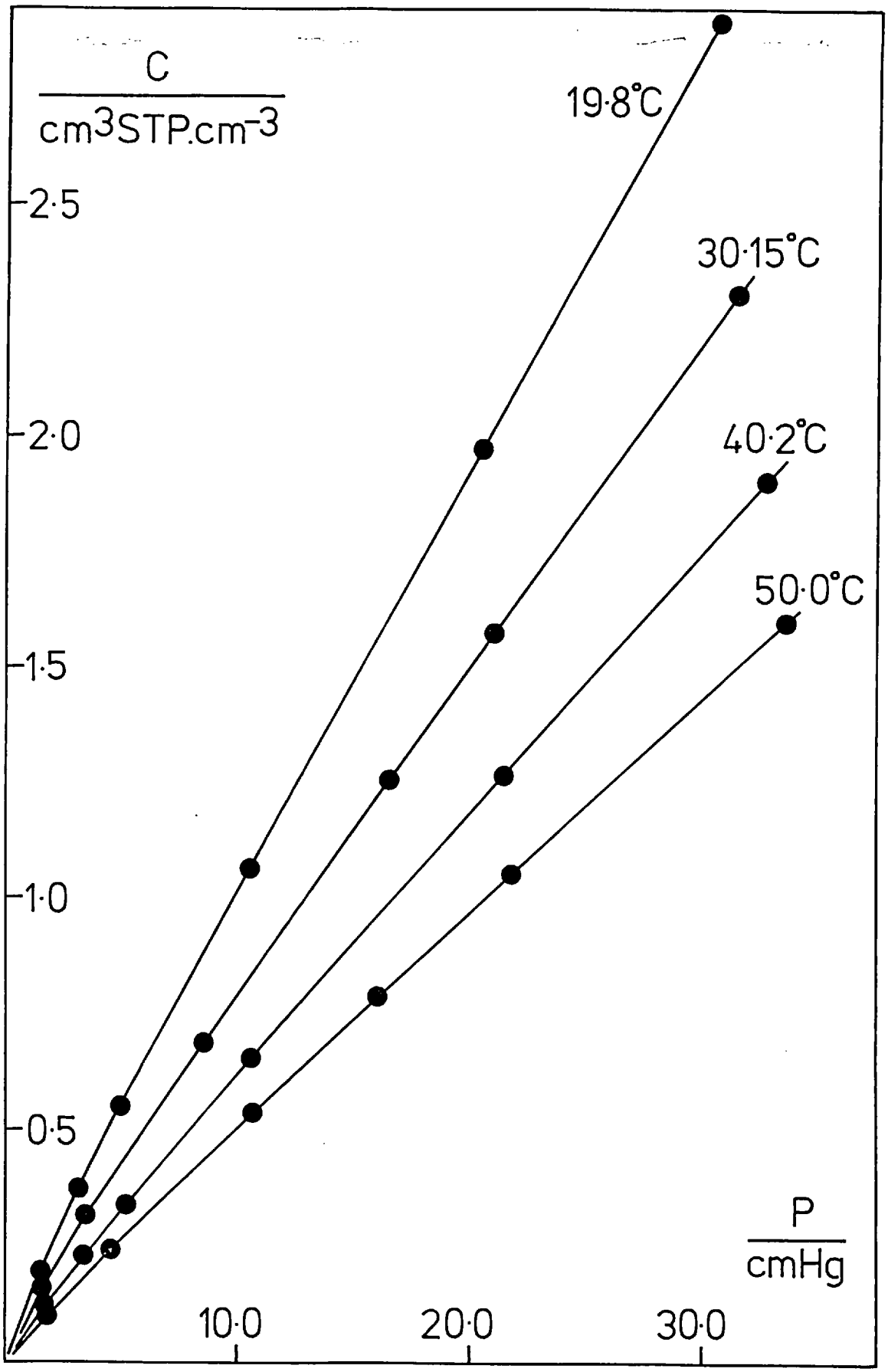


FIG. 6.17 PDMS-60(80:14·6)/PROPANE SORPTION ISOTHERMS

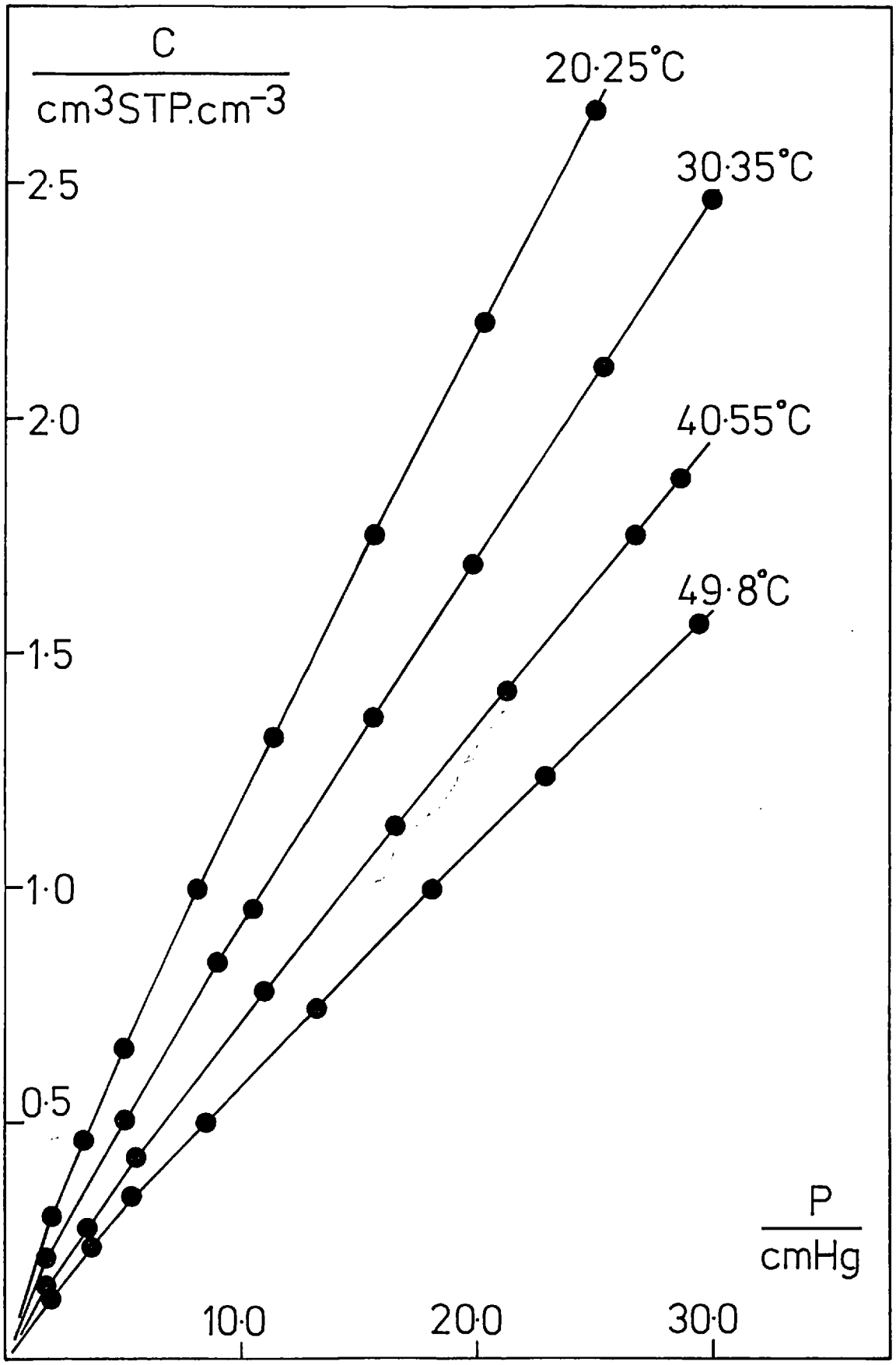


FIG. 6.18 PDMS-64(100:16·5)/PROPANE SORPTION ISOTHERMS

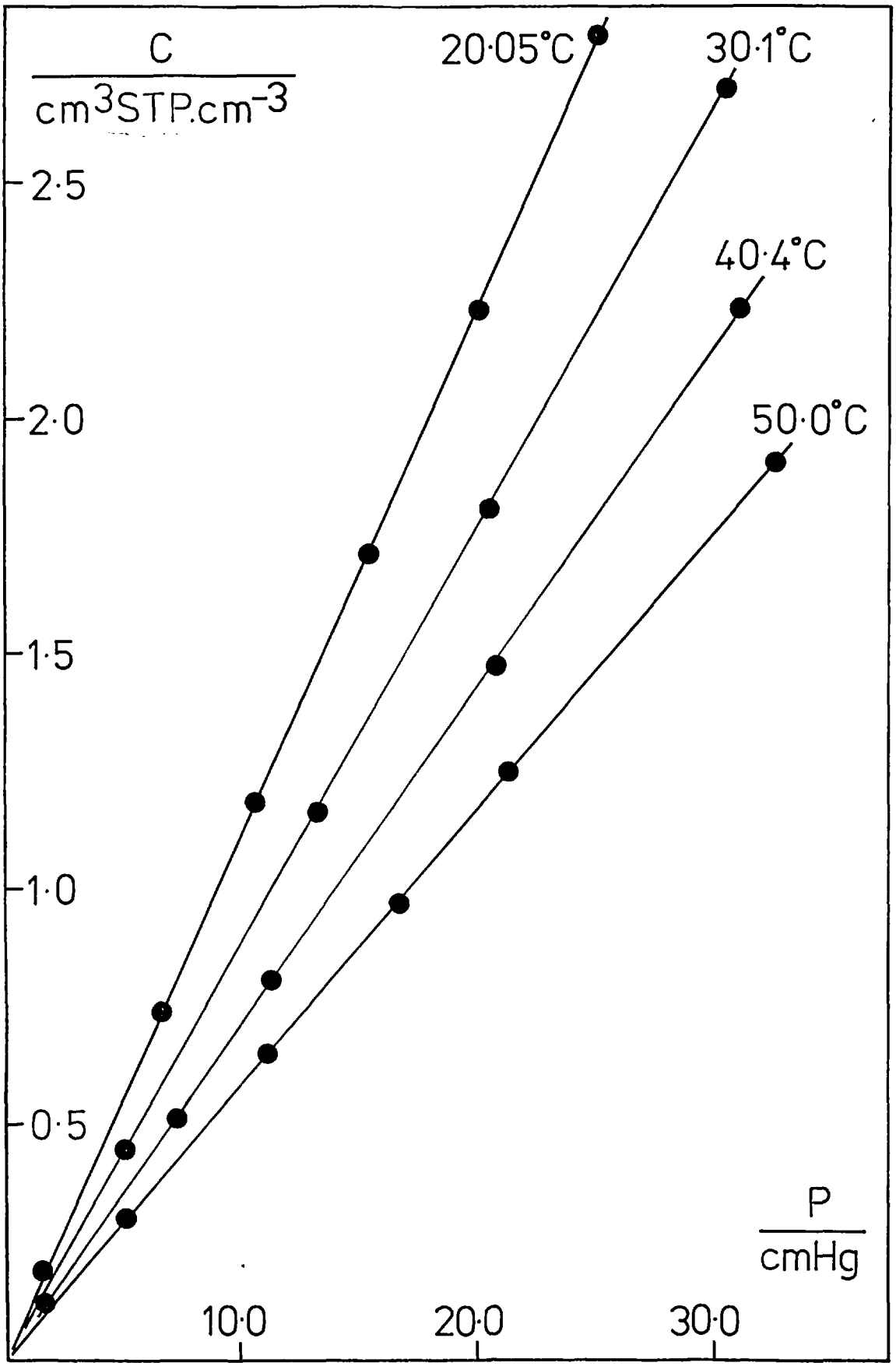


FIG. 6.19 PDMS-83(61:3·6)/PROPANE SORPTION ISOTHERMS

The C_H' results for the three samples each containing 64% PDMS by weight confirm this trend. For the 20-block sample, C_H' is effectively zero; for the 40-block, C_H' is either zero or small and positive; C_H' for the 100-block however has a range 0.338-0.167.

C_H' (which is also rough guide to the amount of cuvature in an isotherm) clearly increases with increasing block-length for a given composition at a single temperature. The effect appears to be more pronounced for samples with higher BPAC contents.

This behaviour is entirely consistent with the earlier postulation that microphase separation becomes easier for longer block lengths. The longer PDMS blocks afford the BPAC blocks (which are themselves longer) more freedom to associate and aggregate. Therefore the longer the block lengths are, the larger are the domains. A large glassy domain would be expected to contain more microcavities than say the same amount of disperse phase subdivided into smaller domains; thus the larger the domains, the larger the number of microcavities and hence the larger is C_H'.

These results are consistent with the permeability data in that both suggest a partial microphase-separated system as the morphology of these membranes with the longer blocks permitting more phase-separation than the shorter ones. For the purpose of comparison, values of k_D, S_L and B (where possible) were interpolated to 50°C and are presented in Table 6.9. Data for pure BPAC and pure PDMS are also included, and the results for k_D and S_L are illustrated in Figs. 6.20 and 6.21.

The plot in Fig. 6.20 strongly suggests that k_D for a membrane of given composition is independent of the block-length distribution. It is debatable whether a minimum occurs near to $\Phi_A = 0.4$. Firstly, the limits of uncertainty for the two points at $\Phi_A = 0.3$ and $\Phi_A = 0.4$ are such that the two corresponding values of k_D could both be 5% higher. The value of k_D for BPAC might also be lower by the same amount. Secondly, the value of k_D for BPAC was determined with the sample unannealed. Tests carried out on PDMS-60 (40:7.2) and PDMS-60(80:14.6) have produced conflicting evidence as to the effect of annealing on sorption parameters. This will be discussed in section 6.6. Thirdly, the density of the BPAC sample was necessarily determined using bulk material; the ultra-thin sheet, which weighed less than 0.2 grams was cast on glass fairly rapidly and it is likely that the density of the sample was less than the density of bulk BPAC. A lower value of the density of BPAC would result in a lower value of k_D.

Table 6.9 Values of k_D, S_L and B at 50°C.

Membrane	Φ_A	$10^2.k_D/(\frac{cm^3 STP}{cm^3 cmHg})$	$10.B/(cmHg)^{-1}$	$10^2 S_L/(\frac{cm^3 STP}{cm^3 cmHg})$
BPAC	0.000	3.80	1.84	23.58
20-blocks:				
PDMS-25(20:17.8)	0.287	3.38	1.03	7.24
PDMS-34(20:11)	0.384	3.21	0.75	4.90
PDMS-50(20:6)	0.547	4.48	-	4.63
PDMS-60(20:3.9)	0.644	4.54	-	(4.54)
PDMS-64(20:3.5)	0.682	4.81	-	(4.81)
40-blocks:				
PDMS-49(41:12.4)	0.537	4.04	-	5.61
PDMS-54(40:10)	0.586	4.34	1.47	5.24
PDMS-60(40:7.2)	0.644	4.67	-	4.97
PDMS-64(40:7)	0.682	4.82	-	5.17
PDMS-82(40:3)	0.846	5.73	-	(5.73)
Misc.				
PDMS-60(80:14.6)	0.644	4.54	1.33	5.61
PDMS-64(100:16.5)	0.682	4.89	1.30	6.89
PDMS-83(61:3.6)	0.855	5.85	-	(5.85)
PDMS	1.000	6.66	-	(6.66)

The expectation for the plot of k_D vs. volume fraction of PDMS was that it would not obey a simple additivity rule as described in Chapter 5 (section 5.3) since this has been found to apply to systems characterised by complete phase-separation such as the PDMS-g-PVAc copolymers. All the evidence so far indicates that the alternating PDMS-b-BPAC system cannot be described in such simple terms.

Shur and Rånby (107) carried out equilibrium sorption experiments to examine the Henry's Law solubility coefficients of carbon dioxide and nitrogen in semi-miscible blends which covered the entire range of volume fractions of the two components. In each case the value of k_D was lower than that predicted by simple additivity of the solubility coefficients and this was believed to be due to some kind of chemical

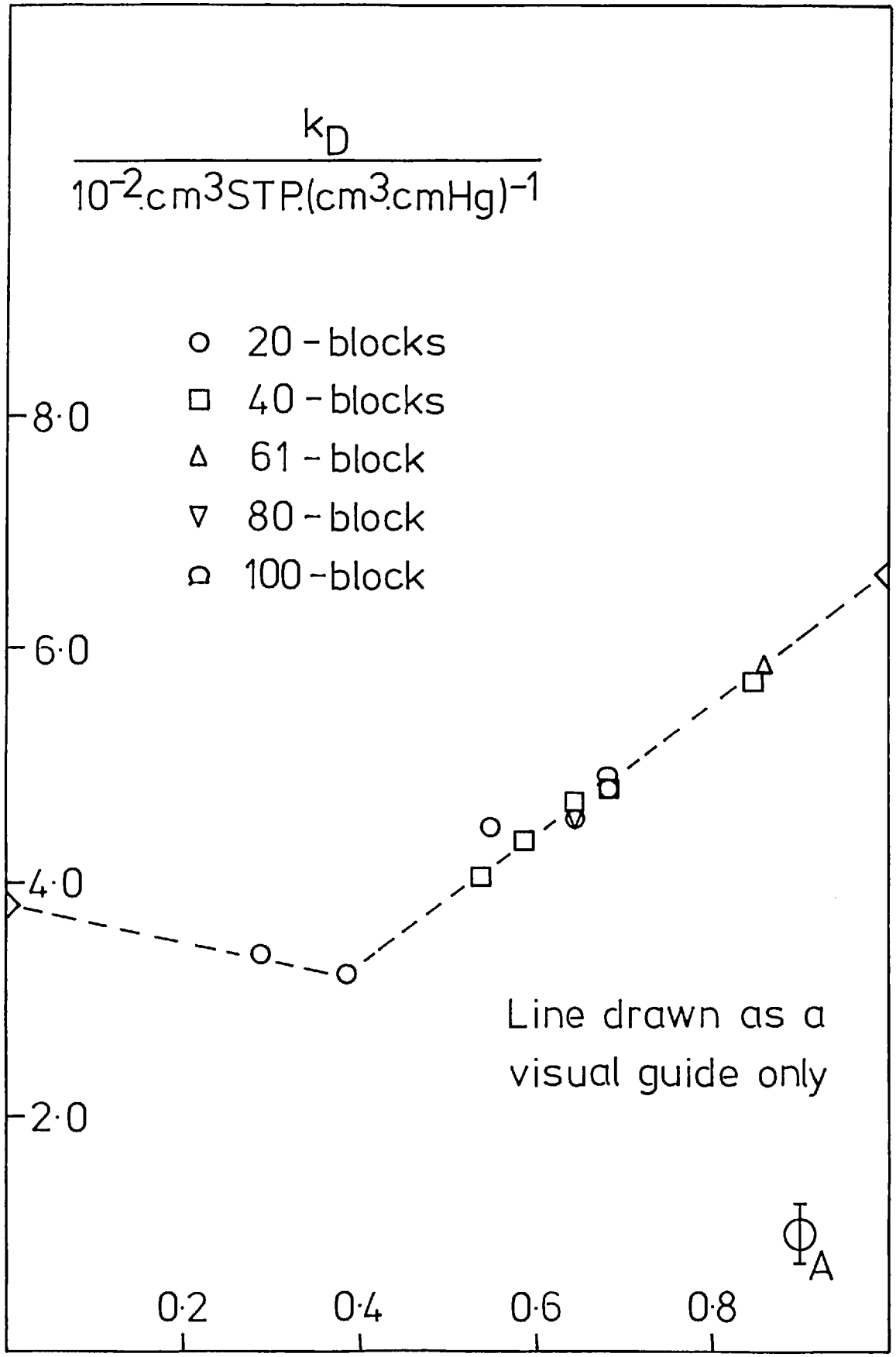


FIG. 6.20 PDMS—b—BPAC/PROPANE
k_D vs. VOLUME FRACTION OF PDMS

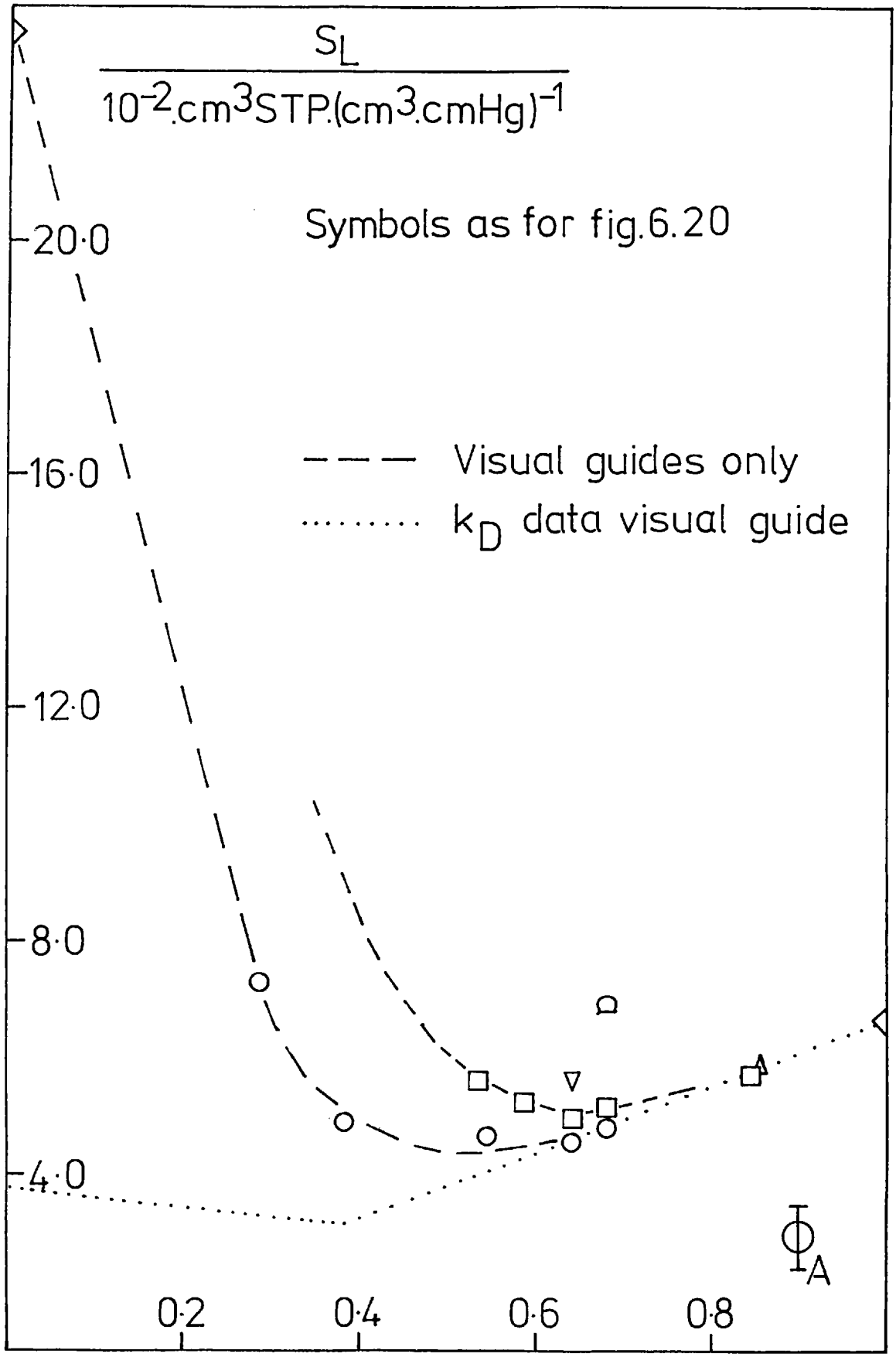


FIG. 6.21 PDMS-b-BPAC/PROPANE

S_L vs. VOLUME FRACTION OF PDMS

(as well as physical) interaction between the two components.

An alternative suggestion which would seem equally applicable to the system under investigation here (since the continuous phase for most of these membranes can be treated as a random copolymer or dilute miscible blend of BPAC in PDMS) is that if one component is essentially "dissolved" in the other, then the system's sorptive capacity is consequently reduced.

The dependence of S_L on the block-length distribution is clearly revealed in Fig. 6.21. For both the 20-blocks and 40-blocks the coefficient for total solubility starts to decrease initially from $\Phi_A = 1$ as some BPAC, which has a lower value of k_D, is introduced. Presumably domain formation is difficult in this region and no significant Langmuir contribution is observed at this stage. As Φ_B increases (Φ_A decreases) further, the domains of BPAC are of sufficient size for microvoids to form in sufficient quantity to make a significant Langmuir contribution to the sorption of the penetrant. The coefficient for total solubility therefore passes through a minimum and starts to rise as the Langmuir component continues to grow.

As suggested earlier for the effect of block-length on C'_H the 40-block membranes are expected to form bigger domains more easily than the 20-blocks for a given composition, so that the minimum in the plot of S_L versus Φ_A occurs at lower values of Φ_B.

The heats of solution are presented in Table 6.10. The uncertainties quoted are based on the scatter in the respective van't Hoff semilog plots (not shown). If account were taken of the errors attached to the sorption parameters themselves, the uncertainties would be considerably greater.

Since $\Delta\overline{H}_H$ represents the energy difference (entropy considerations apart) between the penetrant in the gas state and in the immobilised state in the microcavities of the glassy phase, this parameter should be independent of composition and remain constant at the value for pure BPAC assuming that the glassy domains are pure. Table 6.10 suggests that this is indeed generally the case within the experimental uncertainty of the system.

The results for $\Delta\overline{H}_D$ and $\Delta\overline{H}_{S(C=O)}$ are illustrated in Fig.6.22 and the time-lag (transient) values of $\Delta\overline{H}_S$ have been included for purposes of comparison. No general conclusions are possible, such is the uncertainty in the values and the scatter in the plots. Nevertheless, values of $\Delta\overline{H}_D$

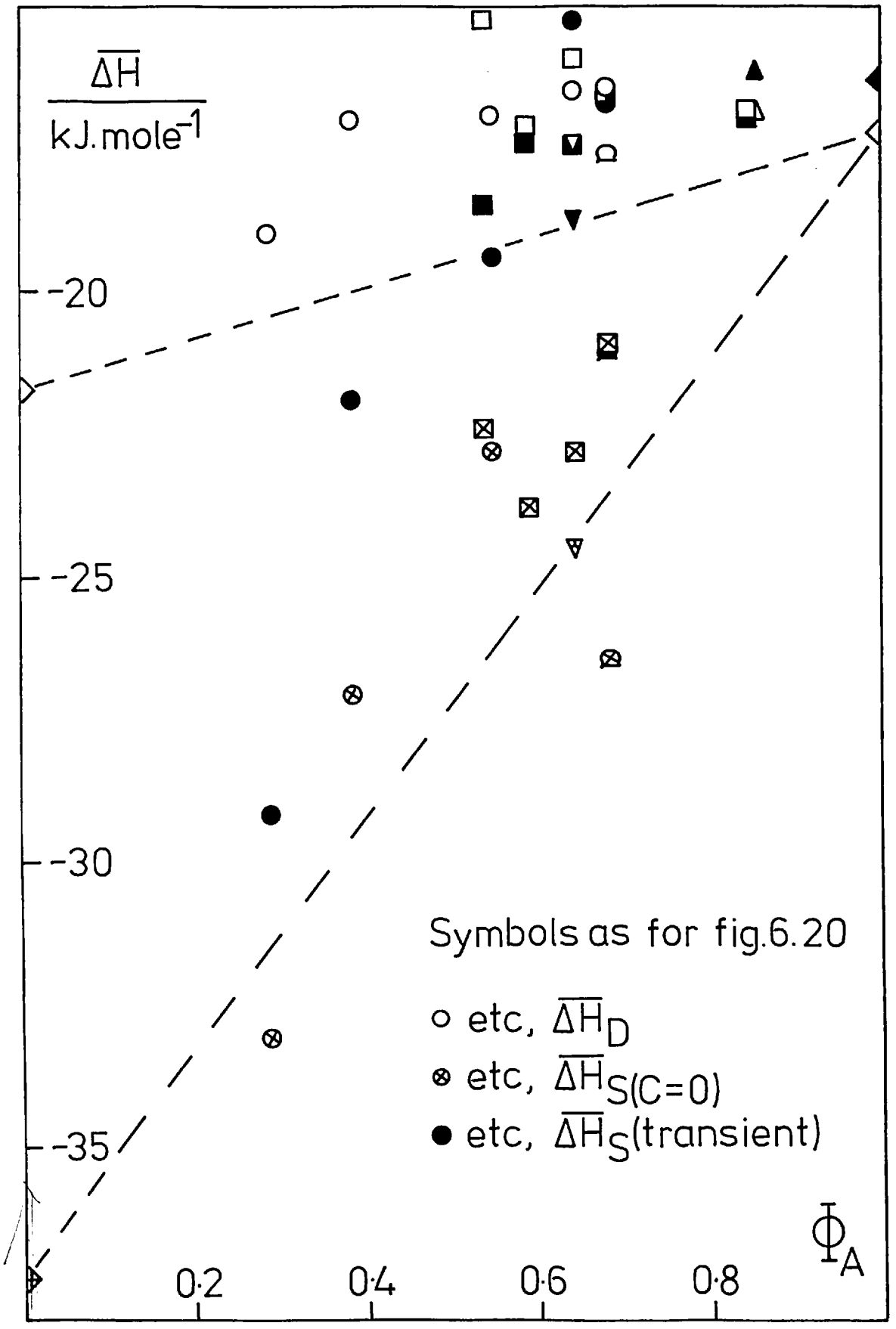


FIG. 6.22 PDMS – b – BPAC/PROPANE
HEATS OF SOLUTION vs. Φ_A

Table 6.10 Enthalpies of solution for PDMS-b-BPAC/propane

Membrane	$\Delta\bar{H}_D$/kJ.mole^{-1}	$\Delta\bar{H}_H$/kJ.mole^{-1}	$\Delta\bar{H}_{S(C=O)}$/kJ.mole^{-1}
BPAC	- 21.7	- 25.2	- 37.3
20-blocks:			
PDMS-25(20:17.8)	- 19.0 (±1.2)	- 19.0 (±5.5)	- 33.1 (±1.2)
PDMS-34(20:11)	- 17.0 (±2.1)	- 19.0 (±6.5)	- 27.1 (±1.4)
PDMS-50(20:6)	- 16.9 (±0.4)	-	- 22.8 (±1.7)
PDMS-60(20:3.9)	- 16.5 (±0.1)	-	(-16.5)
PDMS-64(20:3.5)	- 16.4 (±0.1)	-	(-16.4)
40-blocks:			
PDMS-49(41:12.4)	- 15.2 (±0.9)	-	- 22.4 (±1.11)
PDMS-54(40:10)	- 17.1 (±0.3)	- 13.0 (±5)	- 23.8 (±0.4)
PDMS-60(40:7.2)	- 15.9 (±0.2)	-	- 22.8 (±3.0)
PDMS-64(40:7)	- 16.5 (±0.2)	-	- 20.9 (±2.8)
PDMS-82(40:3)	- 16.8 (±0.1)	-	(-16.8)
Misc.:			
PDMS-60(80:14.6)	- 17.4 (±0.1)	- 22.9 (±0.5)	- 24.5 (±0.5)
PDMS-64(100:16.5)	- 17.6 (±0.3)	- 21 (±5)	- 26.4 (±1.0)
PDMS-83(61:3.6)	- 16.9 (±0.1)	-	(-16.9)
PDMS	- 17.2	-	(-17.2)

appear to be consistently higher than those which would be predicted by a simple additivity rule between the two heats of dissolution for the pure components (the upper dashed line in Fig. 6.22).

6.5 Steady-state diffusion coefficients

The transient diffusion coefficients discussed in section 6.3.5 have been assumed to be weakly dependent on concentration due to the presence, albeit to a small degree in most cases, of a Langmuir component of sorption arising from the immobilisation of penetrant in the microcavities existing in the glassy BPAC domains. The extent of the Langmuir contribution to sorption in the membranes has been estimated in the previous section; the limits of the concentration dependence can now be surmised from the steady-state diffusivities.

In the limit C=0, $D_{C=0}$ can be defined using the limiting solubility coefficient at C=0, S_L.

$$D_{C=0} = \frac{\overline{P}}{S_L} \qquad \ldots (6.21)$$

In the limit $C \to \infty$, pressure P also tends to infinity and the dual mode isotherm (equation (2.37)) reduces to

$$C = k_D P + C'_H \qquad \ldots (2.38)$$

hence the limiting solubility coefficient as P, $C \to 0$

$$S_{P,C\to\infty} = \frac{C}{P} = k_D + \frac{C'_H}{P} \to k_D \qquad \ldots (6.22)$$

D in the limit $C \to \infty$ can also be represented by the diffusion coefficient for the Henry's Law (mobile) species, D_m. Thus

$$D_{C\to\infty} = \frac{\overline{P}}{S_{P,C\to\infty}} = D_m = \frac{\overline{P}}{k_D} \qquad \ldots (6.23)$$

Two steady-state diffusion coefficients, D_m and $D_{C=0}$ define the limits for the diffusion coefficient, D, at $C\to\infty$ and C=0.

Activation energies of diffusion for the two limiting values of D also exist and can be defined as

$$E_{D_m} = E_P - \Delta\overline{H}_D \qquad \ldots (6.24)$$

and

$$E_{DO} = E_P - \Delta\overline{H}_{S(C=0)} \qquad \ldots (6.25)$$

Values of D_m and $D_{(C=0)}$ (at 50°C), E_{D_m} and E_{DO} have been determined using the foregoing equations and the results presented in Tables 6.1, 6.3 6.9 and 6.10. The results are presented in Table 6.11.

For the purposes of comparison, the transient (time-lag) values of D have been included in Fig. 6.23. For the sake of clarity the results for the "misc." membranes have been omitted.

It is immediately evident that with only one exception the time-lag D's, both for the 20- and 40-blocks, are consistently below both the steady-state D's. The expectation was that they should lie between the upper and lower limits which the steady-state D's represent. Experimental error of such consistency is unlikely and one must raise the question of "edge effects" once more.

Table 6.11 Steady-state D's at 50°C and activation energies

Membrane	$10^6 D_m/cm^2.s^{-1}$	$10^6.D_{C=O}/cm^2.s^{-1}$	E_{D_m}/kJ.mole	E_{DO}/kJ.mole^{-1}
BPAC	8.35×10^{-5}	2.23×10^{-5}	66.8	66.6
20-blocks:				
PDMS-25(20:17.8)	0.592	0.276	16.1 (±1.6)	30.2 (± 1.6)
PDMS-34(20:11)	1.45	0.949	15.1 (±2.6)	25.2 (± 1.9)
PDMS-50(20:6)	2.06	2.00	19.2 (±0.6)	25.1 (± 1.9)
PDMS-60(20:3.9)	2.78	(2.78)	18.3 (±0.3)	(18.3)
PDMS-64(20:3.5)	3.04	(3.04)	18.1 (±0.8)	(18.1)
40-blocks:				
PDMS-49(41:12.4)	3.69	2.66	12.2 (±1.1)	19.4 (± 1.3)
PDMS-54(40:10)	4.10	3.40	15.1 (±0.5)	21.8 (± 0.6)
PDMS-60(40:7.2)	4.07	3.82	14.8 (±0.3)	21.7 (± 3.1)
PDMS-64(40:7)	4.71	4.39	15.5 (±0.4)	19.9 (± 3.0)
PDMS-82(40:3)	5.86	(5.86)	15.3 (±0.2)	(15.3)
Misc.:				
PDMS-60(80:14.6)	4.93	3.99	14.9 (±0.3)	22.0 (± 0.7)
PDMS-64(100:16.5)	6.32	4.48	15.0 (±0.4)	23.8 (± 1.1)
PDMS-83 (61:3.6)	6.82	(6.82)	15.0 (±0.2)	(15.0)
PDMS	7.58		14.3	

Factors which may contribute to delaying the attainment of the steady state for a permeation "run" (thus increasing the time-lag and decreasing D) might include the equilibration time for the entire "downstream" side of the permeation apparatus (adsorption to the glass, the grease on the taps, the Baratron head etc), diffusion in the periphery of the membrane gripped by the cups of the permeation cell and even diffusion into the cell sealant. It is puzzling however that the time-lag D for pure PDMS quoted by Alexopoulos et al (154) is higher than the steady-state value.

The graphs for the steady-state values of D warrant close comparison with the graphs of permeability vs. Φ_A for this system at 50°C as shown in Fig. 6.1. The shape of the plots is remarkably similar, especially in comparison to the plot for D_m. The two distinct series are clearly distinguishable. For each series, the graph splits into two (c.f. Fig. 6.21) with $D_{C=O}$ becoming smaller than D_m as Φ_B increases (Φ_A decreases)

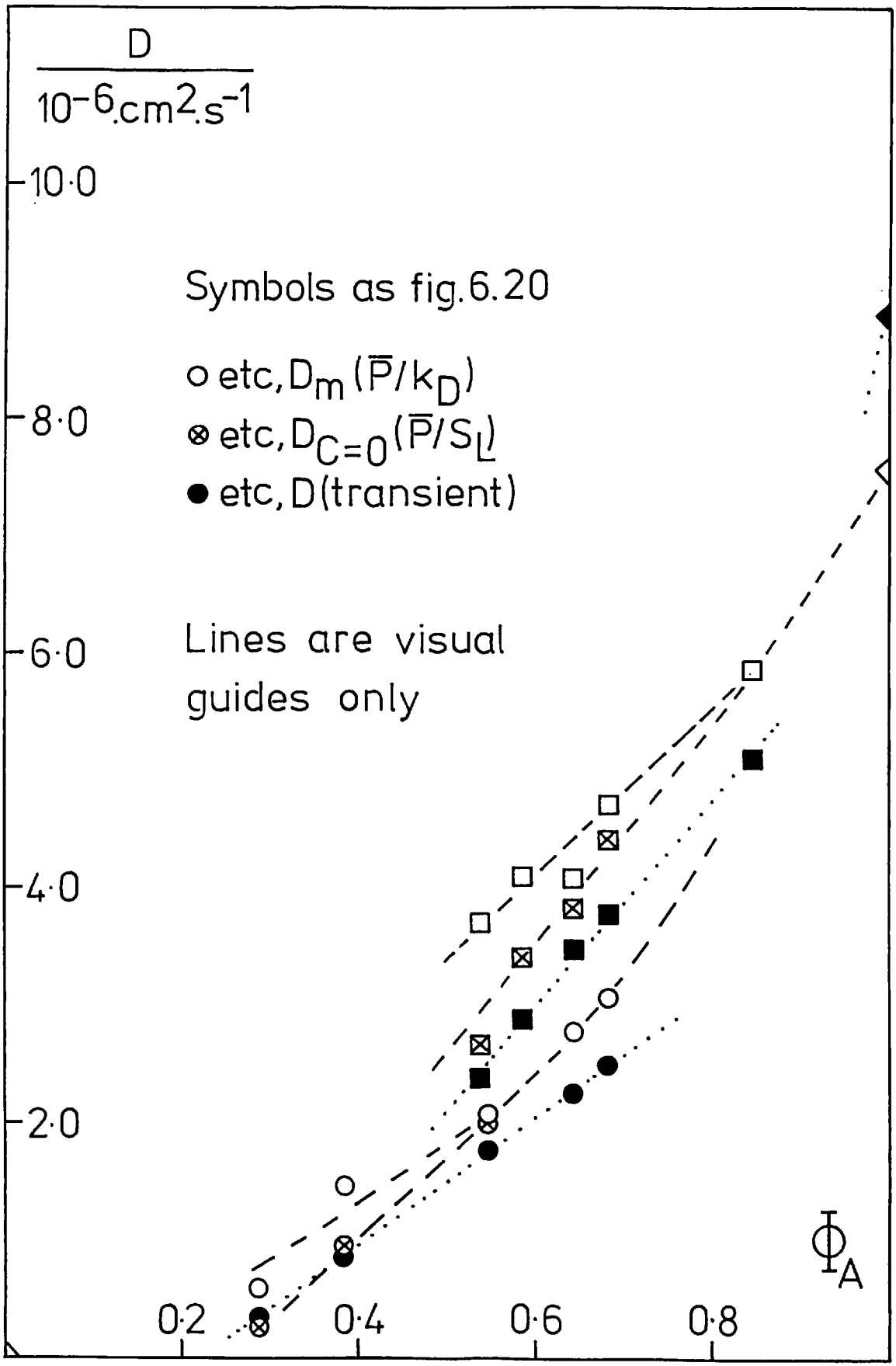


FIG. 6.23 PDMS-b-BPAC /PROPANE

DIFFUSIVITY vs. Φ_A

indicating the growing influence of the Langmuir component representing the degree of penetrant immobilisation which itself is responsible for the consequent lowering of D.

The results for the activation energies of diffusion are plotted in Fig. 6.24 and the time-lag E_D's have been included also.

This figure warrants close comparison with the results for E_P shown in Fig. 6.5. The E_D values (which, in terms of experimental uncertainty, are the most accurate) reveal the same inflection as the E_P values. The physical interpretation of this feature is speculative, but can be based upon the dependence on Φ_A of the quantity $\Delta\Phi$, the volume fraction of BPAC believed to be "blended" with PDMS in the continuous phase.

$\Delta\Phi$ must be zero at $\Phi_A = 1$. As Φ_A decreases, $\Delta\Phi$ rises to its mean value; phase separation occurs, but becomes less complete as Φ_B increases. This accounts for the initial rise in the value of the activation energy. As Φ_A decreases further, the BPAC blocks become sufficiently large so that more complete phase separation becomes possible. The value of $\Delta\Phi$ therefore falls as phase separation becomes more complete and the continuous phase becomes more pure resulting in the activation energy falling.

Finally, as Φ_A decreases further still, phase inversion occurs and E_D rises dramatically, and the same argument applies for E_P. The graph in Fig. 6.24 suggests that phase inversion ought to occur for the 20-blocks at around $\Phi_A = 0.3$ and the electron micrographs of PDMS-25 (20:17.8) (where $\Phi_A = 0.287$) appear to support this possibility (see Appendix 8.9, Figs. 8.1 and 8.2). Both photographs seem to suggest two indistinguishable (PDMS-domain/BPAC-continuum), (BPAC-domain/PDMS-continuum) morphologies which is possibly symptomatic of imminent phase-inversion.

The plots for E_{DO} reflect the growing influence of the Langmuir immobilisation as Φ_A decreases, and appear to rise steadily, although the presence of slight inflections similar to the ones described above cannot be ruled out.

6.6 Effect of annealing on sorption

The earlier suggestion (section 6.4) that comparison of the sorption results for pure BPAC with those of the membranes might be complicated by the fact that the BPAC sample was not annealed before the studies commenced prompted an analysis in terms of the dual mode sorption model of earlier results on two membranes : PDMS-60(80:14.6), unannealed;

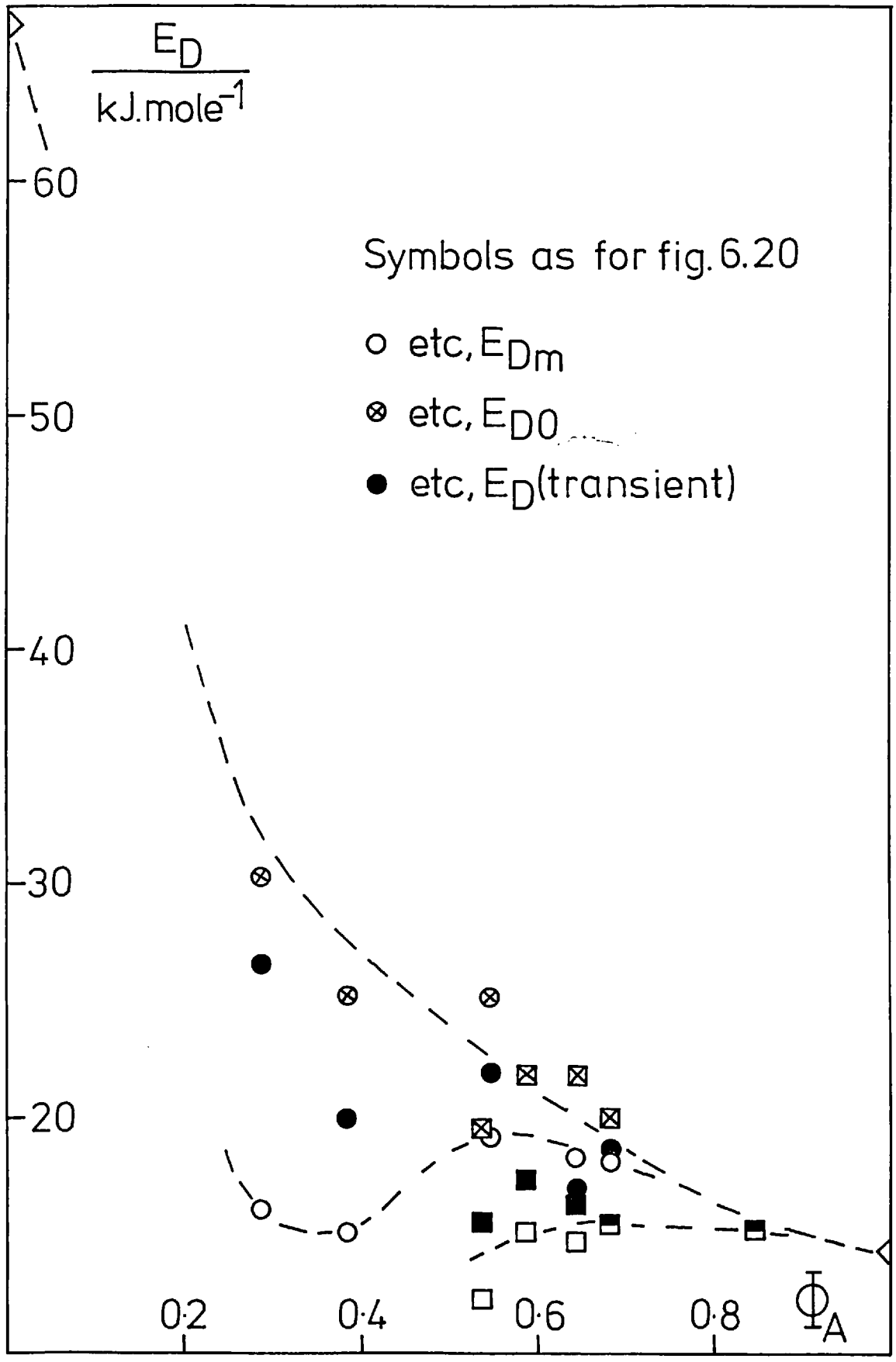


FIG. 6.24 PDMS-b-BPAC/PROPANE
ACTIVATION ENERGY OF DIFFUSION vs. ϕ_A

PDMS-60(40:7.2), unannealed and partially annealed.

The results are presented in Table 6.12 and are illustrated in Figs. 6.25 and 6.26. In each case the annealing temperature was between 130 and 140°C. Annealing beyond the limit of 48 hours produced no further changes.

Table 6.12 Effect of annealing on sorption parameters

Membrane	T/°C	$10^2.k_D/(\frac{cm^3 STP}{cm^3 cmHg})$	$10.C'_H/(\frac{cm^3 STP}{cm^3})$	$10.B/cmHg)^{-1}$	$10^2.S_L/(\frac{cm^3 STP}{cm^3 cmHg})$
PDMS-60(80:14.6)					
Unannealed	50.3	4.33 (± 2%)	3.2	0.78	
Annealed 48 hrs.	50.0	4.53 (± 1%)	0.93 (± 13%)	1.17 (± 18%)	5.62 (± 2%)
PDMS-60(40:7.2)					
Unannealed	50.0	5.16 (± 3%)	0.60	7.1	
Annealed 24 hrs.	50.1	4.63 (± 1%)	0.61(± 24%)	2.3 (± 54%)	6.00 (± 8%)
Annealed 48 hrs.	50.0	4.65 (± 1%)	(0)	(-)	(4.65)

Whilst it is clear from the table and the figures that the Langmuir component in S_L has been radically reduced by annealing, the effect on k_D appears to be less conclusive.

The effect of annealing on sorption is a possible explanation for the discrepancy in results obtained for the sorption of carbon dioxide in polycarbonate at 35°C by Vieth and Eilenberg (128) and Koros, Paul and Rocha (119). A critical comparison of the two sets of parameters is not possible due to the difference in the methods of analysis in each case (Vieth and Eilenberg used the graphical method; Koros et al used a non-linear regression computer program). Nevertheless, the latter investigators made a visual comparison between the two sets of basic experimental data which clearly showed that the polycarbonate sample studied by the former investigators had a sorptive capacity approximately 20-30% lower than the sample studied by the latter.

No details are given as to the sample's preparation and thermal history in both cases. It can be cautiously surmised however that the reduced sorptive capacity of the sample studied by Vieth and Eilenberg may be attributed to annealing of the sample before the studies commenced. Clearly the importance of the effect of annealing on sorption in glassy polymers cannot be over-emphasised if any kind of reproducibility between different sets of investigators is to be achieved.

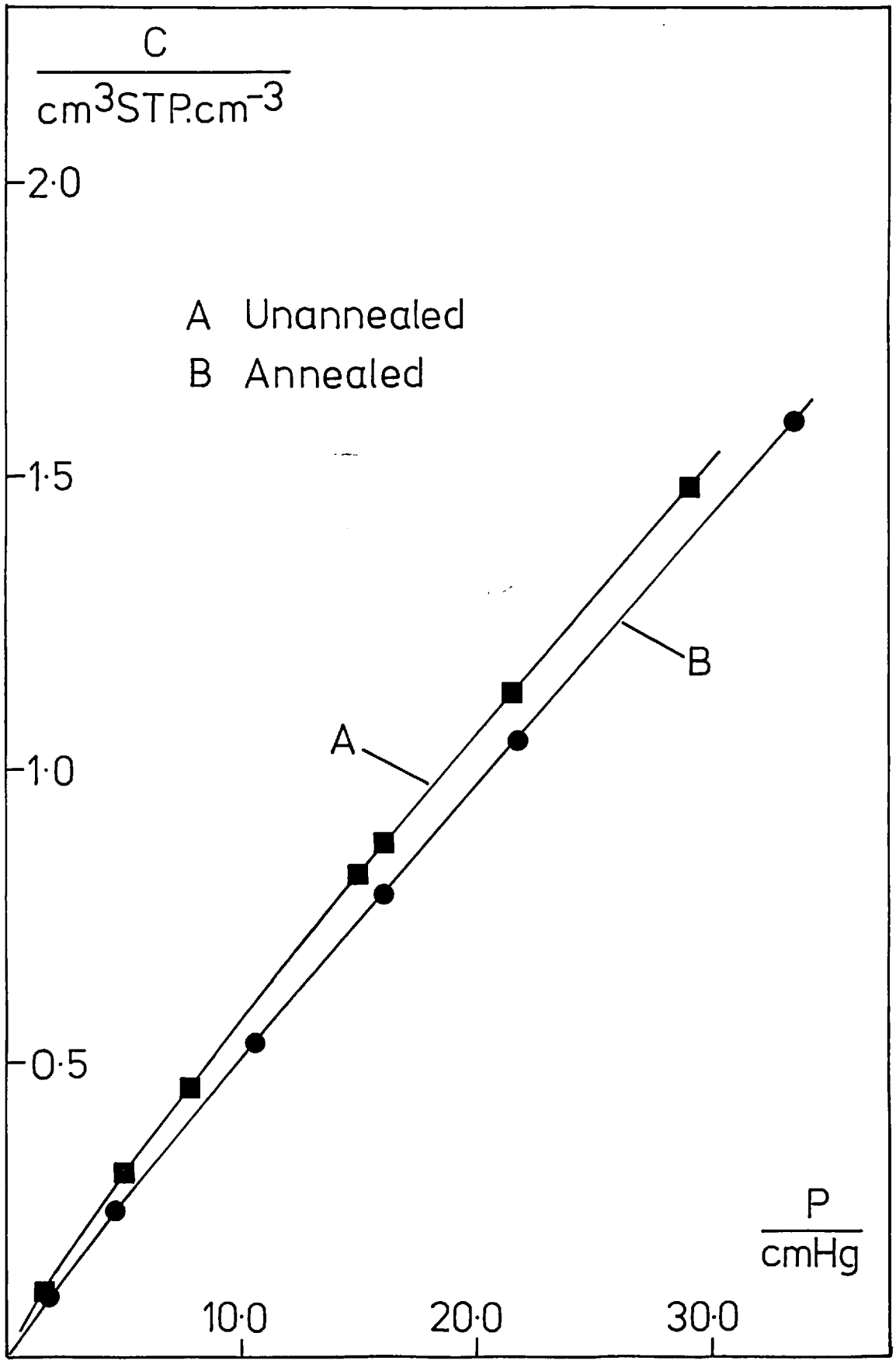


FIG. 6.25 PDMS-60(80:14·6)/PROPANE AT 50°C
EFFECT OF ANNEALING ON SORPTION

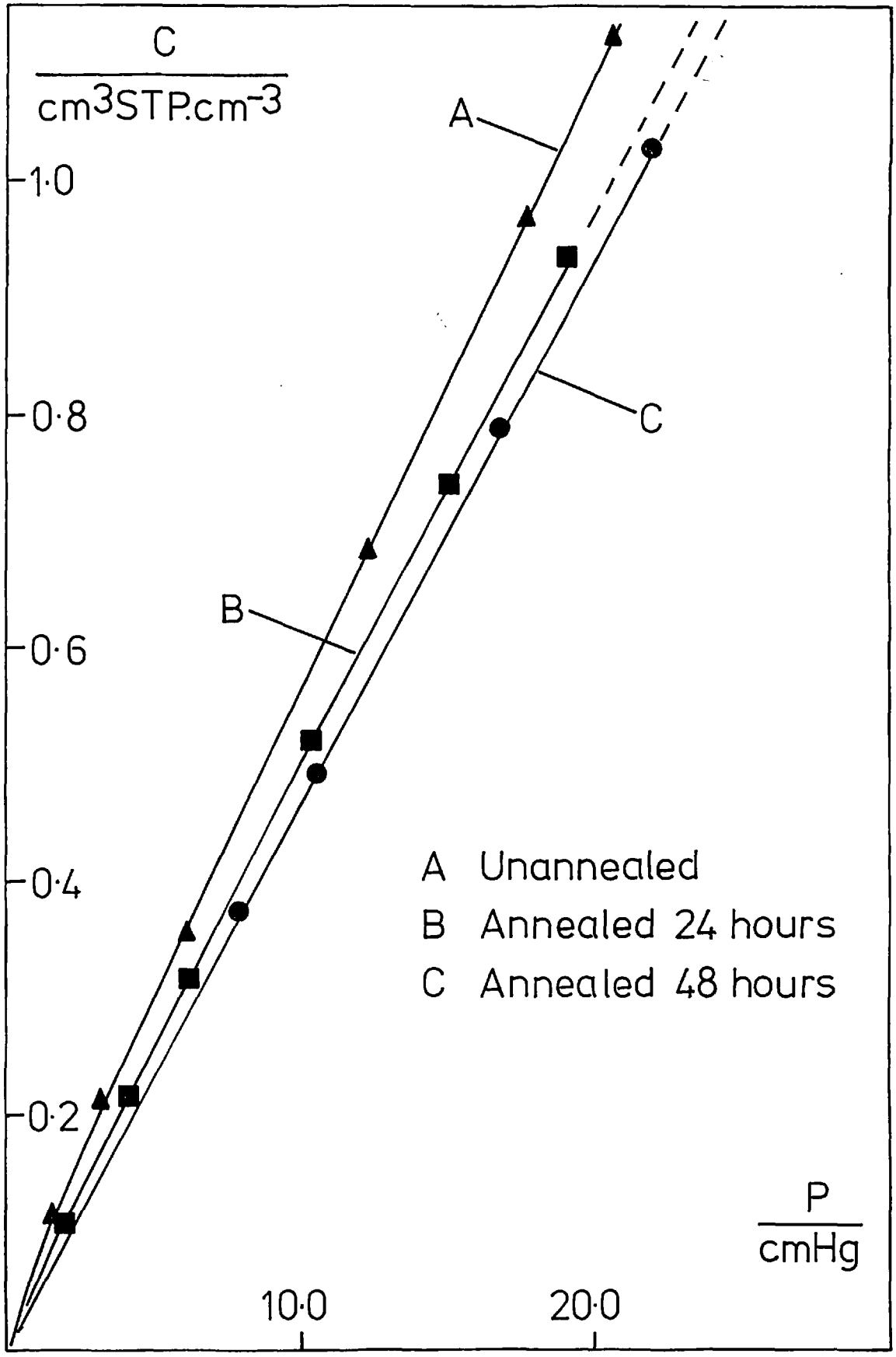


FIG. 6.26 PDMS-60(40:7·2)/PROPANE AT 50°C
EFFECT OF ANNEALING ON SORPTION

CHAPTER 7

CONCLUSIONS

7.1 Summary and appraisal of results.

Some interesting features have emerged in the course of this work and the principal points are discussed briefly in this chapter.

7.1.1 Transport and sorption of propane in pure BPAC

The equilibrium sorption results constitute firm evidence in support of the dual-mode sorption theory, certainly insofar as the mathematical form of the isotherm is concerned. The physical significance of the sorption parameters remains unresolved however, especially in regard to the strong temperature dependence of C'_H and the minimum observed in the concentration dependence of $\Delta\overline{H}_S$.

An analytical method of constraining the "best-fit" sorption parameters to produce mutually compatible parameters has been developed and represents an attempt at interpolating between sets of parameters in tandem. It was entirely fortuitous that the initially constrained results were found to be mutually compatible after just one attempt. A less obliging set of "best fit" parameters might have required several trial-and-error attempts to achieve compatibility.

The sorption kinetics investigation necessitated the development of novel solutions of Fick's equations within the framework of the dual-mode sorption theory based upon Crank's weighted-mean equation; it was necessary also to account for the penetrant immobilisation in the Langmuir mode being incomplete. It has been gratifying to observe the high level of agreement between the theoretical predictions and the experimental data which constitutes firm evidence in favour of the concept of partial immobilisation of penetrant in the Langmuir mode. Although D_i is often a small fraction of the value of D_m, the Langmuir population is much greater than the Henry's Law population at relatively low concentrations. Thus the contribution of the "immobile" component to the diffusive flux must always be considered as significant.

Although the idea of microcavities existing in the glassy state has been widely used throughout this work (and indeed throughout the scientific literature on glassy polymers) the validity of such a concept remains unjustified. No firm conclusions can be drawn regarding their size and shape, or how an immobilised penetrant molecule behaves inside them. Microcavities nevertheless retain at present a conceptual usefulness.

7.1.2 Sorption of propane in PVAc.

The convenience of investigating the sorption behaviour of PVAc grafted to PDMS has been balanced by a commensurate loss of accuracy in the results. In qualitative terms however the data adequately serve the purpose of revealing the presence of a Langmuir mode below T_g and its absence above. The behaviour of glassy polymers in the region of the glass transition remains unresolved and requires further study.

7.1.3 Alternating PDMS-b-BPAC copolymers

The results for density, permeability and equilibrium sorption all support LeGrand's postulate that this system is largely characterised by incomplete microphase separation when the membranes are cast from a solution of methylene chloride. Furthermore, in confirmation of Krause's prediction, microphase separation becomes more difficult as the block-lengths of the components become shorter. Whether this is a thermodynamic effect or perhaps a steric effect is not clear. In general the longer the block lengths, the more complete the phase separation, the closer the permeabilities lie to those predicted by the theoretical expressions for permeation in disperse phase heterogeneous media (Maxwell, Higuchi, etc.); the shorter the block lengths, the more homogeneous the medium becomes and the closer the permeabilities lie to the values predicted by Lichtenecker for permeation in random copolymers and miscible blends.

The E_p results revealed that PDMS forms the principal component of the continuous phase in all the membranes; the $\Delta\overline{H}_H$ results from the sorption studies (discussed shortly) suggested that it was not unreasonable to assume that the domains consisted purely of BPAC.

On this basis the Delta-Phi analysis was developed to evaluate $\Delta\Phi$, which can be defined as the amount of BPAC in the continuous phase. It was assumed that the continuous phase was not two interpenetrating continua as suggested by Kambour and implied by the approach developed by Robeson et al, but a homogeneous phase amenable to treatment according to the Lichtenecker rule. For a given series of membranes which held the number of PDMS mer units constant, $\Delta\Phi$ was found to be fairly constant for the range of volume fractions of PDMS examined. It was gratifying to observe the excellent level of agreement between the theoretical predictions of $\overline{P}$ (based on a constant $\Delta\Phi$) and the experimental data for both membrane series.

Equilibrium sorption studies revealed curved isotherms, characteristic of Langmuir-type immobilisation, for some but not all of the samples. For curvature to be observed it was necessary that sufficient of the BPAC phase was present; this depended not only on the volume fraction of BPAC but also on the average block length of this component being of sufficient size for glassy domains with microcavities to be formed.

The Henry's Law solubility coefficient, k_D was found to be independent of block-length distribution, but C'_H clearly increased with increasing block-lengths of the components for a given composition.

It was found that thermal pretreatment had a significant effect on the sorption behaviour of the membranes by reducing the sorptive capacity. The Langmuir component was clearly reduced by annealing; its effect on k_D was less conclusive.

7.2 Concluding remarks.

7.2.1 Churchill thermocirculator

On the whole the apparatus functioned extremely well. The high accuracy of the microbalance was not, however, fully matched by the thermostatting efficiency of the Churchill thermocirculator. A cursory glance at the sorption studies carried out at 40°C suggests a level of consistency of accuracy often unmatched at other temperatures. This was due to the fact that the Churchill appeared to "hold" this temperature better than any other. Had the thermostat perhaps been more reliable, the accuracy of some of the results could have been higher, though this is by no means certain.

7.2.2 Suggestions for further study

The alternating-block copolymers provide the broadest scope for further investigation in terms of permeation studies. If nothing else, $\Delta\Phi$ is a useful parameter; its physical significance as the amount of BPAC in the continuous phase requires further consideration. For example, $\Delta\Phi$ should be independent of penetrant, so using other penetrants could be a critical test. Should $\Delta\Phi$ not alter with penetrant, one might cautiously surmise that this parameter represents a quantitative assessment of partial microphase-separated morphology.

It is felt intuitively that $\Delta\Phi$ must be a function of Φ_A. This relationship needs to be clearly established using more samples

with even shorter block-lengths, and covering a wider range of Φ_A especially at high BPAC content.

The two principal series of membranes contained fixed PDMS block-lengths; of equal interest would be a series having the BPAC block-lengths fixed. Also, the effect of film morphology of casting from different solvents requires further investigation.

Chapter 8

APPENDIX

8.1 Other theoretical expressions for permeability in heterogeneous media.

(See Chapter 3, table 3.1)

(iii) Bruggeman (Meredith and Tobias adaptation) (75)

$$\overline{P}_M = \overline{P}_C\left(\frac{2(\overline{P}_D+2\overline{P}_C)+2(\overline{P}_D-\overline{P}_C)\Phi_D}{2(\overline{P}_D+2\overline{P}_C)-(\overline{P}_D-\overline{P}_C)\Phi_D}\right) \times \left(\frac{(2-P_D)(\overline{P}_D+2\overline{P}_C)+2(\overline{P}_D-\overline{P}_C)\Phi_D}{(2-P_D)(\overline{P}_D+2\overline{P}_C)-(\overline{P}_D-\overline{P}_C)\Phi_D}\right) \quad \ldots(8.1)$$

For $\overline{P}_C >> \overline{P}_D$, (8.1) becomes

$$\overline{P}_M = \frac{8\overline{P}_C.\Phi_C(1+\Phi_C)}{(5-\Phi_C)(3+\Phi_C)} = \frac{8\overline{P}_C(1-\Phi_D)(2-\Phi_D)}{(4+\Phi_D)(4-\Phi_D)} \quad \ldots (8.2)$$

For $\overline{P}_C << \overline{P}_D$, (8.1) reduces to

$$\overline{P}_M = \frac{\overline{P}_C(2-\Phi_C)(3-\Phi_C)}{\Phi_C(1+\Phi_C)} = \frac{\overline{P}_C(1+\Phi_D)(2+\Phi_D)}{(1-\Phi_D)(2-\Phi_D)} \quad \ldots (8.3)$$

(iv) Böttcher (76)

$$\frac{\overline{P}_M - \overline{P}_C}{3\overline{P}_M} = \Phi_D\left(\frac{\overline{P}_D - \overline{P}_C}{\overline{P}_D + 2\overline{P}_M}\right) \quad \ldots (8.4)$$

(8.4) re-arranges to yield

$$\overline{P}_M = \frac{(b^2 - 8.\overline{P}_C.\overline{P}_D)^{\frac{1}{2}} - b}{4} \quad \ldots (8.5)$$

where $b = (\overline{P}_D - 2\overline{P}_C - 3\Phi_D\overline{P}_D + 3\Phi_D\overline{P}_C)$. $\ldots (8.6)$

(8.5)produces identical results for both $\overline{P}_C >> \overline{P}_D$ and $\overline{P}_C << \overline{P}_D$.

(v) Rayleigh (77), adapted by Runge (78)

$$\overline{P}_M = \overline{P}_C \left(\frac{2\overline{P}_C+\overline{P}_D)(4\overline{P}_C+3\overline{P}_D)-2\Phi_D(\overline{P}_C-\overline{P}_D)(4\overline{P}_C+3\overline{P}_D)- 1.575\Phi_D^{10/3}.(\overline{P}_C-\overline{P}_D)^2}{2\overline{P}_C+\overline{P}_D)(4\overline{P}_C+3\overline{P}_D)+ \Phi_D(\overline{P}_C-\overline{P}_D)(4\overline{P}_C+3\overline{P}_D)- 1.575\Phi_D^{10/3}.(\overline{P}_C-\overline{P}_D)^2} \right) \quad \ldots(8.7)$$

For $\overline{P}_C >> \overline{P}_D$, (8.7) becomes

$$\overline{P}_M = \overline{P}_C \left(\frac{8(1-\Phi_D) - 1.575.\Phi_D^{10/3}}{8 + 4\Phi_D - 1.575.\Phi_D^{10/3}} \right) \quad \ldots(8.8)$$

For $\overline{P}_C << \overline{P}_D$, (8.7) simplifies to

$$\overline{P}_M = \overline{P}_C \left(\frac{3 + 6\Phi_D - 1.575.\Phi_D^{10/3}}{3(1-\Phi_D) - 1.575.\Phi_D^{10/3}} \right) \quad \ldots (8.9)$$

(vi) Rayleigh (77), adapted by Meredith and Tobias (79)

$$\overline{P}_M = \overline{P}_C \left[\frac{\begin{array}{l}(2\overline{P}_C+\overline{P}_D)(4\overline{P}_C+3\overline{P}_D)-2\Phi_D(4\overline{P}_C+3\overline{P}_D)(\overline{P}_C-\overline{P}_D) \\ +1.227.\Phi_D^{7/3}.(2\overline{P}_C+\overline{P}_D)(\overline{P}_C-\overline{P}_D)-6.399.\Phi_D^{10/3}.(\overline{P}_C-\overline{P}_D)^2\end{array}}{\begin{array}{l}(2\overline{P}_C+\overline{P}_D)(4\overline{P}_C+3\overline{P}_D) + \Phi_D(4\overline{P}_C+3\overline{P}_D)(\overline{P}_C-\overline{P}_D) \\ +1.227.\Phi_D^{7/3}.(2\overline{P}_C+\overline{P}_D)(\overline{P}_C-\overline{P}_D) - 2.748.\Phi_D^{10/3}.(\overline{P}_C-\overline{P}_D)^2\end{array}} \right] \quad \ldots (8.10)$$

For $\overline{P}_C >> \overline{P}_D$. (8.10) reduces to

$$\overline{P}_M = \overline{P}_C \left(\frac{8(1-\Phi_D)+ 2.454\Phi_D^{7/3} - 6.399.\Phi_D^{10/3}}{8 + 4\Phi_D+ 2.454\Phi_D^{7/3} - 2.748.\Phi_D^{10/3}} \right) \quad \ldots (8.11)$$

For $\overline{P}_C << \overline{P}_D$, (8.10) becomes

$$\overline{P}_M = \overline{P}_C \left(\frac{3 + 6\Phi_D - 1.227.\Phi_D^{7/3} - 6.399.\Phi_D^{10/3}}{3(1-\Phi_D) - 1.227.\Phi_D^{7/3} - 2.748.\Phi_D^{10/3}} \right) \quad \ldots (8.12)$$

(vii) Series/parallel (80)

Series: most suitable for $\overline{P}_C << \overline{P}_D$,

$$\overline{P}_M = \frac{\overline{P}_C \cdot \overline{P}_D}{\Phi_C \cdot \overline{P}_D + \Phi_D \cdot P_C} \quad \ldots (8.13)$$

Parallel : most suitable for $\overline{P}_C >> \overline{P}_D$,

$$\overline{P}_M = \Phi_C \cdot \overline{P}_C + \Phi_D \cdot \overline{P}_D \quad \ldots (8.14)$$

The models of Fidelle and Kirk (84), Bell and Crank (85) and Baxley, Nicholas and Couper (86) are very complex and have been discussed elsewhere (25).

8.2 Transient permeation : Sample calculations and estimation of errors

The following example illustrates the derivation of the permeability $\bar{P}$, the time-lag diffusion coefficient D, and the transient solubility coefficient S.

PDMS-64 (100:16.5) at 40.5°C

Membrane thickness, ℓ = 0.1332 cm.
Area of membrane, A_c = 4.714 cm^2
Outgoing volume, V = 686.0 cm^3
Room temperature, T_R = 24.2 °C
Transducer output = 6.17 mV
Transducer calibration = 1.196 cmHg. MV^{-1}
∴ Ingoing pressure, P_o = 6.17 x 1.196 = 7.38 cmHg.

Time, t/mins	Pressure, P/mmHg
65	0.2818
70	0.3110
75	0.3400
80	0.3694
85	0.3984
90	0.4274
95	0.4565
100	0.4856
105	0.5147
110	0.5438

Steady-state increases in pressure with time, dP/dt = 9.7014×10^{-5} mmHg.s^{-1}
Steady-state mean time, $< t >$ = 87.5 minutes
Steady-state mean pressure, $< P >$ = 0.41286 mm Hg.

$$\text{Flux, } F = V \times \frac{273.2}{(T_R \times 273.2)} \times \frac{1}{760} \times \frac{1}{A_c} \times \frac{dP}{dt}$$

$$= \frac{686.0 \times 273.2 \times 9.7014 \times 10^{-5}}{(24.2 + 273.2) \times 760 \times 4.714}$$

$$= 1.706 \times 10^{-5} \text{ cm}^3 \text{ STP. cm}^{-2}. \text{ s}^{-1}$$

$$\bar{P} = \frac{F.\ell}{P_o} = \frac{1.706 \times 10^{-5} \times 0.1332}{7.38}$$

$$= \frac{3.08 \times 10^{-7}}{} \quad \frac{\text{cm}^3 \text{ STP. cm}}{\text{cm}^2.\text{s.cm Hg.}}$$

$$\text{Time lag, } L = \langle t \rangle - \langle P \rangle/(dP/dt) = 87.5 \times 60 - \frac{0.41286}{9.7014 \times 10^{-5}}$$

$$= 651 \text{ s.}$$

$$D = \frac{\ell^2}{6L} = \frac{0.1332^2}{6 \times 651} = \underline{2.97 \times 10^{-6}} \text{ cm}^2.\text{s}^{-1}$$

$$S = \bar{P}/D = \frac{3.08 \times 10^{-7}}{2.97 \times 10^{-6}} = 10.36 \times 10^{-2} \frac{\text{cm}^3 \text{ STP}}{\text{cm}^3 . \text{ cm Hg}}$$

The thicknesses of the PDMS-b-BPAC samples were measured in several places with a micrometer screw-guage. The accuracy for the thinnest membrane was estimated to be $\pm$ 1%.

The diameter of the permeation cell was measured to an accuracy of $\pm$ 0.01 cm; this represents an uncertainty in the cross-sectional area of $\pm$ 0.83%.

The outgoing volume, V, was measured by successive gas expansions using accurate buffer volumes to within $\pm$ 0.2%.

The transducer output was estimated accurate to within $\pm$ 1%; the transducer calibration constant to within $\pm$ 0.25%; thus the uncertainty in the ingoing pressure was determined as $\pm$ 0.35%.

The error in the steady-state gradient was estimated statistically from the scatter of points around the least-squares best line representing the slope. This was never greater than $\pm$ 0.2%.

From the above considerations, the uncertainty of the flux was estimated as

$$\Delta F = (\pm 0.83 \pm 0.2 \pm 0.03 \pm 0.2)\%$$

$$= \pm 1.26\%$$

The uncertainty in $\bar{P}$,

$$\Delta\bar{P} = (\pm 1.26 \pm (1\%) \pm 0.35)\%$$

$$\simeq 2.5\%.$$

Experimentally, $\bar{P}$ was found to reproducible to within approximately 1%.

The uncertainties in the time-lags were estimated to be $\pm$ 3%, hence the uncertainty in transient D's is $\pm$ 5% and in transient S's, $\pm$ 7.5%.

8.3 Equilibrium and transient sorption: Sample calculations and estimation of errors.

8.3.1 Equilibrium sorption

The following example illustrates the derivation of penetrant concentration in the polymer, C, and the solubility coefficient, S.

PDMS-64 (100: 16.5)

W_1, weight of sample = 1.06320 grams.
W_2, weight of Pt wire = 0.01175 grams
W_3, weight of Cu counterweight = 1.07665 grams.

ρ_1, density of sample = 1.046 $g.cm^{-3}$
ρ_2, density of platinum = 21.45 $g.cm^{-3}$
ρ_3, density of copper = 8.96 $g.cm^{-3}$

Volume displacement =

$$\frac{W_1}{\rho_1} + \frac{W_2}{\rho_2} - \frac{W_3}{\rho_3} = \frac{1.06320}{1.046} + \frac{0.01175}{21.45} - \frac{1.07665}{8.96}$$

$= 0.8968\ cm^3$ of propane at P cm Hg and T^oC

Using the Archimedean principle, the bouyancy correction, B,

$$B = \frac{0.8968}{22414} \times \frac{273.2}{273.2 + T} \times \frac{P}{76} \times 44.097 \text{ grams propane}$$

where 44.097 is the molecular weight of propane.

$$\therefore B = \frac{6342.6\ P}{273.2 + T} \quad \mu g \text{ propane.}$$

At $T = 30.35^oC$ and P = 15.656 cm Hg,

$$\underline{B = 327.1\ \mu g}$$

Initial weight reading, R_1 = 3172.5 µg
Final weight reading, R_2 = 5582 µg

Total weight uptake,

$$W_T = R_2 - R_1 + B = (5582 - 3172.5 + 327.1)$$
$$= \underline{2736.6\ \mu g \text{ propane}}$$
$$\equiv \frac{2736.6 \times 10^{-6} \times 22414}{44.097}\ cm^3 \text{ STP propane}$$
$$= \underline{1.3910}\ cm^3 \text{ STP propane}$$

$$S = \frac{1.3910}{(\text{sample volume}) \times (\text{penetrant pressure})}$$

$$= \frac{1.3910}{1.016 \times 15.656}$$

$$= \underline{8.745 \times 10^{-2}}\ cm^3 \text{ STP } / cm^3 \text{ . cm Hg}$$

The errors in B are fairly small, and since it always constitutes less than 20% to the total weight uptake the contribution of uncertainty to the solubility coefficient from the buoyancy correction is considered negligible.

The error in absolute terms attributable to the penetrant pressure increased as pressures became larger; however, the overall percentage error tended to fluctuate about $\pm$ 0.5%.

The uncertainty in the volume of the sample is directly attributable to the uncertainty in the density of membrane, i.e. $\pm$ 0.5%, since the weight of the sample could be measured with high precision.

The uncertainty in the difference in weight readings, i.e., $(R_2 - R_1)$ remained constant at $\pm$ 2 μg. For low penetrant pressures, this represents an uncertainty of approximately $\pm$ 2%. At very high pressures, the uncertainty becomes negligible.

From the above considerations, uncertainties can be calculated for the solubility coefficient, S, and for the penetrant concentration, C, where

$$C = \frac{\text{(Total propane uptake expressed in cm}^3\text{ STP)}}{\text{(sample volume)}}$$

At high pressures,

$$\Delta S = (\pm 0.5 \pm 0.5)\% = \pm 1\%$$
$$\Delta C = \pm 0.5\%$$

At low pressures,

$$\Delta S = (\pm 2 \pm 0.5 \pm 0.5)\% = \pm 3\%$$
$$\Delta C = (\pm 2 \pm 0.5)\% = \pm 2.5\%$$

Thus the uncertainties in S and C tended to increase with decreasing penetrant pressure.

8.3.2 Transient sorption

The following example shows the derivation of the penetrant concentration in the sample, C, and the mean diffusion coefficient for sorption, $\overline{D}_S$.

BPAC

Weight of sample, w_1 = 0.18865 grams.
Weight of copper spacers, w_2 = 1.25065 grams.
Weight of copper counterweight, w_3, = 1.38205 grams.

Density of sample, ρ_1 = 1.178 $g.cm^{-3}$

Density of copper, ρ_2, ρ_3 = 8.96 $g.cm^{-3}$

Area of sample sheet, A = 20.4.4 cm^2.

$$\text{Volume displacement} = \frac{w_1}{\rho_1} + \frac{w_2}{\rho_2} - \frac{w_3}{\rho_3}$$

$$= \frac{0.18865}{1.178} \quad \frac{1.25065}{8.96} \quad \frac{1.38205}{8.96}$$

$$= \underline{0.1455} \ cm^3 \text{ of propane at P cm Hg and } T^oC.$$

Using the Archimedean principle, the buoyancy correction, B,

$$B = \frac{0.1455}{22414} \times \frac{273.2}{273.2+T} \times \frac{P}{76} \times 44.097 \text{ grams propane}$$

where 44.097 is the molecular weight of propane

$$\therefore \quad B = \frac{1028.9P}{273.2+T} \ \mu g \text{ propane.}$$

At T = 40.05°C and P = 27.97 cm Hg

$$B = \underline{91.9} \ \mu g$$

Initial weight reading, R_1 = 11372 µg

Final weight reading, R_2 = 12071.5 µg.

Total weight uptake,

$$W_T = R_2 - R_1 + B = (12071.5 - 11372 + 91.9)$$

$$= \underline{791.4 \ \mu g \text{ propane}}$$

$$\equiv \frac{791.4 \times 10^{-6} \times 22414}{44.097} \ cm^3 \text{ STP propane}$$

$$= \underline{0.4023} \ cm^3 \text{STP propane}$$

$$C = \frac{0.4023}{(\text{sample volume})} = \frac{0.4023}{0.1601} = \underline{\underline{2.512}} \ \frac{cm^3 STP}{cm^3}$$

Let $R_{0.5}$ be equal to the reading on the pen-recorder when exactly half the equilibrium amount of propane to be sorbed has been taken up.

$$R_{0.5} = R_2 - \frac{W_T}{2} = R_1 - B + \frac{W_T}{2}$$

$$\simeq \underline{11676} \ \mu g$$

Examination of the pen-recorder trace at T = 40.05°C and P = 27.97 cm Hg reveals at $R = R_{0.5}$, the time, t,

$$t = t_{0.5} = 19.3 \text{ minutes} = \underline{1159} \text{ s.}$$

The thickness of the sample, ℓ,

$$\ell = \frac{W_1}{\rho_1 \times A} = \frac{0.18865}{1.178 \times 204.4} = \underline{7.835 \times 10^{-4}} \text{ cm.}$$

Using equation (2.29)

$$\bar{D}_s = \frac{0.04919\ \ell^2}{t_{0.5}} \qquad (2.29)$$

$$= \frac{0.04919 \times 7.835^2 \times 10^{-8}}{1159}$$

$$\bar{D}_s = 2.606 \times 10^{-11} \text{ cm}^2.\text{s}^{-1}$$

The uncertainties attributable to the concentration are effectively the same as those described in the previous section. The uncertainty in the area of the sheet was ~ 0.5 cm^2, hence the percentage error in A is $\pm$ 0.25%. The uncertainty in the density was estimated at $\pm$ 0.5% and the error in the weight of sample was considered negligible.

$$\Delta\ell = (\pm 0.25 \pm 0.5)\% = 0.75\%$$

The uncertainty in the half-time was estimated at $\sim$ 0.2 minutes. At 60°C, the shorter half-times were $\sim$ 4 minutes and the percentage error is therefore $\pm$ 5% which should decrease for decreasing temperature as values of $t_{0.5}$ become larger. However, at lower temperatures, the final equilibrium point was sometimes unclear due to the uneven thermostatting of the Churchill thermocirculator. A figure of $\pm$ 5% is therefore applicable to the values of $t_{0.5}$ at all the temperatures.

$$\Delta\bar{D}_s = 2\Delta\ell + \Delta t_{0.5} = (\pm 1.5 \pm 5)\%$$
$$= \underline{6.5\%}$$

In practice the figure for the uncertainty in $\bar{D}_s$ at 30°C was slightly higher.

8.4 Sorption data : BPAC

The equilibrium sorption data are presented in Tables 8.1.A and 8.1.B. Values of concentration predicted theoretically have also been listed for purposes of comparison. The first set of theoretical values were computed using the "best-fit" parameters, k_D, C'_H, B. The second set is derived from $\overline{k}_D$, $\overline{C}'_H$, $\overline{B}$.

The transient sorption data are presented in Table 8.2.

Membrane weight = 0.18865 grams
Membrane volume = 0.1601 cm^3
Membrane thickness = 7.835×10^{-4}

The following units are used throughout this section:

Comcentration, C / cm^3 STP. cm^{-3}

Pressure, P / cm Hg

Henry's law solubility, k_D / $\left(\frac{cm^3 \text{ STP}}{cm^3 \text{ cm Hg}} \right)$

Hole saturation constant, C'_H / cm^3 STP. cm^{-3}.

Hole affinity constant, B / $(\text{cm Hg})^{-1}$

Mean diffusion coefficient for sorption, $\overline{D}_s$ / cm^2. s^{-1}.

Table 8.1.A. Equilibrium sorption data for BPAC/propane

T = 30.1°C

P	C(expt'l)	C(calc.)1	C (calc.)2
2.72	0.915	0.928	0.919
6.31	1.511	1.485	1.463
11.15	1.934	1.966	1.944
18.07	2.550	2.504	2.496
19.25	2.606	2.588	2.584
24.97	2.918	2.981	2.995
38.92	3.901	3.885	3.949

$k_D = 6.03 \times 10^{-2}$ $(\bar{k}_D = 6.45 \times 10^{-2})$

$C'_H = 1.67$ $(\bar{C}'_H = 1.56)$

$B = 0.311$ $(\bar{B} = 0.340)$

T = 40.05°C

P	C(expt'l)	C(calc.)1	C (calc.)2
2.15	0.551	0.589	0.552
5.09	0.958	0.960	0.966
10.34	1.428	1.424	1.431
18.77	1.976	1.975	1.978
20.62	2.070	2.084	2.086
27.97	2.512	2.498	2.495
40.92	3.188	3.192	3.177

$k_D = 5.01 \times 10^{-2}$ $(\bar{k}_D = 4.91 \times 10^{-2})$

$C'_H = 1.25$ $(\bar{C}'_H = 1.28)$

$B = 0.254$ $(\bar{B} = 0.248)$

Table 8.1.B. Equilibrium sorption data for BPAC/propane

T = 50.1°C

P	C (expt'l)	C (calc.)1	C (calc.)2
1.728	0.316	0.297	0.316
3.34	0.480	0.498	0.521
5.00	0.655	0.662	0.687
8.38	0.945	0.928	0.948
10.72	1.073	1.081	1.096
10.79	1.096	1.085	1.100
11.07	1.097	1.103	1.116
17.90	1.444	1.478	1.476
17.97	1.507	1.482	1.479
27.60	1.980	1.941	1.914
32.37	2.085	2.154	2.117
41.91	2.617	2.568	2.509
56.93	3.187	3.201	3.107

$k_D = 4.01 \times 10^{-2}$ $(\bar{k}_D = 3.79 \times 10^{-2})$

$C'_H = 1.02$ $(\bar{C}'_H = 1.04)$

$B = 0.167$ $(\bar{B} = 0.183)$

T = 60.0°C

P	C (expt'l)	C (calc.)1	C (calc.)2
4.21	0.470	0.453	0.466
9.09	0.791	0.793	0.787
19.88	1.261	1.299	1.271
29.37	1.657	1.641	1.618
45.06	2.167	2.132	2.141
59.35	2.521	2.543	2.594

$k_D = 2.55 \times 10^{-2}$ $(\bar{k}_D = 2.98 \times 10^{-2})$

$C'_H = 1.22$ $(\bar{C}'_H = 0.925)$

$B = 0.094$ $(\bar{B} = 0.139)$

Table 8.2 Transient sorption data for BPAC/propane

T = 30.1°C

C (expt'l)	$10^{11}.\bar{D}_s$
1.511	0.751
1.934	1.014
2.606	1.071
2.918	1.367
3.901	1.378

$D_m = 1.74 \times 10^{-11}$

$D_i = 3.16 \times 10^{-12}$

T = 50.1°C

C (expt'l)	$10^{11}.\bar{D}_s$
0.316	2.298
0.480	2.827
0.945	3.868
1.097	4.613
1.444	4.613
2.085	5.990

$D_m = 8.29 \times 10^{-11}$

$D_i = 1.02 \times 10^{-11}$

T = 40.05°C

C (expt'l)	$10^{11}.\bar{D}_s$
0.551	1.006
0.958	1.413
1.428	1.804
1.976	2.246
2.512	2.606
3.188	2.684

$D_m = 3.46 \times 10^{-11}$

$D_i = 5.74 \times 10^{-12}$

T = 60.0°C

C (expt'l)	$10^{11}.\bar{D}_s$
0.470	6.368
0.791	8.388
1.261	11.18
1.657	-2.28
2.167	13.98
2.521	14.81

$D_m = 1.84 \times 10^{-10}$

$D_i = 1.87 \times 10^{-11}$

8.5 Sorption data : PDMS

The equilibrium sorption data are presented in Table 8.3

Membrane weight = 1.32440 grams

Membrane volume = 1.3584 cm^3

The following units are used throughout this section:-

Comcentration, C / cm^3 STP.cm^{-3}.

Pressure, P/cm Hg.

Solubility coefficient, S /($\frac{cm^3 \text{ STP}}{cm^3 . \text{ cm Hg}}$)

Table 8.3 Equilibrium sorption data for PDMS/propane

T = 1.5°C

P	C	10^2.S
1.48	0.305	20.63
7.96	1.648	20.70
10.54	2.173	20.62
14.29	2.967	20.77
20.30	4.259	20.99

S = 0.2074

T = 11.65°C

P	C	10^2.S
1.756	0.275	15.64
5.96	0.934	15.73
10.90	1.714	15.72
16.12	2.547	15.80
21.28	3.367	15.82

S = 0.1573

T = 20.4°C

P	C	10^2.S
1.811	0.227	12.53
10.51	1.322	12.58
15.90	2.003	12.59
21.44	2.714	12.66
28.01	3.550	12.68

S = 0.1261

T = 30.0°C

P	C	10^2.S
5.34	0.537	10.06
11.12	1.120	10.07
15.72	1.585	10.09
21.43	2.164	10.10
30.04	3.049	10.15

S = 0.1008

T = 40.4°C

P	C	10^2.S
5.22	0.421	8.07
10.73	0.866	8.07
16.39	1.328	8.07
22.16	1.788	8.07
31.19	2.517	8.07

S = 8.07×10^{-2}

T = 50.0°C

P	C	10^2.S
6.29	0.426	6.66
10.81	0.719	6.65
16.53	1.101	6.66
22.14	1.474	6.66
31.98	2.132	6.67

S = 6.66×10^{-2}

T = 59.9°C

P	C	10^2.S
5.43	3.038	5.59
10.80	0.599	5.54
16.66	0.925	5.55
21.35	1.183	5.54
32.01	1.777	5.55

S = 5.55×10^{-2}

8.6 Sorption data : PDMS-g-PVAc and PVAc (extracted).

The equilibrium sorption data for PDMS-g-PVAc are presented in Tables 8.4.A and 8.4.B; the extracted data for PVAc are presented in Tables 8.5.A and 8.5.B.

For the grafted copolymer,

membrane weight = 0.36575 grams

membrane volume = 0.3413 cm^3

The following units are used throughout this section:-

Concentration, C / cm^3. STP cm^{-3}

Pressure, P / cm Hg

Solubility coefficient, S /($\frac{cm^3 \text{ STP}}{cm^3 . \text{ cm Hg}}$)

Henry's Law solubility k_D /($\frac{cm^3 \text{ STP}}{cm^3 . \text{ cm Hg}}$)

Hole saturation constant, C'_H / cm^3 STP. cm^{-3}

Hole affinity constant, B /$(cm\ Hg)^{-1}$

N.B. Above T_g, $k_D \equiv S$.

Table 8.4.A Equilibrium sorption data for PDMS-g-PVAC (containing 44.2% PVAc by volume)/propane, below T_g

$T = 2.7^{\circ}C$

P	C(expt'l)	C(calc)
1.76	0.256	0.256
5.22	0.707	0.709
7.55	1.003	1.003
10.47	1.366	1.366
15.39	1.974	1.972
21.99	2.778	2.779
27.35	3.432	3.431

$k_D = 0.1212$

$C'_H = 0.133$

$B = 0.255$

$T = 22.4^{\circ}C$

P	C(expt'l)	C(calc.)
1.93	0.162	0.161
5.31	0.425	0.425
8.08	0.637	0.638
10.75	0.841	0.842
15.95	1.241	1.238
20.91	1.614	1.615
24.28	1.870	1.871

$k_D = 7.584 \times 10^{-2}$

$C'_H = 0.0319$

$B = 0.464$

$T = 12.1^{\circ}C$

P	C(expt'l)	C(calc.)
1.82	0.204	0.205
5.00	0.534	0.532
8.36	0.865	0.866
11.01	1.125	1.126
16.22	1.637	1.635
20.19	2.021	2.022
24.80	2.470	2.469

$k_D = 9.676 \times 10^{-2}$

$C'_H = 0.0787$

$B = 0.316$

Table 8.4.B Equilibrium sorption data for PDMS-g-PVAc (containing 44.2% PVAc by volume)/propane, above T_g.

T = 40.15°C

P	C	10^2.S
1.853	0.099	5.34
6.64	0.355	5.35
10.71	0.573	5.35
16.46	0.880	5.35
21.03	1.125	5.35
24.96	1.335	5.38

S = 5.35×10^{-2}

T = 60.2°C

P	C	10^2.S
5.24	0.193	3.78
8.06	0.296	3.67
10.95	0.402	3.67
12.94	0.477	3.68
21.99	0.811	6.69
26.08	0.960	3.68
40.00	1.481	3.702

S = 3.69×10^{-2}

T = 50.0°C

P	C	10^2.S
1.837	0.080	4.38
5.20	0.229	4.41
10.52	0.462	4.40
10.98	0.490	4.46
16.39	0.729	4.45
21.22	0.946	4.46
25.30	1.125	4.45

S = 4.45×10^{-2}

Table 8.5.A Equilibrium sorption data for PVAc/propane, below T_g
(extracted and scaled to $\Phi_{PVAc} = 1$)

T = 2.7°C

P	C(extr'd)	C(calc.)
1.76	0.137	0.134
5.22	0.287	0.291
7.55	0.370	0.370
10.47	0.458	0.458
15.39	0.596	0.591
21.99	0.755	0.757
27.35	0.886	0.887

$k_D = 2.29 \times 10^{-2}$

$C'_H = 0.300$

$B = 0.257$

T = 22.4°C

P	C(extr'd)	C(calc.)
1.93	0.072	0.071
5.31	0.151	0.152
8.08	0.208	0.210
10.75	0.262	0.264
15.95	0.373	0.366
20.91	0.460	0.461
24.28	0.524	0.526

$k_D = 1.89 \times 10^{-2}$

$C'_H = 0.073$

$B = 0.459$

T = 12.1°C

P	C(extr'd)	C(calc.)
1.82	0.104	0.106
5.00	0.226	0.226
8.36	0.315	0.317
11.01	0.382	0.385
16.22	0.516	0.513
20.19	0.605	0.607
24.80	0.715	0.714

$k_D = 2.24 \times 10^{-2}$

$C'_H = 0.179$

$B = 0.315$

Table 8.5.B Equilibrium sorption data for PVAc/propane, above T_g (extracted and scaled to $\Phi_{PVAc} = 1$)

$T = 40.15^{\circ}C$

P	C(extr'd)	$10^2.S$
1.853	0.034	1.82
6.64	0.121	1.82
10.71	0.196	1.83
16.46	0.300	1.82
21.03	0.385	1.83
24.96	0.456	1.83

$S = 1.83 \times 10^{-2}$

$T = 50.0^{\circ}C$

P	C(extr'd)	$10^2.S$
1.837	0.027	1.45
5.20	0.081	1.56
10.52	0.161	1.53
10.98	0.186	1.69
16.39	0.272	1.67
21.22	0.357	1.68
25.30	0.419	1.66

$S = 1.66 \times 10^{-2}$

$T = 60.2^{\circ}C$

P	C(extr'd)	$10^2.S$
5.24	0.075	1.42
8.06	0.113	1.40
10.95	0.153	1.40
12.94	0.185	1.43
21.99	0.315	1.44
26.08	0.370	1.42
40.00	0.587	1.47

$S = 1.44 \times 10^{-2}$

8.7 Transient permeation data for PDMS-b-BPAC/propane

The following units will be used throughout this section:-

Permeability, $\overline{P}$ / $\left(\frac{cm^3 STP.cm.}{cm^2.s.\ cm\ Hg}\right)$

Diffusivity, D / $cm^2.\ s^{-1}$

Solubility, S / $\left(\frac{cm^3 STP}{cm^3.\ cm\ Hg}\right)$

Membrane area, A / cm^2.

Membrane thickness, ℓ/cm.

Outgoing volume, V/cm^3.

Membrane temperature, T/^oC.

Ingoing pressure, P_o/cmHg

Time-lag, L/s.

8.7.1 20-block membranes

The transient permeation data for the 20-block membranes are presented in Tables 8.6 - 8.10.

Table 8.6 PDMS-25 (20 : 17.8) (Data of Spencer (155)).

ℓ = 0.031

T	$10^8.\overline{P}$	$10^7.D$	$10^2.S$
30.0	2.12	1.72	12.32
40.1	2.09	2.53	8.26
49.5	2.01	3.35	6.01
59.2	1.91	4.32	4.42
69.5	1.88	5.83	3.22

Table 8.7. PDMS - 34 (20:11)

A = 4.714 ℓ = 0.0637 V = 690.1

T	P_o	L	$10.\overline{P}$	$10^7.D$	$10^2.S$
30.25	10.49	1281	4.92	5.28	9.32
30.25	5.30	1285	4.93	5.26	9.35
40.00	9.18	1013	4.68	6.68	7.02
40.25	10.55	982	4.74	6.89	6.89
50.15	6.92	801	4.73	8.45	5.60
60.40	11.79	616	4.53	10.98	4.12
60.40	5.49	614	4.55	11.01	4.13

Table 8.8 PDMS-50(20:6) (Data of Spencer (155))

ℓ = 0.0440

T	$10^8.\overline{P}$	$10^6.D$	$10^2.S$
30.0	8.78	1.02	8.53
39.8	9.03	1.34	6.74
47.3	9.14	1.63	5.61
55.5	9.43	2.02	4.67
63.1	9.62	2.39	4.03

Table 8.9 PDMS-60 (20: 3.9)

A = 5.309 ℓ = 0.0665 V = 2271.0

T	P_o	L	$10^7\overline{P}$	$10^6.D$	$10^2.S$
26.90	9.87	544	1.21	1.35	8.90
30.20	9.87	499	1.20	1.48	8.12
34.75	9.69	452	1.22	1.63	7.48
37.10	10.11	433	1.22	1.70	7.12
37.45	8.43	419	1.24	1.76	7.01
41.20	11.36	396	1.23	1.86	6.61
43.80	9.81	375	1.24	1.97	6.31
46.30	9.57	360	1.26	2.05	6.15
46.30	9.99	356	1.25	2.07	6.02

Table 8.10 PDMS-64 (20:3.5) (Data of Spencer (155)).

ℓ = 0.1280

T	$10^7.\bar{P}$	$10^6.D$	$10^2.S$
30.0	1.36	1.56	8.68
40.0	1.38	1.99	6.95
49.5	1.49	2.52	5.89
57.9	1.49	2.93	5.08
66.3	1.49	3.45	4.32
73.6	1.45	3.90	3.71

8.7.2 40-block membranes

The transient permeation data for the 40-block membranes are presented in Tables 8.11 - 8.15.

Table 8.11 PDMS-49 (41:12.4)

A = 4.714 ℓ = 0.1023 V = 686.6

T	P_o	L	$10^7.\bar{P}$	$10^6.D$	$10^2.S$
35.15	10.75	943	1.57	1.85	8.49
40.40	12.27	901	1.55	1.94	7.99
45.20	9.95	835	1.52	2.09	7.27
49.95	9.30	699	1.47	2.49	5.91
50.10	9.66	750	1.48	2.33	6.37
54.80	9.99	684	1.46	2.55	5.74
60.20	9.59	616	1.43	2.83	5.05
64.50	10.45	572	1.43	3.05	4.69

Table 8.12 PDMS-54 (40:10)

A = 4.714 ℓ = 0.0849 V = 684.3

T	P_o	L	$10^7.\bar{P}$	$10^6.D$	$10^2.S$
30.25	10.05	637	1.88	1.88	9.96
35.30	9.85	570	1.84	2.11	8.72
40.45	9.77	516	1.82	2.33	7.79
45.20	9.79	462	1.80	2.60	6.91
50.00	10.25	410	1.77	2.93	6.03
50.00	9.36	419	1.76	2.87	6.16
55.00	10.50	379	1.76	3.17	5.57
60.40	11.04	345	1.75	3.49	5.02

Table 8.13 PDMS-60 (40: 7.2)

A = 4.909 ℓ = 0.0650 V = 699.2

T	P_o	L	$10^7.\bar{P}$	$10^6.D$	$10^2.S$
30.75	12.68	297	1.96	2.37	8.27
35.70	11.43	270	1.94	2.61	7.43
40.95	13.34	241	1.92	2.92	6.60
45.50	11.69	220	1.91	3.20	5.96
50.30	11.90	202	1.89	3.49	5.43
50.50	11.60	201	1.90	3.51	5.43
55.10	11.09	185	1.88	3.80	4.96
60.55	11.35	167	1.89	4.21	4.48

Table 8.14 PDMS-64 (40:7)

A = 4.714 ℓ = 0.0610 V = 684.3

T	P_o	L	$10^7.\bar{P}$	$10^6.D$	$10^2.S$
30.70	9.45	235	2.31	2.64	8.76
35.10	9.08	218	2.33	2.85	8.18
40.15	9.21	199	2.30	3.12	7.36
45.40	9.48	178	2.28	3.49	6.54
50.20	9.36	161	2.26	3.84	5.89
50.20	8.06	167	2.24	3.71	6.03
55.10	9.78	148	2.27	4.19	5.42
60.00	8.93	138	2.25	4.50	5.01

Table 8.15 PDMS-82 (40:3)

A = 4.524 ℓ = 0.0700 V = 658.5

T	P_o	L	$10^7.\bar{P}$	$10^6.D$	$10^2.S$
31.20	10.15	228	3.50	3.58	9.78
31.20	10.36	226	3.48	3.62	9.62
40.45	10.07	194	3.41	4.21	8.12
40.45	10.00	190	3.40	4.29	7.93
50.55	9.22	159	3.35	5.13	6.53
60.20	9.90	135	3.32	6.04	5.49
60.20	9.19	133	3.31	6.13	5.39

8.7.3 Misc. membranes

The transient permeation data for the miscellaneous membranes are presented in Tables 8.16 - 8.18.

Table 8.16 PDMS-60 (80:14.6)

A = 4.714 ℓ = 0.0580 V = 689.4

T	P_o	L	$10^7.\bar{P}$	$10^6.D$	$10^2.S$
30.50	13.41	218	2.39	2.57	9.29
35.30	11.69	199	2.34	2.82	8.27
40.50	10.92	179	2.29	3.13	7.32
45.15	12.72	162	2.27	3.46	6.57
50.45	11.06	147	2.22	3.82	5.82
55.30	12.88	134	2.20	4.20	5.24
60.10	13.25	125	2.19	4.49	4.87

Table 8.17 PDMS-64 (100:16.5)

A = 4.714 ℓ = 0.1332 V = 686.0

T	P_o	L	$10^7.\bar{P}$	$10^6.D$	$10^2.S$
35.45	10.18	1060	3.24	2.79	11.61
35.45	8.23	1102	3.23	2.68	12.05
40.50	7.15	994	3.18	2.97	10.69
50.00	9.89	773	3.09	3.83	8.07
50.00	9.57	780	3.09	3.79	8.15
55.00	7.92	699	3.04	4.23	7.18

Table 8.18 ODMS-83 (61: 3.6)

A = 4.524 ℓ = 0.1080 V = 658.5

T	P_o	L	$10^7.\bar{P}$	$10^6.D$	$10^2.S$
32.45	9.33	442	4.16	4.40	9.47
32.60	2.14	443	4.12	4.38	9.40
32.60	4.27	450	4.13	4.32	9.57
32.60	6.71	449	4.15	4.33	9.57
32.60	8.31	449	4.17	4.33	9.64
32.60	10.16	459	4.18	4.24	9.87
32.60	15.29	451	4.20	4.31	9.75
36.10	7.63	432	4.11	4.50	9.12
40.00	10.49	394	4.11	4.93	8.33
51.95	7.50	319	3.97	6.09	6.53
55.40	7.83	310	3.95	6.27	6.30
59.95	7.09	282	3.91	6.90	5.66

8.8 Equilibrium sorption data for PDMS-b-BPAC/propane

The following units will be used throughout this section:-

Concentration, $C/cm^3 STP.cm^{-3}$

Pressure. P/cm Hg.

Henry's Law solubility, k_D /($\frac{cm^3\ STP}{cm^3.cm\ Hg}$)

Hole saturation constant, $C'_H/cm^3\ STP.cm^{-3}$

Hole affinity constant, $B/cm\ Hg)^{-1}$

Solubility coefficient, S /($\frac{cm^3\ STP}{cm^3.cm\ Hg}$)

Weight of membrane, W_M/grams.

Volume of membrane, V_M/cm^3

N.B. When the isotherm curvature is effectively negligible, $S = k_D$.

8.8.1 20-block membranes

The equilibrium sorption data for the 20-block membranes are presented in Tables 8.19 - 8.23.

Table 8.19 PDMS-25 (20:17.8)

W_M = 0.66155

V_M = 0.5768

T = 19.95

P	C(expt'l)	C(calc.)
0.826	0.206	0.190
2.11	0.420	0.419
4.02	0.672	0.682
5.71	0.867	0.874
8.55	1.157	1.156
11.43	1.419	1.412
17.55	1.920	1.913
22.59	2.298	2.304

$k_D = 7.15 \times 10^{-2}$
$C'_H = 0.821$
$B = 0.230$

T = 30.35

P	C(expt'l)	C(calc.)
1.956	0.268	0.259
3.76	0.448	0.448
4.83	0.544	0.548
5.55	0.607	0.609
8.68	0.848	0.852
11.36	1.039	1.039
17.37	1.423	1.418
22.85	1.743	1.740
27.46	1.996	2.000

$k_D = 5.14 \times 10^{-2}$
$C'_H = 0.742$
$B = 0.139$

T = 40.3

P	C(expt'l)	C(calc.)
1.987	0.193	0.188
3.04	0.274	0.272
4.24	0.357	0.359
5.53	0.441	0.446
8.40	0.621	0.618
11.22	0.771	0.773
16.81	1.062	1.056
21.85	1.288	1.295
23.73	1.385	1.382

$k_D = 4.22 \times 10^{-2}$
$C'_H = 0.502$
$B = 0.133$

T = 50.1

P	C(expt'l)	C(calc.)
0.891	0.063	0.061
1.88	0.124	0.124
2.87	0.183	0.181
3.83	0.234	0.234
5.63	0.324	0.326
8.53	0.459	0.461
11.32	0.581	0.582
17.53	0.835	0.831
22.75	1.028	1.029
27.26	1.196	1.196

$k_D = 3.41 \times 10^{-2}$
$C'_H = 0.359$
$B = 0.105$

Table 8.20 PDMS-34 (20:11)

W_M = 1.11325

T = 20.05

P	C(expt'l)	C(calc.)
1.63	0.211	0.203
4.46	0.483	0.488
8.53	0.821	0.828
12.40	1.131	1.119
16.52	1.397	1.412
20.45	1.698	1.682
20.50	1.694	1.686
26.30	2.054	2.075
30.48	2.358	2.350

$k_D = 6.31 \times 10^{-2}$

$C'_H = 0.523$

B = 0.146

V_M = 1.0076

T = 40.1

P	C(expt'l)	C(calc.)
1.793	0.113	0.109
4.87	0.273	0.273
10.68	0.542	0.545
16.41	0.786	0.789
21.18	0.986	0.984
27.23	1.232	1.224
32.01	1.404	1.410

$k_D = 3.69 \times 10^{-2}$

$C'_H = 0.309$

B = 0.0892

T = 30.1

P	C(expt'l)	C(calc.)
1.68	0.150	0.146
3.63	0.290	0.291
4.90	0.378	0.377
7.50	0.538	0.539
10.39	0.702	0.707
15.18	0.968	0.968
20.75	1.266	1.257
20.75	1.254	1.257
26.80	1.564	1.563
31.12	1.776	1.778

$k_D = 4.77 \times 10^{-2}$

$C'_H = 0.365$

B = 0.131

T = 50.0

P	C(expt'l)	C(calc.)
1.81	0.084	0.084
4.03	0.179	0.176
5.11	0.218	0.219
10.50	0.424	0.418
16.91	0.640	0.644
21.54	0.799	0.805
26.97	0.986	0.991
32.42	1.182	1.177

$k_D = 3.37 \times 10^{-2}$

$C'_H = 0.102$

B = 0.165

Table 8.21 PDMS-50 (20:6)

W_M = 0.87805

T = 20.2

P	C(expt'l)	C(calc.)
1.877	0.185	0.187
3.83	0.364	0.363
5.38	0.503	0.500
8.40	0.761	0.762
11.26	1.010	1.008
16.69	1.470	1.475
22.04	1.932	1.933
24.99	2.189	2.186

$k_D = 8.54 \times 10^{-2}$

$C'_H = 0.055$

B = 0.511

V_M = 0.8004

T = 40.85

P	C(expt'l)	C(calc.)
1.878	0.108	0.109
4.05	0.232	0.231
5.56	0.316	0.316
8.59	0.482	0.483
11.29	0.632	0.631
17.31	0.950	0.960
22.63	1.250	1.250
26.50	1.460	1.460

$k_D = 5.42 \times 10^{-2}$

$C'_H = 0.030$

B = 0.165

T = 30.45

P	C(expt'l)	C(calc.)
1.873	0.139	0.139
3.76	0.273	0.274
5.54	0.399	0.398
8.62	0.612	0.611
11.27	0.789	0.791
17.08	1.187	1.184
22.12	1.520	1.523
25.82	1.771	1.770

$k_D = 6.63 \times 10^{-2}$

$C'_H = 0.075$

B = 0.128

T = 49.95

P	C(expt'l)	C(calc.)
1.908	0.091	0.090
4.13	0.194	0.194
5.82	0.272	0.273
8.63	0.404	0.403
11.32	o.528	0.528
17.52	0.812	0.813
22.85	1.057	1.056
27.13	1.251	1.251

$k_D = 4.48 \times 10^{-2}$

$C'_H = 0.075$

B = 0.033

Table 8.22 PDMS-60 (20:3.9)

W_M = 0.71570

T = 20.1

P	C	10^2.S
2.266	0.200	8.83
6.14	0.528	8.60
10.94	0.934	8.54
15.69	1.333	8.50
20.39	1.734	8.50
29.94	2.539	8.48

S = 8.50×10^{-2}

V_M = 0.6803

T = 40.05

P	C	10^2.S
1.666	0.095	5.72
10.87	0.602	5.53
15.20	0.839	5.52
21.19	1.168	5.51
31.22	1.721	5.51

S = 5.52×10^{-2}

T = 30.05

P	C	10^2.S
1.81	0.127	6.99
5.29	0.368	6.95
10.70	0.726	6.78
16.28	1.105	6.79
20.73	1.405	6.78
25.05	1.694	6.76
30.48	2.055	6.74
30.59	2.077	6.79

S = 6.77×10^{-2}

T = 50.1

P	C	10^2.S
1.917	0.088	4.59
4.93	0.226	4.59
10.87	0.494	4.54
21.45	0.971	4.53
32.60	1.481	4.54

S = 4.54×10^{-2}

Table 8.23 PDMS-64 (20: 3.5)

W_M = 1.35215

T = 20.1

P	C	10^2.S
2.04	0.184	9.00
4.01	0.361	8.99
5.35	0.479	8.91
7.96	0.709	8.90
10.97	0.977	8.90
15.97	1.420	8.89
22.09	1.969	8.91
26.40	2.356	8.93

S = 8.91 x 10^{-2}

V_M = 1.3001

T = 40.7

P	C	10^2.S
1.762	0.103	5.86
3.95	0.228	5.76
5.44	0.314	5.77
8.80	0.505	5.75
12.57	0.723	5.75
17.74	1.019	5.75
27.06	1.555	5.75

S = 5.75 x 10^{-2}

T = 30.45

P	C	10^2.S
1.830	0.131	7.18
5.26	0.375	7.14
8.55	0.610	7.13
14.46	1.033	7.14
19.15	1.366	7.13
26.00	1.855	7.14

S = 7.14 x 10^{-2}

T = 50.1

P	C	10^2.S
5.11	0.245	4.79
10.01	0.479	4.79
15.25	0.730	4.79
20.24	0.969	4.79
27.72	1.327	4.79

S = 4.79 x 10^{-2}

8.8.2 40-block membranes

The equilibrium sorption data for the 40-block membranes are presented in Tables 8.24 - 8.28

Table 8.24 PDMS-49 (41: 12.4)

W_M = 1.23355 V_M = 1.1520

T = 20.60

P	C(expt'l)	C(calc.)
1.91	0.239	0.231
5.15	0.552	0.557
10.79	1.039	1.044
16.11	1.472	1.467
20.30	1.787	1.789
23.13	2.011	2.003
29.74	2.492	2.497

$k_D = 7.17 \times 10^{-2}$
$C'_H = 0.453$
$B = 0.137$

T = 40.40

P	C(expt'l)	C(calc.)
1.39	0.097	0.094
4.88	0.306	0.306
10.79	0.626	0.629
16.24	0.908	0.908
22.17	1.205	1.203
28.03	1.490	1.488
33.81	1.765	1.767

$k_D = 4.67 \times 10^{-2}$
$C'_H = 0.247$
$B = 0.095$

T = 30.75

P	C(expt'l)	C(calc.)
1.67	0.155	0.148
4.98	0.403	0.405
10.78	0.797	0.803
16.03	1.136	1.138
19.17	1.342	1.337
23.93	1.622	o.623
29.41	1.955	1.953
33.95	2.221	2.224

$k_D = 5.78 \times 10^{-2}$
$C'_H = 0.332$
$B = 0.110$

T = 50.0

P	C(expt'l)	C(calc.)
1.64	0.088	0.088
5.36	0.263	0.263
7.59	0.360	0.362
10.46	0.490	0.486
16.14	0.728	0.727
18.41	0.821	0.823
21.19	0.937	0.939
24.93	1.097	1.095

$k_D = 4.12 \times 10^{-2}$
$C'_H = 0.083$
$B = 0.199$

Table 8.25 PDMS-54 (40:10)

W_M = 1.35400

T = 20.0

P	C(expt'l)	C(calc.)
1.84	0.219	0.214
3.59	0.390	0.391
5.33	0.554	0.555
8.39	0.828	0.831
11.27	1.083	1.082
17.10	1.583	1.580
22.48	2.036	2.033
26.64	2.378	2.382

$k_D = 8.27 \times 10^{-2}$

$C_H' = 0.208$

B = 0.231

V_M = 1.2410

T = 40.55

P	C(expt'l)	C(calc.)
2.10	0.136	0.134
3.53	0.220	0.221
5.47	0.333	0.333
8.56	0.504	0.506
11.26	0.656	0.655
17.45	0.988	0.988
22.10	1.237	1.237
27.98	1.548	1.548

$k_D = 5.23 \times 10^{-2}$

$C_H' = 0.105$

B = 0.147

T = 30.2

P	C(expt'l)	C(calc.)
1.95	0.166	0.165
3.95	0.316	0.318
5.51	0.432	0.431
8.67	0.654	0.653
11.24	0.832	0.830
16.62	1.194	1.195
21.99	1.554	1.556
27.61	1.933	1.931

$k_D = 6.62 \times 10^{-2}$

$C_H' = 0.121$

B = 0.220

T = 49.75

P	C(expt'l)	C(calc.)
1.93	0.099	0.098
3.91	0.193	0.194
6.38	0.309	0.309
10.63	0.502	0.502
15.18	0.705	0.705
19.51	0.897	0.896
24.03	1.096	1.096
28.30	1.283	1.283

$k_D = 4.36 \times 10^{-2}$

$C_H' = 0.062$

B = 0.157

Table 8.26 PDMS-60 (40:7.2)

W_M = 0.92750 V_M = 0.8620

T = 19.75

P	C(expt'l)	C(calc.)
1.367	0.149	0.146
3.98	0.396	0.399
10.04	0.946	0.946
17.73	1.620	1.619
24.98	2.247	2.247
30.51	2.723	2.724

$k_D = 8.58 \times 10^{-2}$
$C'_H = 0.123$
$B = 0.221$

T = 40.05

P	C(expt'l)	C(calc.)
1.818	0.112	0.113
4.18	0.251	0.250
9.24	0.543	0.539
15.27	0.878	0.881
21.56	1.235	1.238
32.14	1.839	1.837

$k_D = 5.66 \times 10^{-2}$
$C'_H = 0.018$
$B = 0.694$

T = 30.1

P	C(expt'l)	C(calc.)
1.02	0.086	0.085
1.77	0.142	0.142
4.16	0.313	0.315
7.19	0.531	0.529
14.17	1.016	1.016
21.13	1.500	1.500
26.04	1.840	1.840

$k_D = 6.93 \times 10^{-2}$
$C'_H = 0.038$
$B = 0.584$

T = 50.0

P	C(expt'l)	C(calc.)
7.85	0.376	4.79
10.48	0.493	4.71
16.76	0.789	4.71
21.94	1.027	4.68
27.16	1.257	4.63
33.71	1.561	4.63

$S = 4.65 \times 10^{-2}$

Table 8.27 PDMS-64 (40:7)

W_M = 0.80440

V_M = 0.7668

T = 20.15

P	C(expt'l)	C(calc.)
1.496	0.152	0.154
2.98	0.294	0.293
4.99	0.479	0.478
7.51	0.710	0.708
10.36	0.965	0.967
13.97	1.293	1.295
18.09	1.671	1.669
22.68	2.085	2.085
23.98	2.199	2.203
30.36	2.784	2.781

$k_D = 9.06 \times 10^{-2}$

$C'_H = 0.032$

B = 0.870

T = 40.4

P	C	$10^2.S$
1.777	0.108	6.08
3.24	0.194	6.00
5.28	0.318	6.03
7.77	0.463	5.96
10.69	0.630	5.90
14.07	0.828	5.88
17.40	1.019	5.86
23.94	1.396	5.83
29.46	1.714	5.82
34.07	1.986	5.83

$S = 5.84 \times 10^{-2}$

T = 30.05

P	C(expt'l)	C(calc.)
1.738	0.134	0.135
3.73	0.284	0.283
5.29	0.398	0.398
8.05	0.600	0.599
10.92	0.805	0.806
14.47	1.062	1.062
18.60	1.360	1.360
22.35	1.629	1.629
26.67	1.939	1.940
29.98	2.179	2.178

$k_D = 7.18 \times 10^{-2}$

$C'_H = 0.0287$

B = 0.320

T = 50.0

P	C	$10^2.S$
1.793	0.089	4.98
3.34	0.165	4.95
5.19	0.256	4.94
8.26	0.406	4.91
11.02	0.535	4.86
15.83	0.766	4.84
21.42	1.032	4.82
21.42	1.032	4.82
27.02	1.305	4.83
34.08	1.643	4.82

$S = 4.83 \times 10^{-2}$

Table 8.28 PDMS-82 (40:3)

W_M = 1.19050 V_M = 1.1764

T = 19.9

P	C	10^2.S
2.05	0.224	10.93
5.09	0.551	10.83
10.85	1.179	10.87
17.19	1.870	10.88
25.70	2.817	10.96

S = 10.93 x 10^{-2}

T = 40.05

P	C	10^2.S
3.54	0.249	7.05
6.95	0.485	6.98
10.84	0.755	6.96
20.67	1.449	7.01
31.07	2.182	7.02

S = 7.01 x 10^{-2}

T = 30.15

P	C	10^2.S
1.95	0.168	8.61
5.01	0.430	8.58
10.89	0.938	8.62
17.35	1.491	8.59
25.67	2.212	8.62

S = 8.61 x 10^{-2}

T = 50.0

P	C	10^2.S
1.64	0.940	5.73
4.54	0.258	5.69
10.95	0.628	5.73
21.08	1.205	5.72
31.19	1.789	5.74

S = 5.73 x 10^{-2}

8.8.3 Miscellaneous block membranes

The equilibrium sorption data for the miscellaneous block membranes are presented in Tables 8.29 - 8.31.

Table 8.29 PDMS (80:14.6)

W_M = 0.60950 V_M = 0.5819

T = 19.8

P	C(expt'l)	C(calc.)
1.563	0.196	0.196
3.20	0.372	0.372
4.94	0.545	0.545
10.51	1.068	1.068
20.53	1.972	1.972
30.70	2.879	2.879

$k_D = 8.84 \times 10^{-2}$
$C'_H = 0.183$
$B = 0.297$

T = 40.2

P	C(expt'l)	C(calc.)
1.726	0.119	0.120
3.41	0.226	0.226
5.29	0.341	0.341
10.62	0.653	0.652
21.38	1.262	1.263
32.68	1.898	1.898

$k_D = 5.57 \times 10^{-2}$
$C'_H = 0.089$
$B = 0.205$

T = 30.15

P	C(expt'l)	C(calc.)
1.715	0.161	0.160
3.62	0.316	0.317
8.58	0.688	0.689
16.47	1.253	1.254
20.99	1.574	1.572
31.52	2.307	2.308

$k_D = 6.93 \times 10^{-2}$
$C'_H = 0.141$
$B = 0.242$

T = 50.0

P	C(expt'l)	C(calc.)
1.81	0.099	0.098
4.67	0.244	0.245
10.60	0.532	0.532
16.01	0.786	0.786
21.71	1.051	1.051
33.58	1.596	1.596

$k_D = 4.53 \times 10^{-2}$
$C'_H = 0.093$
$B = 0.117$

Table 8.30 PDMS-64 (100: 16.5)

W_M = 1.06320

V_M = 1.0164

T = 20.25°C

P	C(expt'l)	C(calc.)
1.97	0.301	0.301
3.30	0.472	0.468
4.98	0.658	0.661
8.11	0.992	0.996
11.34	1.325	1.323
15.65	1.752	1.750
20.33	2.206	2.204
25.02	2.654	2.656

$k_D = 9.44 \times 10^{-2}$
$C'_H = 0.338$
$B = 0.262$

T = 40.55

P	C(expt'l)	C(calc.)
1.75	0.149	0.149
3.45	0.277	0.277
5.60	0.427	0.428
11.01	0.784	0.783
16.59	1.133	1.134
21.23	1.422	1.420
27.01	1.774	1.774
28.63	1.873	1.873

$k_D = 6.00 \times 10^{-2}$
$C'_H = 0.186$
$B = 0.175$

T = 30.35

P	C(expt'l)	C(calc.)
1.79	0.214	0.208
5.05	0.505	0.512
8.95	0.837	0.837
10.51	0.962	0.962
15.66	1.369	1.365
19.82	1.687	1.686
25.38	2.110	2.111
30.08	2.466	2.467

$k_D = 7.50 \times 10^{-2}$
$C'_H = 0.240$
$B = 0.248$

T = 49.8

P	C(expt'l)	C(calc.)
1.93	0.127	0.126
3.65	0.230	0.228
5.30	0.322	0.323
8.52	0.498	0.500
13.16	0.743	0.743
18.04	0.993	0.993
22.87	1.239	1.237
29.42	1.562	1.563

$k_D = 4.87 \times 10^{-2}$
$C'_H = 0.167$
$B = 0.119$

Table 8.31 PDMS-83 (61:3.6)

W_M = 1.32860 V_M = 1.3115

T = 20.05

P	C	10^2.S
1.679	0.186	11.08
6.63	0.735	11.08
10.62	1.180	11.12
15.41	1.715	11.13
20.05	2.231	11.13
25.14	2.807	11.17

S = 11.14×10^{-2}

T = 40.4

P	C	10^2.S
1.725	0.123	7.14
7.20	0.510	7.09
11.30	0.802	7.09
20.82	1.476	7.09
31.16	2.230	7.13

S = 7.13×10^{-2}

T = 30.1

P	C	10^2.S
5.08	0.446	8.79
13.23	1.164	8.80
20.47	1.807	8.83
30.59	2.705	8.84

S = 8.83×10^{-2}

T = 50.0

P	C	10^2.S
5.15	0.299	5.80
11.11	0.648	5.83
16.64	0.971	5.84
21.37	1.246	5.83
32.64	1.909	5.85

S = 5.84×10^{-2}

8.9 Electron microscopy

The electron micrographs of PDMS-25(20:17.8) are presented in Figs. 8.1 and 8.2 and were produced using an "Hitachi" system and a "Temscan" system respectively. The basic difference in the systems is apparently associated with the orientation of the X-ray probe. Silicon analyses are included in each case and it is evident that the dark regions correspond to PDMS and the white regions to BPAC.

Both (BPAC-domain/PDMS-continuous) and (PDMS-domain/BPAC-continuous) morphologies seem to be present to some extent suggesting perhaps the imminence of phase-inversion. The "domains", if they can be said to exist here, are small with diameters of $\sim$ 100 - 150A.

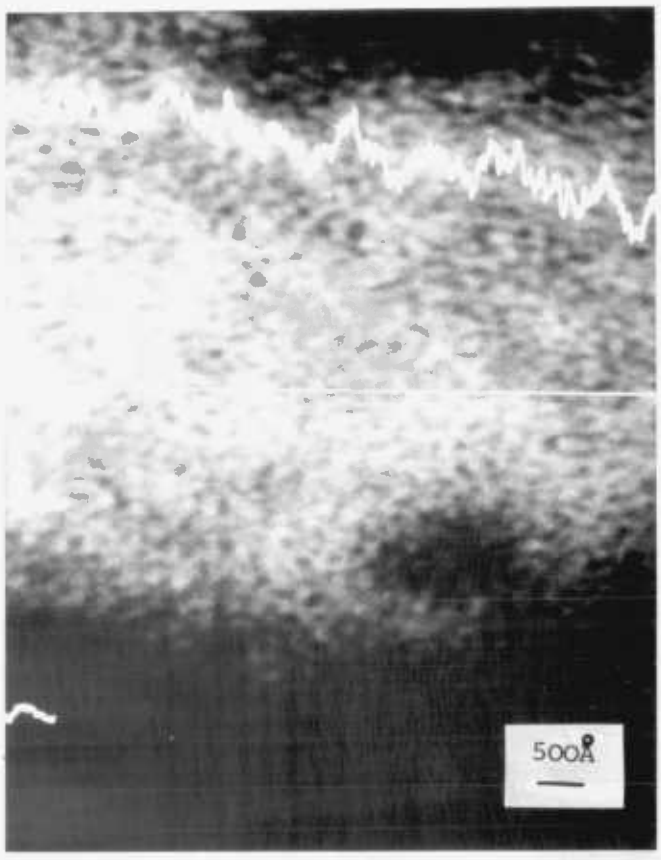


Fig. 8.1. PDMS-25 (20:17·8) x 120,000 (including silicon analysis).

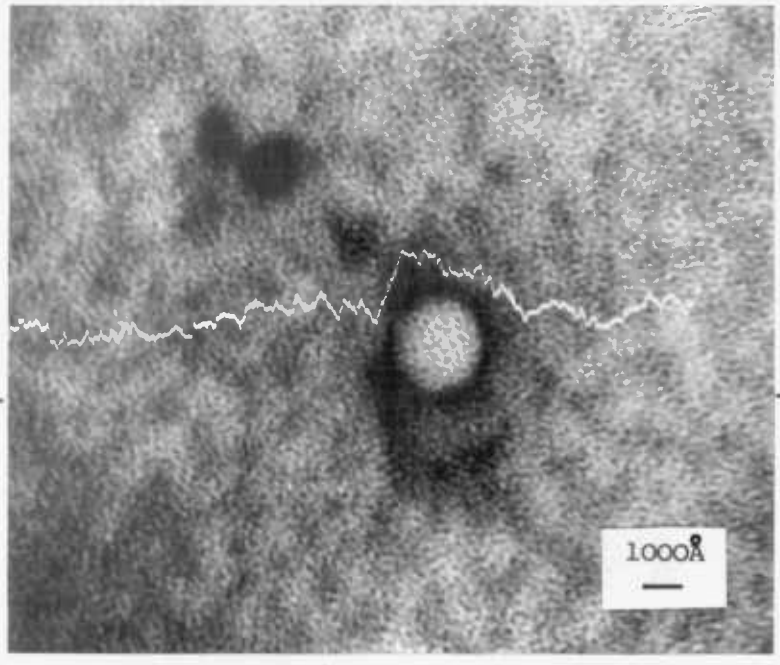


Fig. 8.2. PDMS-25 (20:17·8) x 50,000 (including silicon analysis).

REFERENCES

1. T. Graham. Phil. Mag. 32, 401 (1866).
2. J. Crank and G.S. Park "Diffusion in Polymers", Academic Press, London (1968).
3. H. Fujita. Fort. Hochpoly. - Forsch. 3, 1 (1961).
4. P. Meares. Ch. 12 in "Polymers : Structure and Bulk Properties", Reinhold Corporation, London (1965).
5. C. E. Rogers. Ch.6 in "Physics and Chemistry of the Organic Solid State" Vol. 2, (D. Fox, M.M. Labes and A. Weissberger, Eds.), Interscience, New York (1965).
6. G. J. van Amerogen. Rubb. Chem. Tech. 37, 1065 (1964).
7. Polymer Handbook (2nd Edition), (J. Brandup and E.H. Immergut, Eds.), p.III - 229, Wiley-Interscience, New York (1975).
8. V. Stannett. Op.cit., ref.2, chapter 2.
9. H. Fujita. Op.cit., ref.2, chapter 3.
10. J.A. Barrie, Op.cit., ref.2, chapter 8.
11. Op.cit., ref.7, p.III-230.
12. R.M.Barrer. Nature (Lond.) 140, 106 (1937).
13. J.van Amerongen. J. Poly. Sci. 5, 307 (1950).
14. C.A. Kumins and T.K. Kwei. Op.cit., ref.2., chapter 4.
15. C.A. Kumins and R. Roteman. J. Poly. Sci. 55, 683 (1961).
16. V. Stannett and J.L. Williams, J. Poly. Sci. C 10, 45 (1966).
17. C.A. Kumins and J. Roteman. J. Poly.Sci. 55, 699 (1961).
18. P. Meares. J. Amer. Chem. Soc. 76, 3415 (1954).
19. P. Meares. Trans. Faraday Soc. 54, 40 (1958).
20. R.M. Barrer and G. Skirrow. J. Poly. Sci. 3, 549 (1948).
21. A. Aitken and R.M. Barrer. Trans. Faraday Soc. 51, 116 (1955).
22. R.M. Barrer. Op. cit., ref.2., chapter 6.
23. J.A. Barrie, J.D. Levine, A.S. Michaels and P. Wong. Trans. Faraday Soc. 59, 869 (1963).
24. J.H. Petropoulos. I.U.P.A.C.: 4th Discussion Conference on Macromolecules (1974).
25. J. Crank. "The Mathematics of Diffusion" (2nd Edition), Clarendon Press, Oxford (1975). (Chapter 12).
26. R.E. Meredith and C.W. Tobias. Chapter 2 in "Advances in Electrochemistry and Electrochemical Engineering", Vol.2, (Ed. C.W. Tobias), Interscience, New York (1963).
27. A.C. Sheer. Ph.D. Thesis, University of London (1976).
28. R.J. Ceresa. "Block and Graft Copolymers", Butterworths, London (1962).

29. H.A.J. Battaerd and G.W. Tregear. "Graft Copolymers", Interscience, New York (1967).
30. W.J. Burlant and A.S. Hoffman "Block and Graft Copolymers", Reinhold Corporation, New York (1960).
31. "Block and Graft Copolymerisation", Vol.1, (Ed. R.J. Ceresa, Wiley, London (1973).
32. A.S. Hoffmann and R. Bacskai. Chapter 6 in "Copolymerisation", High Polymer Series Vol.18, (Ed. G.E. Ham), Interscience, London (1964).
33. M. Szwarc, M. Levy and R. Milkovich. J. Amer. Chem. Soc. 78, 2656 (1956).
34. M. Szwarc. Nature 178, 1168 (1956).
35. F.A. Bovey "The Effects of Ionising Radiations on Natural and Synthetic High Polymers", Interscience, New York (1958).
36. A. Chapiro. "High Polymers. XV. Radiation Chemistry of Polymeric Systems, "Interscience, New York (1962).
37. J.W.T. Spinks and R.J. Wood. "An Introduction to Radiation Chemistry", Wiley, New York (1964).
38. R.B. Fox and R.F. Cozzens. Encycl. Polym. Sci. Technol. 11, 702 (1969).
39. A. Fick. Annln. Physik. (Leipzig) 170, 59 (1855).
40. J.B. Fourier. "Theorie analytique de la chaleur" (1822), English translation by A. Freeman, Dover publishers, New York (1955).
41. G.S. Hartley and J. Crank. Trans. Faraday Soc. 45, 801 (1949).
42. R.M. Barrer. "Diffusion in and through Solids" (2nd Edition), Cambridge University Press, London (1951).
43. W. Jost. "Diffusion in solids, liquids, gases", p.63, Academic Press, New York (1952).
44. M.H. Jacobs. "Diffusion Processes", Springer-Verlag, Berlin (1967).
45. R.M. Barrer. Trans. Faraday Soc. 35, 629 (1939).
46. W.A. Rogers, R.S. Buritz and D. Alpert. J. Appl. Phys. 25, 868 (1954).
47. H.L. Frisch. J. Phys. Chem., Wash. 61, 93 (1957).
48. J. Crank. Op. cit., ref. 25, p.222.
49. P. Meares. J. Appl. Poly. Sci. 9, 917 (1965).
50. J. Crank. Op. cit., ref. 25, p.250.
51. J. Crank and G.S. Park. Trans. Faraday Soc. 45, 240 (1949).
52. S. Prager and F.A. Long. J. Amer. Chem. Soc. 73, 4072 (1951).
53. M.J. Hayes and G.S. Park. Trans. Faraday Soc. 52, 949 (1956).
54. R.J. Kokes, F.A. Long and J.L. Hoard. J. Chem. Phys. 20, 1711 (1952).
55. R.M. Barrer and D.W. Brook. Trans. Faraday Soc. 49, 1049 (1953).

56. J. Crank. Trans. Faraday Soc. 51, 1632 (1955).
57. J.A. Barrie and D. Machin. Trans. Faraday Soc. 67, 2970 (1971).
58. J. Lin Hwang. J. Chem. Phys. 20, 1320 (1952).
59. H. Fujita and A. Kishimoto. Text. Res. J.22, 94 (1952).
60. S. Prager. J. Chem. Phys. 19, 537 (1951).
61. A. Kishimoto and Y. Enda. J. Poly. Sci. A1, 1799 (1963).
62. J. E. Wilkins. J. Soc. 2nd App. Maths. 11, 632 (1963).
63. M.H. Cohen and D. Turnbull. J. Chem. Phys. 31, 1164 (1959).
64. R.M. Barrer. J. Phys. Chem. 61, 178 (1957).
65. R.M. Barrer. Trans. Faraday Soc. 39, 237 (1943).
66. W.W. Brandt. J. Phys. Chem. Wash. 63, 1080 (1959).
67. A.T. DiBenedetto and D.R. Paul. J. Poly. Sci. A2, 1001 (1964).
68. A.T. DiBenedetto. J. Poly. Sci. A1, 3477 (1963).
69. D.R. Paul and A.T. DiBenedetto. J. Poly. Sci. C 10, 17 (1965).
70. W.R. Vieth, J.M. Howell and J.H. Hsieh. J. Membrane Sci. 1, 177 (1976).
71. K. Munday. Unpublished work.
72. W.R. Vieth and K.J. Sladek. J. Colloid Sci. 20, 1014 (1965).
73. J.C. Maxwell. "Treatise on Electricity and Magnetism" Vol.1, p.365, Oxford University Press, Oxford (1873).
74. D.A.G. Bruggeman. Annln. Physik. (Leipzig) 24, 636 (1935).
75. R.E. Meredith and C.W. Tobias. J. Electrochem. Soc. 108, 286 (1961)
76. C.J.F. Böttcher. "Theory of electric polarisation", Elsevier, Amsterdam (1952).
77. Lord Rayleigh. Phil. Mag. 34, 481 (1892).
78. I. Runge. Z. Tech. Phys. 6, 61 (1925).
79. R.E. Meredith and C.W. Tobias. J. Appl. Phys. 31, 1270 (1960)
80. O. Wiener. Abhandl. Sachs. Ges. Wiss. 32, 509 (1912).
81. W.I. Higuchi. J. Phys. Chem. 62, 649 (1958).
82. W.I. Higuchi and T. Higuchi. J. Amer. Pharm. Assoc. 49, 598 (1960).
83. K. Lichtenecker. Physik. Z. 27, 115 (1926).
84. P.T. Fidelle and R.S. Kirk. A.I.Ch.E.J. 17, 1427 (1971).
85. G.E. Bell and J. Crank. J. Chem. Soc. Faraday Trans. II 70, 1259 (1974).
86. A.L. Baxley, C.H. Nicholas and J.R. Couper. 7th Conference on Thermal Conductivity, p.685. Nat. Bur. Stand. U.S.A. Spec. Publ. No. 302.
87. H. Fricke. Phys. Rev. 24, 575 (1924).
88. R.L. Hamilton and O.K. Crosser. Ind. Eng. Chem. Fund. 1, 187 (1962).
89. C.A.R. Pearce. Br. J. Appl. Phys. 6, 113 (1955).

90. J.A. Reynolds and J.M. Hough. Proc. Roy. Soc. (London), B70, 769 (1957).
91. S.P. Mitoff. Chapter 4 in "Advances in Materials Research" Vol.3, (Ed. H. Herman), Interscience, New York (1968).
92. C.M. Peterson. J. Appl. Poly Sci. 12, 2649 (1968).
93. K.D. Ziegel. J. Macromol. Sci. (Phys) B5, 11 (1971).
94. D.R. Paul and W.J. Koros. J. Poly. Sci. A2. 14, 675 (1976).
95. L.M. Robeson, A. Noshay, A Matzner and C.N. Merriam. Die Angew. Makromol. Chemie 29/30, 47 (1973).
96. A.E. Barnabeo, W.S. Creasy and L.M. Robeson. J. Poly. Sci. (Poly. Chem. Ed.) 13, 1979 (1975).
97. R.Y.M. Huang and P.J.F. Kanitz. J. Appl. Poly. Sci. 14, 669 (1969).
98. P.J.F. Kanitz and R.Y.M. Huang, J. Appl. Poly Sci. 15, 67 (1971).
99. K. Toi, K. Igarashi and T. Tokuda. J. Appl. Poly. Sci. 20, 703 (1976).
100. H. Odani, K. Taira, N. Nemoto and M. Kurata. Bull. Inst. Chem. Res., Kyoto University, 53, 216 (1975).
101. J. Barbier. Rubb. Chem. Tech. 28, 814 (1955).
102. H.B. Hopfenberg and D.R. Paul. Chapter 10 in "Polymer Blends", (D.R. Paul and S. Newman, Eds.), Academic Press, New York (1978(?)).
103. B.G. Ranby. J. Poly. Sci. C 51, 89 (1975).
104. Y.J. Shur and B. Rânby. J. Appl. Poly. Sci. 19, 1337 (1975).
105. Y.J. Shur and B. Rânby. Ibid. 19, 2143 (1975).
106. Y.J. Shur and B. Rânby. Ibid. 20, 3105 (1976).
107. Y.J. Shur and B. Rânby. Ibid. 20, 3121 (1976).
108. J. Ito. Kogyo Kagaku Zasshi 63, 2016 (1960).
109. E.T. Pieski "Polythene" (Eds. A. Renfrew and P. Morgan), 2nd Edition, p. 379 (1960).
110. R.L. Stallings, H.B. Hopfenberg and V. Stannett. J. Poly. Sci. C. 41, 23 (1973).
111. H.L. Frisch. Polym. Eng. Sci. 17, 81 (1977).
112. P. Meares. Trans. Faraday Soc. 53, 101 (1957).
113. R.M. Barrer, J.A. Barrie and J. Slater, J. Poly. Sci. 27, 177 (1958).
114. A.H. Chan, W.J. Koros and D.R. Paul. J. Membrane Sci. 2, 117 (1977).
115. A.S. Michaels, W.R. Vieth and J.A. Barrie. J. Appl. Phys. 34, 1 (1963).
116. W.R. Vieth, H.H. Alcalay and A.J. Frabetti. J. Appl. Poly. Sci. 8, 2125 (1964).
117. K. Toi, J. Poly. Sci. A2. 11, 1829 (1973).

118. W.J. Koros, D.R. Paul, M. Fujii, H.B. Hopfenberg and V. Stannett. J. Appl. Poly. Sci. 21, 2899 (1977).
119. W.J. Koros, D.R. Paul and A.A. Rocha. J. Poly. Sci. A2 14, 687 (1976).
120. A.S. Michaels, W.R. Vieth and J.A. Barrie. J. Appl. Phys. 34, 13 (1963).
121. W.R. Vieth, C.S. Frangoulis and J.A. Rionda Jr. J. Colloid. Interface Sci. 22, 454 (1966).
122. W.R. Vieth, P.M. Tam and A.S. Michaels. J. Colloid Interface Sci. 22, 360 (1966).
123. D.R. Paul. J. Poly. Sci. A2. 7, 1811 (1969).
124. J. H. Petropoulos. Ibid. 8, 1797 (1970).
125. R.M. Barrer and D. Nicholson. Z. Physik. Chem. (Frankfurt) 37, 18 (1963).
126. V.M. Patel, C.K. Patel, K.C. Patel and R.D. Patel. Makromol. Chem. 158, 65 (1972).
127. E.G. Davis and M.L. Rooney. Kolloid Z. 249, 1043 (1971).
128. W.R. Vieth and J.A. Eilenberg. J. Appl. Poly Sci. 16, 945 (1972).
129. S. Kubo and M. Dole. Macromolecules 7, 190 (1974).
130. A.S. Michaels and H.J. Bixler. J. Poly. Sci. 50, 393 (1961).
131. J. A. Tshudy and C. von Frankenberg. J. Poly. Sci. A2. 11, 2027 (1973).
132. D. R. Paul and D. R. Kemp. J. Poly. Sci. C 41, 79 (1973).
133. D. R. Kemp and D. R. Paul. J. Poly. Sci. A2 12, 485 (1974).
134. W. R. Vieth, A. S. Douglas and R. Bloch. J. Macromol. Sci. (Phys.) B3, 737 (1969).
135. W. R. Vieth and M. A. Amini. "Permeability of Plastic Films and Coatings to Gases, Vapours and Liquids" (H.B. Hopgenberg, Ed.), p.49, Plenum Press, New York (1974).
136. R.A. Assink. J. Poly Sci. A2. 13, 1665 (1975).
137. J.A. Barrie, K. Munday and M.J.L. Williams. In "Organic Coatings and Plastics Chemistry", (in press) (1978).
138. S.A. Stern and A.H. de Meringo. J. Poly. Sci. A2 16, 735 (1978).
139. H.A. Vaughn U.S. Pat. 3, 189, 662 (1965).
140. H.A. Vaughn J. Poly. Sci. B7, 569 (1969).
141. E. P. Goldberg. U.S. Pat. 2,999, 845 (1961).
142. R.P. Kambour. Polymer Letters 7, 573 (1969).
143. D.G. LeGrand. Ibid. 7, 579 (1969).
144. T. L. Magila and D. G. LeGrand. Poly. Eng. Sci. 10, 349 (1970).
145. D. G. LeGrand. Polymer Letters 9, 145 (1971).

146. D. G. LeGrand. Trans. Soc. Rheology 15:3, 541 (1971).

147. D. G. LeGrand. "Structure and properties of polymer films" (R. W. Lenz and R. S. Stein, Eds.), p81, Plenum Press, New York (1972 (?)).

148. S. Krause. Macromolecules 3, 84 (1970).

149. J.V. Dawkins. Chapter 8A, "Block Copolymers" (D.C. Allport and W. H. Janes, Eds.), Applied Science Publishers, London (1973).

150. P. G. Grohmann. Unpublished data.

151. S. Brunauer. "The Adsorption of Gases and Vapours", Princeton University Press, Princeton, N.J. (1943).

152. W. J. Koros, A. H. Chan and D. R. Paul. J. Membrane Sci. 2, 165 (1977).

153. K. Munday. Private communication.

154. J. B. Alexopoulos, J. A. Barrie, J. C. Tye and M. Fredrickson. Polymer 9, 57 (1968).

155. H. G. Spencer. Unpublished data.

156. R. P. Kambour, F. E. Karasz and J. H. Daane. J. Poly. Sci. A. 2, 327 (1966).

157. R. M. Barrer, J. A. Barrie and M. G. Rogers. J. Poly. Sci. A 1, 2565 (1963).

SORPTION AND DIFFUSION OF HYDROCARBON VAPOURS IN GLASSY POLYMERS

JAMES A. BARRIE, KEITH MUNDAY and MICHAEL J.L. WILLIAMS

Chemistry Department,
Imperial College of Science and Technology,
London SW7 2AY.

ABSTRACT

SORPTION AND DIFFUSION OF HYDROCARBON VAPOURS IN GLASSY POLYMERS

J.A. Barrie, M.J.L. Williams and K. Munday, The Chemistry Department, Imperial College of Science and Technology, London SW7 2AY.

Sorption isotherms in the region of low relative pressures have been determined at several temperatures for methane, propane and chlorodifluoromethane in polystyrene and for propane in bisphenol-A polycarbonate and polyvinylacetate. The results are well represented by the isotherm equation of Dual Sorption Theory as applied to glassy polymers. The temperature dependence of the isotherm parameters is examined and discussed; the Langmuir component to sorption decreases as the glass transition temperature is approached and measurements with polyvinylacetate confirm that this component is absent above the transition. Average diffusion coefficients were obtained from sorption (desorption) rate curves at constant pressure for propane in polystyrene and polycarbonate and a procedure developed for their analysis to yield the diffusion coefficients of the two sorbed species of penetrant. For the polycarbonate there is evidence of mobility in that fraction of the penetrant population exhibiting Langmuir-type sorption.

INTRODUCTION

The concept of microcavities frozen into polymer structures below the glass transition temperature and the subsequent formation of a dual mode mechanism for the sorption of gases and vapours in glassy polymers has played an important part in the interpretation of the transport process for penetrants in these systems. It is postulated that in addition to the dissolution of penetrant in the matrix similar to the sorption mode of the rubbery state there is a component associated with localized sorption of penetrant in microvoids; in the region of lower relative pressures dissolution obeys Henry's law while microvoid sorption may be described by the Langmuir isotherm. To develop a model for the transport of penetrant it was assumed in earlier treatments that both species of penetrant were in local equilibrium and further that penetrant sorbed in microvoids was immobilized relative to dissolved species. In later studies the effect of relaxing these constraints was examined and there is now evidence that the microvoid population can contribute to the flux. Much of this work has been reviewed (1,2) or discussed in more recent publications (3,4). It should be noted that the concept of mobile and immobile species had already been used by several investigators to describe the diffusion of water in polymers; also the use of combined isotherm equations for these systems had been considered by several workers (5).

Although a large number of polymer-penetrant systems has been examined only in a few of these (6,7,8) has the temperature dependence of the dual sorption parameters been studied in any detail. In the present investigation sorption equilibria have been studied at several temperatures for propane in polycarbonate, polystyrene and polyvinyl-acetate and for chlorodifluoromethane and, to a lesser extent, methane in polystyrene; also sorption kinetic measurements have been made for propane in polycarbonate and polystyrene. The results are analysed and discussed in terms of the dual-sorption model.

EXPERIMENTAL

The samples studied were polystyrene in both film and powder form, polycarbonate film and a thin sheet of polydimethylsiloxane-g-polyvinylacetate. Films of polystyrene and bisphenol A polycarbonate were cast from methylene chloride solutions on mercury and glass surfaces respectively and were outgassed for several days in the temperature range 50 to 70°C. Average film thicknesses were determined from mass and density measurements and were 107 and 27.2 μm for polystyrene used in the methane and propane studies respectively and 7.8 μm for the polycarbonate; the corresponding film areas were 179, 75 and 200 cm^2. For sorption measurements each film was wound in the form of a spiral with copper wire spacers.

Polydimethylsiloxane-g-polyvinylacetate containing 44.2% vol. polyvinylacetate was prepared by γ-irradiation from a ^{60}Co source of a lightly crosslinked polydimethylsiloxane sheet (~ 100 μm) swollen with vinyl acetate. Irradiation was performed in the absence of air which inhibited grafting, after which the sheet was refluxed with ethyl acetate for several days to constant weight to remove homopolymer and finally outgassed under high vacuum. Electron micrographs indicated that the polyvinylacetate was present as heterodisperse domains of average size 0.08 μm in a continuum of polydimethylsiloxane.

A monodisperse sample of emulsion polymerized microspheres of polystyrene was prepared and characterized by the B.F. Goodrich Company Research Centre, Brecksville, Ohio; the particle diameter was 0.53 μm.

Glass transition temperatures determined by differential scanning calorimetry were as follows; polystyrene film and polystyrene powder 101, polycarbonate film 147 and polyvinylacetate disperse phase 32°C.

The purity of the propane and methane was > 99.9 mol % and of the chlorodifluoromethane > 99.5 mol %; the latter was subjected to several freeze-pump-thaw cycles before use.

Sorption isotherms and kinetics were measured with an electronic vacuum microbalance (Model 4102, Sartorius Instruments Ltd., U.K.) as described earlier (9) and corrections made for buoyancy effects.

RESULTS AND ANALYSIS

SORPTION

Sorption isotherms for the various penetrant-polymer systems at several temperatures are shown in Figures 1 to 6. Those for polystyrene and polycarbonate exhibit clearly the curvature now well established for vapour sorption in glassy polymers at lower relative pressures and characteristic of isotherms of the Langmuir type; an exception is the methane-polystyrene system where the range of relative pressure is not sufficiently large to observe departure from Henry's law. A small but definite amount of curvature is also present in the isotherms for the graft copolymer below the glass transition temperature; at higher temperatures the isotherms are linear as are those for crosslinked polydimethylsiloxane. Isotherms for the polyvinylacetate disperse phase were "extracted" from those of the graft copolymer and of the polydimethylsiloxane and are shown in Figure 6 ; the accuracy here is less than for the other systems studied as the major part of the sorption occurs in the continuous polydimethylsiloxane phase. Dispersion of the polyvinylacetate in this manner gave short equilibration times and avoided possible problems arising from softening of the polymer above the glass transition temperature.

The results were analysed in terms of the dual-sorption theory as applied to glassy polymers for which the isotherm equation is

$$C = C_D + C_H = k_D p + \frac{C'_H b p}{1+bp} \qquad (1)$$

where C, the total concentration of sorbed penetrant comprises a component C_D for dissolved species and a component C_H for molecules localized in microvoids. It is assumed that sorption of the dissolved component obeys

Henry's law and that the microvoid component obeys the Langmuir equation for sorption on a fixed number of equivalent sites with not more than one molecule per site. The temperature dependence of k_D, the Henry's law constant for dissolved species is given by $k_D = (k_D)_o \exp(-\Delta\bar{H}_D/RT)$ where $\Delta\bar{H}_D$ is the heat of sorption for this component. From a statistical thermodynamic consideration of ideal localized monolayers the Langmuir parameter b is given by $b = b_o \exp(q/kT)$ where q is the minimum energy required to evaporate a molecule from its lowest energy state in the monolayer and b_o is a weak function of temperature. The quantity C'_H is the value of C_H in the limit $p \to \infty$ and corresponds to saturation of the adsorption sites; if C'_H is independent of temperature then q is simply related to the isosteric heat of adsorption on sites $-\Delta\bar{H}_H = -R\left(\frac{\partial \ln p}{\partial 1/T}\right)_{C_H}$

A non-linear regression analysis described in the Appendix was used to obtain values for k_D, b and C'_H which are shown in Table 1. The programme also estimated by what amount each parameter could be altered within the limits of a standard deviation; these values are quoted as average percentages in parenthesis in Table 1. Clearly the uncertainties in the sorption parameters are relatively large especially for C'_H and b, however, for the product $C'_H b$ they are much less as has already been pointed out (10). Because of the larger uncertainties attached to the isotherms for polyvinylacetate as a disperse phase the errors in the parameters C'_H and b were too large for a meaningful analysis, accordingly individual values of C'_H and b are not recorded in Table 1; also included in Table 1 are values of the Henry's law constant for the limit $p \to 0$, namely $k = k_D + C'_H b$. The temperature dependence of k is given by $k = k_o \exp\left\{-(\Delta\bar{H})_{c=o}/RT\right\}$ where $-(\Delta\bar{H})_{c=o}$ is the isosteric heat of sorption in the limit $C \to o$.

The temperature dependence of k_D, b and k is illustrated in Figure 7 with some typical examples and values of $\Delta\bar{H}_D$, q and $(\Delta\bar{H})_{c=o}$ are given in Table 2. The temperature dependence of k_D and k for the polyvinylacetate disperse phase both above and below the glass transition temperature is shown in Figure 8; no attempt was made to estimate the

heats of sorption below the glass transition temperature. Finally, in Figure 9 the variation with concentration of $\Delta\overline{H}$, the overall heat of sorption, is shown.

DIFFUSION

Integral sorption (desorption) rate curves were measured with constant pressure maintained at the film interface and diffusion coefficients obtained from the initial slopes by conventional procedures. For the propane-polystyrene system average coefficients were obtained from conjugate sorption-desorption curves and the arithmetic mean approximation used to relate these to the differential coefficient D such that $\overline{D} \equiv (\overline{D}_s+\overline{D}_d)/2 = \frac{1}{C}\int_o^C DdC$ (11). For the propane-polycarbonate system, sorption rate curves only were measured and the average and differential coefficients were related through the weighted-mean approximation $\overline{D}_s = rC^{-r}\int_o^C C^{r-1}DdC$ where r = 1.67 (11). The concentration dependence of $\overline{D}$ and $\overline{D}_s$ is shown in Figures 10 and 11 respectively.

In the development and application of dual-sorption theory several notations have been used for the experimental diffusion coefficient and the diffusion coefficient for dissolved penetrant some examples of which are, $D_{eff}D$ (2,12), D_aD_{eff} (13), DD' (3), D_aD' (14) and DD' (15). In what follows the experimental diffusion coefficient determined from the total flux and gradient of the total concentration is denoted by D.

Extensions of the earlier analyses of gas transport in glassy polymers assign diffusion coefficients to penetrant both in dissolved state and sorbed in microvoids respectively. Denoting these coefficients by D_D and D_H respectively and assuming that the populations of these two states obey Henry's law and the Langmuir isotherm respectively then the flux per unit area is given by (3,4)

$$J = -D_D\frac{\partial C_D}{\partial x} - D_H\frac{\partial C_H}{\partial x} \equiv -D\frac{\partial C}{\partial x} \qquad (2)$$

It follows that,

$$D = (D_D - D_H)\frac{\partial C_D}{\partial C} + D_H \tag{3}$$

From equation (1),

$$\frac{\partial C_D}{\partial C} = 1/\left\{1 + \frac{C'_H b/k_D}{(1+bp)^2}\right\} \tag{4}$$

and hence D is obtained as a function of pressure. Alternatively, from equation (1),

$$p = \frac{\left\{(C'_H b + k_D - bC)^2 + 4k_D bC\right\}^{\frac{1}{2}} - (C'_H b + k_D - bC)}{2k_D b} \tag{5}$$

which with equations (3) and (4) gives D as a function of C or C_D (12). The resulting expressions are quite general in the sense that D_D and D_H may be functions of concentration; however, it is generally assumed that both coefficients are constant and this approach is adopted from here on. In the limit $bp \ll 1$,

$$D_{c=o} = \frac{D_D k_D + D_H C'_H b}{k_D + C'_H b} \tag{6}$$

and for $p \to \infty$, $D = D_D$. In principle, the concentration dependence of D can be obtained from the plots of $\bar{D}$ against C by conventional methods involving differentiation, graphical or otherwise, of the data and a best fit made with equation (3) using D_D and D_H as adjustable parameters. However, as the expression for D(C) is cumbersome and differentiation introduces additional errors it is better to make the comparison with the average diffusion coefficient data. The corresponding theoretical expressions are easily obtained as follows,

$$\bar{D}_s \equiv rC^{-r}\int_o^C C^{r-1} D\,dC$$

$$= rC^{-r}\left\{\int_o^C C^{r-1}(D_D - D_H)\frac{\partial C_D}{\partial C} + \int_o^C C^{r-1} D_H\,dC\right\} \tag{7}$$

$$= (D_D - D_H)X + D_H \tag{8}$$

The integral X which may be computed by numerical integration was expressed as follows using integration by parts,

$$X = rC^{-r}\left\{C^{r-1}k_D p - k_D(r-1)\int_o^C C^{r-2} p\,dC\right\} \tag{9}$$

$$= \frac{C_b}{C}$$

A plot of $\overline{D}_s$ versus X is then linear with slope $(D_D - D_H)$ and intercept D_H; If the arithmetic mean of the average coefficients from conjugate sorption and desorption rate curves is used to obtain $\overline{D} = \frac{1}{C}\int_0^C DdC$ then the corresponding expressions for $\overline{D}$ are obtained with r = 1 in equations (7) to (9) and reduce to the relatively simple expression

$$\overline{D} = \frac{pD_D}{C}\left\{k_D + \frac{D_H}{D_D}\frac{C'_H b}{(1+bp)}\right\} \equiv (D_D - D_H)\frac{C_D}{C} + D_H \qquad (10)$$

In this instance the average coefficient $\overline{D}$ is identical with that obtained from steady-state permeation so that using Fick's equation for the permeability $\overline{P}$,

$$\overline{P} = \overline{D}\,\frac{C}{p} = k_D D_D\left\{1 + \frac{D_H}{D_D}\frac{(C'_H b/k_D)}{(1+pb)}\right\} \qquad (11)$$

which is the expression obtained earlier (3,4) for the steady-state permeability as a function of the pressure. The corresponding expressions for the concentration dependence of $\overline{D}$ and $\overline{P}$ are obtained using equation (5). In the limit $p \to o$ equation (10) reduces to equation (6) and for $p \to \infty$ $\overline{D} = D_D$.

The results for the C_3H_8- polycarbonate system plotted according to equation (8) are shown in Figure (12) and indicate a finite but small D_H for microvoid population. Attempts to analyse or curve fit the results with $D_H = 0$ were not successful in that the values of D_D displayed a small but definite trend with concentration. The solid curves in figure (11) were computed using equation (8). For the C_3H_8- polystyrene (film) system the accuracy of the data was such that it was not possible to establish whether or not $D_H = 0$; within the limits of experimental error the results were represented satisfactorily by equation (10) with $D_H = 0$. Values of D_D and D_H are given in Table (3); also included are values of the limiting coefficients $D_{c=o}$ calculated from equation (6) and of the activation energy in the limit $C \to o$.

DISCUSSION

SORPTION

The solid curves of Figures 1 to 6, computed using equation (1) and the parameters of Table 1, are in good agreement with the experimental points but the errors in the sorption parameters are comparatively large and tend to increase with temperature. This may be partly a reflection of the difficulty in ensuring that relaxation and hysteresis effects are negligible in glassy polymer systems. This aspect was studied in more detail with the microsphere samples; it was observed that the bulk of the sorption was rapid followed by a small uptake which slowly approached an equilibrium value while in all cases desorption was rapid (16). Thus even at low levels of sorption, less than 1% by volume, some degree of relaxation would appear to be present; also some thermal hysteresis was observed on cycling the sample over the temperature range. Although the uncertainties introduced by these effects were in general small, at worst not more than a few per cent, nevertheless they limit the accuracy with which one may determine the sorption parameters in these systems. The value of .0069 for the overall solubility k determined directly for methane in polystyrene at 30°C may be compared with the value of 0.00126 obtained earlier from a dual-sorption analysis of high pressure isotherm data for the same system at 25°C. The discrepancy between the two figures is not serious in view of the difference in temperature and sample preparation and the use of a graphical rather than a least-squares regession analysis to fit the high pressure data (18)

According to equation (1) the ratio C_H/C_D varies from C'_Hb/k_D to zero as the pressure changes from 0 to ∞ and so from the results in Table 1 it is inferred that for sorption in glassy polymers the Langmuir component is the major one in the region of lower pressures. A comparison of the propane data for the polystyrene film and powder indicates that although the overall solubility k for both samples is similar, the Langmuir component for the powder is higher and has

increased at the expense of the Henry's law component; this behaviour may reflect differences in the thermal histories of the samples with the microspheres having a larger microvoid volume. It has already been demonstrated that annealing of the microspheres has quite a significant effect on their sorption behaviour (16). Although chlorodifluoromethane is sorbed more strongly than propane the ratio $C_H'b/k_D$ is not significantly different for these two vapours. In polycarbonate, propane is sorbed more strongly than in polystyrene in both the Langmuir and Henry's law modes; also the ratio $C_H'b/k_D$ is relatively large but this may simply reflect the higher glass transition of the polycarbonate and the fact that this ratio increases steadily as the temperature is lowered below the transition temperature for all of the polymers studied.

The decline in the relative magnitude of the Langmuir component as the glass transition temperature is approached is in accord with earlier observations and the view that this component of the sorption should tend to zero in the region of the transition (7). The results for the polyvinylacetate disperse phase demonstrate directly that this is the case with no Langmuir component to the sorption in evidence above the glass transition temperature. Somewhat similar behaviour has been reported for the vinylchloride-polyvinylchloride system (16) and reference has also been made to the system CO_2-poly(ethyleneterephthalate) (17).

The parameter C_H' has been used as a measure of the surface area bounding the microvoids by assuming that the molecules sorbed in these have the same hexagonal packing as the plane of closest packing in the liquid state (18) or as a measure of the microvoid volume using an appropriate density for the sorbed phase, generally that of the liquid for vapours above their critical temperature (7,10). The density of liquid propane decreases from ~ 0.5 at 20°C to ~ 0.425 at 60°C; the corresponding variation of C_H' particularly for the propane-polystyrene system is much larger and in terms of these earlier analyses (18,7,10) one may conclude that the microvoid surface area or microvoid volume decreases as the temperature is increased.

It is pertinent at this stage to re-emphasize some observations which have been made with regard to testing theoretical isotherm equations. It has long been recognized that agreement between the theoretical and experimental isotherm does not constitute proof of the model on which the theoretical equation is based and furthermore even if sensible values of the parameters emerge these may result from a mutual cancellation of different effects (19,20,21,22,23). It is unlikely that sorption of penetrant in microvoids conforms exactly to the ideal localized model of sorption according to which molecules are sorbed on a set of sites with no interaction between sorbed molecules and no more than one molecule allowed per site; on this basis C'_H is constant and independent of temperature and is a measure of the number of sorption sites in the system. Invariably C'_H is observed to vary with temperature and it has been argued that for several reasons this effect may be more apparent than real (19, 20, 21) Nevertheless this parameter has been used to estimate saturation capacities of real systems such as the zeolites where Langmuir-type sorption is often observed (24). In experiments with glassy polymers the degree of saturation C_H/C'_H attained is usually large and in the present investigation was rarely less than 80% and usually greater than 90% so that good agreement with the Langmuir equation is obtained over a large part of the isotherm. In the light of these earlier observations it would appear that the parameter C'_H is related to the saturation capacity but that some care should be exercised in the use of absolute values.

Similar strictures apply to the interpretation of the parameter b and its temperature coefficient q; in terms of the Langmuir model q is constant and a measure of the isosteric heat of sorption in the microvoids. A comparison of the data of Table 2 indicates that in general q is numerically larger than $\Delta\overline{H}_D$ which might have been anticipated; however, in some instances the difference is small and in others $|q| < |\Delta\overline{H}_D|$. Similar

behaviour was observed for hydrocarbon vapours in ethylcellulose (7) and for methane in oriented polystyrene (6). The isosteric heat of sorption in microvoids in the limit C→0 is given by $-(\Delta\bar{H}_H)_{c=o} = \frac{d\ln C'_H b}{d1/T}$ and values are included in Table 2; if C'_H is temperature independent then $(\Delta\bar{H}_H)_{c=o} = -q$. Also since $k = k_D + C'_H b$ it follows that

$$\Delta\bar{H}_{c=o} = \frac{k_D}{k}\Delta\bar{H}_D + \frac{C'_H b}{k}(\Delta\bar{H}_H)_{c=o} \qquad (12)$$

The difference in the values of q and $-(\Delta\bar{H}_H)_{c=o}$ of Table 2 is substantial and the question arises as to which of these two quantities is more representative of the true heat of sorption in microvoids. Using the parameters C'_H and b of Table 1 adsorption isosteres were constructed for the Langmuir component of the sorption for constant values of C_H. Smoothed values of $\Delta\bar{H}_H$ were obtained from linear isosteres only and the variation with concentration is shown in Figure (14); at higher concentrations approaching saturation the isosteres became non-linear. $\Delta\bar{H}_H$ tends to become more exothermic as C_H increases; it is conceivable that this behaviour is more apparent than real and associated with a perturbation of the polymer matrix as for example, a change in the microvoid content with temperature. If this were so, then $\Delta\bar{H}_H$ would not reflect accurately the heat of sorption in microvoids. The small minimum observed in Figure (9) is also probably associated with the increase in $|\Delta\bar{H}_H|$ with concentration; at higher concentrations the relative contribution to $\Delta\bar{H}$ from the dissolved species increases and $\Delta\bar{H}$ tends towards $\Delta\bar{H}_D$.

The results for the polyvinylacetate disperse phase in Figure (8) are of interest in that they indicate that $\Delta\bar{H}_D$ may be more exothermic above the glass transition temperature than below it, suggesting perhaps that hole formation in the dissolved state is more endothermic below the transition. In view of the reduced accuracy of the isotherms for this system a more detailed study over a wider range of temperature is required to substantiate these observations.

DIFFUSION

The earlier work on the application of dual-sorption theory in this area made use of pressure decay in a system of finite volume; the analysis was then based on an empirical correlation relating parameters obtained from a numerical solution of the diffusion equation and has been described in detail elsewhere (2). In later developments the restriction $D_H=0$ was removed and the pressure dependence of the steady-state permeability and the time-lag analysed to obtain D_D and D_H (3,4). The procedure developed here and incorporated in equations (8) and (9) enables one to determine both D_D and D_H from the initial slopes of either sorption or desorption rate ($\sqrt{t}$) curves determined at constant pressure; the accuracy of the method will depend among other things on that of the weighted-mean approximation.

The data for polycarbonate in Table 2 support the view that immobilization of the Langmuir component is only partial (7,10). Although D_H is relatively small the contribution to the flux from this component can be large at low pressures; for example, in the limit $p \to o$, the ratio of the flux of dissolved species to that of penetrant in microvoids is $\frac{C'_H b}{k_D} \frac{D_H}{D_D}$ and at 30°C is estimated as 1.95. Substituting 1.95 for the ratio of the fluxes in equation (11) it is estimated that the permeability for propane in polycarbonate varies from $\sim 3.2.\ 10^{-12}$ to $1.6.\ 10^{-12}$ cc stp. cm/cm^2 s. cm Hg as the pressure changes from 0 to 10 cm g and thereafter approaches asymptotically the limiting value of $k_D D_D = 1.07.\ 10^{-12}$. The results for polystyrene in Fig.13 are inconclusive and/more data points are required to establish whether $D_H=0$. As indicated earlier (3) the average coefficient $\bar{D}$ may be converted to the corresponding $\bar{P}$ ($=\bar{D}\,\frac{C}{p}$) and the latter examined for pressure dependence. In this instance no advantage is gained as the scatter in the $\bar{P}$ values obscures any trend with pressure; The average values of $\bar{P}$ at 30 and 50°C are $3.72.10^{-12}$ and $5.12.10^{-12}$ respectively.

The temperature dependence of the diffusion coefficients is shown in Figure (15) and the corresponding energies of activation in Table 2. From equation (6) it follows that

$$(E_D)_{c=o} = -(\Delta\overline{H})_{c=o} + (E_{D_D} + \Delta\overline{H}_D)\frac{D_D k_D}{D_{c=o}k} + \left\{E_{D_H} + (\Delta\overline{H}_H)_{c=o}\right\}\left(1-\frac{D_D k_D}{D_{c=o}k}\right) \quad (13)$$

and the $\Delta\overline{H}$ terms are related through equation (12). In view of the relatively large errors attached to the values of D_H it is not possible to attach too much significance to the relative values of E_{D_D} and E_{D_H}. One might have anticipated E_{D_H} to be larger than E_{D_D}; this tends to be so for hydrocarbon diffusion in ethylcellulose although in general the differences are not large (7). It is conceivable that the transition state for penetrant diffusing out of microvoids into the dissolved state differs from that for penetrant diffusing in the dissolved state.

In conclusion the analysis is consistent with the view that the localized microvoid space may be a function of temperature and, in particular, decreases as the temperature of the glass approaches Tg but it is difficult to draw firm conclusions. Essentially the dual- sorption theory postulates two modes of sorption the isotherms for which are described by the Henry's law and Langmuir equations; in this respect the theory gives good agreement with experiment in a large number of systems. If one proceeds further and identifies the parameters of the Langmuir equation with those of the Langmuir model for ideal localized sorption then it should be borne in mind that isotherm equations of this form are not specific to this mode of sorption and too literal an interpretation of the isotherm parameters and their temperature dependence in this fashion could be misleading. Finally a method for analysing average diffusion coefficient data from constant pressure sorption analysis is suggested; the results for polycarbonate indicate a component to the flux from the Langmuir component but for polystyrene are inconclusive.

Acknowledgements

We thank the SRC for maintenance awards (to K.M. and M.J.L.W.) and both the SRC and the University of London Research Fund for grants to purchase equipment. We are grateful to Professor H.B. Hopfenberg for the sample of polystyrene microspheres.

APPENDIX

The least-squares values of the dual-mode sorption coefficients cannot be determined by any simple closed expression. If α, β and γ are approximations to the desired coefficients k_D, C_H and b, we define

$$C' = \alpha p + \beta \left(\frac{\gamma p}{1+\gamma p}\right) \tag{1}$$

and

$$S = \sum_{i=1}^{n}(C'-C)^2$$

$$= \alpha^2\Sigma p^2+\beta^2\Sigma f(p)^2+2\alpha\beta\Sigma p f(p)$$

$$-2\alpha\Sigma Cp-2\beta\Sigma C f(p)+\Sigma C^2 \tag{2}$$

where $f(p) = \frac{\gamma p}{1+\gamma p}$ and C,p are the experimental values.

Then for any given value of γ the corresponding approximations α and β are uniquely defined by the simultaneous equations

$$\frac{\partial S}{\partial \alpha} = 2\alpha\Sigma p^2+2\beta\Sigma p.f(p)-2\Sigma Cp = 0 \tag{3}$$

$$\frac{\partial S}{\partial \beta} = 2\beta\Sigma f(p)^2+2\alpha\Sigma p.f(p)-2\Sigma C.f(p) = 0 \tag{4}$$

It is then required only to find the value of γ giving the minimum value of the sum of the squares of the deviations, S, which is easily achieved by a computer program employing a systematic variation in γ. We then define the mean deviation of the experimental points as $S/(n-3)$, where n is the number of points and n-3 the remaining degrees of freedom, and estimate the uncertainties in the best fit parameters k, C_H', and b, from the maximum variations of these parameters giving isotherms which lie within one mean deviation of the best fit isotherm over the range of the experimental data.

REFERENCES

1. H.B. Hopfenberg and V. Stannett, "The Physics of Glassy Polymers", (Ed. R.N. Haward), Chapter 9. Applied Science Publishers, London (1973).
2. W.R. Vieth, J.M. Howell and J.H. Hsieh, J. Membrane Sci., 1, 177 (1976).
3. J.H. Petropoulos, J. Polym. Sci., Pt.A-2, 8, 1797 (1970).
4. D.R. Paul and W.J. Koros, J. Polym. Sci.; Polym. Phys. Ed., 14, 675 (1976).
5. J.A. Barrie "Diffusion in Polymers" (Eds. J. Crank and G.S. Park), Chapter 8, Academic Press. London and New York (1968).
6. W.R. Vieth, C.S. Fragoulis and J.A. Rionda, Jr., J. Colloid Interface Sci., 22, 454 (1966).
7. A.H. Chan, W.J. Koros and D.R. Paul, J. Membrane Sci., 3, 117 (1978).
8. S.A. Stern and A.H. De Meringo, J. Polym. Sci.; Polym. Phys Ed., 16, 735, (1978).
9. J.A. Barrie and D. Machin, J. Macromol Sci. Phys. B3(4) 645 (1969).
10. W.J. Koros, A.H. Chan and D.R. Paul, J. Membrane Sci., 2, 165 (1977).
11. J. Crank, "The Mathematics of Diffusion" p 244, 250 Clarendon Press, Oxford (1975).
12. W.J. Koros, D.R. Paul and A.A. Rocha, J.Polym. Sci.; Polym. Phys. Ed., 14, 687 (1976).
13. K. Toi, J. Polym. Sci.; Polym.Phys. Ed., 11, 1829 (1973).
14. A.S. Michaels, W.R. Vieth and J.A. Barrie, J. App. Phys., 34, 13 (1963).
15. J.A. Barrie, A.S. Michaels and W.R. Vieth, J. Polym. Sci.; Polym. Phys. Ed., 13, 859 (1975)

16. A.R. Berens, J. Membrane Sci., 3, 247 (1978).

17. W.J. Koros, D.R. Paul, M. Fujii, H.B. Hopfenberg and V. Stannett, J. App. Polym. Sci., 21, 2899 (1977).

18. W.R. Vieth, Phi M. Tam and A.S. Michaels, J. Colloid Interface Sci., 22, 360 (1966).

19. D.H. Everett, Trans. Faraday Soc., 46, 453 (1950).

20. D.H. Everett, Trans. Faraday Soc., 46, 942, (1950).

21. D.H. Everett, Trans. Faraday Soc., 46, 957, (1950).

22. D.H. Everett, Proc. Chem. Soc. (London) 37 (1957).

23. D.M. Young and A.D. Crowell "Physical Adsorption of Gases" Chapter 3,4. Butterworth, London (1962).

24. L.V.C. Rees and C.J. Williams, Trans. Faraday Soc., 60, 1973 (1964).

Table 1. Dual Sorption Parameters

T/°C	$10^2 k_D$ $cm^3(stp)/cm^3 cmHg$	C'_H $cm^3(stp)/cm^3$	b $(cmHg)^{-1}$	10k $cm^3(stp)/cm^3 cmHg$	$C'_H b/k_D$
		CH_4/Polystyrene			
30	-	-	-	0.069	5.0*
50	-	-	-	0.044	
		C_3H_8/Polystyrene (film)			
30	4.69	1.01	0.18	2.29	3.88
50	2.82	0.735	0.071	0.804	1.85
		C_3H_8/Polystyrene (powder)			
20	4.39(±5%)	1.32(±9%)	0.209(±18%)	3.2(±9%)	6.28
30	3.30(±11%)	1.36(±17%)	0.136(±28%)	2.18(±11%)	5.60
40	2.93(±6%)	0.90(±12%)	0.127(±20%)	1.43(±8%)	3.80
50	2.46(±6%)	0.70(±16%)	0.106(±23%)	0.984(±7%)	3.02
60	2.29(±14%)	0.51(±45%)	0.108(±62%)	0.776(±17%)	2.41
		$CHClF_2$/Polystyrene (powder)			
20	7.34(±8%)	2.16(±15%)	0.18(±28%)	4.71(±13%)	5.3
30	5.42(±9%)	1.95(±14%)	0.150(±25%)	3.47(±11%)	5.4
40	4.49(±7%)	1.50(±13%)	0.110(±20%)	2.10(±7%)	3.67
50	3.81(±7%)	1.20(±15%)	0.089(±20%)	1.45(±6%)	2.80
60	3.18(±18%)	0.80(±59%)	0.071(±63%)	0.89(±9%)	1.79
		C_3H_8/Polycarbonate			
30	6.03(±7%)	1.67(±11%)	0.311(±30%)	5.79(±18%)	8.6
40	5.01(±2%)	1.25(±4%)	0.254(±9%)	3.68(±5%)	6.3
50	4.01(±8%)	1.02(±21%)	0.167(±43%)	2.10(±19%)	4.3
60	2.55(±17%)	1.22(±31%)	0.094(±50%)	1.40(±19%)	4.5
		C_3H_8/Polyvinylacetate (disperse)			
2.7	2.29(±5%)	-	-	0.999(±8%)	3.4
12.1	2.24(±5%)	-	-	0.786(±14%)	2.5
22.4	1.89(±5%)	-	-	0.52	1.76
40.15	1.83(±1%)	-	-	-	
50.0	1.66(±5%)	-	-	-	
60.2	1.45(±3%)	-	-	-	

* data from (18)

Table 2. Heats of Sorption.

System	$-\Delta\overline{H}_D$ kJmol^{-1}	q kJmol^{-1}	$-(\Delta\overline{H})_{c=o}$ kJmol^{-1}	$-(\Delta\overline{H}_H)_{c=o}$ kJmol^{-1}
CH_4-polystyrene (film)	-	-		18†
C_3H_8-polystyrene (film)	21†	38†	51†	43†
C_3H_8-polystyrene (powder)	13	13	34	30
$CHClF_2$-polystyrene (powder)	17	20	39	34
C_3H_8-polycarbonate	24	34	43	41
C_3H_8-polyvinylacetate (T > Tg)	10	-	-	-
C_3H_8-polydimethylsiloxane	17	-	-	-

† From two temperatures only.

TABLE 3. Diffusion Coefficients and Activation Energies for Diffusion

T/°C	$10^{11}D_D$	$10^{12}D_H$	$10^{11}D_{c=o}$	E_{D_D}	E_{D_H}	$E_{D_{c=o}}$
	cm^2/s	cm^2/s	cm^2/s	kJ/mol	kJ/mol	kJ/mol
			CH_4/Polystyrene			
30	-	-	1270	-	-	39
50	-	-	3330	-	-	
			C_3H_8/Polystyrene (film)			
30	8	-	1.64	33	-	55
50	18	-	6.3			
			C_3H_8/Polycarbonate			
30	1.77(±4%)	4.0(∓9%)	0.54			
40	3.43(±1.5%)	5.4(∓1.4%)	0.93			
50	8.3(±12%)	6.6(∓17%)	2.12	69	49	67
60	20.3(±19%)	27.1(∓88%)	5.9			

CAPTIONS FOR FIGURES

Figure 1. Sorption isotherms for polystyrene (film).

C_3H_8: ○ 30°, ● 50°C. Solid lines computed from equation (1); dotted line is the asymptote at 30°C.

CH_4: ordinate is CX4; □ 30° ■ 50°C.

Figure 2. Sorption isotherms for propane in polystyrene (powder).

■ 20, ▲ 30, ● 40, ◆ 50, ▼ 60°C. Solid lines computed for equation (1); dotted line is the asymptote to the curve at 20°C.

Figure 3. Sorption isotherms for propane in polycarbonate

■ 30, ▲ 40, ● 50, ▼ 60°C. Solid lines computed from equation (1); dotted line is the asymptote to the curve at 30°C.

Figure 4. Sorption isotherms for chlorodifluoromethane in polystyrene (powder).

■ 20, ▲ 30, ● 40, ◆ 50, ▼ 60°C. Solid lines computed from equation (1); dotted line is the asymptote to the curve at 20°C.

Figure 5. Sorption isotherms for propane in polydimethylsiloxane-g-polyvinylacetate and polydimethylsiloxane.

PDMS-g-PVAc: ■ 2.7, ▲ 12.1, ● 22.4°C; ▼ 50°C, typical linear isotherm obtained above Tg. Solid lines computed from equation (1).

PDMS : ○ 11.7°C, typical linear isotherm.

Figure 6. Sorption isotherms for propane in polyvinylacetate disperse phase.

■ 2.7, ▲ 12.1, ● 22.4; ▼ 50°C, typical linear isotherm obtained above Tg. Solid lines computed from equation (1); dotted line is the asymptote to the curve at 2.7°C.

Figure 7. Temperature dependence of dual-sorption parameters; typical behaviour illustrated by results for the propane-polycarbonate system.

● $Z = k$, ▲ $Z = b$, ■ $Z = k_D$, ▼ $= C'_H b$.

Figure 8. Temperature dependence of k_D and k for the propane–polyvinylacetate (disperse phase) system.

● $Z = k_D$, ■ $Z = k$.

Figure 9. Concentration dependence of the heat of sorption $\Delta\overline{H}$; smoothed values obtained from the curves computed from equation (1).

—— C_3H_8-polystyrene, --- $CHClF_2$-polystyrene, ····· C_3H_8-polycarbonate.

Figure 10. Concentration dependence of the average diffusion coefficient $\overline{D}$ for the propane-polystyrene (film) system.

○ 30, ● 50 °C; Solid curves computed from equation (10) with $D_H=0$.

Figure 11. Concentration dependence of the average diffusion coefficient $\overline{D}_s$ for propane-polycarbonate system.

■ 30, ▲ 40, ● 50, ▼ 60 °C; solid curves computed from equation (8).

Figure 12. Plots of $\overline{D}_s$ versus X, where X is given by equation (9), r=1.67 for propane in polycarbonate.

■ 30, ▲ 40, ● 50, ▼ 60 °C.

Figure 13. Plots of $\overline{D}$ versus X, where X is given by equation (9), r=1, for propane in polystyrene.

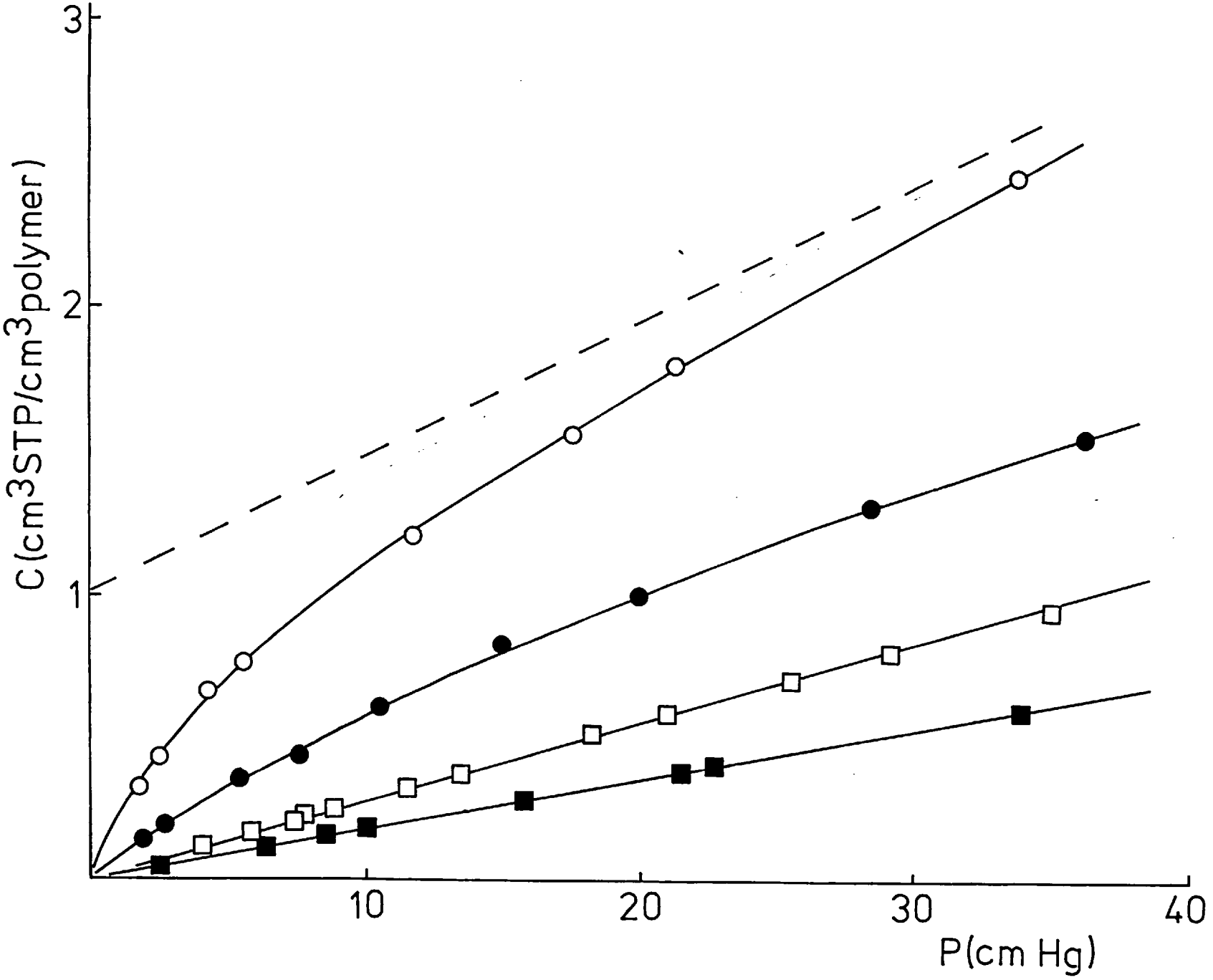
○ 30, ● 50 °C.

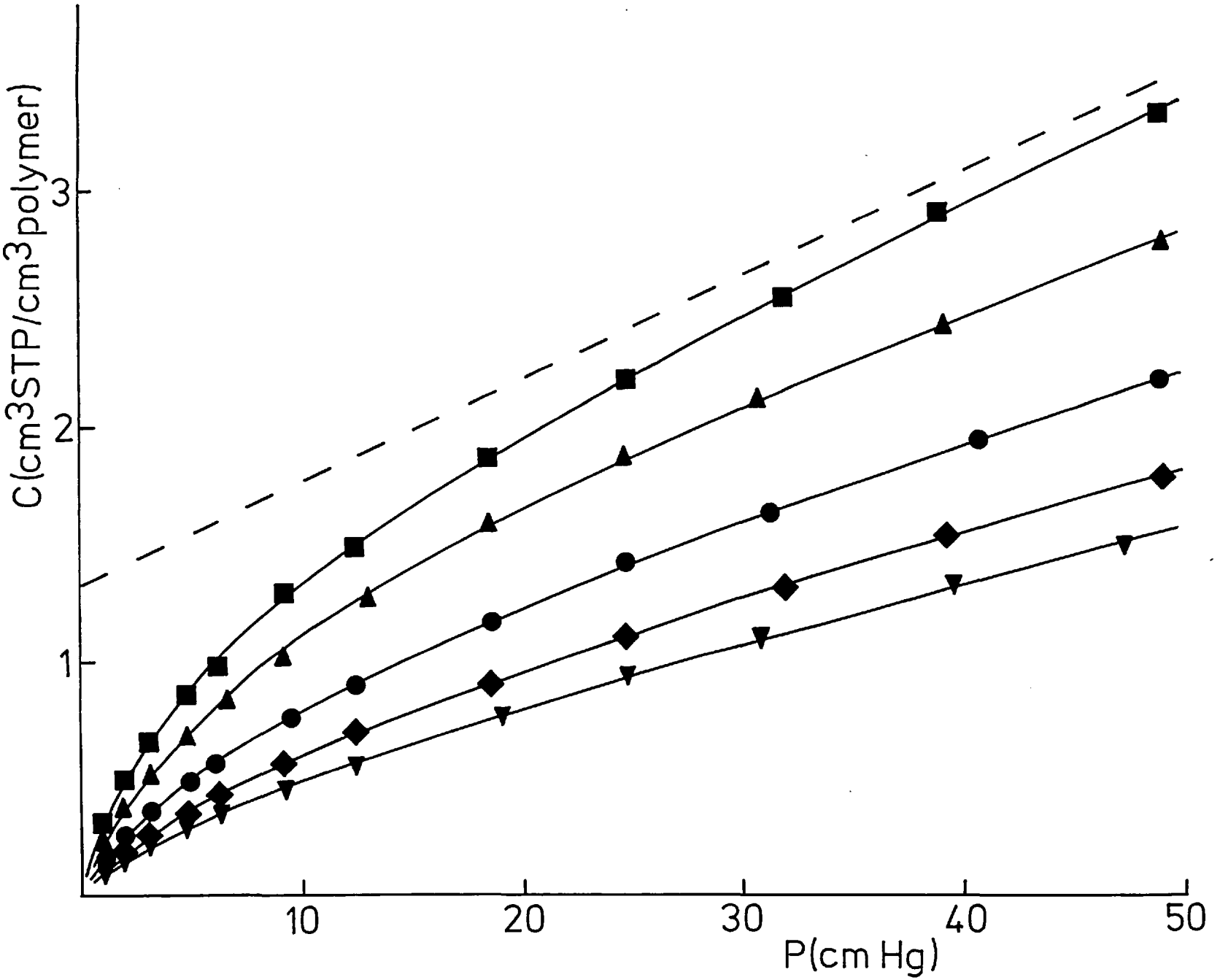
Figure 14. Concentration dependence of the heat of sorption $\Delta\overline{H}_H$.

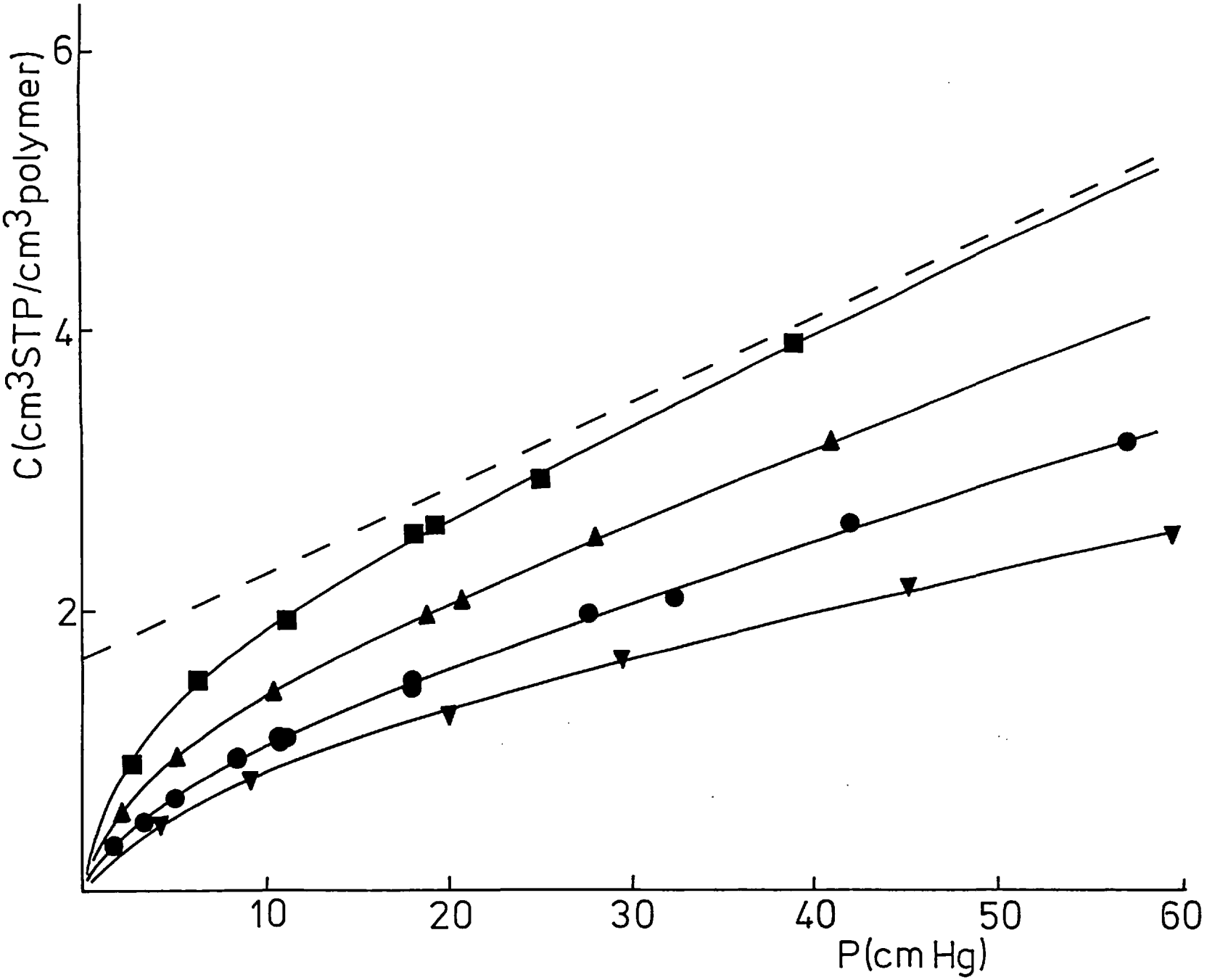
-·-·-· C_3H_8-polystyrene (sheet), ····· C_3H_8-polystyrene (powder), ----- C_3H_8-polycarbonate, ——— $CHClF_2$-polystyrene (powder).

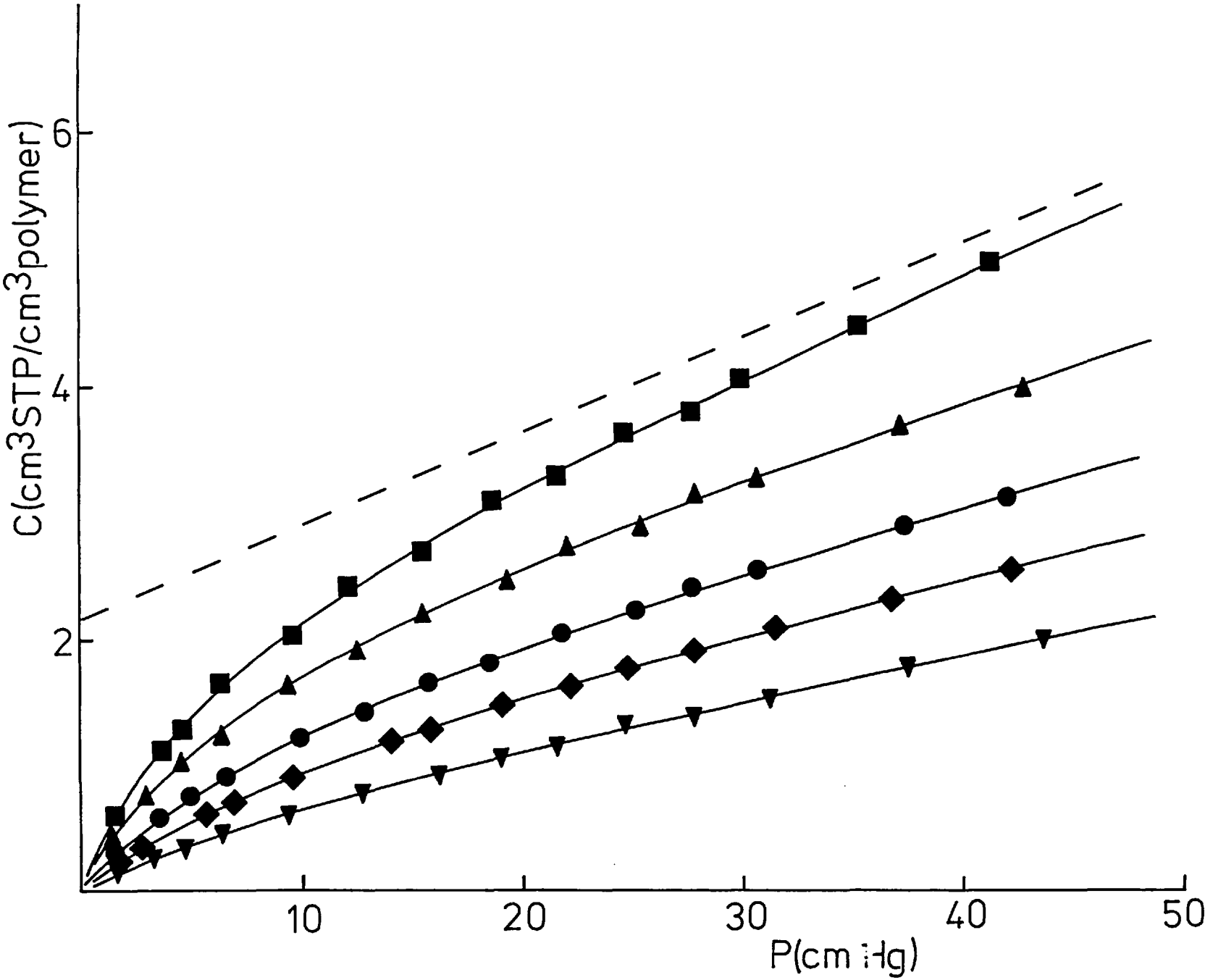
Figure 15. Temperature dependence of diffusion coefficients; typical behaviour as illustrated by results for the propane–polycarbonate system.

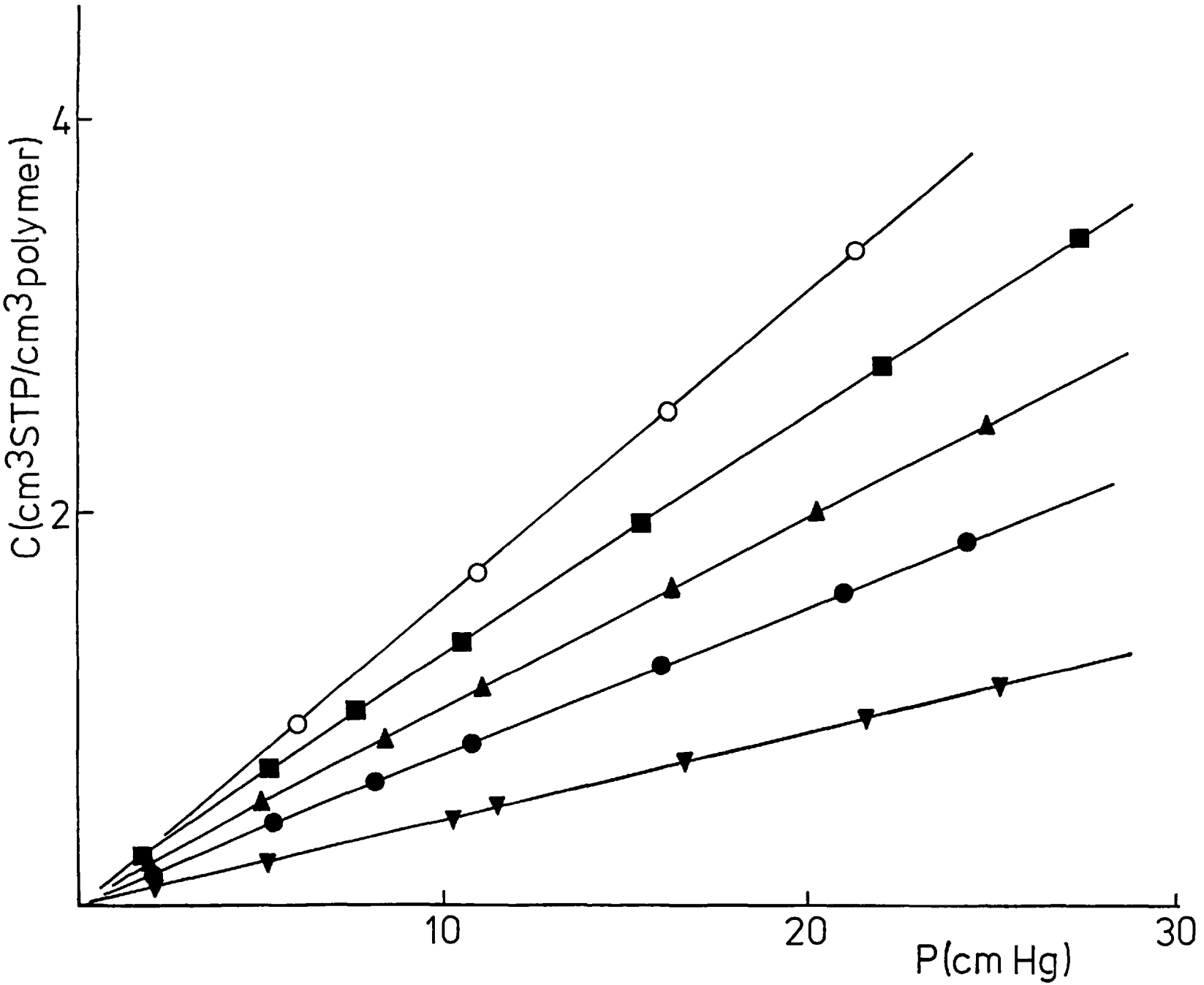
● D_D, ▲ $D_{c=o}$, ■ D_H.

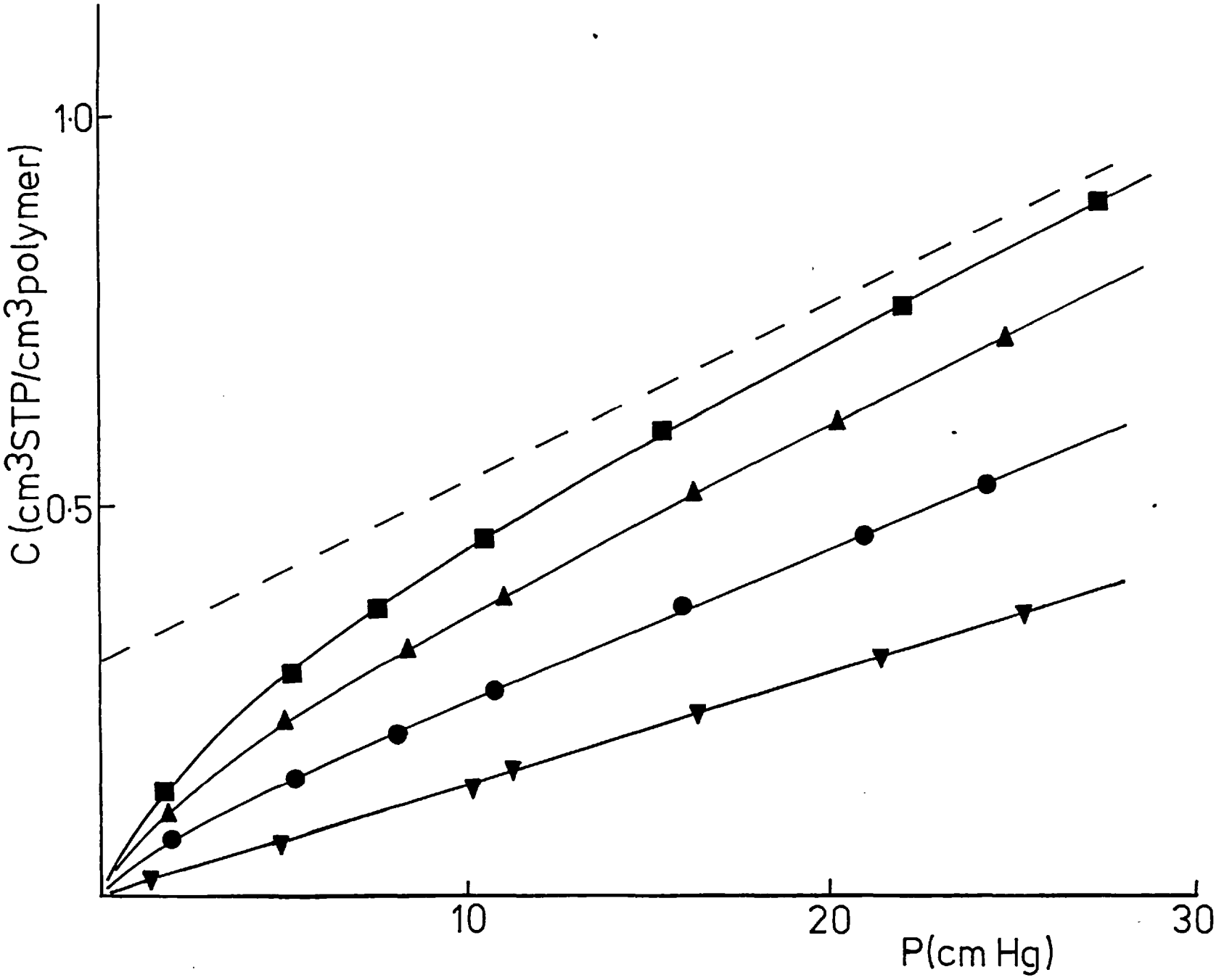

3
2
1
C(cm3STP/cm3polymer)
10
20
30
40
P(cm Hg)

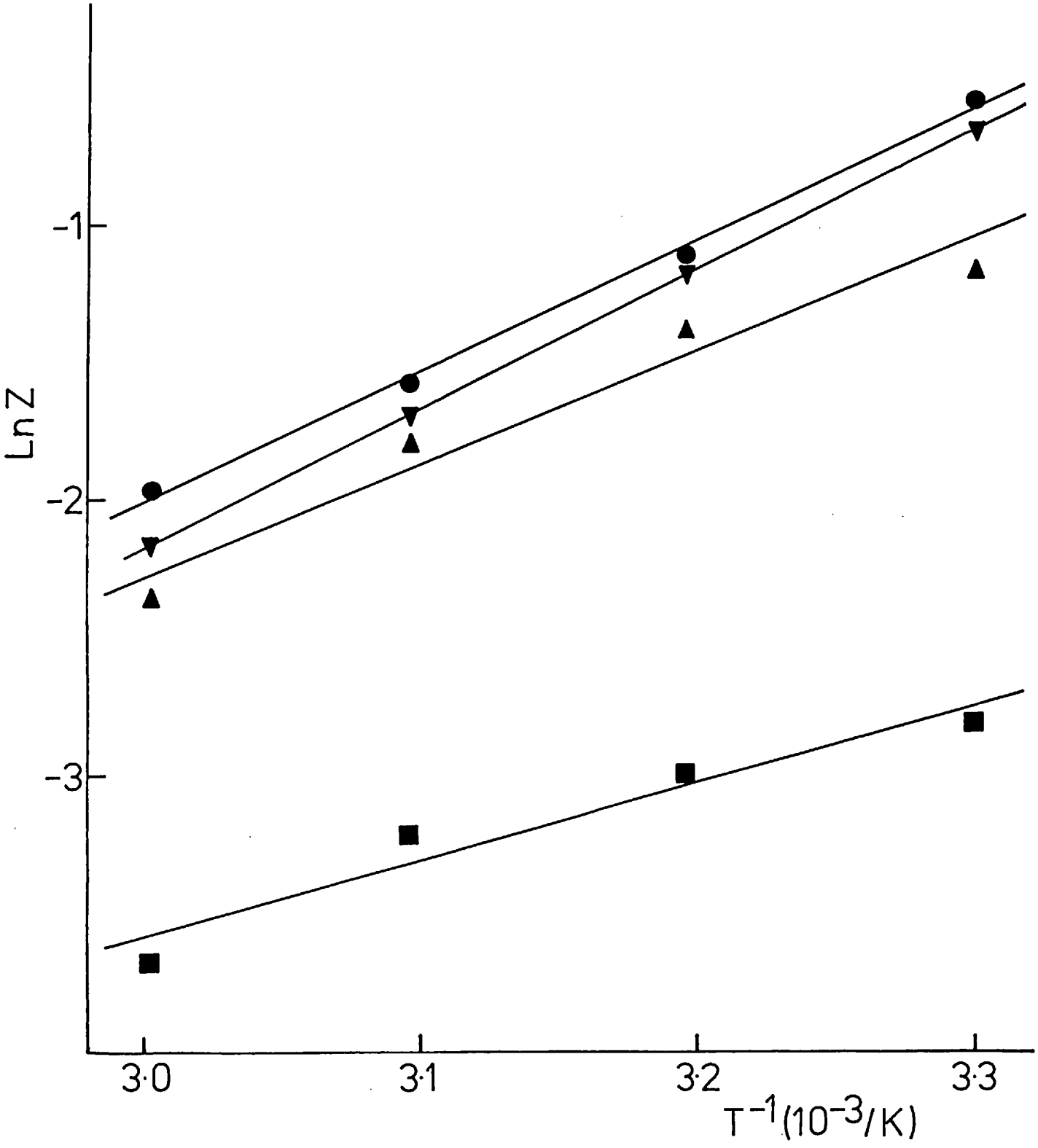

C(cm3STP/cm3polymer)
3
2
1
10
20
30
40
50
P(cm Hg)

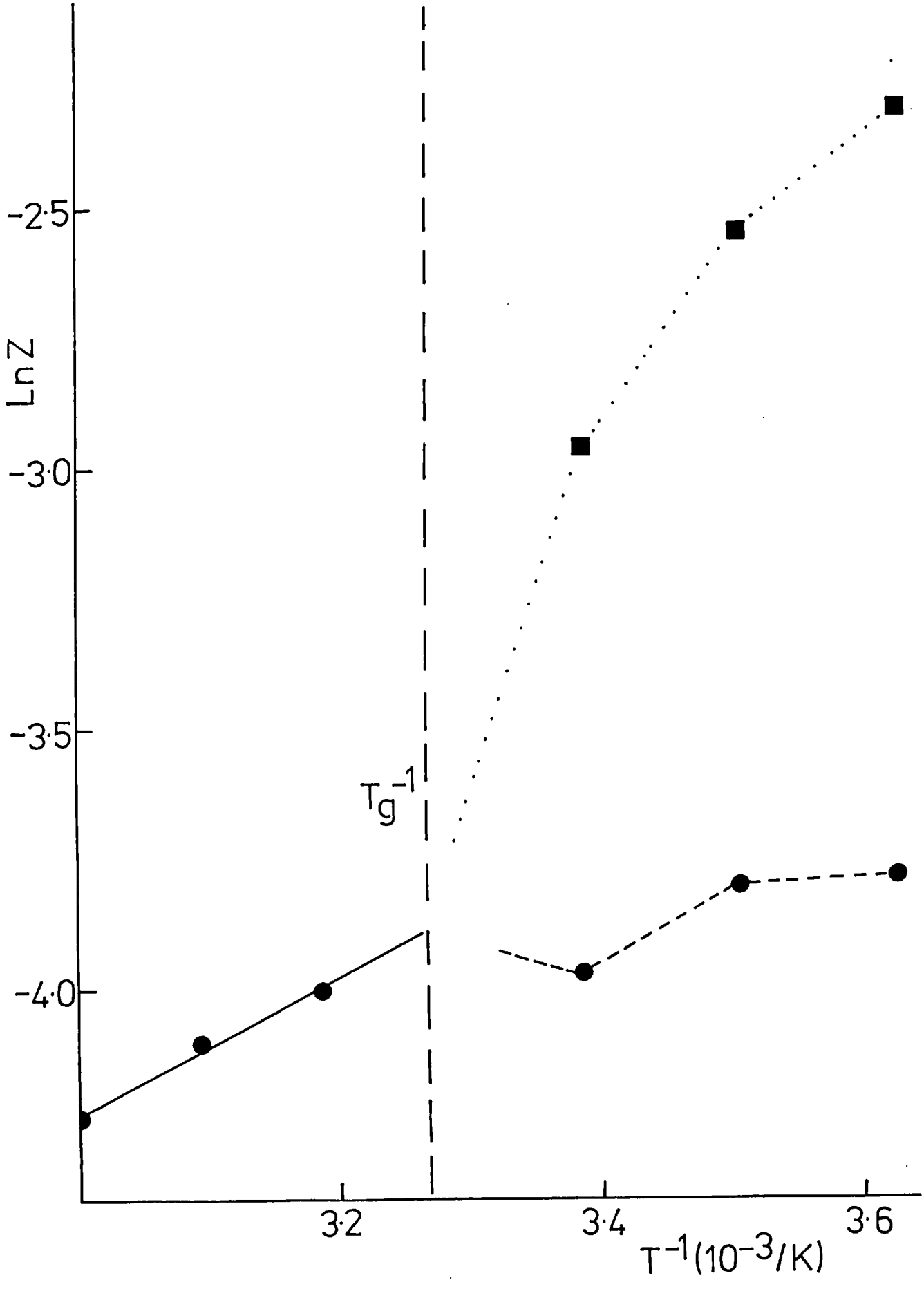

C(cm3STP/cm3polymer)
6
4
2
10
20
30
40
50
60
P(cm Hg)

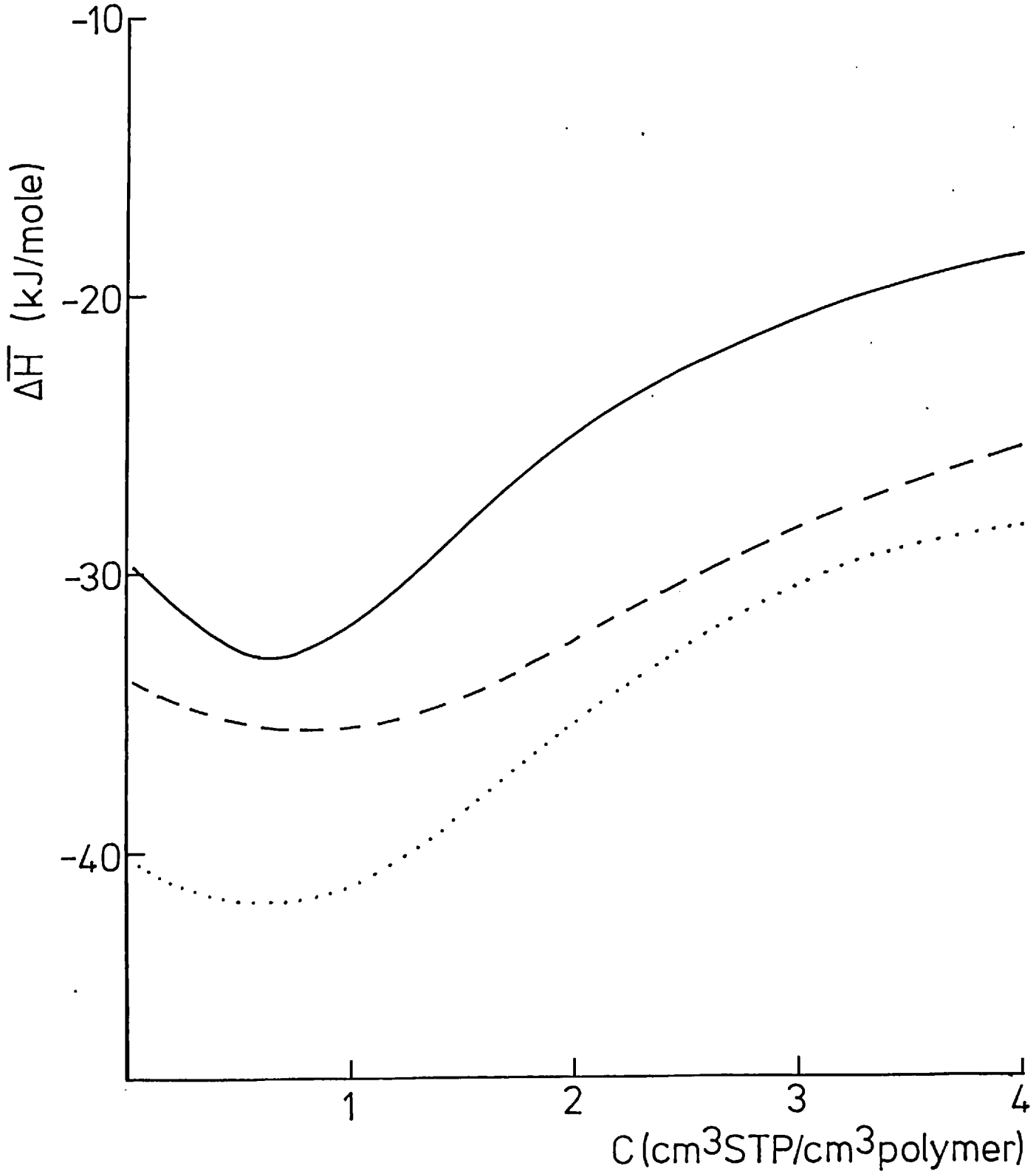

C(cm3STP/cm3polymer)
6
4
2
10
20
30
40
50
P(cm Hg)

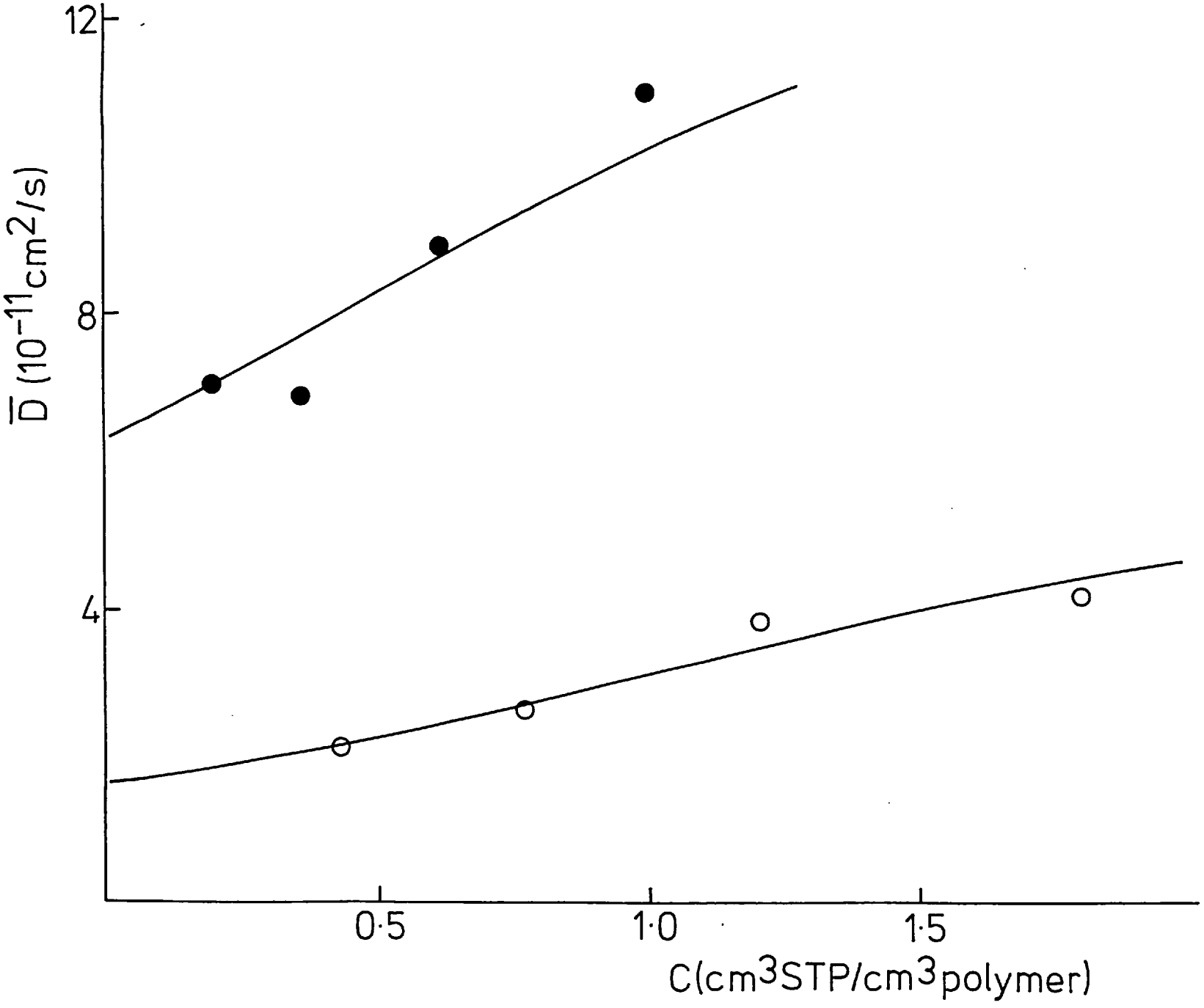

C(cm3STP/cm3polymer)
4
2
10
20
30
P(cm Hg)

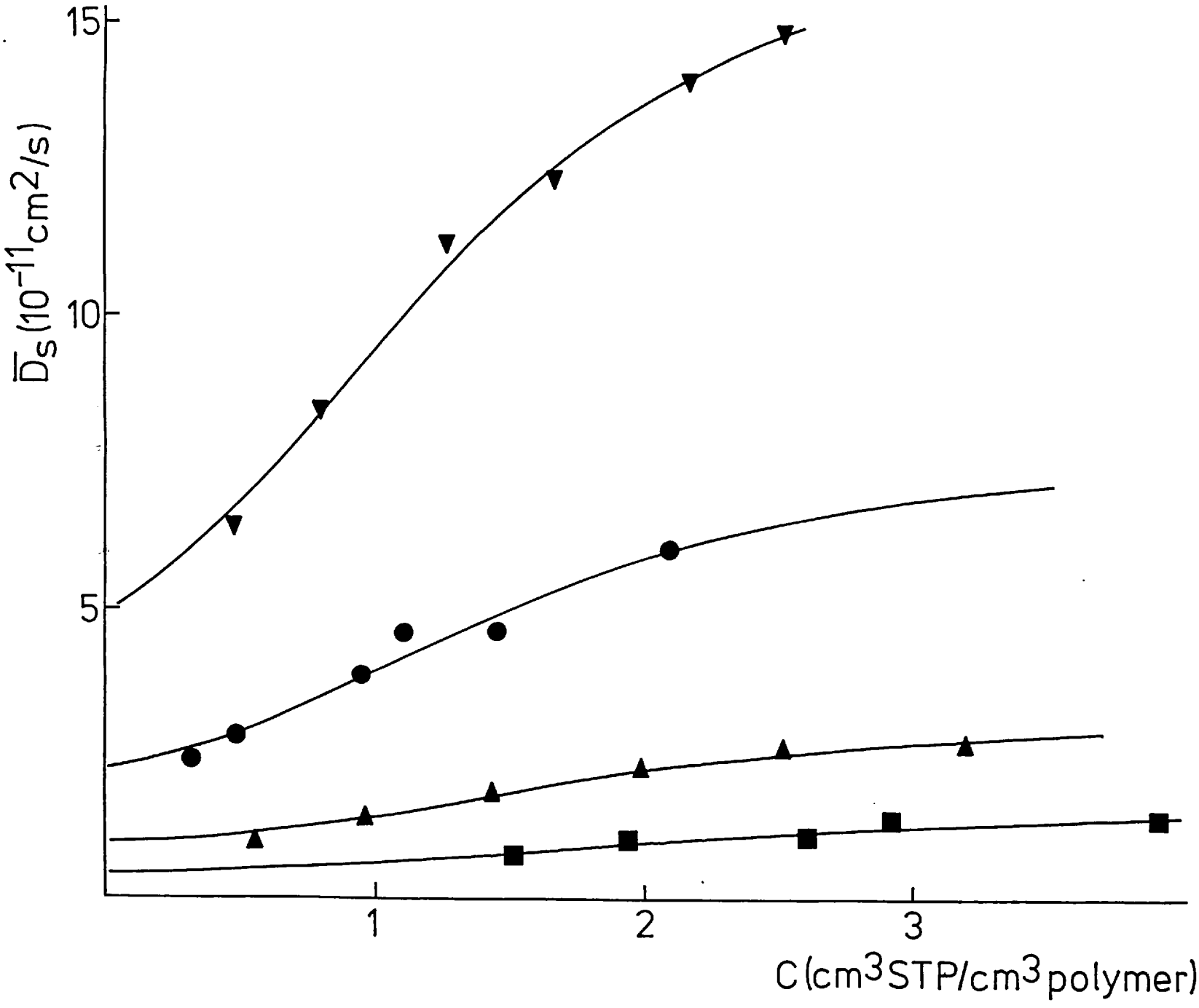

C (cm3STP/cm3polymer)
1·0
0·5
10
20
30
P(cm Hg)

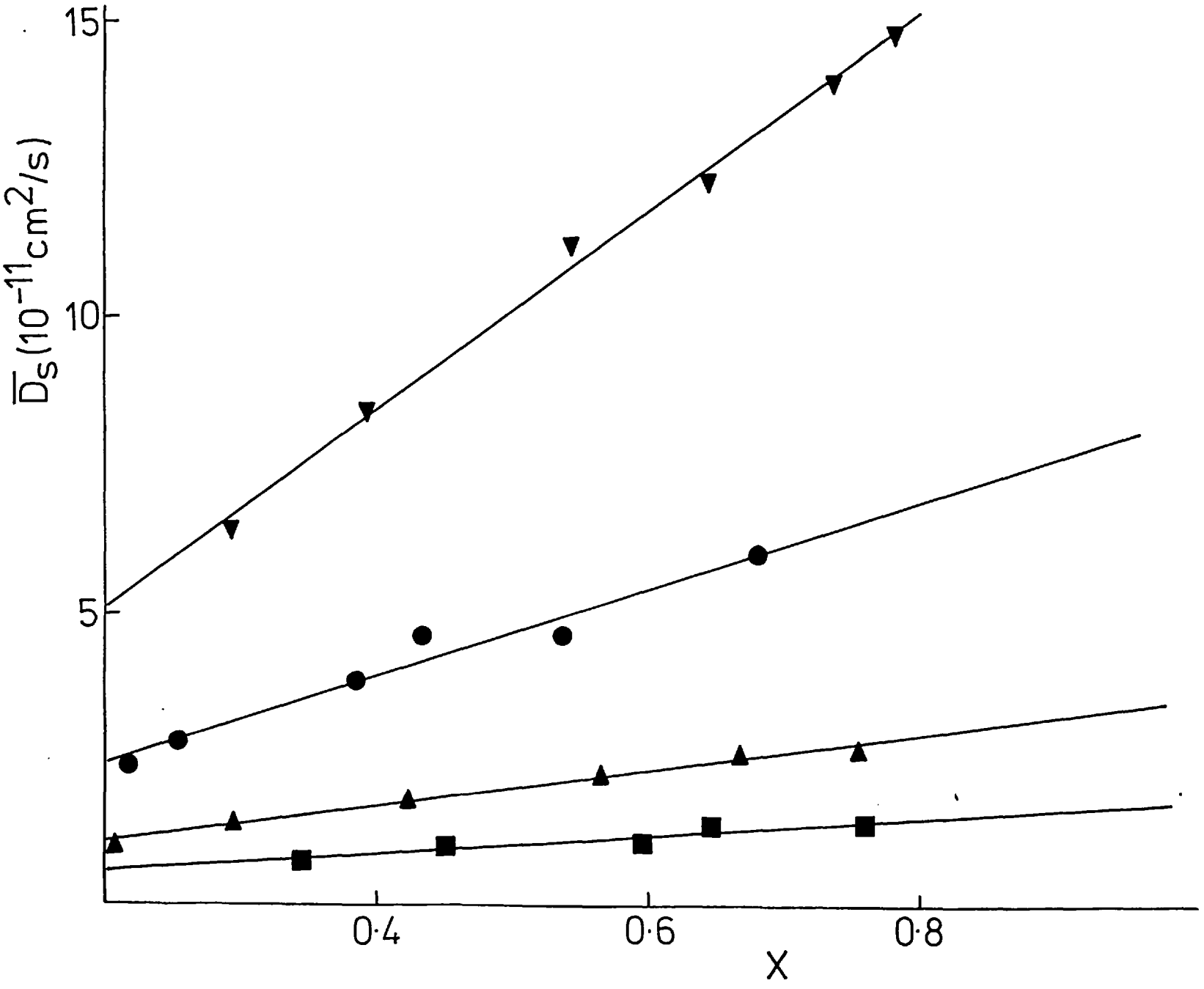

-1
-2
-3
Ln Z
3·0
3·1
3·2
3·3
T⁻¹(10⁻³/K)

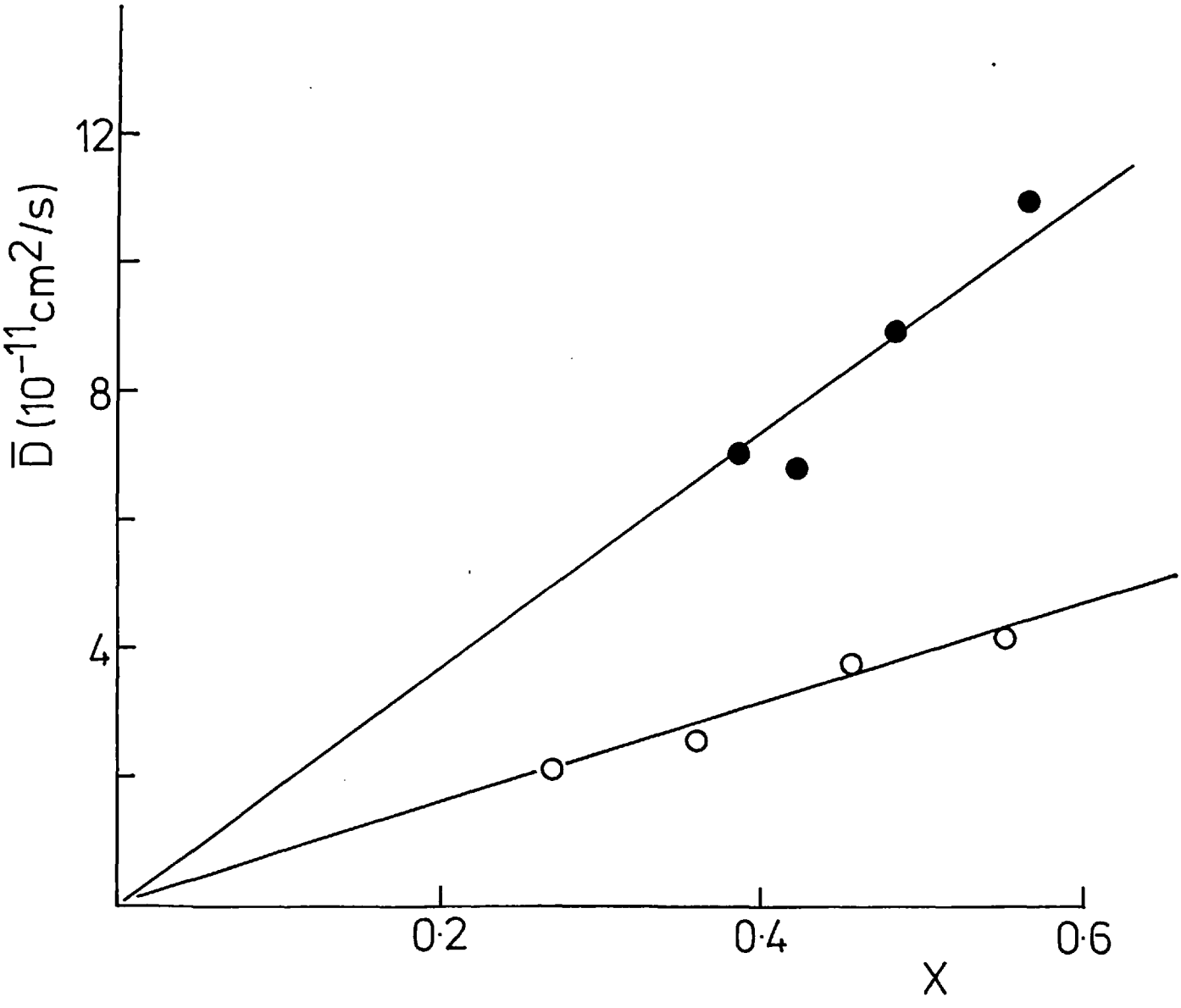

-2·5
-3·0
-3·5
-4·0
Ln Z
T_g^{-1}
3·2
3·4
3·6
$T^{-1}(10^{-3}/K)$

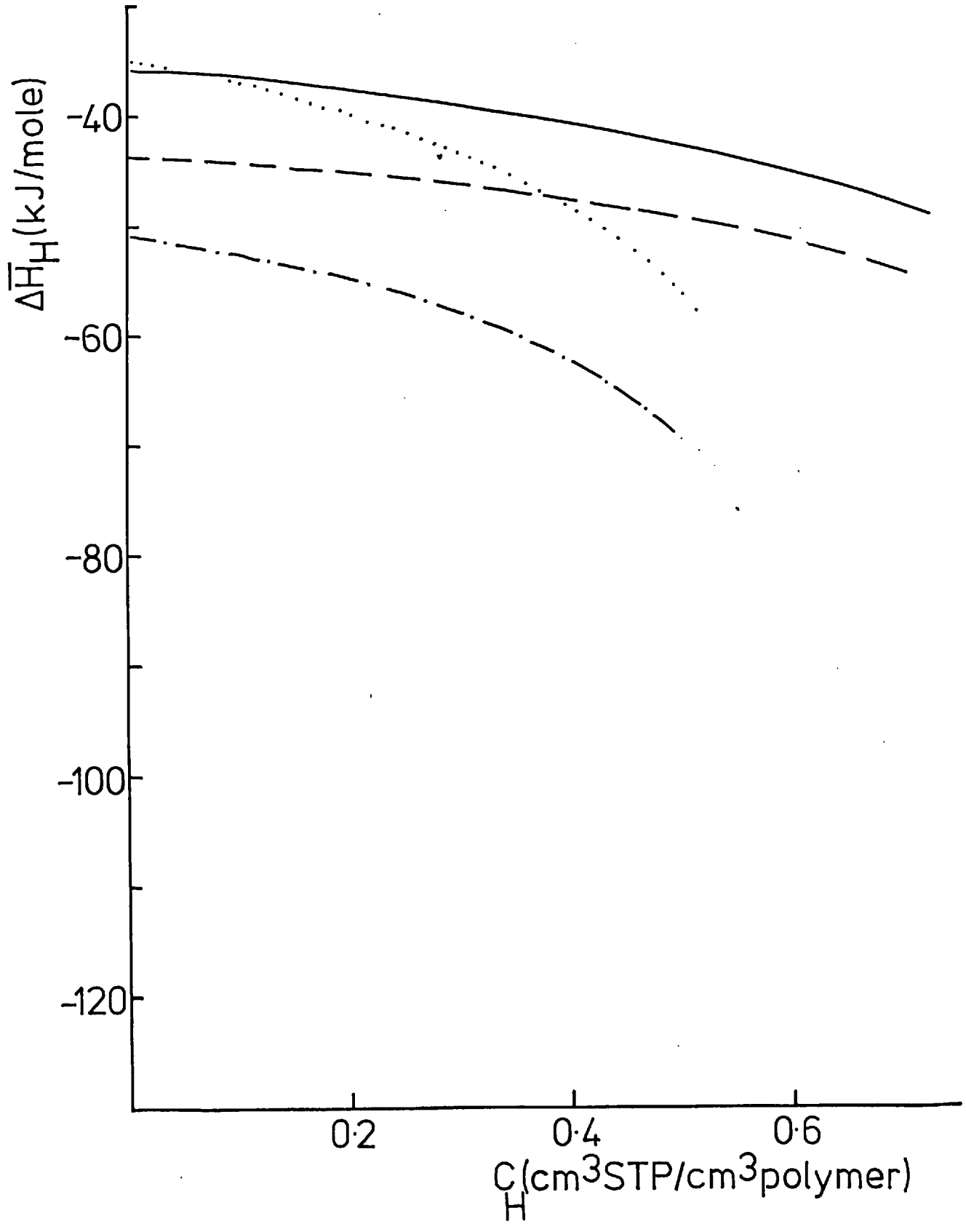

-10
-20
-30
-40
$\overline{\Delta H}$ (kJ/mole)
1
2
3
4
C (cm³STP/cm³polymer)

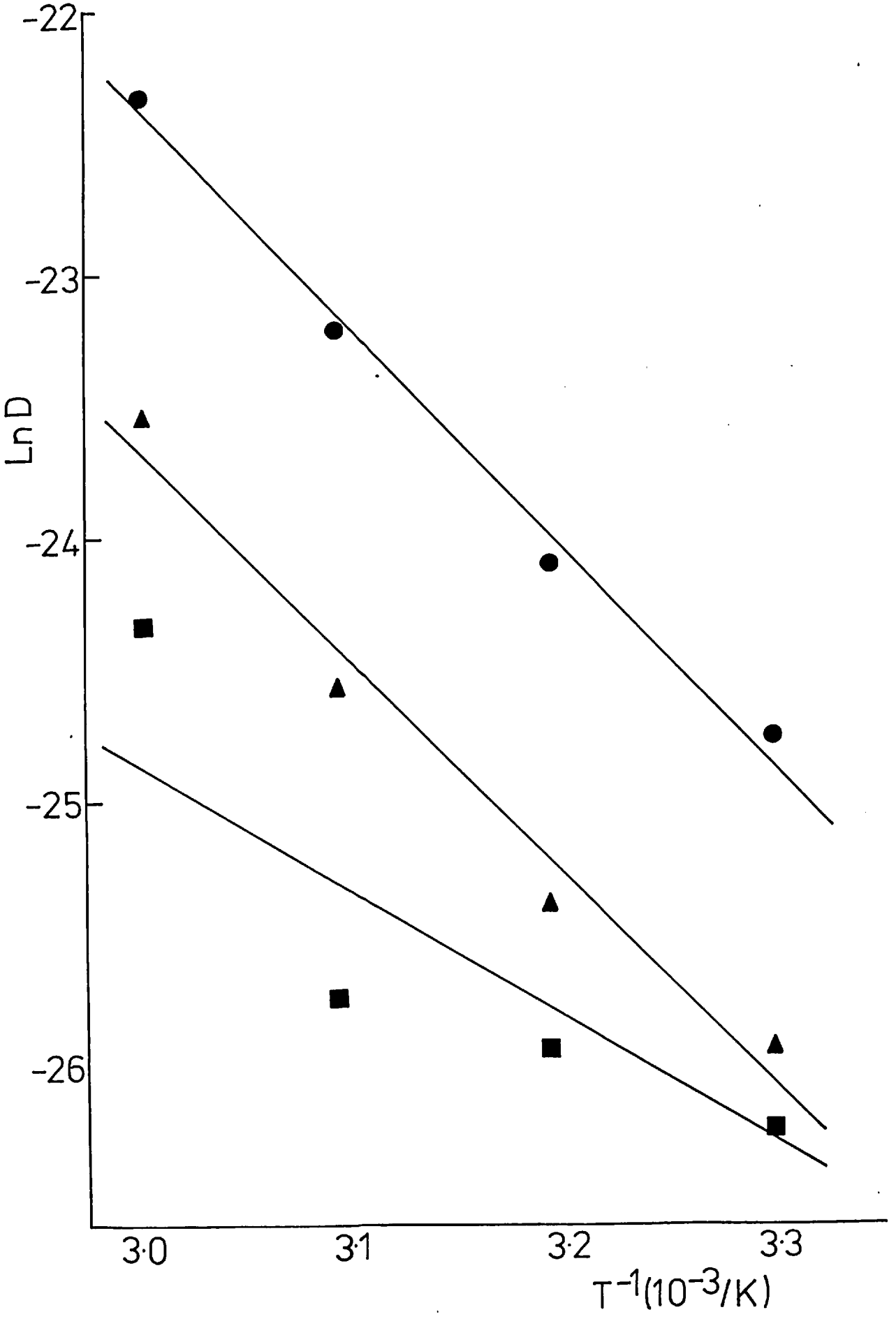

12
8
4
$\overline{D}$ (10^{-11} cm^2/s)
0·5
1·0
1·5
C(cm^3STP/cm^3polymer)


15
10
5
$\overline{D}_S$ (10^{-11} cm^2/s)
1
2
3
C (cm^3 STP/cm^3 polymer)


15
10
5
$\overline{D}_S(10^{-11}cm^2/s)$
0·4
0·6
0·8
X


$\bar{D}$ (10^{-11} cm^2/s)
12
8
4
0·2
0·4
0·6
X


$\Delta\bar{H}_H$(kJ/mole)
-40
-60
-80
-100
-120
0·2
0·4
0·6
C_H(cm³STP/cm³polymer)


-22
-23
-24
-25
-26
LnD
3·0
3·1
3·2
3·3
T⁻¹(10⁻³/K)